DETECTION OF METALLOENZYMES EMPLOYING FLUORESCENT-POLYMERS AND LIPOSOMES

A Dissertation
Submitted to the Graduate Faculty
of the
North Dakota State University
of Agriculture and Applied Sciences

By

Rinku Dutta

In Partial Fulfillment of the Requirements
for the Degree of
DOCTOR OF PHILOSOPHY

Major Department:
Pharmaceutical Sciences

March 2012

Fargo, North Dakota

North Dakota State University
Graduate School

Title

Detection of Metalloenzymes Employing Fluorescent-Polymers and Liposomes

By

Rinku Dutta

The Supervisory Committee certifies that this ***disquisition*** complies with North Dakota State University's regulations and meets the accepted standards for the degree of

DOCTOR OF PHILOSOPHY

SUPERVISORY COMMITTEE:

Sanku Mallik

Chair

Jagdish Singh

Estelle Leclerc

Anne Denton

Approved:

03.22.2012 — Date

Jagdish Singh — Department Chair

ABSTRACT

In the biological systems, proteins are important constituents. Protein-protein interactions play vital roles in physiological environments and any disruption in these interactions lead to adverse effects. However, designing artificial receptor molecules or scaffolds to imitate or replace these endogenous partners could be an avenue for better drug designing and detection tools creation. We are primarily interested in polymer and liposomal systems to detect two crucial metalloenzymes of the living world. Matrix metalloproteinases are zinc-containing endopeptidases which are required for wound healing, pregnancy and angiogenesis in normal bodily conditions. However, when overexpressed, these cause cancer, arthritis, cardiovascular disorders and fibrosis. Carbonic anhydrases (CAs) are another class of Zn^{2+} metalloenzymes involved in glaucoma, diabetes, epilepsy and hypertension. Sulphonamide-based inhibitors are prevalent in the market for targeting CAs, but they lack specificities in isozyme-selective inhibition or detection. Usually most of the broad spectrum inhibitors for MMPs have failed the clinical trials due to adverse side effects such as musculoskeletal pain or the inhibition of other non-targeted isozymes.

Our strategy was to develop isozyme selective fluorescent water soluble polymers incorporating an active site binding inhibitor for each enzyme class and different charged and uncharged moieties for surface binding with the exposed residues of the isozymes. We have incorporated fluorophores in our polymers which acted as our detection signal generator through fluorescence. For MMPs, one of the optimized polymers was able to detect MMP-9 selectively compared to MMP-7 and -10 (discussed in Chapter 1). This polymer had shown potency in differentiating and subtyping various breast and prostate cancer cell lines from non- cancerous

cell lines based on interactions with the secreted MMP-9 from these cell lines (discussed in Chapter II). Chapter III deals with the selective detection of CA II from CA VII and XII even in the complex mixture of biomacromolecules using our synthesized polymers. In Chapter IV, we investigated dye-encapsulated liposomal formulations for detection of catalytically active MMP-7. The synthesized polymers and liposomes could serve as an alternative detection tool for detection and isozyme selective interactions of these metalloenzymes.

ACKNOWLEDGEMENTS

I sincerely thank my major advisor Dr. Sanku Mallik for guiding me all throughout my doctoral studies. I found him to be an excellent teacher, researcher and guide. During my entire stay at his laboratory, he had been always patient and considerate whenever I faced difficulties in my research. He is not only a great guide, but also a wonderful listener. He had always been a very beneficial critique when it came to prepare for my seminars or poster presentations. During the group meetings he had always supported me with new ideas at the time of difficulties. I really appreciate his suggestions, help, motivation and encouragement.

I wish my gratitude to Dr. Jagdish Singh for allowing me to work in the department and use all the instruments that were needed for my experiments. As a committee member, he had always been very enthusiastic about my work and had helped me with his feedbacks and support.

I am grateful to Dr. Estelle Leclerc for being in my committee and helping me in my research. She had been really nice to me and very supportive. I would like to thank Dr. Anne Denton for being my external committee member. Dr. Denton had always come up with positive criticisms which were very beneficial for my research and her comments were really helpful.

I owe my gratefulness to Dr. Manas Haldar, the post doctoral researcher in our laboratory for his assistance, guidance and help. Dr. Haldar helped me in many of my syntheses and whenever I faced trouble dealing with any reactions, he had always assisted me in troubleshooting them with his valuable opinions and suggestions.

I would like to thank Dr. D. K. Srivastava and his laboratory for supplying me with the necessary enzymes whenever needed and helping me in completing my studies.

I thank the Department of Pharmaceutical Sciences and the Department of Chemistry and Biochemistry at the North Dakota State University for completing necessary experiments for my research. I appreciate Jean and Janet for their help, support and assistance.

I sincerely thank Dr. Daniel L. Friesner for doing all the statistical analyses for my experiments.

I would like to thank my senior labmates Dr. Jayati Banerjee, Dr. Rajesh Subramaniam, Tapas, Ryan and my present labmates and colleagues Mike, Erin, Rahul, Prajakta for their help and allowing me to work in a friendly and healthy environment in the lab. I also appreciate all the undergraduates and pharmacy students who worked with me in those years and being really helpful in my work. I thank Jane, Jessica, Chantal, Mohammed and Andrea for their help.

I would like to thank Dr. Partha Sengupta, Bud and his wife, Chumkidi, Kruthi, Arshi, Amit, Geetanjali, Ruchi, Faidat, Anna and all my fellow graduate students in the Department of Pharmaceutical Sciences for being nice and friendly to me throughout all these years.

I thank my parents for their blessings and love without which this wouldn't have been possible. I owe my heartiest gratitude and thankfulness to all my family members for their support, encouragement and motivations.

Finally I thank the funding agencies, National Institute of Health (NIH) (National Cancer Institute, 1 R01 CA132034) and the Department of Pharmaceutical Sciences, NDSU.

Above all I thank the Almighty, for helping me in my hard days and allowing me to keep patience, perseverance and complete my goal.

DEDICATION

With love to ma and baba

TABLE OF CONTENTS

LIST OF TABLES

LIST OF FIGURES

LIST OF SCHEMES

LIST OF ABBREVIATIONS

AChE……Acetylcholinesterase

ADAM……...A disintegrin and metalloproteinase

ADAMTS…….. A disintegrin and metalloproteinase with thrombospondin

AIBN……. Azobisisobutyronitrile

Ala……. Alanine

APMA……... 4-aminophenylmercuric acetate

Ara-C……Cytosine arabinoside

Arg……Arginine

Asn…….Asparagine

Asp…….Aspartic acid

Boc…… Di-tertbutyl dicarbonate

BOP……... Benzotriazol-1-yloxytris(dimethylamino)-phosphonium Hexafluorophosphate

BSA……... Bovine Serum Albumin

CAD……...Computer-aided detection

CARP…….....Carbonic anhydrase-related proteins

CAs……....Carbonic Anhydrases

CC……..Cytochrome *c*

CD……. Cyclodextrin

CEA……... Carcinoembryonic antigen

CF…….. Carboxyfluorescein

ChT……....Chymotrypsin

CL…….. Conventional liposomes

Conc…….. Concentration

Cryo-TEM……..... Transmission electron microscopy at cryogenic temperature

CS…….. Citrate Synthase

CXCL12……..... Chemokine (C-X-C motif) ligand 2

d……. Doublet

DA……. Dansylamide

DLS……... Dynamic Light Scattering

DMF…….. Dimethylformamide

DMSO……... Dimethyl sulfoxide

DNA…….. Deoxyribonucleic acid

DOPC……..... 1, 2-Dioleyl-sn-glycero-3-phosphocholine

DOPE…….....1,2-Dioleoyl-sn-Glycero-3-phosphoethanolamine

DPPC……. 1,2-dihexadecanoyl-sn-glycero-3-phosphocholine

DRE……... Digital rectal examination

DRS……... Diffuse Reflectance Spectroscopy

DSPC…….....1,2-Distearoyl-sn-glycero-3-phosphocholine

DSPE……..... 1,2-Distearoyl-sn-glycero-3-phosphoethanolamine

ECL……... Electrochemiluminescence

ECM…….. Extracellular matrix

EDTA……..... Ethylenediaminetetraacetic acid

ELISA……....Enzyme Linked Immunosorbent Assay

EMMPRIN……..... Extracellular MMP inducer

EPR……....Enhanced permeability and retention effect

ER……..Estrogen receptor

EtOAc……....Ethylacetate

FasL……...Fas ligand

FBS……....Fetal Bovine Serum

FC……..Ferrocene carboxylic acid

FDA……...Food and Drug Administration

FISH…….. Fluorescence *in situ* hybridization

FITC…….. Fluorescein isothiocyanate

FFDM…… Full-field digital mammography

FRET……. Förster resonance energy transfer

fTHP…….. fluorogenic triple-helical peptide

ΔG……..Gibbs free energy Change

Glu……Glutamic acid

GPC……... Gel Permeation Chromatography

GPI-linked……..... Glycophosphatidylinositol-linked

GUV…….. Giant Unilamellar Vesicle

ΔH…….....Enthalpy change

h……Human

HA……. Hemagglutinin

HBTU…… O-Benzotriazole-N,N,N´,N-tetramethyl-uronium-Hexafluorophosphate

HBBS…….Hank's Balanced Salt Solution

HEPES…….....N-2-Hydroxyethylpiperazino-N□-2-ethanesulfonic acid

HER2…….....Human epidermal receptor protein-2

His……. Histidine

HOBT……..... 1-Hydroxybenzotriazole

HPLC……High Performance Liquid Chromatography

HRP……... Horse radish peroxidase

IC_{50}……..... Half maximal inhibitory concentration

ICH……..... Immunohistochemistry

IDA……....Iminodiacetic acid

IFETS……..... Intra-molecular fluorescence energy transfer substrate

IFS…….....Intrinsic fluorescence spectroscopy

ITC…….....Isothermal titration microcalorimetry

J……..... Coupling constant

K_a……...Association constant

k_{cat}……..Rate constant of catalysis

K_d……...Dissociation constant

K_i……... Inhibition constant

kJ……... Kilojoule

K_M……..Michaelis Menton constant

LCL……... Long Circulatory liposomes

LDA……...Linear Discriminant Analysis

LDH……...L-Lactate dehydrogenase

Leu…….....Leucine

LHA……...Liquid Hybridization Assay

LUV……...Large Unilamellar Vesicle

M……... Molar

m……....Multiplet

MALDI-ToF……..Matrix assisted laser desorption/ionization- time of flight

Met…….....Methionine

MHz……...Megahertz

MIPs…….. Molecular Imprinting Polymers

MLV…….. Multilamellar Vesicle

MMPi……Matrix Metalloproteinase inhibitor

MMPs…….... Matrix Metalloproteinases

MRI……... Magnetic resonance imaging

mRNA……... Messenger Ribonucleic acid

MT-MMPs…….....Membrane type matrix metalloproteinases

MWCNT…….....Multiwalled carbon nanotubes

NaCl……...Sodium chloride

NASBA……. Nucleic Acid Sequence-based Amplification

ng……...Nanogram

NIPAM…….. N-isopropylacrylamide

nm……..Nanometer

nM……. Nanomolar

NMM……N-methylmorpholine

NMR……..Nuclear Magnetic Resonance

NS……..Naphthalenesulphonamide

ns……... Nanosecond

OPD……... *o*-Phenylenediamine

PEG……... Polyethylene glycol

PET……....Positron emission mammography

P.I…….. Polydispersity Indices

PMDETA……...N,N,N',N,N Pentamethyldiethylenetriamine

PNPA…….*p*-Nitrophenyl acetate

POPC……. 1-Palmitoyl-2-oleoyl-sn-glycerol-3-phosphocholine

PPE……. p-Phenyleneethynylene

PR…….. Progesterone receptor

PSA……Prostate specific antigen

QSAR…….. Quantitative-structure-activity-relationship

RAFT……Reversible addition-fragmentation chain transfer

RASI-1……...Rheumatoid Arthritis Synovium Inflamed-1

RCC……... Renal cell carcinoma

RECK…… Reversion-inducing cysteine-rich protein with kazal motifs

RES……Reticuloendothelial system

RNA……...Ribonucleic acid

rpm…….Revolutions per minute

RSVE……Reconstituted sendai virus envelopes

ΔS…….. Entropy change

s……. Singlet

SDS……....Sodium dodecyl sulphate

STI…….....Soyabean trypsin inhibitor

SUV……...Small Unilamellar Vesicle

TF…….. Transferrin

TFA……... Trifluoroacetic acid

Thr……..... Threonine

TIMPs……....The Tissue inhibitor of metalloproteinases

TIPS…….....Triisopropylsilane

TLC……..... Thin layer chromatography

TMB……..... 3,3´,5,5-Tetramethylbenzidine

TMS…….....Tetramethylsilane

TRUS…….....Trans-rectal ultrasound

uPA……....Urokinase type plasminogen activator

US…….....Ultrasound

UV-Vis……..... Ultraviolet visible

Val……..... Valine

VHL…….....Von Hippel-Lindau

µg…….....Microgram

µL……..... Microliter

µM……..... Micromolar

LIST OF APPENDIX TABLES

LIST OF APPENDIX FIGURES

GENERAL INTRODUCTION

Dissertation Organization

Developing water soluble fluorescent-polymers as detection tools for two physiologically relevant enzymes, Matrix metalloproteinases (MMPs) and Carbonic anhydrases (CAs) covers the major portion of this document. The first three chapters deal with the syntheses and interaction studies of various monomers and polymers for these two metalloenzymes. Liposomes were studied in Chapter IV for detection of one of the isozymes of MMPs, MMP-7 as another detection avenue.

Prior to these chapters, a general review of the main topics of the thesis has been discussed under the chapter called Literature Review. Four relevant topics have been described here about their origin, classifications, therapeutic and diagnostic applications, various progresses in the respective field and their important developments till date. The chapter starts with a discussion of the enzymes matrix metalloproteinases, followed by carbonic anhydrases and then the protein surface recognition concept and finally shifting to liposomes.

Part of my dissertation work has been published and the rest is under preparation. All the chapters comprised of a common format starting with abstract and followed by introduction, materials and methods, results and discussions and ending with a conclusion. In Chapter 1, syntheses and interactions of the various water soluble fluorescent-polymers with MMPs have been studied and reported. One of the statistical tools, Logit Regression Analyses was used for identifying the optimal polymer for isozyme selective detection of MMP-9. This work was published in Dutta, R., Scott, M. D., Haldar, M. K., Ganguly, B., Srivastava, D. K., Friesner, D.

L., and Mallik, S. (2011) Fluorescent water soluble polymers for isozyme-selective interactions with matrix metalloproteinase-9, *Bioorg Med Chem Lett 21*, 2007-2010.

Chapter II presents the use of the optimal polymer developed in Chapter I for distinguishing various cancer cell lines from non cancerous cell lines. Part of the studies involving differentiation and subtyping prostate cell lines has been published in Scott, M. D., Dutta, R., Haldar, M. K., Guo, B., Friesner, D. L., and Mallik, S. (2012) Differentiation of Prostate Cancer Cells Using Flexible Fluorescent Polymers, *Anal Chem 84*, 17-20. The rest of the chapter deals with the distinguishing and subtyping of various breast cancer cell lines from non cancerous cell lines. The content of this part has been already written up and will be submitted to the *Journal of the American Chemical Society*.

Chapter III delineates the isozyme selective detection of carbonic anhydrases with the aid of another set of fluorescent polymers. The chapter describes the syntheses and characterizations of the inhibitor monomer and various polymers used, the inhibition assays and lifetime studies along with steady state fluorescence experiments. With the combination of isothermal titration microcalorimetry and inhibition data, it was established that one of the polymers had higher binding affinity with CA II compared to the inhibitor itself. This work will be submitted as a full article to the journal *Organic and Biomolecular Chemistry*.

Chapter IV describes the syntheses and use of various peptides and liposomes. Releases of a self quenching dye, carboxyfluorescein from encapsulated liposomes for detection of active MMP-7 enzyme were studied. A detailed account of various formulations and application of a state-of-the art "click" reaction has been put forward in understanding the role of charged peptides for interaction with MMP-7.

A general conclusion and future studies have been presented at the end. Finally the dissertation ends with the citation of an overall list of references that were used throughout the dissertation followed by an appendix for all the chapters.

LITERATURE REVIEW

Matrix Metalloproteinases (MMPs)

Matrix metalloproteinases (MMPs) or Matrixins belong to the Metzincin class of Zinc metalloproteinases. The name "Metzincin" comes from the zinc ion and a methionine residue which is conserved, both present at the active site of the protease (*1*). These endopeptidases play crucial roles in degrading various extracellular matrix (ECM) and basement membrane proteins, namely various collagens, gelatin, aggrecan, fibronectin, laminin, proteoglycan link protein, elastin, casein, tenacin, entactin, and transferring (*2*). Due to the broad substrates specificities of the members of this family their nomenclature based on substrate classification has been replaced by the order of their discovery. However, earlier classification based on substrate choice is still prevalent.

MMPs are regulated at three stages, transcription, activation and inhibition (*3*). Under normal physiological conditions the proteolytic activities of MMPs are tightly controlled by endogenous inhibitors, α_2-macroglobulin, thrombospondin-1, RECK (reversion-inducing cysteine-rich protein with kazal motifs) and the immensely studied TIMPs (The tissue inhibitor of metalloproteinases) -1, -2, -3 and -4 (*4*). Normal *in vivo* functions of MMPs include bone and tissue modelling and remodelling, embryonic vascular development, pregnancy, growth, wound healing and innate immunity (*5*). Imbalance between the MMPs and the mentioned inhibitors leads to pathological conditions like metastasis, cancer, rheumatoid and osteoarthritis, multiple sclerosis and Alzheimer's disease (*1*),(*6*).

The collagenolytic activity of matrix metalloproteinases was first discovered in 1962 when J. Gross and C. M. Lapiere demonstrated the presence of these enzymes during the

metamorphosis of tadpole tail (*1*). However over the decades, MMPs have attracted interests of researchers due to their upregulation in tumor progression and cancers. Since their first discovery, molecular biologists had identified various new members in this family. Till date almost 23 human MMPs isozymes have been reported and are divided into two broad categories, namely secreted and membrane-type MMPs (MT-MMPs) (*7*). Classification of MMPs based on structure and trivial substrate recognition is as follows (Table 1).

However MMP-4, 5 and 6 were abandoned from this classification since they were found to be similar to other isozymes of the family. Although MT-MMPs are anchored to the cell surface covalently, secreted MMPs are also found to tether to the cell surface via binding to multiple moieties such as integrins, CD44, proteoglycans, collagen type IV and extracellular MMP inducer (EMMPRIN) (*4*). MMPs are calcium-dependent and zinc-containing endopeptidases which are secreted by connective tissues and pro-inflammatory cells such as fibroblasts, endothelial cells, various osteoblasts, macrophages, neutrophils and lymphocytes (*8*). They are secreted as inactive zymogens and gets activated by various proteolytic enzymes such as serin proteases, furin, plasmin, urokinase type plasminogen activator (uPA) and by many MMPs themselves (*2*). Although high levels of these metalloproteinases are considered as prognostic markers of varied cancer types but downregulation or even absence of MMP-3 and MMP-8 are found to be correlated with elevated skin cancer (*9*).

Structurally MMPs consist of a pre-peptide domain, a N-terminal pro-domain, a catalytic domain (~180 residues), a hinge region and C-terminal hemopexin-like domain (Figure 1). MMP-7 lacks the C-terminal domain and thus is the smallest of all the isozymes (*10*). The pre-peptide domain is also called autoinhibitory domain because as long as this domain remains uncleaved from the protease, it stays in latent form. Most of the MMPs consist of the hemopexin

domain (MMP 1, 3, 8, 10, 12, 13, 18, 19, 20, 22 and 27) which resembles a four-bladed β-propeller structure and participate for the enzyme's internalization, activation, substrate identification and destruction (*1*).

Table 1. Classification of human MMPs based on structure and their substrates.

MMP designation	Structure-based class	Substrate-based class
MMP-1	Simple hemopexin domain	Collagenase-1
MMP-2	Gelatin-binding	Gelatinase A, type IV collagenase
MMP-3	Simple hemopexin domain	Stromelysin-1
MMP-7	Minimal domain	Matrilysin
MMP-8	Simple hemopexin domain	Collagenase-2
MMP-9	Gelatin-binding	Gelatinase B, type IV collagenase
MMP-10	Simple hemopexin domain	Stromelysin-2
MMP-11	Furin-activated and secreted	Stromelysin-3
MMP-12	Simple hemopexin domain	Metalloelastase
MMP-13	Simple hemopexin domain	Collagenase-3
MMP-14	Transmembrane	#MT1-MMP
MMP-15	Transmembrane	#MT2-MMP
MMP-16	Transmembrane	#MT3-MMP
MMP-17	*GPI-linked	#MT4-MMP
MMP-18	Simple hemopexin domain	Collagenase-4
MMP-19	Simple hemopexin domain	**RASI-1
MMP-20	Simple hemopexin domain	Enamelysin
MMP-21	Vitronectin-linked insert	Homologue of *Xenopus* XMMP
MMP-22	Simple hemopexin domain	No human analogue known yet
MMP-23	Type II transmembrane	Cysteine array MMP (CA-MMP)
MMP-24	Transmembrane	MT5-MMP
MMP-25	*GPI-linked	MT6-MMP, leukolysin
MMP-26	Minimal domain	Matrilysin-2
MMP-27	Simple hemopexin domain	Not characterized
MMP-28	Furin-activated and secreted	Epilysin

*GPI-linked = Glycophosphatidylinositol-linked , #MT= Membrane type, **RASI-1= Rheumatoid Arthritis Synovium Inflamed-1.

The active site of all the MMPs is evolutionarily conserved between the different MMPs and the sequence motif HEXXHXXGXXH coordinates with the catalytic Zn^{2+} ion where X is

any amino acid (*11*). However the S1´ pocket in the active site varies considerably among the isozymes (*8*).

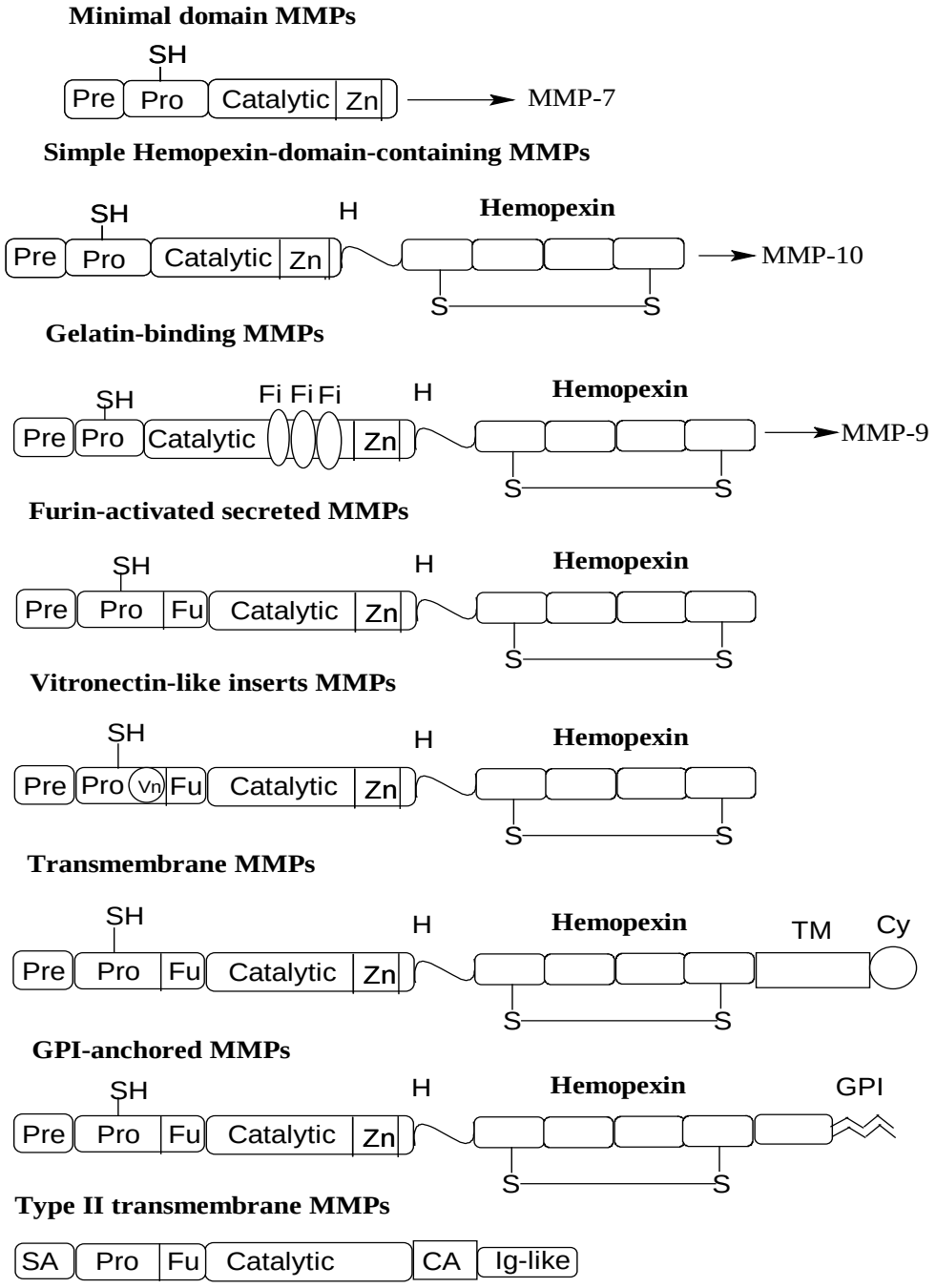

Figure 1. The domain structures of various classes of Matrix metalloproteinases.

Post-translational modifications of the zymogens take place in the endoplasmic reticulum where the pre-peptide domain cleaves off. The conserved cysteine residue coordinated with the active site zinc ion stays intact in the pro-peptide domain in the inactive enzymes (*2*). The pro-peptide domain has a conserved sequence PRCGXPD and consists of ~ 80 residues. The active site tetrahedral zinc ion is coordinated with three histidine residues and cysteine and thus remain shielded from water and substrates (*12*).

During activation the pro-peptide domain gets cleaved off by various activators (4-aminophenylmercuric acetate, APMA ; urea; oxidized glutathione) and thus the cysteine breaks contact with the zinc and the enzyme loses its latency. This mechanism is widely accepted as the "cysteine switch" (Figure 2) (*2*). As soon as the cysteine and zinc contact is ruptured, the active site becomes available for entry of water as well as substrate molecule, thus getting access to interact with the active site Zn^{2+}. With this the earlier tetrahedral zinc (II) ion attains the pentavalent structure coordinating with three His residues, the water molecule and the carbonyl group of the substrate. Hydrogen bonds are formed between the water and Glu-198 (MMP-8) and between the substrate and Ala-161. Thus the pK_a of the water is lowered and gets deprotonated by the glutamate. The carbonyl group of the substrate coordinated to the metal ion leads to its increased electrophilicity, thus helping the hydroxide ion of the water to easily attack as the negative charge on the oxygen of the carbonyl group is stabilized by the zinc ion. The proton taken up by the glutamate ion from the water molecule is transferred to the peptide amine group of the substrate and the resulting charge on the nitrogen is stabilized by the Ala through hydrogen bonding. The negative charge of the carbonyl oxygen forms the π-bond, thus cleaving the amide bond of the substrate peptide. The H^+ from the formed carboxylic acid is transferred to the amine by the conserved Glu and thus completing the hydrolysis steps (*13*).

In our study we have extensively used human recombinant MMP-7, -9 and -10 in the Chapters 1, 2 and 4. So a brief description of each of these metalloproteinases and their related isozymes has been discussed. MMP-2 (Gelatinase A; 72 kD) and MMP-9 (Gelatinase B; 92 kD) cleaves collagen type IV and type V, elastin and gelatin. High serum levels of MMP-9 have been attributed to rapid tumor progression and metastasis in cancer patients with melanoma. Both the enzymes carry fibronectin type II inserts within the catalytic domain which contributes to collagen binding (*14*).

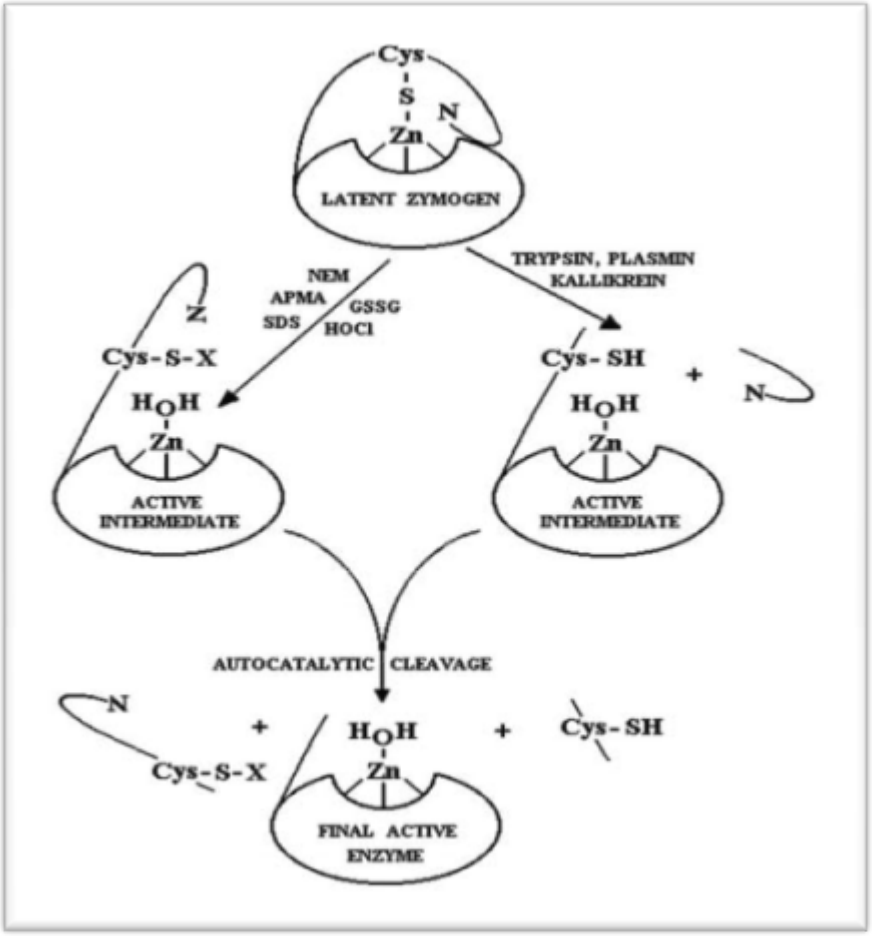

Figure 2. Cysteine Switch mechanism of MMPs. (Used with permission from Ref. 2).

MMP-7, MMP-23 and MMP-26 (matrilysins) are the smallest in the class with a pro-peptide domain and zinc binding catalytic domain (*15*). MMP-7 is expressed in multiple organs such as normal mammary, peribronchial and parotid glands, liver, pancreas, prostate and lungs (*16*). They are key players in shedding various cell-surface molecules, like tumor necrosis factor-α, E-cadherin, Fas ligand (FasL) and β4-integrin (*17*). Matrilysins have been found to be overexpressed in organ cancers such as stomach, colon, skin, breast, prostate, liver and pancreas (*15*). X-ray crystallography suggested that 'bipolar' distribution of positive and negative charges on the enzyme surface leads to differential interactions with the charged lipid membranes (*18*).

MMP-10 or stromelysin-2 are not only involved in cancer but are also found in human osteophytic and neonatal rib bone. MMP-3 (stromelysin-1) and MMP-10 are expressed by squamous epithelial and fibroblastic cells (*19*). Non-collagen substrates which are components of connective tissues like proteoglycans, laminin, fibronectin are degraded by stromelysins (*20*).

Conventional methodologies for MMP detection involves ELISA, western blotting and gelatin zymography (*21*). Once detected, MMPs require effective design of specific inhibitors for treating various diseases. Targeting a particular isozyme without interfering the functions of other isozymes has been the most intriguing part of MMP research. Since these enzymes are crucial for normal physiological as well as pathological settings, their importance cannot be overlooked and in fact for decades numerous groups have delved into developing synthetic as well as peptidomimetic MMP inhibitors (MMPi) (*22*). The roles of each of the isozymes are so overlapped, particularly in cancer, that the strategy for MMP inhibition was not successful as it was thought to be. Among endogenous substrates, MMP-1,-2,-8 and -13 are found to degrade collagen I, fibronectin is cleaved by MMP-2,-3, -7,-10 and -11. Various peptide-based substrates have been examined to identify the substrate specificities of MMPs and it has been understood

that there remains a mix matching when it comes to cleave a substrate by the entire family. Usually the cleavage site motif of a MMP is denoted by P3-P2-P1 ~ P1´-P2´-P3´(P is any amino acid) where P1´ and P2 are usually hydrophobic amino acids, P2´ is preferably hydrophobic or basic amino acid and P3 is proline and P1 contains serine. The cleavage site is primarily between P1 and P1´. Exceptionally MMP-3,-7 and-14 requires Met at P3´ and Glu at P1 by MMP-2,-3 and-7. Thus although the cleavage site motif is common to all the isozymes, differences in the selection of amino acids for substrate design can be an opportunity to develop specificities (*23*).

Usually MMP upregulation is accomplished by the stromal cells surrounding the cancer tissues, but in some cases such as for MMP-7 and MMP-2, -9 and 14 they are expressed by the glandular epithelial cells (*3*). It has been found that cleavage of the same substrate, leads to cancer progression in some cases and suppression in other. Usually MMP genes are not muted, but activation of tumor progression genes as well as suppression of tumor-suppression genes are usually noticed (*4*). The whole biochemical cascade of MMP regulation is perplexing and so design of inhibitor for definite target often leads to detrimental effects on anti-targets causing adverse side effects as well as increased tumorigenesis. It has been proved by many groups that the active site pocket of all the MMP isozymes are more or less similar, but the subsite pocket S_1´ residues in the active site loop makes the actual differences among the isozymes as well as regarding their substrate specificity. Overall et al have reported that for MMP- 1 and -7, this pocket is shallow whereas for most of the other important ones (MMP – 2, 3, 8, 9, 12, 13) it is deep (*24*). Chen et al used side pocket of S_1´ or S_1´* for designing inhibitor for MMP-13 particularly. The earlier dogma that MMPs are solely responsible for degrading the extracellular matrix (ECM) was challenged when they were found to participate in innate immunity as well as

to maintain the homeostasis of the ECM environment. These are achieved by a cascade of various cell signaling pathways like cleaving, activating as well as inactivating growth factors, chemokines, monocyte-chemotactic proteins 1-4, CXCL12 (a stromal-cell-derived-factor-1α) and disruption of cellular contacts (*25*) - (*26*), (*4*). Thus MMPs play a pivotal role in the signaling pathways in healthy conditions and any non regulation or alteration at any of the steps can be directly or indirectly related to pathogenesis. In tumor progression and growth, these driving forces have been examined and multiple challenges evolved when it came to target these biomarkers of cancer.

The questions that tormented the scientific world were which MMP isoforms are elevated in which cancer, how their cascades of expression and activation are related and how their biochemical actions were interrelated in various stages of tumor progressions. For effective inhibition of MMPs, various approaches have been used at different stages of MMP from transcription, through translation, following the diverse signaling pathways, zymogen and enzyme activation step. Various monoclonal antibodies, natural products, anti-angiogenic factors, glucocorticoid drugs, toxin-fused substrates have been employed in cancer treatment at the different stages of MMP regulation described above (*27*)- (*28*). In the field of inhibitor design, small molecules are targeted for active site inhibition, restricting the enzyme's natural substrate to get access to the inner core (*29*). However, these small molecules can also interact with the other pockets beyond the active site and can cause conformational changes of the enzyme and thus inhibiting the enzyme. Synthetic inhibitors can be broadly divided into two categories, peptidomimetic and non-peptidomimetic. Broader classification of the non-peptidomimetic class involves hydroxamates, carboxylates, thiols, tetracycline-analogues, barbiturates, hydroxypyrone, pyrimidine-based and phosphonates (Figure 3) (*8*).

Among the peptidomimetic inhibitors, collagen-based hydroxamate inhibitors were pioneer in the field. Batimastat (BB-94) (Figure 4), a British Biotech Inc. drug was the first synthetic collagen-mimicking hydroxamate-based MMP inhibitor that was studied for advanced human malignancies (*30*).

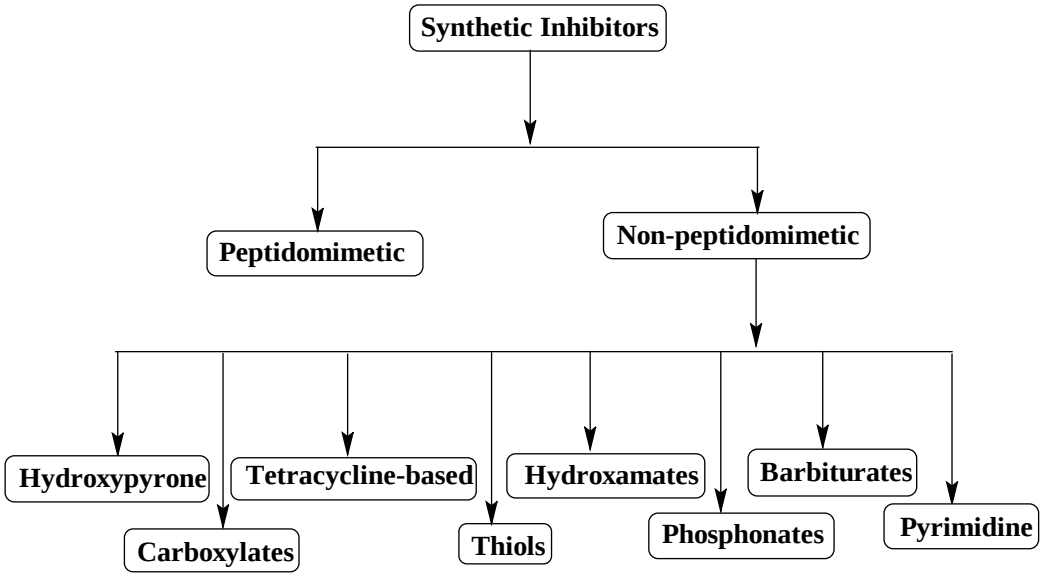

Figure 3. Classification of Synthetic inhibitors of MMPs (*8*).

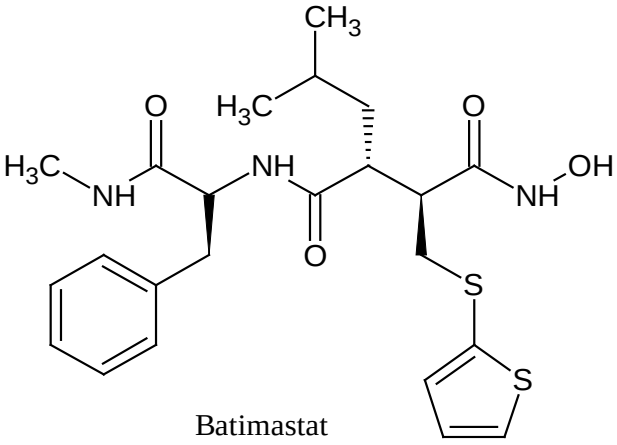

Figure 4. Structure of Batimastat (BB-94).

Later various other drugs such as Ilomastat, Marimastat, Tanomastat and Prinomastat proceeded for clinical trials but till date only Periostat is the only Food and Drug Administration (FDA) approved MMPi (*30*),(*31*). The active compound of Periostat is Doxycycline and is used for periodontal diseases. Musculoskeletal pain, inflammation, poor bioavailability were the main reasons why the MMP inhibitors could not pass the clinical trials although they showed promising results in animal models (*32*).

Although the hydroxamate inhibitors were effective in many ways, they suffer from non-selective interaction with other metal ions beyond zinc and susceptible to metabolic transformations. Thus new generation of MMP inhibitors were designed, but one disadvantage which could not be overcome was that these inhibitors could inhibit related ADAM and ADAMTS enzymes in addition to MMPs. Thus for effective designing thorough structural-based studies such as QSAR, NMR, X-ray, detailed pharmacophore mapping needed to be undertaken.

One of the pyrone MMP inhibitor (Figure 5) was found to be effective against MMP-3 with IC_{50} = 20 nM compared to MMP-1 and -2 (IC_{50} >50 µM) (*32*). Among the phosphonate-based inhibitors, the molecule RXP-03 (Figure 5) was found to be very promising as a broad-spectrum inhibitor (*32*). It had K_i values in the nanomolar range for MMP-2, -9, -8, -10, -11 and -13 but micromolar for MMP-1 and -7. The molecule showed excellent stability in mice model with colon carcinoma and its efficacy was found to be dose and stage of tumor dependent (*33*). Tetracycline-based inhibitors derived from antibacterial tetracyclines and chemically modified are the ones which were studied elaborately. Metastat, also called COL-3 (Figure 5) was found to reduce the bronchoalveolar lavage fluid MMP-2 and -9 activities in the porcine model.

Doxycycline and Minocycline are the other important tetracyclines that showed efficacy in various neurological diseases in addition to MMP inhibitions (*32*).

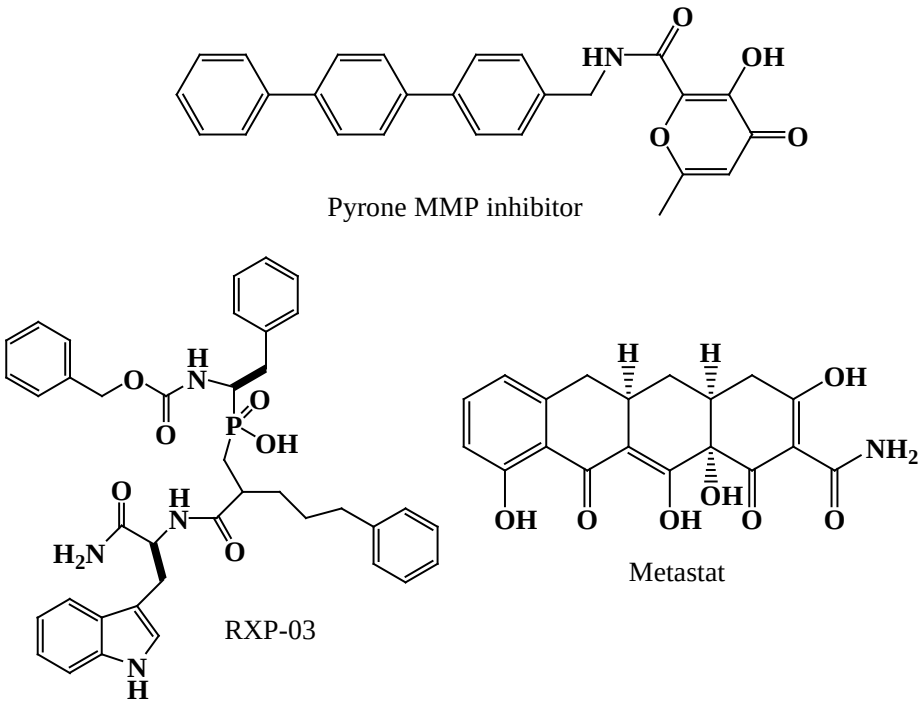

Figure 5. Structures of some synthetic inhibitors.

Among the natural product inhibitors, various polyphenols, flavanoids and terpenoids have been proved to be very effective MMP antagonists (*34*)-(*35*). Catechins, curcuminoids, resveratrol derivatives can directly act as natural substrate blockers or could interfere in the transcription pathways. The main drawbacks for commercial natural substrates are their limited availability, time consuming extraction and difficult large scale production.

There are multiple reasons for cancer and metastasis, such as activation of MMPs, overexpression of oncogenes or suppression of tumor-suppression genes. Although thousands of molecules have been designed and tested for MMP inhibition, but overall the application of MMP inhibitors has been disappointing. The inhibitors showed much efficacy at the preclinical

studies, but they failed badly in the clinical studies when involved in patients with metastatic and later stage cancers. The questions which came up with the failure of the most promising drugs in Phase III clinical trial like Tanomastat (BAY-12-9566), Prinomastat (AG-3340) were the contribution of which isozymes are important for cancer, at what stage of cancer has a drug the highest efficacy and the least adverse toxicity, the level of MMP activity at various stages of cancer, the activity of which isozymes are synchronized and to what extent in the tumor progression, and so on (*36*), (*37*).

Thus researchers and companies are still trying to face these extremely important challenges for better and effective treatment for cancer, metastasis and invasion. While treatment is crucial, early detection of cancer is relevant for choice of drugs and kind of treatments. Various assays such as immunoassay, zymography assay, fluorimetric assay, activity-based profiling, etc have been reported for detecting various isozymes of the family (*21*). Among the assays designed for MMP detection, bioassays rely on the degradation of the natural substrates of the enzymes. MMP-2 and -9 as mentioned earlier are called gelatinase after their substrate of choice 'gelatin'. In this assay avidin was first coated on the microtiter plates and the biotinylated gelatin was added. Upon cleavage of the gelatin substrate by the enzyme, the amount of biotin left attached to avidin was quantified by the peroxidase activity of streptavidin-peroxidase which is spectrophotometrically detected using peroxide and TMB as the coloring agents (*38*). With this system 0.16 ng/mL of MMP-2 could be detected from tumor samples of patients (*39*). In this area succinylated gelatin has also been helpful by which nanomolar concentrations (1 to 2 nM) of MMP-9 and -2 could be detected respectively (*40*).

Gelatin zymography is a very accurate and widespread technique for quantitative determination of MMPs. Usually gelatin is incorporated in the gel which when subjected to

electrophoresis, the protease in the sample comes in contact with its substrate. Triton X replace SDS, and once the Triton is washed with washing buffer, the enzyme refolds and becomes active again. The portions of the gel where the substrate gets digested is devoid of protein staining proving the activity of the enzyme. Because MMP reference standards are not easily available, this method though very helpful suffers from extensive usage. In zymography, there are other classifications such as collagen zymography, *in situ* zymography, reverse zymography, real time zymography and *in vivo* zymography (*21*). Although these strategies are available for MMP detection, they lack in isozyme specificity, most of them are expensive and time consuming, requires native substrates and specific antibodies (*41*), (*42*).

For radio isotopic assays, ^{14}C and ^{3}H –labeled natural substrates have been used as devices for MMP-2 and -9 detection (*43*), (*44*). Among the fluorometric assays, FITC-labeled proteins, intra-molecular fluorescence energy transfer substrates (IFETS) and fluorogenic triple-helical peptide (fTHP) are widely in use.

Immunoassays are developed for measurement of both pro and active forms of MMPs and monoclonal antibodies are powerful tools in immunodetection (*21*). Western blotting utilizes electrophoresis techniques where the immobilized proteins bind to the antibodies as detected by a color change. The limiting factors for this technique are time and cost (*45*). ELISA (Enzyme-linked immunosorbent assay) involves immunosorbent techniques for detecting enzymes. Total collagenase (both pro and active) can be measured using either two monoclonal antibodies or in combination with a monoclonal and polyclonal antibody. ELISA kits are really handy and sensitive but they need proper storage and are time-consuming (*21*).

Mallik et al have demonstrated that liposomes composed of collagen-mimetic peptides in the bilayer and encapsulating carboxyfluorescein dye acted as good MMP detecting agents (*46*).

In another study it was also proved that when liposomes encapsulating the enzyme Horseradish Peroxidase (HRP) came in contact with MMP-9, the HRP enzyme was released from the vesicles and came in contact with a chromogenic HRP substrate (OPD) in the assay buffer forming a brown colored precipitate. The response was proportional to the concentration of the MMP-9 (*47*).

Thus various strategies have been explored for MMP detection and in this endeavor we studied various fluorescent polymers and liposomal formulations for isozyme selective interaction and detection of matrix metalloproteinases (MMP-7, -9 and -10). To further support our data we have also demonstrated that the synthesized polymers could detect a particular isozyme in the conditioned cancer cell culture media, thus could also differentiate cancerous cell lines from non-cancerous ones based on the levels of secreted MMPs in these culture media.

Carbonic Anhydrases (CAs)

Carbonic anhydrases (CAs, EC 4.2.1.1.) are zinc-containing metalloenzymes whose primary physiological function is to catalyze the reversible hydration of carbon dioxide to bicarbonate and proton (Equation 1) (*48*).

$$CO_2 + H_2O \rightleftharpoons HCO_3^- + H^+ \qquad \textbf{(Equation 1)}$$

As a result they are involved in very crucial processes within the body namely, pH regulation, CO_2 homeostasis, ion transport, water and electrolyte balance. They play vital roles in various biosynthetic and metabolic processes for example, gluconeogenesis, lipogenesis, ureagenesis, bone resorption, gastric and pancreatic juice secretion, and production of cerebrospinal fluid and aqueous humor (*49*). Other reactions of CAs include hydration of

cyanate to carbamic acid, cyanamide to urea, hydration of aldehyde to gem-diols, and hydrolysis of various acids (*48*).

There are four unrelated gene families known till date, α-CAs, β-CAs, γ-CAs and δ-CAs. The α-CAs are found in vertebrates, algae, eubacteria and cytoplasm of green plants whereas the γ-CAs are present mainly in Archaea and few eubacteria. The β-CAs are predominantly available in chloroplasts of mono and dicotyledonous plants along with some algae and eubacteria. The δ-CAs are primarily found in marine diatoms. In human 16 isoforms of α-CAs have been reported yet, of which three are CARP or CA-related proteins (Table 2) (*48*).

Table 2. Distribution of α-Carbonic anhydrases among higher vertebrates.

Distribution	**Isozymes**
Cytosolic	CA I, II, III, VII, XIII
Mitochondrial	CA V (A and B)
Transmembrane	CA IX, XII, XIV
Membrane-bound	CA IV, XV
Secreted	CA VI
CARP (CA-related Proteins)	CA VIII, X, XI

Cytosolic forms include CA I, II, III, VII and XIII, peripheral membrane proteins are CA IV and CA XV, transmembrane isozymes are CA IX, XII and XIV. CA V is the mitochondrial form and CA VI is the secreted isozyme. CARP or CA-related proteins share the same sequence homology with the CAs but their activities are different from them (*48*), (*50*).

The catalytic and inhibition mechanisms of CAs are served by the metallic Zn^{2+} ion which sits in the 15 Å deep active site cleft and bound by three histidine residues, His 94, His 96 and His 119 along with a water molecule or a hydroxide ion (Scheme 1) (*50*).

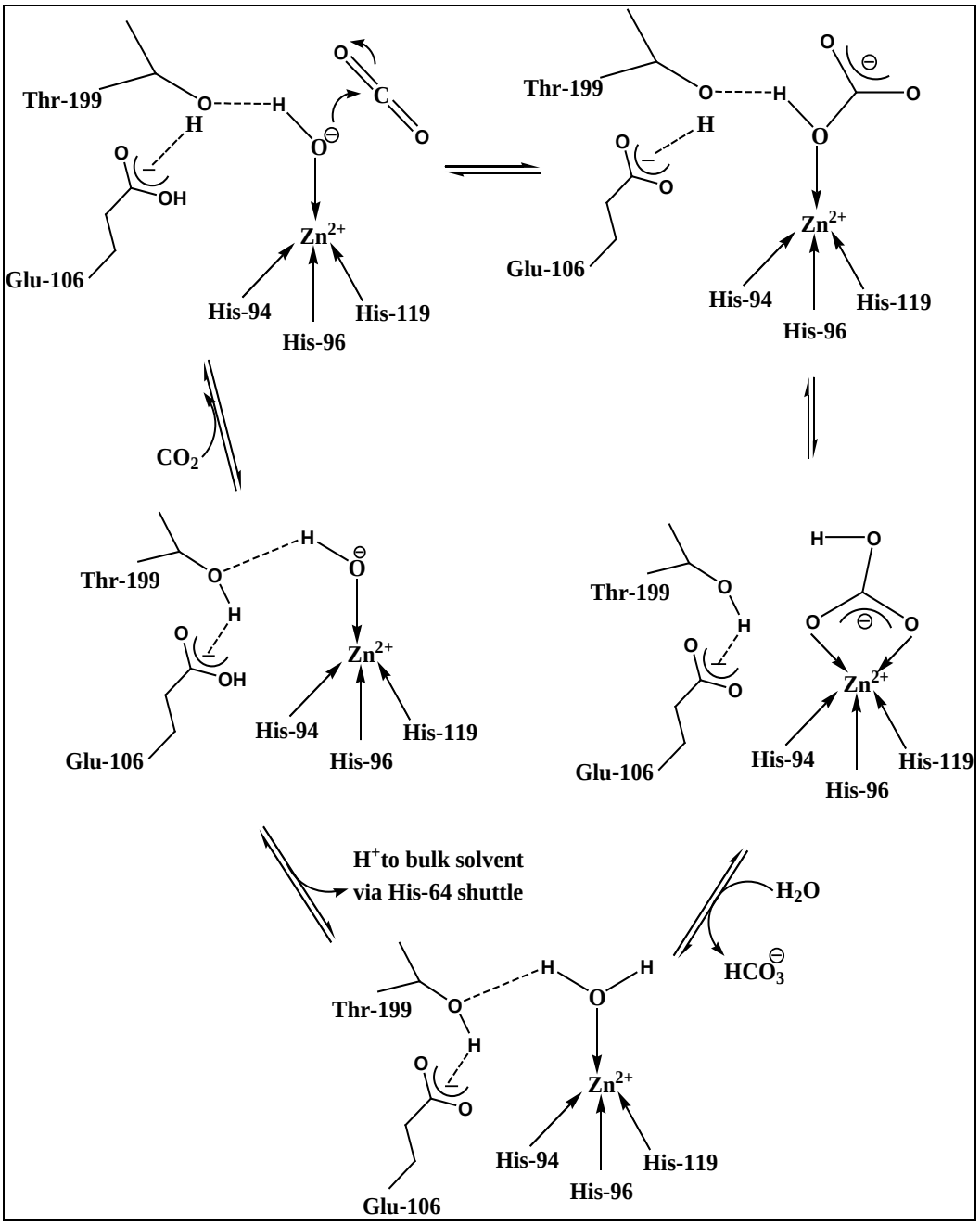

Scheme 1. Catalytic mechanism of CA II showing its role in reversible hydration of carbon dioxide to yield bicarbonate and a proton (*50*).

The hydroxyl group of Thr 199 is hydrogen bonded with the zinc-bound water molecule and is also connected to the carboxylate group of Glu 106. Because of these interactions there

occurs an enhancement of the nucleophilicity of the water molecule that favors the carbon dioxide for nucleophilic attack.

The substrate carbon dioxide binds to the hydrophobic pocket of CA, comprised of Val 121,Val 143 and Leu 198 and eventually gets attacked by the strong nucleophilic zinc bound hydroxide. The basic form (the hydroxide bound Zn^{2+} ion) is the active state of the enzyme. CO_2 gets converted to the bicarbonate which remains coordinated to the zinc ion. Water displaces the bicarbonate ion from the zinc, rendering the enzyme back to the inactive form (*49*). To activate the CAs, a proton needs to be transferred from the active site turning the enzyme to the basic form. In case of CA I and II, His 64 accomplish this purpose and in others the buffering medium. CA II is one of the active isozymes with reported $k_{cat}/K_m = 1.5 \times 10^8\ M^{-1}\ sec^{-1}$ (*50*).

CA II isozymes are the only soluble form in renal epithelial cells and expressed in various amounts in kidney intercalated cells, proximal tubules, collecting duct cells and loop of Henle (*51*). CA II has been detected in the normal as well as neoplastic ductal cells of pancreatic exocrine tissues and CA I in both normal and malignant pancreatic endocrine tissues (glucagon-producing). Colorectal cancer patients' stool samples are examined to be abundant with CA I/CA II in comparison with healthy individuals (*52*). Leppilampi et al studied the presence of CA isozymes in various hematopoietic cell lines and also blast cells of bone marrow from leukemia patients. It was found that CA II was expressed in leukemia blast cells as well as in the myeloid and lymphatic cells (*53*).

Although CA II is the most widely studied isozyme in the class, other isozymes also require attention since some of them are directly or indirectly involved in pathogenesis. Among these, CA IX and CA XII are found to be overexpressed in various malignancies (*54*). In 2001

Ivanov et al studied the expressions of CA IX and CA XII genes in von Hippel-Lindau (VHL)-defective tumors using Northern blot and immunostaining techniques. Various cancer cell lines as well as tumor specimens were compared with normal tissues and it was concluded that these transmembrane enzymes are induced highly under hypoxic and acidic conditions which are common phenomenon of tumor environment (*55*). Another group in 2006 explored the expression of these two isozymes in mouse embryos at the organogenesis stage. With the help of immunohistochemistry the researchers were able to prove that CA IX was well distributed in various organs like lung, brain, pancreas and liver and CA XII was mostly available in the stomach and choroid plexus of brain including the above mentioned organs (*56*). Chiche et al analyzed CA IX and CA XII isoforms to demonstrate that these two isozymes share their roles in promoting tumor growth by the tight regulation of intracellular pH and by counteracting acidosis. This was proved in xenograft tumor model where appropriate gene silencing and measuring mRNA levels confirmed that CA XI and CA XII could be held responsible as anticancer targets (*54*). In order to identify the role of CA IX as a biomarker in renal cell carcinoma (RCC), Hulick et al studied ELISA for CA IX correlation before and after nephrectomy. It was observed that those patients with clear cell RCC, who underwent nephrectomy, had CA IX level significantly lower than those with non-clear cell RCC and followed by nephrectomy for metastatic disease. In 2010 Hsieh et al showed the relation of CA XII with MMP-2 and -9 for tumor migration where they used MDA-MB-231 (breast cancer cell line) for proving their hypothesis. CA XII knockdown resulted in the reduction in cell growth due to CDK6 and cyclin D1 expression inhibition (*57*).

Supuran et al discussed the inhibition strategies of CAs for designing synthetic molecules. Inhibitors can be classified into two categories, first the anions which complex with

the metal and the second those which bind to the active site zinc (II) ion by either coordinating in the metal sphere or by substitution. Thiocyanates belong to the second category and the adduct can form either tetrahedral or trigonal-bipyramidal structure. Sulphonamides form tetrahedral geometry where their nitrogen atom coordinates to the Zn (II) and supported by hydrogen bonds from Glu 106 and Thr 199 residues for anchoring the inhibitor at the active site pocket. The sulphonamides such as acetazolamide, brinzolamide and dorzolamide (Figure 6), bind to the zinc ion in its deprotonated form imparting tetrahedral structure to the binding complex (*48*).

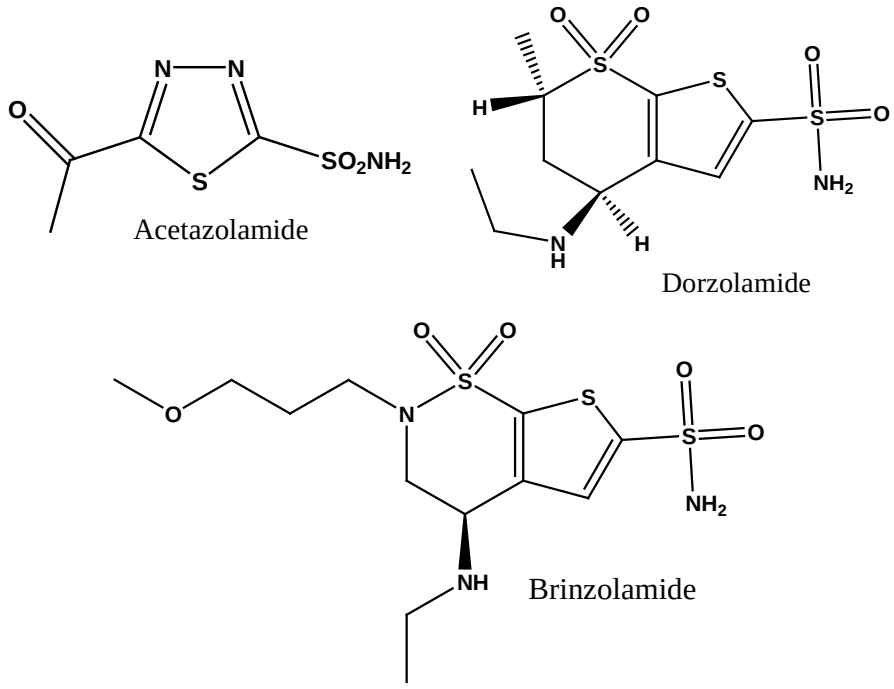

Figure 6. Structures of Sulphonamide inhibitors of Carbonic Anhydrases.

In addition to sulphonamide, various sulphamate and sulphamide (Figure 7) inhibitors were found to inhibit CA I, II and IV (*58*), (*59*). But all of these bind to the zinc ion and form adduct like the sulphonamides.

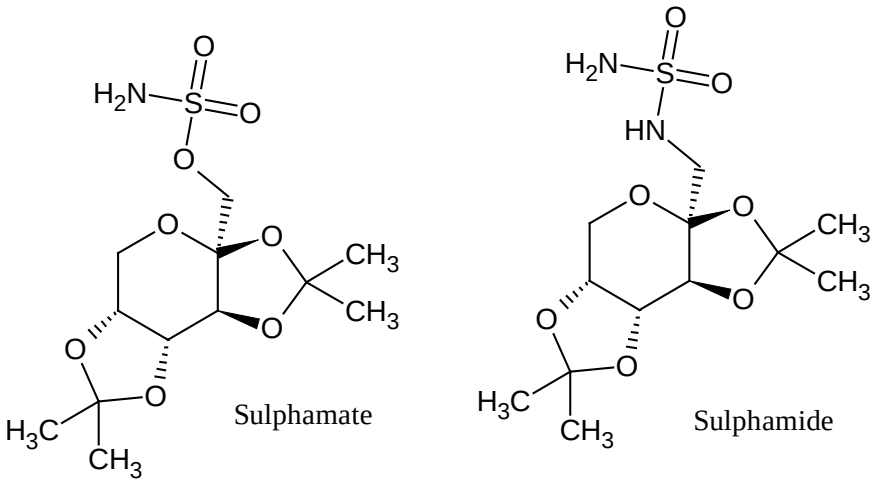

Figure 7. Structures of Sulphamate and Sulphamide Inhibitors.

Mann and Keilin in 1940 published a paper where they first reported Sulphanilamides (Figure 8) as specific carbonic anhydrase inhibitors. It was found that with the N-substitution of the sulphonamide moiety, the derivatives lose their potency and so extensive structure-activity correlation studies were performed over the years. Based on these molecules various CA inhibitors have been synthesized and used as anti glaucoma agents, hypoglycemic agents as well as chemotherapeutic agents (*50*). Among these agents, acetazolamide has been found to be very potent antiglaucoma agent which acts by reducing increased intraocular pressure. The K_i value for this compound against CA II , CA IV and CA I were 10 nM, 66 nM and 200 nM in human (*50*), (*60*). However dorzolamide (TRUSOPT^{TM}, Merck & Co) and brinzolamide (AZOPT^{TM}, Alcon Laboratories) entered clinics as antiglaucoma agents in 1995 and 1999 respectively after acetazolamide's first introduction in 1956 (*61*), (*50*).

When it comes to design inhibitors specific for a particular isozyme for CAs, results of available drugs become daunting because of lack of specificity. Since almost all the inhibitors are targeted for active site zinc binding, it was relatively difficult to obtain molecules for a

selected member of the family. So an alternative strategy that was followed consisted in designing compounds that not only could bind to the zinc ion but could also interact with other amino acid moieties that were present in the pocket and which actually differentiate each isozyme from other member of the family.

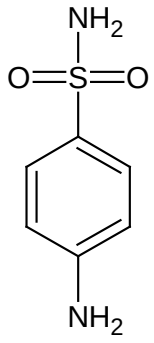

Sulphanilamide

Figure 8. Structure of Sulphanilamide.

For example, from the crystal structure of CA I and CA II, it was found that presence of His residues (other than His 94, His 96 and His 119 already described before) varies from isozyme to isozyme (Figure 9) (*62*). CA II consists of His 3, His 10, His 15, His 17 and His 64 which are not found in CA I. Inhibition experiments have shown that CA II responded better to sulphonamides than CA I and the latter had actually higher affinity for cyanides, cyanates, halides and thiocyanates (*50*).

CA III is resistant to sulphonamide although it had K_i to be 0.9 μM for $CF_3SO_2NH_2$ (*63*). For CA IV, there exist four Cys residues at the entrance of the active site pocket and form two disulfide bonds. Schiff bases of aromatic/heterocyclic sulphonamides although discovered accidentally showed specificities towards CA IV (Figure 10) (*64*).

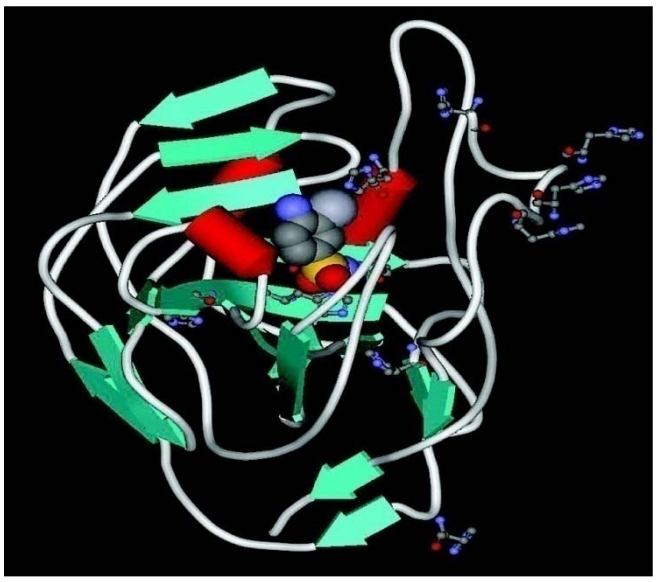

Figure 9. Schematic illustration of the human carbonic anhydrase II. (Used with permission from Ref. 66).

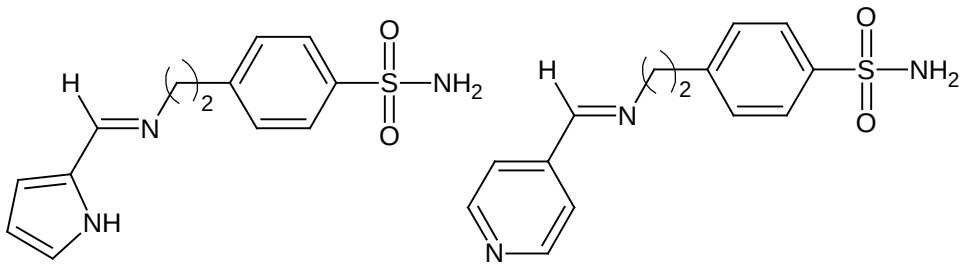

Figure 10. Schiff bases of aromatic/heterocyclic Sulphonamides.

Since application of single synthetic molecules to inhibit a particular isozyme could not meet the requirement of highest selectivity, an alternative approach that could help in this field was taking the help of multivalencies of the designed compounds. Since in nature protein-protein interaction is carried out with respect to polyvalency, so designing molecules that could manipulate or imitate this concept might solve the problem for selective inhibition among the isozymes.

Following this methodology, our group has previously demonstrated that effective inhibition could be achieved by designing molecules following the "two-prong" approach for isozyme selective interactions. It was reported that when an inhibitor is attached with an extra anchoring group that could bind to the surface-exposed His residues, the binding affinity of the inhibitor increased many fold. For this purpose, an iminodiacetate- Cu^{2+} (IDA-Cu^{2+}) was attached to the benzene sulphonamide derivates thus enhancing its affinity 40-fold. A triethylene glycol spacer was used which acted as a bridge between the other two portions thus taking care of the steric hindrance factor. Steady-state kinetic data and binding study results proved that designing molecules based on this strategy could be a potential outcome for isozyme selective inhibitor synthesis (*65*). In another report in 2006, the group showed that the IDA-Cu^{2+} portion of a promising inhibitor BR30 (K_d = 28 nM for CA II and 120 nM for CA I) was able to bind both CA I and II but at two different His residues (His 200 for CA I and His 64 for CA II) (*66*).

Based on the strategy of polyvalency, in chapter 3, we have constructed another methodology that could serve as the toolkit for isozyme selection. The approach primarily stands on the concept of protein surface recognition which is discussed elaborately in the next section and various polymers were synthesized consisting of charged and uncharged amino acids along with the active-site binding inhibitor and a reporter to distinguish between the CA isozymes.

Protein Surface Recognition

Proteins are polymeric biomacromolecules of amino acids which are present in all cells and almost in every organelle (*67*). In general, proteins have two sites in their structures for binding substrates and maintaining stability within the system. These two sites are (i) the interior surface which comprised of the active site cleft and concave in most cases and (ii) the exterior

surfaces which are responsible for interaction with large molecules and imparting stability to the structure. Usually small hydrophobic substrates bind to the more hydrophobic interior core and the exterior site hold macromolecules due to multiple binding contacts. Water is shielded from the interior portion of the protein and the exterior surface stays in direct contact with the bulk aqueous phase (*68*).

Protein-protein interactions play vital roles in various processes like growth, differentiation, immune response, metabolic processes, signal transduction and cell cycle (*69*), (*70*), (*29*). Hormone-receptor connectivity, antigen-antibody complexes, proteases-inhibitor binding are other examples of protein-protein interactions in the biological world (*71*). Abnormal pathologies occur if the natural protein-protein interaction is disrupted, for example, sickle cell anemia, respiratory diseases, unusual cell growth and so on (*72*). The protein-protein interactions involve primarily non-covalent bonding and weak interactions. Most of the interactions consist` of intermolecular contacts, namely, H-bonding, hydrophobic effect, and electrostatic interactions (*70*).

The average area buried due to most protein-protein interactions per protein is 800 $Å^2$ with a total area buried per complex is 1600 $\pm$ 350 $Å^2$ also known as “hot-spots” (Figure 11) (*71*), (*69*). Korn et al have demonstrated with the help of “hydropathy level diagram” that the contact surfaces of most protein-protein interactions are more hydrophobic than the exterior part of the subunits, although there are exceptions to this observations (*73*).

Generally, it has been found that arginine contribute to 9.9% of the interfacial amino acids followed by valine which is 7.3%. Polar residues Arg and Asn are normally found in the interfaces which are more similar to the exterior than the interior compositions as reported by Jones et al. Tyr, Met and Pro are the other amino acids that are found in the interfaces (*74*).

Researchers have come to the point that the critical protein-protein binding mechanism is generally hydrophobic in nature with hydrophobic residues as well as with the hydrophobic parts of hydrophilic residues (*71*).

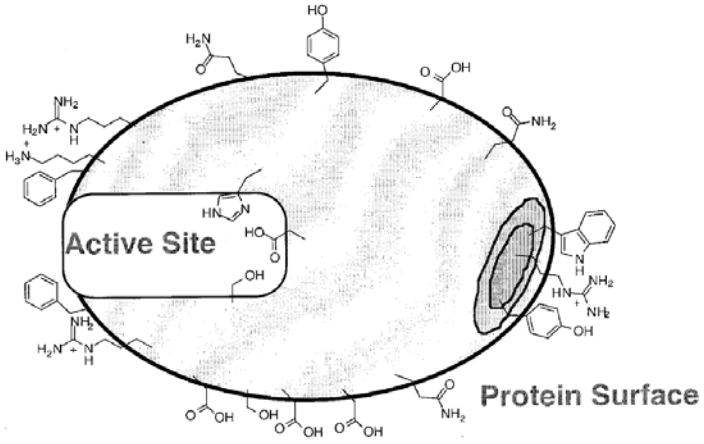

Figure 11. Schematic illustration of a protein's active site with the hot spot and the exterior surface. (Used with permission from Ref. 69).

Proteins/enzymes can be targeted for specific alteration of functions or to eliminate abnormal functions by synthetic small molecule receptors. Major area of drug development involves inhibiting protein/enzymes with small synthetic molecules (*29*). Traditionally the synthetic receptors were aimed towards the active site pocket of the target enzyme. The goal was to hinder the endogenous ligands or to alter their functions. For MMPs, for example, hundreds of inhibitor molecules and peptidomimetics have been designed for binding to the active site zinc ion. Designing inhibitors for targeting the active site seems to be easily achieved for the metalloenzymes where the active catalytic site consists of a metal within an enzyme (*75*). Highest substrate selectivity is achieved by the deep active cleft. However, constructing molecules for binding to the solvent exposed exterior surface area becomes challenging due to the complexities of the functional groups as well as the large surface areas. Usually for any enzyme class the residues of the active site are somehow evolutionarily conserved. But what

makes the isozymes of the class different from each other are the pattern of the amino acids on the surface area (*76*).

Protein-protein interactions can be controlled by Protein Surface Recognition and it has emerged to be an useful modality in designing multivalent molecules for treatment of various disease conditions, including Alzheimer's disease, arthritis, diabetes and glaucoma (*70*). For this field of research appropriate modeling and docking studies are required to know the effective pattern of the protein surface structure in a subsequent protein-protein surface binding. Another important criterion for designing molecules for Protein Surface Recognition is to develop complementary functional moieties on the molecule that will provide better interaction with the target protein than its natural partner. Enzyme action enhancement and inhibition with protein disaggregation, dimerization or stabilization all can be accomplished by successful construction of molecules for Protein Surface Recognition.

Extensive work has been done by Hamilton and his group in the area of protein Surface Recognition. Calixarene and Porphyrin scaffolds were used to modulate various derivatives of these compounds for proteins like Chymotrypsin (ChT) and Cytochrome *c* (CC) respectively (*70*), *(72*), (*77*). The aim was to disrupt the binding of the proteins with their endogenous inhibitor and target the proteins with the synthesized compounds. One of the calixarene compounds was particularly able to turn down the natural soyabean trypsin inhibitor (STI) of ChT and acted as an inhibitor itself. The compound disrupted the calixarene-STI interaction and was bound to the exterior surface of the enzyme. The interactions mainly were electrostatic and hydrophobic as designed for the ChT which has cationic and hydrophobic residues close to the active site (*70*).

In a similar study, tetraphenyl porphyrins have been modified with various amino acids that were anchored to the porphyrin scaffold thus a large surface area (300-400 $Å^2$) was created for effective protein-ligand interactions by Hamilton et al (Figure 12). The porphyrin derivatives were fluorescent in nature, however quenching was found upon addition to cytochrome *c* solution because of the complex between the heme Fe (III) and the ligand. Out of the four synthesized derivatives, one had better dissociation constant (20 ± 5 nM) compared to the rest of the derivatives. This compound had eight aryl groups with a net negative charge of eight and was better in binding to the enzyme compared to its natural ligand, cytochrome peroxidase *c* (K_d = 2.4 μM). The group concluded that the anionic charge and the presence of aryl groups lead to electrostatic as well as hydrophobic interactions with the cationic and hydrophobic portions of the protein target (*77*).

Trauner *et al.* explored the protein surface recognition principles by developing ligands for potassium channels. Tetraphenylporphyrin derivatives (water-soluble) were designed based on the four-fold symmetry to mimic and interact with the channels to gain strong polyvalency. Membranes from human $K_v1.3$ channel transfected HEK-293 cells were studied for ^{125}I-$HgTX_1$A19Y/Y37F (hongo toxin) binding to the porphyrin ligands and positively charged ligands strongly interacted with the channels in agreement with the conserved anionic Asp residues (D381). This was a strong evidence of the partial binding of the ligands with the outer vestibule of potassium channels reversibly (*78*).

Molecular Imprinting polymers (MIPs) technique offers another detecting technology for protein recognitions. In this technique the synthetic materials get embedded with recognition sites when interacting with a template. The synthetic materials (monomers) get polymerized in the presence of the template molecule via cross-linking with the bound template molecule. Upon

removal of the template, the polymeric material is left with cavities which fit the suitable target molecule. These MIPs act as excellent biosensors for biological receptors like antibodies, proteins and DNA. Careful development of polymerization and selection of suitable templates have proved to yield superior recognition platforms (*79*). The most part of this thesis is based on the concept of Protein surface recognition.

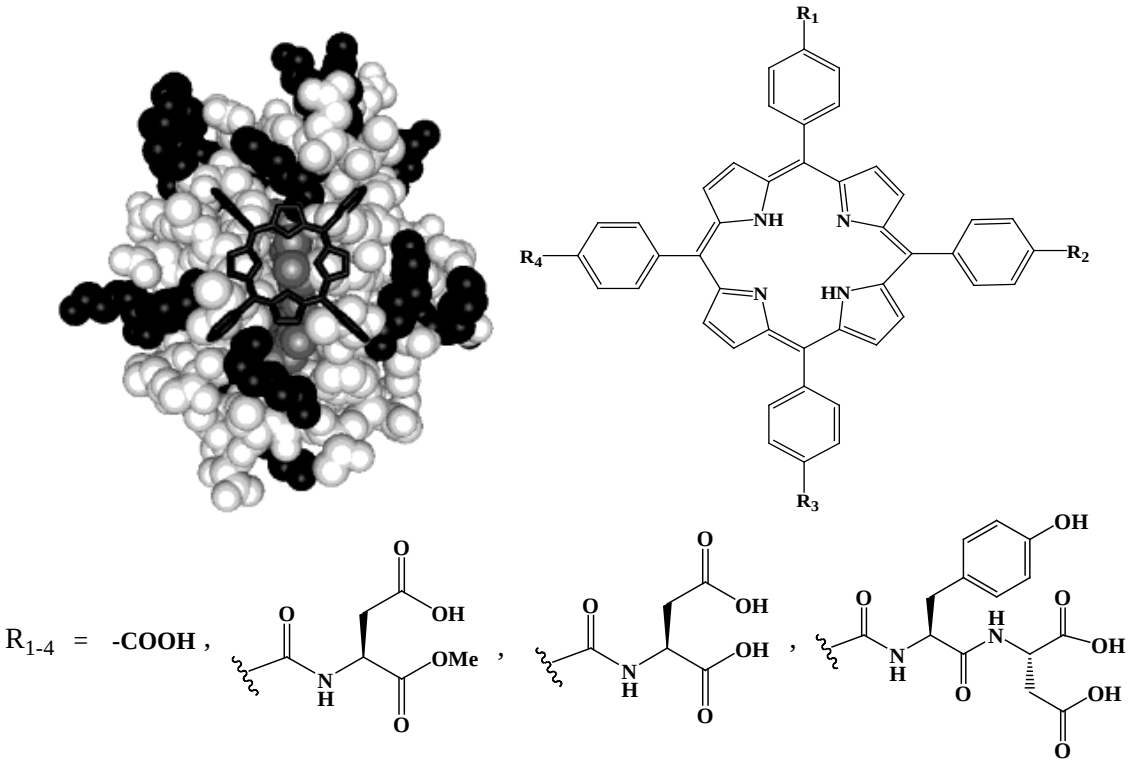

Figure 12. (a) Cartoon depicting X-ray crystal structure of cytochrome *c* (horse heart) with the tetraphenylporphyrin group at the centre. The white portions represent other residues except lysine and arginine which are depicted by the black spheres. The middle grey ones are the heme group. (Used with permission from Ref. 77). **(b)** The tetraphenylporphyrin scaffold (with various derivatives).

Liposomes

Liposomes bear resemblance to the cell membrane bilayer structure. These are microscopic spherical vesicles, consisting of lipid layers arranged concentrically and enclosing

an aqueous core (*80*). The discovery of liposomes dates back to 1961 by Bangham and his group at the Babraham University, Cambridge while they were trying to test a new electron microscope. Upon adding negative stain to dry phospholipids they found surprising resemblance to the plasmalemma and that was the very first evidence of the structure of the cell membrane to be composed of lipid bilayer (*81*).

Liposomes serve as models for biological membranes and have been studied for drug delivery by encapsulating various drug moieties. Hydrophilic molecules can be enclosed within the aqueous core and lipid soluble drugs are entrapped within the lipophilic membranes of liposomes (*82*). Because of these unique properties they have been used for targeted drug delivery in cancer therapeutics where these liposomes are found to be accumulated by enhanced permeability and retention (EPR) effect in the solid tumor versus normal tissues (*83*). The composition of the liposomes have made it biocompatible and their cellular uptake by endocytosis without extracellular release of contents have imparted potentials for systemic drug and gene delivery. The toxicity of the otherwise chemotherapeutic agents (drugs) can be concealed within the liposomes, while carrying the cargo through the blood stream to the desired location of delivery (*84*).

Liposomes with controlled sizes from microscale to nanoscale (50-5000 nm in diameter) have been prepared. In order to attain active targeting, surface modification of liposomes have been achieved by peptide, protein and antibody tagging on the liposomes (*82*). In spite of the fact that liposomes have been proved to be excellent carriers for various biological compounds as well as therapeutic drugs, there remains certain disadvantage also, mainly they are rapidly degraded by the reticuloendothelial system (RES) after systemic administration and sustained drug delivery cannot be achieved for an extended period of time (Figure 13). The phagocytic

cells present in the liver and spleen uptake the injected liposomes, thus leading to the destruction of the macrophages and interfering in the defense mechanism of the host *(80)*. Usually liposomes with more than 200 nm diameter are engulfed by the RES and smaller ones remain in the blood circulation for longer period (*83*). In order to overcome these drawbacks two approaches have been developed. Polyethylene glycol (PEG) is a hydrophilic polymer and its incorporation in the liposomal lipids leads to reduction in opsonization and imparts long-circulating ability in the blood stream. Due to the longer half-life of these PEG-liposomes, they can circulate in the blood for longer time without getting cleared away by the RES and can have better distribution (*85*). Another approach is to incorporate the drug-loaded liposomes within the depot polymer-based systems. Various synthetic and natural polymers have been used as depot for drugs since these polymeric materials are biodegradable, biocompatible and nontoxic. Many hydrogels and natural polymers (chitosan, collagen, dextran) have been very promising in forming temporary depot systems. The composite system have certain advantages over the polymeric-based system such as increased stability, controlled drug delivery over a prolonged period and preservation of the encapsulated bioactive drug within the liposomes. PEG-ylated liposomes, also called stealth liposomes or sterically stabilized liposomes have enhanced biocompatibility, low toxicity and immunogenicity along with increased circulation time. DOXIL/Caelyx is the PEG-ylated liposomal formulation (Doxorubicin) that was both US FDA and Europe Federation approved for the treatment of Kaposi's sarcoma (*82*).

There are different methods by which liposomes can be classified, of which structure and composition deserve special attention. Unilamellar liposomes consist of one bilayer and multilamellar liposomes have multiple lipid bilayers. Depending on the diameter size of the vesicles sizes, liposomes can be diverse in lamellar numbers (*86*). Table 3 and Table 4 below

indicate the various vesicle types of liposomes depending on their sizes and their classification based on their composition. Various sizes of liposomes can be formed depending on the method of preparation. Reverse phase evaporation, freeze and thaw, extrusion techniques, and dehydration and rehydration methods are some of the conventional ways by which liposomes can be made (*80*).

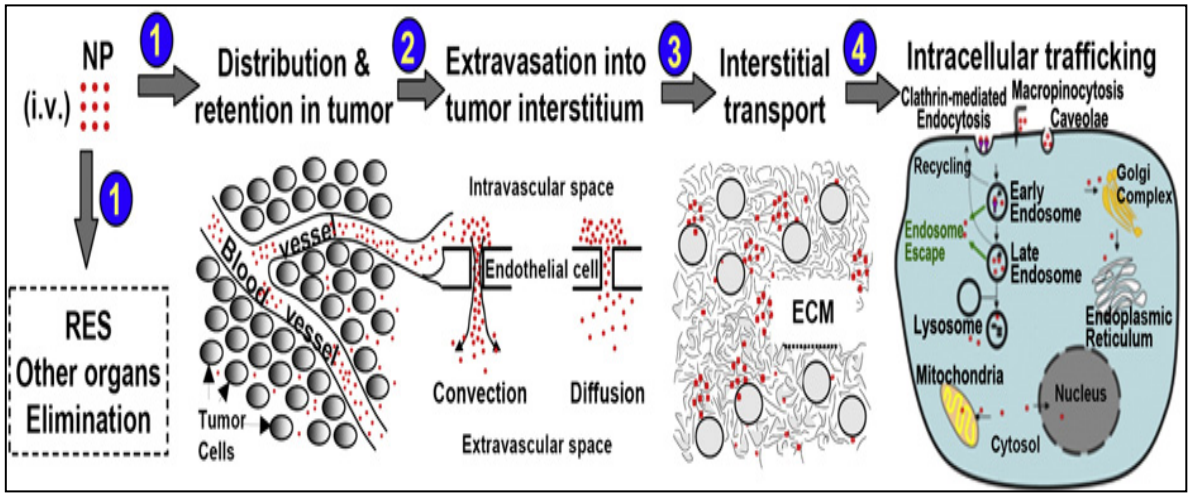

Figure 13. Schematic diagram showing how nanoparticulate carriers (NP) transfer from i.v. injection site to target sites. (Used with permission from Ref. 84).

Particle size distribution and polydispersity of liposomes are measured by dynamic light scattering (DLS) and flow field-flow fractionation coupled with multiangle light scattering methods (*86*). Since DLS measurement often does not give reliable size distribution, cryo-TEM (Transmission electron microscopy at cryogenic temperature), freeze-fracture TEM and quasi-elastic light scattering are used for better mean radii and size distribution measurements (*87*).

Gel exclusion chromatography can separate liposomes of the size ranging from 30-300 nm. For clinical applications liposomal stability and shelf-life are important aspects. Normally the lipid molecules undergo hydrolysis and oxidation and so they are always recommended for low temperature storage (*86*).

Table 3. Classification of liposomes based on their structure.

Vesicle type	Diameter size of the vesicles	Number of lipid bilayer present	Preparation Techniques
Unilamellar Vesicle (UV)	All size range	1	All of the below techniques and mechanical agitation of MLVs
Small Unilamellar Vesicle (SUV)	20 – 100 nm	1	Extrusion, solvent injection, high-energy sonic fragmentation, homogenization
Large Unilamellar Vesicle (LUV)	< 100 nm	1	Freeze-thaw cycling, detergent dialysis, reverse evaporation, extrusion, swelling in non-electrolytes
Giant Unilamellar Vesicle (GUV)	< 1 µm	1	Solid-film hydrolysis, electroformation, de-/rehydration, detergent dialysis
Multilamellar Vesicle (MLV)	< 0.5 µm	5 -25	Thin film hydration (evaporation-dried, spray-dried or lyophilized lipid material)

Table 4. Classification of liposomes based on composition.

Types of liposomes	Composition
Conventional liposomes (CL)	Neutral or negatively charged phospholipids and cholesterol
Fusogenic liposomes (RSVE)	Reconstituted sendai virus envelopes
pH sensitive liposomes	Phospholipids such as DOPE
Cationic liposomes	Cationic lipid with DOPE
Long circulatory liposomes (LCL)	Neutral high temp, cholesterol and 5-10 % PEG
Immunoliposomes	Attached with monoclonal antibody or recognition sequences.

Various synthetic, semi- synthetic as well as natural phospholipids are used for liposomal preparation. In addition to natural lipids, various phosphatidylcholine derived from egg and soybean lecithins, sphingomyelin are also used for conventional liposomal formulations. POPC, DSPC, DPPC and DSPE are some of the important phospholipids that are usually used in

liposome synthesis. The phospholipids form the lipid bilayer and sometimes cholesterol is incorporated within the bilayer to impart buffer fluidity, intercalating with the phospholipid molecules and restricting the trans to gauche conformation transformation (*80*). Presence of cholesterol also helps in the reduction of fast release of the encapsulated compound into the plasma (*82*). Many formulations are currently available in the market and are found in Ambisone, Myocet, Daunoxome and Daunorubicin which use conventional liposomes as formulations. However, Doxil is the first FDA approved liposome formulation to be available in the market for Kaposi's sarcoma and ovarian cancer (*83*).

Liposomes can release their cargo either upon passive diffusion or active targeting. By circulation in the blood stream the lipid carriers can diffuse their payload but advanced and better targeting is achieved by triggered release at the site of action. Usually for active delivery, liposomes are constructed with enzyme-cleavable specific peptides or selective antibodies (monoclonal antibodies in many cases) (*83*), (*84*). Liposomes can be ruptured at their target by various external stimuli such as pH, temperature, light, enzymes or ultrasound (*88*), (*89*). Once activated, the encapsulated content leaks out of the liposomes due to multiple factors of which membrane instability, structural changes in the bilayer lipid motifs occur to be the primary reasons. Sakaguchi et al synthesized various carboxylated poly (glycidol) derivatives to prepare pH-sensitive phosphatidylcholine (egg yolk) liposomes for cytoplasmic delivery of proteins and genes (*90*). Transferrin receptors are responsible for the transport of ferric ions through endocytosis within the cells. It has been reported that transferrin receptors are found in larger amount in tumor cells than in normal cells (*91*). So these receptors are excellent targets for targeted drug delivery in cancer cells. One group in the year 2004, fabricated liposomes with pH-sensitive fusogenic peptides for encapsulating rhodamine dye. Transferrin was anchored to

the liposomal surface for internalization of the lipid vesicles to the target cells. Confocal laser microscopy images of K562 cells revealed that the cholesterol conjugated peptide on the liposomal surface achieved improved intracellular delivery and endosomal escape (*92*). The same group in 2008 used the same pH-sensitive peptide for developing plasmid DNA encapsulated liposomes. These liposomes were PEG-ylated and acted synergistically with the cholesterol-conjugated peptides for enhanced release and transfection efficiency (*93*). Ultrasound application for liposomal trigger release was manifested by many researchers where enhanced delivery of drugs and genes has been achieved. For targeted drug delivery the thermal or mechanical properties of ultrasound have been explored for reaching deeper areas which are inaccessible by other triggers for local treatment of disease (*94*). Microbubbles and echogenic liposomes both entrap gas bubbles whose oscillation upon ultrasound treatment leads to disturbance in the caging agent thus releasing the payload at the site of interest. For the tumor targeted gene delivery to syndecan-2 overexpressing cancer cells, Negishi et al developed AG73 peptide conjugated PEG-liposomes and bubble liposomes and ultrasound exposure resulted in 60 fold increase in the transfection efficiency (*89*).

In 2005, Srivastava and colleagues designed lipids incorporating *o*-nitrobenzyl group which were photocleavable and applied these lipids to synthesize liposomes encapsulating the dye 6-carboxyfluorescein (*95*).

Enzymes are ubiquitous biomarkers in various disease conditions. Their catalysis reactions on certain peptides have been explored tremendously for on the site release of liposomal contents (*96*). Proteases are normally found to be overexpressed in tumor and cancerous conditions (*97*). Matrix metalloproteinases-9 (MMP-9) is one such enzymes which are found to be upregulated in disease conditions such as cancer, arthritis, fibrosis, etc (*21*).

Mallik et al have synthesized various lipopeptides which attain triple-helical conformations in the liposomes thus resembling the enzyme's endogenous substrate collagen. A detailed mechanistic study was performed for the substantial release of the encapsulated dye carboxyfluorescein (CF) upon triggered release by MMP-9 compared to other MMPs (-7 and -10) from the liposomal core (*46*). Later in 2009, the group performed experiments with metastatic cancer cells (MCF-7) secreted MMP-9 for the liposomal release of CF dye, thus once again demonstrated their "proof-of concept" from their earlier work (*98*).

Polymerized liposomes are made up of polymerizable groups that are attached either to the polar head groups of the liposomes or to the fatty acid tails. Use of different polymerizable groups such as methacryloyl, diacetylene, styryl and vinyl pyrrolidone has been demonstrated in the synthesis of polymerized liposomes (polymerizable phosphocholine as the major lipid) by many researchers. The polymerization is carried out either thermally or photochemically and the resulting lipid vesicles formed are more stable than saturated liposomes (*99*). Mallik et al in 2004 presented a work which was based on the application of polymerized liposomes for detection of proteins. Lanthanide ion Eu^{3+} was used which was conjugated with the chelating agent ethylenediaminetetraacetic acid (EDTA) and 5-aminosalicylic acid (5As) acting as the sensitizer. The Eu^{3+} - EDTA - 5As was incorporated as the head group in the polymerized lipid for the liposomes. Various proteins (BSA, CA, bovine serum γ-globulin) were tested and the luminescence signals from the lanthanide ion upon protein interaction and the change in the lifetime data gave a sensitive platform for identification of different protein molecules (*100*).

In 2007, UV irradiated polymerized liposomes were used by the same group for selective isozyme recognition of carbonic anhydrases (CAs) (*101*). Various lipids were synthesized for the bilayer build up, one of them had a weak CA inhibitor attached (5% by weight) and the other

lipid (5%) was constructed with an iminodiacetate (IDA) chelated Cu^{2+} ion for interacting with the histidine moieties present on the enzyme's surface. The major portion of the liposome construct comprised of a mixed chain polymerizable lipid (85%) phosphatidylcholine and Eu^{3+}-complexed lipid for luminescent reporter (5%). Different isozymes (CA I, II, VII, XII and bovine erythrocyte CA) behaved differently against the liposomes as observed from the lifetime and dissociation constants data.

In the field of cancer research, liposomes have been used extensively for targeted drug delivery for tumor cells. Due to the leaky blood vessels in tumor tissues (EPR effect), liposomes can penetrate the vascular networks and stay there for extended period of time (*83*). Kullberg et al. reported that using thermosensitive and Herceptin antibody conjugated liposome can leads to intracellular disruption of liposomes due to hyperthermia. These liposomes showed increased targeting specificity for Her-2-overexpressing cancer cells (*102*). Folate receptors are overexpressed in cancer cells compared to normal tissues. Targeting folate receptors with liposomes conjugated with folate ligands have been proved to be a useful way for targeting cancer cells (*103*). Various anti-cancer drugs such as Doxorubicin and Mitoxantrone have been found to present excellent anti-tumor activity when used within the folate targeted liposomal carrier. However, these formulations suffer from one drawback which is the slow release of the drug upon cellular uptake of the liposomes. Kawano et al have shown that using lipids with enhanced fluidity can overcome this drawback, thus leading to higher toxicity of tumor cells with folate-targeted liposomal Mitoxantrone (*104*). Leroux et al have reported that pH-sensitive immunoliposomes composed of a copolymer *N*-isopropylacrylamide (NIPAM) and anti-CD33 monoclonal antibody could be very specific to the CD33 cell surface antigen of targeted leukemic cells. This group demonstrated that these liposomes were highly toxic against CD33

positive human monocyte HL60 cells where intact cytosine arabinoside (ara-C) was able to escape in the endosomes due to the polymeric structural change of NIPAM after receptor-mediated internalization (*88*).

Use of transferrin-conjugated PEG-ylated liposomes (TF-PEG-liposomes) as potential cancer drug carrier was reported by Suzuki et al in 2008. Cisplatin has the inherent property of kidney (nephrotoxicity) toxicity due to the poor renal clearance of the metal platinum present in the drug. The group demonstrated when Oxaliplatin, a cisplatin derivative was encapsulated in the TF-PEG-liposomes that lead to higher concentration of the drug in the tumor when compared with just PEG-liposomes, the drug itself or just bare liposomes (*105*). Sadzuka et al studied the modification of liposomes with mixed PEG molecules (molecular weight ranging from 340 to 2000) for the enhanced delivery of doxorubicin to the tumor cells (*85*). The group studied the effect of fixed aqueous layer thickness on the mixed PEG-modified liposomes and found that the layered thickness enhanced the antitumor activity of the liposomes.

A promising avenue of liposomal use is in the detection where they can be used as biosensors as well as imaging probes. Zheng et al. have demonstrated in their work how chemiluminescence immunoassay can be developed using antibody-modified liposomes. Sandwich assay was constructed where prostate specific antigen (PSA) was detected in picogram level using horseradish peroxidase (HRP) encapsulated liposomes. Using triton as the surfactant for lysis of the liposomes, the released HRP molecules upon chemical reaction with luminol and H_2O_2, gave an indirect measurement of the amount of analyte (PSA) bound to the capture antibody on the microwell plates (Figure 14) (*106*).

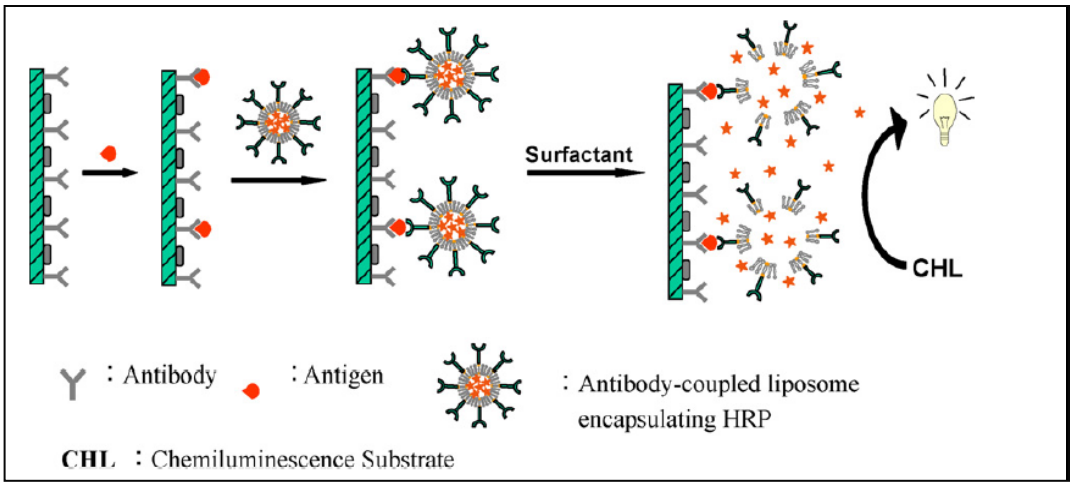

Figure 14. Schematic illustration of application of chemiluminescence liposomes for detection of prostate specific antigen. (Used with permission from Ref. 106).

Kamidate and colleagues showed the application of 4-Iodophenol as an enhancer for direct detection of HRP encapsulated liposomes via luminal chemiluminescence. The chemiluminescence in presence of the iodophenol-luminol-hydrogen peroxide when catalyzed by HRP resulted in 150 times greater in intensity when compared with a lipid-free bulk solution. Definitely the presence of 4-Iodophenol resulted to be an advantage as an effective enhancer (*107*).

Viswanathan and his group used monoclonal anti-carcinoembryonic antigen antibodies (α CEA) tagged liposomes as biosensors for detection of CEA which is a vital biomarker for early diagnosis of cancer. Ferrocene carboxylic acid (FC) was encapsulated within the liposomes to form FCL and a sandwich immune complex was developed with the multiwalled carbon nanotubes (MWCNT) screen-printed electrode bound α CEA-CEA- α CEA-FCL (*108*). Upon lysis of the liposomes the ferrocene moieties were released on the electrode surface and the voltametric response was related to the concentration of CEA. The method provided an efficient

tool kit for detection of CEA in human serum and saliva samples from cancer patients up to a detection limit of 1 x 10^{-12} g/mL (*108*).

Vamvakaki et al utilized an unstable enzyme (Acetylcholinesterase; (AChE)) encapsulated in the phosphatidylcholine liposomes which resulted in the formation of optical nano-biosensors thus protecting and stabilizing the bioactive molecule. Porin was used in the lipid bilayer for the easy transport of the substrate (acetylcholine chloride) to the inner aqueous core of the liposomes. However, porins were relatively small in size for the outside access of the enzymes from the liposomes. Pyranine was used as the fluorescent indicator which has a pK_a value 7.3 close to the pH which AChE requires for its catalytic action. The enzymatic activity on the substrate resulted in the formation of acetic acid thus changing the pH of the interior of liposomes. This change in the pH caused differences in the fluorescence signals which were monitored at the fluorophore excitation/emission (460 nm /513 nm) wavelengths. This method provided a unique technique for detecting enzyme stabilization within the sol-gel matrices of the liposomes and biosensing capabilities of the entire system (*109*).

Edwards and Baeumner used fluorescein-tagged DNA oligonucleotides loaded antibody-tagged liposomes for detection of antigen protein *Bacillus anthracis*. The group performed a sandwich immunoassay where the antigen was bound to the antibodies immobilized in the microwell plates. The secondary antibody conjugated liposomes were allowed to attach with the antigen followed by lyses of the liposomes leading to the release of the dye-coupled DNA. The released DNA then was hybridized with a complementary sequence that was previously coated in another microwell plate. Another liposome encapsulating sulforhodamine-B was then added to bind to the fluorescein dye on the hybridized probe. Upon lysis of the secondary liposomes

with surfactant, the fluorescence signals were produced which were proportional to the concentration of the antigen protein added initially (*110*).

Egashira et al prepared immunoliposomes encapsulating a ruthenium (Ru) complex to detect hemagglutinin (HA) molecule of influenza virus. The Ru complex upon adsorption on the gold electrodes yielded electrochemiluminescence (ECL) which attributed a high sensitive detection of the HA upto a concentration of 10^{-14} g/mL (*111*). Detection of dengue virus using DNA probe attached to the dye-encapsulating liposomes were demonstrated by Baeumner et al (*112*). Astrovirus detection in fecal samples using DNA-tagged liposomes was shown by Jennifer et al. The group used various methodologies such as electrochemiluminescence, ethidium bromide staining, liquid hybridization assay (LHA) including liposome-strip assay. For the liposomal study they used sulforhodamine dye for encapsulation and the RNA required for the assay was amplified by nucleic acid sequence-based amplification (NASBA) (*113*). In chapter 4 of the thesis, we have described the detailed procedure of synthesizing dye encapsulated liposomes and their release studies in presence of active MMP-7.

CHAPTER I. SYNTHESES AND APPLICATION OF FLUORESCENT WATER-SOLUBLE POLYMERS FOR ISOZYME-SELECTIVE INTERACTIONS WITH MATRIX METALLOPROTEINASE-9

Abstract

Matrix Metalloproteinases play crucial roles in various pathogenic diseases, including cancer. Over 26 isozymes are reported in this family of proteases, out of which most of them are overexpressed in cancerous conditions and tumors. The isozymes share similar active site patterns; however the exposed amino acids on their surfaces are different. The functions of the isozymes overlap with each other and so designing selective inhibitors is difficult. Most of the clinical trials with MMP inhibitors have failed due to their lack of recognition of the different isozymes and selectively inhibiting each separately. In normal healthy conditions 100-200 ng/mL of MMP-2 and -9 are found and this value rises to 1-2 µg/mL in various cancerous conditions (*6*), *(22*). The conventional ways by which MMPs are detected are gelatin zymography, western blotting and ELISA. But each one has its own limited advantages and disadvantages. Although synthetic polymers have been reported in literature to detect structurally different proteins, the use of polymers for isozyme selective detection within an enzyme class has not been reported yet.

Herein we report the synthesis of fluorescent water soluble polymers for isozyme-selective interactions with one of the MMPs, MMP-9 which is found to be upregulated not only in many cancers but also in multiple sclerosis or arthritis. The reported polymers were synthesized randomly with a reporter fluorophore and an inhibitor. We have used a hydroxamate

inhibitor for the binding of the Zn^{2+} present in the active site cleft. For the recognition of the surface charges on the enzymes, positively charged, negatively charged and hydrophobic amino acids were incorporated within the polymers. For these reasons we have attached lysine, aspartic acid and alanine to our polymers. Various combinations were made to synthesize many polymers using free radical copolymerization procedure. These polymers were tested against MMP-7, -9 and -10 in fluorescence experiments for isozyme selective detection. Selective interactions were noticed for MMP-9 against MMP-7 and MMP-10. The data were analyzed by logit binary regression analysis and one of the polymers showed significant interactions with MMP-9 proving that the particular polymer could distinguish between the three isozymes. These results were supported by human serum experiments as well by inhibition studies.

Introduction

Proteins constitute a major fraction of biological systems. Their proper regulation leads to complex but beneficial life processes (*67*). Structurally all proteins are different with respect to interior and exterior surface residues. A unique distribution of amino acid moieties is a signature pattern for each protein which makes them distinct from each other. Various functional groups (polar, nonpolar, charged, aromatic and hydrophobic) on the exterior surfaces of proteins lead to interactions with other proteins as well as with endogenous ligands (*114*). Antigen-antibody, hormone-receptor and protease-inhibitors are examples of such binding interactions (*71*). Designing artificial molecules could lead to better regulation, modulation or inhibition of proteins in disease conditions. The synthetic compounds are targeted for protein surface recognition depending on the subsequent match between the specific binding motifs on the protein surfaces with the designed molecules' tailored units.

Use of synthetic receptors for protein surface recognition has gained tremendous importance for manipulating the natural protein-protein interactions. Apart from active site interactions, molecular interactions also take place on the solvent-exposed exterior surfaces of the enzymes. In natural conditions large surface area is required (about 1600 $Å^2$) for effective protein-protein interactions (*68*). Usually Coulomb interactions take place between the polar residues on the protein surfaces, and the complementary bindings are reinforced by the hydrophobic residues or the domains on the surfaces (*115*). Disrupting protein-protein and protein-ligand interactions by synthetic molecules can be a fundamental approach for novel drug discovery as well as better inhibitor design (*116*).

Various approaches have been implemented for developing artificial synthetic receptors for gaining high molecular recognition and protein surface binding. Use of peptides on various scaffolds has led to significant protein surface interactions. Hamilton et al. pioneered in this field by exploring calixarene and porphyrin scaffolds for chymotrypsin (ChT) and cytochrome c surface recognition respectively (*70*), (*77*). For designing inhibitors for α-ChT, tetrapeptide loops were attached to the calixarene scaffold with the approximate 450 $Å^2$ surface area and these aspartate-rich scaffolds bound to the surface-exposed lysine (Lys 36, 90, 175, 177) and arginine (Arg 145) on the protein surface, thus blocking the natural substrate (trypsin inhibitors) to approach to the active site of the enzyme. The inhibition constants of one promising designed inhibitor were K_i = 0.81 μM and K_i* = 0.11 μM (K_i = dissociation constant for the initial enzyme-inhibitor complex; K_i* = dissociation constant of the second enzyme-inhibitor complex) and it was found to bind to the cationic residues close to the actual active site cleft of the enzyme (*70*).

Hamilton's group also focused in developing tetraphenylporphyrins with various amino acid derivatives attached and having flat and semi rigid surface area of 300-400 $Å^2$. One of the designed receptors (glutamate-rich porphyrin derivative) containing eight negative charges and eight phenyl groups had K_d value of 20 nM for cytochrome c (*77*). Thus efficient designing on the porphyrin template leads to geometrical match between the cationic and hydrophobic side chains of the particular target enzyme. The porphyrins excelled calixarenes in view of synthetic ease, large size, rigidity and photophysical properties (*77*), (*70*).

Cyclodextrin (CD) scaffolds were studied by Breslow et al. for inhibiting multimerization of various enzymes, such as Glucose-6-phosphate dehydrogenase, D-Galactose dehydrogenase, Citrate Synthase (CS), Phosphohexose isomerase, L-Lactate dehydrogenase (LDH), Fumarase, and Sorbitol dehydrogenase. Two of the compounds were good in inhibiting CS and LDH and Tyr and Trp for CS and Phe, Tyr, and Trp for LDH were responsible for interations with the CD dimers (*117*).

Metal-ligand interactions have been explored by Mallik et al. for protein surface recognition. "Two-prong" approach have been applied for an inhibitor to bind to the active site pocket of the enzyme and the Cu (II) binding to the surface exposed histidine residues on the carbonic anhydrase enzyme. Thus conjugating a poor inhibitor (benzene sulphonamide) to the surface binding group (cupric iminodiacetate) increased the receptor's affinity for human carbonic anhydrase (CA II) 40-fold (*65*). hCA I differs from hCA II in having four surface histidine residues as opposed to six in the latter. One of the designed compounds actually had better K_d value (0.017 ± 0.001 μM) as compared to benzene sulphonamide itself (4.5 ± 0.1 μM) (*118*).

Among the synthetic receptors, polymers have gained immense importance in molecular recognition amongst other artificial protein sensors (*119*). Polymers have been long used for binding different proteins (*79*). Due to the flexibility of the polymeric backbone, formation of multiple, complementary interaction sites is possible between the polymer and the amino acid residues on the protein surface (*120*). Polymers are used for developing affinity membranes where they act as switches thus, turning on enzyme activity. They have been also reported as "protein sensors" where they act as selective protein immobilization agents (*121*), (*72*). Methacrylamide-based polymeric sensors have been developed by Schrader and its group for selective detection of various proteins (*121*). Not only proteins, but also sulfated polysaccharides, such as heparin could be detected by the fluorescent copolymers. Physiologically relevant concentrations of heparin (25 - 250 nM) could be quantitatively detected by these methods (*122*).

Rotello and his coworkers had developed an array of gold nanoparticle based fluorescent polymers for detection and quantification of various proteins (BSA, Cyt *c*, β-galactosidase, lipase, subtilisin A, acid phosphatase and alkaline phosphatase) and with the help of linear discriminant analysis (LDA), they were able to dictate the fluorescence fingerprints of each the proteins in their study (*123*).

Koch et al. have developed the novel concept of statistical copolymerization and have shown that this approach was applicable for designing synthetic copolymers for 'induced-fit' binding models for similar sized proteins but varying in biological functions. The group also used methacrylamide-based monomers have been mentioned which were polymerized by free-radical copolymerization methodology. Depending on the protein surfaces, monomers were selected from the pool of synthesized molecules and copolymerized. Noncovalent interactions

(hydrophobic, van der Waals and π-stacking interactions) dominated over polar attractions for the linear polymers to achieve protein surface binding. Fluorescence titrations and IC_{50} values were concomitant in choosing one of the polymers for unique selectivity for lysozyme from cytochrome c and Bovine serum albumin (*120*).

Tominey et al synthesized a set of linear polymers for detection of lysine and arginine-rich proteins using reversible addition-fragmentation chain transfer (RAFT) polymerization technique (*115*). Molecular Imprinting Polymers or MIPS are other elegant polymeric scaffolds that are used for protein sensing. These biomimetic materials provide excellent robustness and specific recognition sites for the target analyte (*79*).

Water soluble, flexible polymers have been used as biosensors to selectively bind to different proteins. Because of polyvalent interactions, the flexibility of the polymer backbone aids in the formation of multiple, complementary interaction sites between the polymer and the amino acid residues on the protein surface. The proteins used by researchers in most of the studies for these selective recognition experiments were structurally very different (e.g., lysozyme, bovine serum albumin or cytochrome c) (*124*), (*121*). To the best of our knowledge, selective binding of polymers to different isozymes of an enzyme family has not been demonstrated.

Matrix metalloproteinases (MMPs) are a group of Zn^{2+} containing metalloenzymes whose primary function is to hydrolyze the extracellular matrix components (*8*), (*125*). There are 26 isozymes in this family and they share their roles in a number of different physiological processes such as cell proliferation, apoptosis, differentiation, angiogenesis, chemokine/cytokine activation and the expression levels of these enzymes are strictly regulated at multiple levels (*4*), (*27*). MMP-9 including other isozymes have been shown to be overexpressed in degenerative

diseases like arthritis, multiple sclerosis or metastatic cancers (*126*), (*127*). In healthy individuals, the serum concentration of MMP-9 is found to be about 5–10 nM (*128*). However, in lung cancer patients, the concentration of this enzyme can be as high as 100–200 nM in the bronchial lavage fluids (*129*). The levels of MMP-9 serve as diagnostic and prognostic markers for cancer and metastasis (*128*), (*129*).

Since isozymes catalyze the same chemical reaction, their active sites are remarkably similar. However, the pattern of amino acid residues on the surface of the isozymes are not under evolutionary pressure and are usually not conserved (*130*). We reasoned that this difference in the surface pattern if exploited for selective binding of polymers (which are composed of various charged and uncharged moieties) could result in the specific interaction of one isozyme only for the polymer (Scheme 2). From the knowledge gained from our earlier work based on the "two-prong" approach of multivalency for multiple binding of ligands to the surface of a single biological entity, herein, we report our results on selective binding to recombinant human matrix metalloproteinase-9 (MMP-9) by a set of water soluble, flexible polymers (*118*), (*76*).

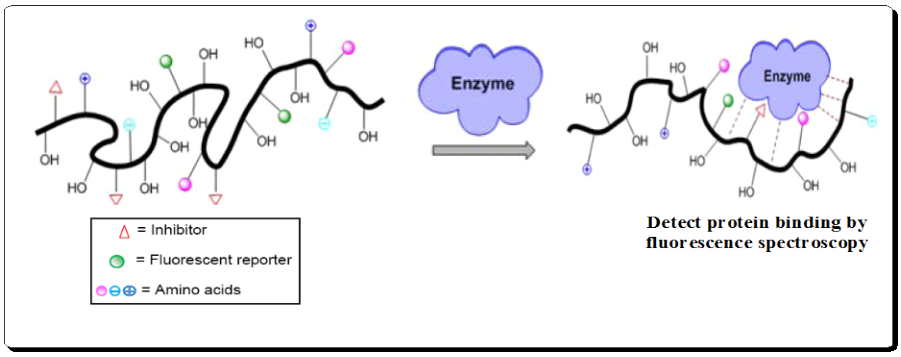

Scheme 2. Schematic representation of the polymer structure and its interaction with enzyme.

Materials and Methods

All commercial reagents were purchased from Alfa Aesar, TCI America and Aldrich. Various solvents used for synthesis were used as purchased without further purification. Most of the syntheses were carried out under nitrogen atmosphere. Among the equipments that were used were rotary evaporator for solvent evaporation, desiccators for drying, automated flash chromatography (Combiflash RF system by Teledyne Isco) for purification, 300, 400 and 500 MHz (Varian) spectrometers for ^{1}H and ^{13}C NMR spectra. NMR solvents used were $CDCl_3$, D_2O, DMSO-d_6 with TMS as the internal standard. NMR spectral data processing was performed using ACD Labs software processor. TLC plates used were Adsorbosil plus IP, 20 X 20 cm plate, 0.25 mm (Altech Associates, Inc.). Chromatography plates were visualized under UV or iodine chamber. Melting points of the compounds were determined with a micro melting point apparatus. Polymers were characterized using Gel permeation chromatography (Waters 2690) and dimethylformamide as the solvent. Fluorescence spectroscopic studies were carried out using a Fluoromax-4 fluorescence instrument by Horiba Jobin-Yvon. For inhibition studies, Spectramax Spectrophotometer was used and MMP-2/MMP-7 commercial fluorogenic substrate (MCA-Pro-Leu-Gly-Leu-Dpa-Ala-Arg-NH_2. TFA) was purchased from EMD Biosciences. Human Serum was purchased from BioWhittaker, Lonza.

Synthesis of methacrylamide-based monomers: We synthesized a set of monomers using water soluble methacrylamide as the polymerizable moiety. We conjugated the polymerizable moiety to an alcohol (for increased water solubility and hydrogen bonding with amino acid residues on the surface of MMPs), to the fluorogenic dansyl group and to a non-selective hydroxamate MMP inhibitor. Different amino acids such as lysine, aspartic acid and

alanine were also linked to the polymerizable groups to impart electrostatic and hydrophobic properties to the polymers.

Dansyl monomer: Dansyl chloride (1.5 g, 5.6 mmol) was dissolved in dichloromethane (30 mL) and the solution was added dropwise into 1,2-ethylenediamine (48.80 mL, 3.341 g, 55.6 mmol) under stirring at 0°C. After addition, the solution was stirred for 3 hours at room temperature. The reaction mixture was acidified with dilute HCl and then extracted with CH_2Cl_2 (2 X 20 mL). The aqueous layer was made basic (pH = 9) using 10 M NaOH and again extracted with CH_2Cl_2 (2 X 20 mL). The organic layer was dried over Na_2SO_4, filtered and dried under vacuum to obtain a yellowish-green solid.

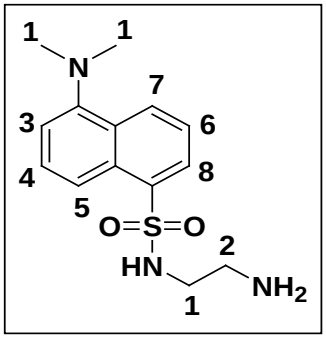

5-Dimethylamino-naphthalene-1-sulfonic acid (2-amino-ethyl)-amide

5-Dimethylamino-naphthalene-1-sulfonic acid (2-amino-ethyl)-amide: ^{1}H NMR (400 MHz,$CDCl_3$, 25˚C, TMS); δ ppm 2.69 (s., 2 H, $C2H_2$) 2.90 (s, 8 H, $C1H_8$) 7.19 (s, 1 H, $C3H_1$) 7.52 (s.,1 H, $C4H_1$) 7.58 (s, 1 H, $C5H_1$) 8.30 (s, 1 H, $C7H_1$) 8.26 (s, 1 H, $C6H_1$) 8.55 (d, J=8.5 Hz, 1 H,$C8H_1$).

The intermediate product (1.122 g, 3.8 mmol) and triethylamine (0.6 mL, 4.18 mmol, 1.1 eq.) were dissolved in 200 mL dichloromethane. A solution of methacryloyl chloride (437 mg, 4.18 mmol, 1.1 eq.) in 50 mL dichloromethane was added slowly to the ice-cold yellow fluorescent solution and then stirred for 6 hours. The solvent was removed under reduced

pressure and the product was purified by automated flash chromatography over silica gel with ethylacetate/hexane (**R_f = 0.1**; EtOAc : Hex = 3:1) as the mobile phase. Yield: 0.5 g (45%) of greenish yellow fluorescent solid flakes. mp =116-117 °C.

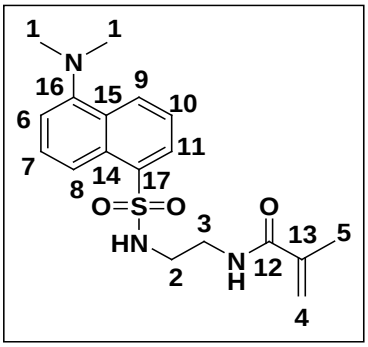

N-[2-(5-Dimethylamino-naphthalene-1-sulfonylamino)-ethyl]-2-methyl-acrylamide

N-[2-(5-Dimethylamino-naphthalene-1-sulfonylamino)-ethyl]-2-methyl-acrylamide: ^{1}H NMR (400 MHz, $CDCl_3$, 25˚C, TMS); δ ppm 1.86 (s, 3 H, $C5H_3$) 2.89 (s, 7 H, $C1H_6$, NH) 3.08 (s.,2 H, $C2H_2$) 3.37 (s., 2 H, $C3H_2$) 5.27 (s, 1 H, $C4H_1$) 5.61 (s, 1 H, $C4H_1$) 6.30 (s., 1 H, $C6H_1$) 7.20(s, 1 H, $C7H_1$) 7.50 - 7.59 (m, 2 H, $C9H_1$, $C10H_1$) 8.26 (s, 2 H, $C8H_1$, NH) 8.54 (s, 1 H, $C11H_1$). ^{13}C NMR (100 MHz, $CDCl_3$, 25˚C, TMS); δ ppm 18.66 (C5), 39.74 (C3), 43.39 (C1), 45.62 (C2),115.52 (C6), 118.75 (C8), 120.43 (C4), 123.37 (C11), 128.82 (C10), 129.68 (C7), 129.85 (C9),130.18 (C15), 130.88 (C14), 134.56 (C13), 139.43 (C17), 152.32 (C16), 169.25 (C12).

Alcohol monomer: 3-amino-1, 2-propanediol (1.367 g, 15 mmol) and triethylamine (4.17 mL, 30 mmol, 2.0 eq.) were dissolved in 50 mL acetonitrile. Methacrylic anhydride (2.8 g, 18 mmol, 1.2 eq.) in 25 mL acetonitrile was added slowly to the ice-cold solution and stirred overnight at room temperature. The solvent was removed under reduced pressure and the product was purified by automated flash chromatography over silica gel with

dichloromethane/methanol (**R_f = 0.3**; CH_2Cl_2 : MeOH = 10 : 1) as the mobile phase. Yield: 0.4 g (30%) of a white hygroscopic solid.

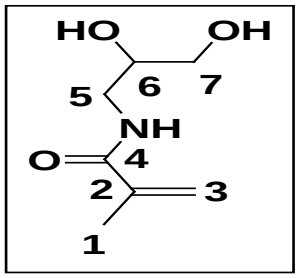

N-(2, 3-Dihydroxy-propyl)-2-methyl-acrylamide

N-(2,3-Dihydroxy-propyl)-2-methyl-acrylamide: ^{1}H NMR (400 MHz, DMSO, 25°C, TMS); δ ppm 1.84 (s, 3 H, C1H_3) 3.01 - 3.11 (m, 1 H, C5H_1) 3.24 (d, J=13.37 Hz, 2 H, C5H_1, C6H_1) 3.29 (d, J=5.12 Hz, 2 H, C7H_2) 5.32 (s., 1 H, C3H_1) 5.65 (s, 1 H, C3H_1) 7.78 (s., 1 H, NH). ^{13}C NMR (400 MHz, DMSO, 25°C, TMS); δ ppm 19.29 (C1), 43.32 (C5), 64.55 (C7), 71.01 (C6), 119.77 (C3), 140.54 (C2), 168.52 (C4).

Lysine monomer: N-Boc-L-lysine-t-butyl ester hydrochloride (3.39 g, 10 mmol, 1.0 eq.) and triethylamine (2.02 g, 20 mmol, 2.0 eq.) were dissolved in 100 mL dichloromethane. A solution of methacryloyl chloride in 25 mL dichloromethane (1.05 g, 10 mmol, 1.0 eq.) was added slowly to the ice-cold solution and was stirred for 18 hours under nitrogen gas at room temperature. The solution was washed with 15% brine solution, 10% citric acid (2X) and the organic layer collected was treated with 4% sodium bicarbonate solution (2X). The organic layer was dried over Na_2SO_4, filtered and the solvent was removed under reduced pressure. The white solid was purified using automated flash chromatography over silica gel with dichloromethane/methanol (**R_f = 0.5**; CH_2Cl_2 : MeOH = 10 : 1) as the mobile phase.

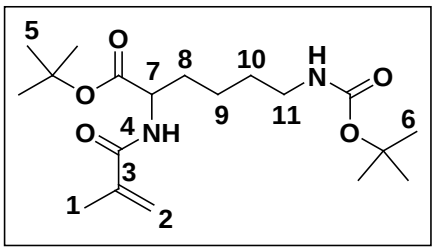

6-*tert*-Butoxycarbonylamino-2-(2-methyl-acryloylamino)-hexanoic acid *tert*-butyl ester

6-*tert*-Butoxycarbonylamino-2-(2-methyl-acryloylamino)-hexanoic acid *tert*-butyl ester: ^{1}H NMR (400 MHz, $CDCl_3$, 25˚C, TMS); δ ppm 1.48 (s, 12H, $C6H_9$, $C9H_2$, $C8H_1$) 1.43 (s, 10 H, $C5H_9$, $C10H_1$) 1.68 (s., 1 H, $C8H_1$) 1.86 (s., 1 H, $C10H_1$) 1.98 (s, 3 H, $C1H_3$) 3.11 (s., 2 H, $C11H_2$) 4.53 (s., 1 H, $C7H_1$) 5.37 (s., 1 H, $C2H_1$) 5.76 (s, 1 H, $C2H_1$).

HCl (3 mL of 4 N in dioxane) was added to the purified product for deprotection and stirred under nitrogen gas at room temperature for 4 hours. The solvent was evaporated under vacuum and the dried product was stored in the freezer. Yield: 2.1 g (60%) of a white sticky precipitate.

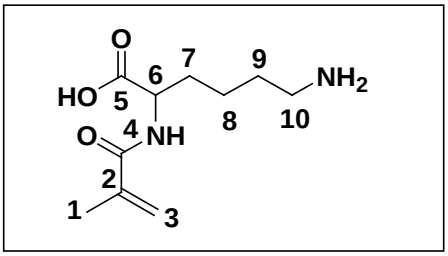

6-Amino-2-(2-methyl-acryloylamino)-hexanoic acid

6-Amino-2-(2-methyl-acryloylamino)-hexanoic acid: ^{1}H NMR (400 MHz, DMSO, 25˚C, TMS); δ ppm 1.34 (s., 2 H, $C8H_2$) 1.51 - 1.59 (m, 2 H, $C9H_2$) 1.73 (s., 2 H, $C7H_2$) 1.86 (s, 3 H, $C1H_3$) 2.76 (s., 2 H, $C10H_2$) 4.21 (s., 1 H, $C6H_1$) 5.38 (s., 1 H, $C3H_1$) 5.74 (s., 1 H, $C3H_1$) 8.04 (s., 1 H, NH). ^{13}C NMR (100 MHz, DMSO, 25˚C, TMS); δ ppm 19.30 (C1), 23.38 (C8), 27.15 (C7), 30.60 (C9), 39.13 (C10), 52.70 (C6), 120.36 (C3), 140.09 (C2), 168.44 (C4), 174.29 (C5).

Aspartic Acid monomer: 1-Hydroxybenzotriazole (HOBT) (0.676 g, 5 mmol, 1.0 eq.) and O-benzotriazole-N,N,N',N'-tetramethyl-uronium-hexafluorophosphate (HBTU) (1.896 g, 5 mmol, 1.0 eq.) were added to 1.409 g (5 mmol) of L-aspartic acid di-tert-butyl ester hydrochloride and 1.292 g (10 mmol, 2.0 eq.) of di-isopropylethylamine in 25 mL dichloromethane. Methacrylic acid (0.43 g, 5 mmol, 1.0 eq.) in 10 mL dichloromethane was added to the ice-cold solution dropwise and the reaction solution was stirred for 18 hours under nitrogen gas at room temperature. Solution was washed with 10% brine and the organic layer was collected. Aqueous 10% citric acid (2X) was used for washing next and the organic layer collected was treated with 4% sodium bicarbonate solution (2X). The organic layer was dried over Na_2SO_4, filtered and the solvent was removed under reduced pressure. The solid mass was purified using automated flash chromatography over silica gel with ethylacetate/hexane (**R_f = 0.5**; EtOAc : Hex = 1:1) as the mobile phase. White crystalline solids were obtained as the purified product.

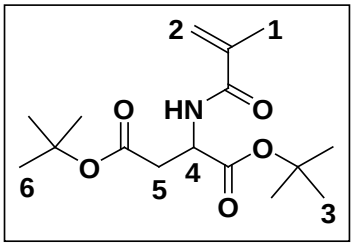

2-(2-Methyl-acryloylamino)-succinic acid di-tert-butyl ester

2-(2-Methyl-acryloylamino)-succinic acid di-tert-butyl ester: ^{1}H NMR (300 MHz, $CDCl_3$, 25˚C, TMS); δ ppm 1.46 (d, J=8.06 Hz, 18 H, $C3H_9$, $C6H_9$) 1.99 (s., 3 H, $C1H_3$) 2.74 (s., 1 H, $C5H_1$) 2.89 (s., 1 H, $C5H_1$) 4.74 (s., 1 H, $C4H_1$) 5.38 (s., 1 H, $C2H_1$) 5.78 (s, 1 H, $C2H_1$) 6.83 (s., 1 H, NH).

The product was treated with 3 mL of trifluoroacetic acid for deprotection. The solution was stirred under nitrogen for 6 hours. The solvent was evaporated and yellowish hygroscopic solidwas obtained. Yield: 0.92 g (65%).

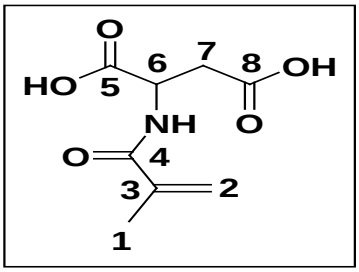

2-(2-Methyl-acryloylamino)-scuccinic acid

2-(2-Methyl-acryloylamino)-scuccinic acid : ^{1}H NMR (400 MHz, CD_3OD, 25˚C, TMS); δ ppm 1.96 (s., 3 H, C1H_3) 2.75 - 2.98 (m, 3 H, C7H_2, NH) 4.72 (s., 1 H, C6H_1) 5.43 (s., 1 H, C2H_1) 5.76 (s., 1 H, C2H_1). ^{13}C NMR (100 MHz, CD_3OD, 25˚C, TMS); δ ppm 19.15 (C1), 36.44 (C7), 49.61 (C6), 120.41 (C2), 140.04 (C3), 167.89 (C4), 172.50 (C5), 173.17 (C8).

Alanine monomer: 1-Hydroxybenzotriazole (HOBT) (0.676 g, 5 mmol, 1.0 eq.) and Obenzotriazole- N,N,N',N'-tetramethyl-uronium-hexafluorophosphate (HBTU, 1.896 g, 5 mmol, 1.0 eq.) were added to L-alanine-t-butyl ester hydrochloride (0.9085 g, 5 mmol) and diisopropylethylamine (1.2925 g, 10 mmol, 2.0 eq.) in 25 mL dichloromethane. Methacrylic acid (0.43 g, 5 mmol, 1.0 eq.) in 10 mL dichloromethane was added to the ice-cold solution drop wise and the reaction solution was stirred for 18 hours under nitrogen gas at room temperature. Solution was washed with 10% brine solution and the organic layer was collected. Aqueous 10% citric acid (2X) was used for washing next and the organic layer collected was treated with 6% sodium bicarbonate solution (2X). The organic layer was dried over Na_2SO_4, filtered and the solvent was removed under reduced pressure. The solid mass was purified using automated

flash chromatography over silica gel with ethylacetate/hexane ($\mathbf{R_f = 0.6}$; EtOAc : Hex = 1:1) as the mobile phase. White flakes were obtained as the purified product.

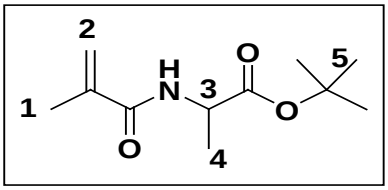

2-(2-Methyl-acryloylamino-propionic acid tert-butyl ester

2-(2-Methyl-acryloylamino-propionic acid tert-butyl ester: ^{1}H NMR (400 MHz, $CDCl_3$, 25˚C, TMS); δ ppm 1.11 (d, J=7.11 Hz, 3 H, $C4H_3$) 1.18 (s, 9 H, $C5H_9$) 1.67 (s, 3 H, $C1H_3$) 4.21 (s, 1H, $C3H_1$) 5.05 (s, 1 H, $C2H_1$) 5.45 (s, 1 H, $C2H_1$) 6.23 (s., 1 H, NH).

The intermediate was treated with 3 mL of trifluoroacetic acid for deprotection. The solution was stirred under nitrogen for 6 hours. The solvent was evaporated and whitish solid was obtained. Yield: 0.92 g (65%).

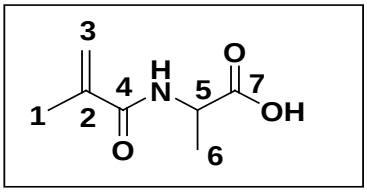

2-(2-Methyl-acryloylamino)-propionic acid

2-(2-Methyl-acryloylamino)-propionic acid: ^{1}H NMR (400 MHz, DMSO, 25˚C, TMS); δ ppm 1.12 (s, 3 H, $C6H_3$) 1.66 (s, 3 H, $C1H_3$) 4.08 (s., 1 H, $C5H_1$) 5.17 (s., 1 H, $C3H_1$) 5.53 (s, 1 H, $C3H_1$) 7.88 (s., 1 H, NH). ^{13}C NMR (100 MHz, $CDCl_3$, 25˚C, TMS); δ ppm 17.32 (C1), 18.56 (C6), 48.72 (C5), 121.74 (C3), 138.86 (C2), 169.13(C4), 176.38 (C7).

Inhibitor monomer: To a stirred solution 3-(trityloxycarbamoyl) propanoic acid (1.78 g, 4.74 mmol) and BOC deprotected methacrylic acid and spacer conjugation adduct [N-(2-(2-(2-

aminoethoxy)ethoxy)ethyl)-methacrylamide hydrochloride] (1.198 g, 4.74 mmol) in dichloromethane (60 mL) NMM (1.563 mL, 14.24 mmol) was added. The reaction mixture was stirred for 5 minutes and BOP (2.1 g, 4.74 mmol) was added all at a time. After overnight stirring at room temperature, the reaction was quenched with brine. Reaction mixture was further diluted with dichloromethane (100 mL) and the organic layer was washed with 10% citric acid, 5% $NaHCO_3$ solution. The resulting organic layer was dried over sodium sulfate, solvent evaporated off and the residue obtained was purified by flash chromatography (**R_f = 0.4**, 5% methanol in CH_2Cl_2) yielding 2.34 g of pure product. (Yield: 86%).

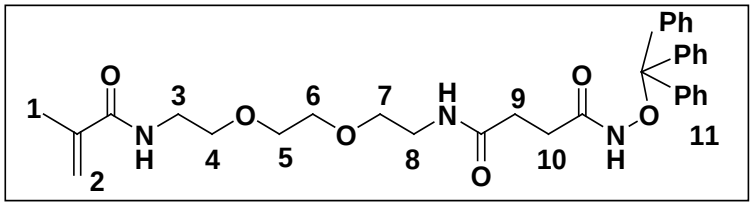

N-(2-{2-[2-(2-Methyl-acryloylamino)-ethoxy]-ethoxy}-ethyl)-N'-trityloxy-succinamide

N-(2-{2-[2-(2-Methyl-acryloylamino)-ethoxy]-ethoxy}-ethyl)-N'-trityloxy-succinamide: ^{1}H NMR (400 MHz, $CDCl_3$, 25°C, TMS); δ ppm 1.76 - 1.85 (m, 1H, $C9H_1$) 1.90 (s, 3 H, $C1H_3$) 2.01 -2.10 (m, 1 H, $C9H_1$) 2.11 - 2.20 (m, 1 H, $C10H_1$) 2.22 - 2.33 (m, 1 H, $C10H_1$) 3.21 - 3.64 (m, 12H, C3H-C8H) 5.64 (s, 1 H, $C2H_1$) 6.15 - 6.29 (m, 1 H) 6.30 - 6.50 (m, 1 H, NH) 6.53 - 6.71 (m, 1H, NH) 7.16 - 7.46 (m, 15 H, $C11H_{15}$) 8.04 - 8.19 (s, 1 H, NH).

This product (1.5 g, 2.61 mmol) was treated with 5% TIPS in TFA (5 mL) in dichloromethane (20 mL) for 2 hours. Majority of the solvent was evaporated off and excess ether was added to the reaction mixture after cooling. Resulting semisolid precipitation was allowed to settle for sometime and clear supernatant was decanted off. The precipitate was washed with ether and dried under vacuum. Final product obtained 0.6 g (64%); mp: 92-93 °C.

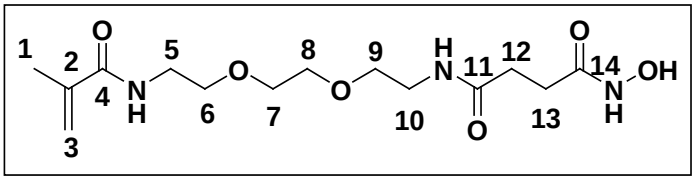

N-Hydroxyl-N'-(2-{2-[2-(2-methyl-acryloylamino)-ethoxy]-ethoxy}-ethyl)-succinamide

N-Hydroxyl-N'-(2-{2-[2-(2-methyl-acryloylamino)-ethoxy]-ethoxy}-ethyl)-succinamide: ^{1}H NMR (400 MHz, Methanol-d4, 25˚C, TMS); δ ppm 1.90 (s, 3H, C1H_3), 2.33 (s, 2H, C12H_2), 2.46 (s, 2H, C13H_2), 3.27 (s, 1H, C5H_1), 3.40 (s, 2H, C8H_2), 3.47-3.52 (m, 2H, C6H_2), 3.58 (s, 7H, C5H_1, C7H_2, C9H_2, C10H_2), 5.34 (s, 1H, C3H_1), 5.66 (s, 1H, C3H_1). ^{13}C NMR (100 MHz, DMSO, 25˚C, TMS); δ ppm 18.61 (C1), 27.80 (C12), 30.49 (C13), 38.53 (C10), 38.78 (C5), 68.80 (C7, C8), 69.09 (C6), 69.52 (C9), 119.04 (C3), 139.84 (C2), 167.51 (C4), 168.42 (C14), 171.13 (C11).

General procedure for polymer synthesis: All the monomers were weighed in proper mole % and dissolved in DMF (Table 5) for each polymer composition. Catalytic amount of the initiator AIBN in DMF (10-20 mg) was added to the reaction mixture. The reaction was degassed for 15 minutes and stirred for 24 hours at 60-62ºC. The reaction mixture was next diluted with 2 to 3 mL of methanol and the whole mixture was added to 10 times volume of ethylacetate. The polymers precipitated out. The solution was kept in freezer for 2-3 hours, centrifuged, washed with ethylacetate twice, dried in vacuum and kept in the freezer. The polymers were characterized by GPC using DMF as the solvent containing 0.1% LiBr (Table 6).

Fluorescence Spectroscopic Studies: The polymers (2 mg) were weighed and dissolved in 1 mL of 30 mM phosphate buffer (pH=7.4). Proper dilutions were performed to achieve the desired concentrations in the cuvette (Table 7). The fluorescence spectra of polymer was taken first with excitation wavelength to be 325 nm and emission recorded from 350 to 750 nm. Then

human recombinant MMP-9 (10 µL of 4.2 µM) was added to the cuvette and the solution was again excited at 325 nm. The emission spectra were recorded between 350 nm and 750 nm. Similarly for MMP-7 and -10, the same procedures were followed for each of the eleven polymers separately. Since for each polymer, the experiments with MMP-7, -9 and -10 were done separately for each of the isozymes, the fluorescence spectra were adjusted for the overlay graphs (Figure 15; Appendix Figure A.1.1-A.1.10). However, for the statistical data analysis, the ratios of the fluorescence intensities at 541nm before and after addition of isozymes from original fluorescence spectra were analyzed. The fluorescence of the solutions in absence and presence of the enzymes were recorded six times and the ratios of these six cycles were subjected to statistical analyses.

Table 5. Monomers used for the preparation of the polymers (**R1-R11**).

Polymers	Dansyl (mole %)	Asp. (mole %)	Lys. (mole %)	Alcohol (mole %)	Inhibitor (mole %)	Ala (mole %)
R1	10	-	-	80	10	-
R2	10	-	-	90	-	-
R3	10	-	10	80	-	-
R4	10	10	-	80	-	-
R5	10	10	10	70	-	-
R6	10	10	10	60	10	-
R7	10	10	-	70	10	-
R8	10	-	10	70	10	-
R9	10	-	-	80	-	10
R10	10	-	-	70	10	10
R11	10	10	10	50	20	-

Inhibition Assays: The inhibition assays were conducted using a 96-well fluorescence microplate containing 250 nM of the recombinant human MMP-9. Polymer samples were prepared in aqueous phosphate buffer (30 mM, pH = 7.4) and 50 nM or 100 nM of **R11** was used (final concentrations in the wells). The commercially available fluorogenic substrate (MCA-Pro-Leu-Gly-Leu-Dpa-Ala-Arg-NH_2.TFA) was used in the assay. The final concentration of the

substrate in the wells was 28 μM. The samples were excited at 325 nm and the emission intensity was monitored at 395 nm as a function of time for 30 minutes (Figure 16).

Table 6. The weight average (M_w), number average (M_n) molecular weights, polydispersity indices (P.I.) of the polymers (**R1-R11**).

Polymers	M_w	M_n	P.I.
R1	128,920	66,623	1.93
R2	107,291	43,945	2.44
R3	99,486	50,436	1.97
R4	119,800	52,727	2.27
R5	96,232	37,139	2.59
R6	94,514	52,959	1.78
R7	116,450	47,670	2.44
R8	93,405	47,258	1.98
R9	117,010	76,187	1.54
R10	106,802	67,273	1.59
R11	117,191	64,577	1.81

Table 7. Polymer concentrations used for the fluorescence experiments.

Polymers	Conc. used (nM)
R1	27
R2	34
R3	31
R4	28
R5	32
R6	34
R7	26
R8	36
R9	27
R10	30
R11	31

Results and Discussions

Using azoisobutyronitrile (AIBN) as the free-radical initiator, various random copolymers were synthesized. The synthesized sets of polymers were screened for selective interactions with MMP-9. The starting monomer compositions were varied systemically and the resultant polymers were tested for interaction with recombinant human MMP-7, -9 and -10.

Nanomolar concentrations of the polymer solutions (26-36 nM in 30 mM phosphate buffer, pH 7.4) were prepared and the enzymes were added to make 200 nM of the final enzyme concentration.

The changes in the emission spectra of the polymer-incorporated dansyl group were recorded in the region 350-750 nm (λ_{ex} = 325 nm). It was found that with the addition of the enzymes, the emission intensity decreased for all the isozymes (Figure 15; Appendix Figure A.1.1-A.1.10). One possible explanation for the reduced emission intensity could be that the polymer-incorporated dansyl groups were experiencing more hydrophilic microenvironments in the presence of the recombinant enzymes.

It was found that the relative decrease in emission intensity at 541 nm for all the eleven polymers depended on the polymer used and the MMP isozyme tested. The ratios of the fluorescence emission intensities in the absence and presence of the MMP isozymes were calculated and subjected to statistical analysis to determine their significance (Table 8; Appendix Table A.1.1, A.1.2).

Statistical Analysis: Statistical analysis was implemented to determine whether and to what extent each of the polymers selectively interacts with MMP-9 isozyme. A commonly used approach for such a large group (11 random polymers, three isozymes, and 6 replications) is the binary logistic regression. More specifically, each of the 18 x 1 data matrices containing the fluorescence intensities for a given polymer (6 replications and 3 MMPs per polymer) were 'stacked' or 'blocked together in order to create a large vector i.e. 198 x 1 of fluorescence intensity readings (11 polymers with 18 observations per polymer).

In the data matrix more additional columns were created by forming a series of binary variables which identify each polymer, and these binary indicator variables were subsequently

interacted with the fluorescence data to create a fully interacted data matrix (198 x 22). Finally three columns of binary variables were appended, where each new column identified a particular MMP (-7, -9 and -10).

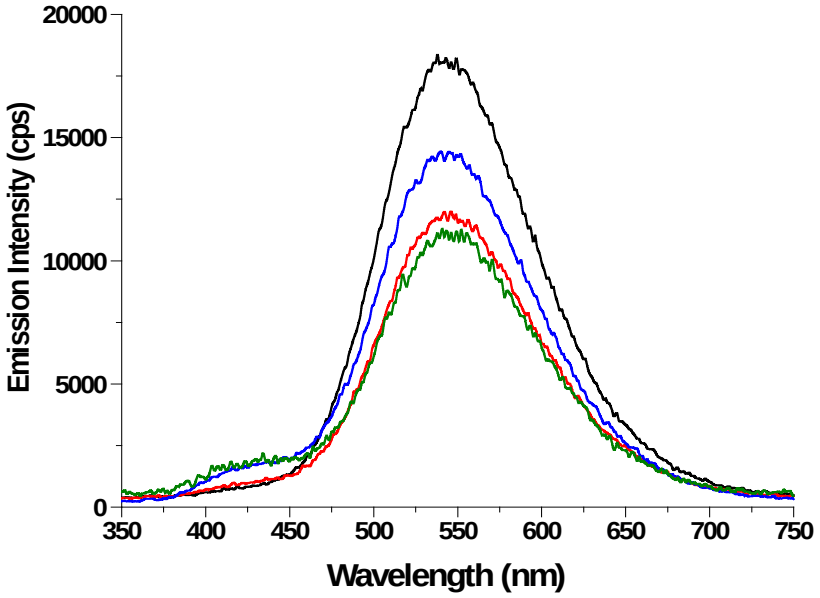

Figure 15. Fluorescence emission spectra of the polymer **R11** (31 nM in 30 mM phosphate buffer, pH = 7.4, λ_{ex} = 325 nm, black trace) in presence of 200 nM of recombinant human MMP-7 (red trace), MMP-9 (blue trace) and MMP-10 (green trace).

Table 8. Fluorescence ratios at 541 nm for polymers **R1-R11** against MMP-9 for 6 repetitions.

Polymers	Cycle 1	Cycle 2	Cycle 3	Cycle 4	Cycle 5	Cycle 6
R1	1.161	1.184	1.256	1.260	1.260	1.312
R2	1.090	1.081	1.060	1.039	1.074	1.036
R3	1.152	1.087	1.103	1.085	1.077	1.068
R4	1.151	1.192	1.165	1.191	1.103	1.170
R5	1.081	1.129	1.111	1.113	1.108	1.135
R6	1.205	1.201	1.205	1.157	1.117	1.080
R7	1.194	1.258	1.255	1.183	1.183	1.159
R8	1.276	1.206	1.227	1.184	1.142	1.110
R9	1.169	1.143	1.135	1.132	1.108	1.073
R10	1.337	1.368	1.298	1.304	1.283	1.225
R11	1.259	1.265	1.295	1.297	1.252	1.265

The value of this approach is that it allows for the estimation of a fully interacted logit model of the following form:

$$P(MMP_i^k = 1 \mid D, F) = \sum_{j=1}^{J} D_i^j \left(\beta_j + \gamma_j F_i^j\right) \quad \textbf{(Equation 2)}$$

$$P\,(MMP_i^k = 0 \mid D, F) = 1 - P\,(MMP_i^k = 1 \mid D, F) \quad \textbf{(Equation 3)}$$

where: i indexes each observation; P() denotes the cumulative logistic distribution; D is a binary indicator of each (j = 1,...,J) polymer, k denotes each isozyme (MMP-7, -9, and -10), F is the fluorescence of each isozyme; J denotes the number of polymers (11) and β, γ are parameter estimates. While this is estimated as single maximum likelihood estimation, the stacked data matrix allows separate intercept and slope estimates for each polymer included in the regression. That is, each of the polymer-specific response functions in a given group is "stacked" and estimated together to preserve adequate degrees of freedom to run the regression.

Because the goal of the analysis was to indentify which polymers selectively interacted with MMP-9, equation (3) was estimated as a binary logit model, where the dependent variable took a value of one for a MMP-9 isozyme, and zero if the isozyme was in the remaining categories (MMP-7, -10). This ensured a parsimonious estimation procedure without being forced to estimate equation (2) multiple times for each isozyme-copolymer grouping (MMP-9 versus MMP-7, MMP-9 versus MMP-10, etc.). Additionally, because each polymer had a separate response function with two parameter estimates (a slope and an intercept), results were presented using an odds ratio (with accompanying 95% profile confidence intervals) capturing the joint effects of these intercept and slope parameters for a given polymer on the MMP-9 isozyme. Values greater than unity (and whose confidence intervals did not contain a value of

one) indicated that the polymer significantly predicted or identified the given MMP relative to its alternatives (Appendix Table A.1.3-A.1.6).

Appendix Table A.1.6 identifies the polymers whose odds ratios were significantly greater than unity. This statistical analysis revealed that it was possible to design polymers that were able to selectively interact with isozymes within the MMP family. In particular, it was noted that polymer **R11** uniquely and significantly interacts with the MMP-9 isozyme out of all the eleven copolymers (Table 9).

R11 polymer contains the aspartic- and the lysine monomers (10 mol% each) and 20 mol% of the inhibitor monomer. Decreasing the amount of the inhibitor monomer to 10 mol% (i.e., polymers **R7**, **R8**) or omitting this monomer from the polymers (i.e., **R5**) led to the loss of selective interactions of the polymers with MMP-9 (Appendix Table A.1.3-A.1.6). Reducing the amount of inhibitor monomer (to 10 mol %) (i.e., polymer **R6**) or incorporation of the alanine-based monomer in the polymer (i.e., **R10**) also had negative effect on the selective interactions with MMP-9 (Appendix Table A.1.3-A.1.6).

Table 9. Estimates and p-values from the logit regression analyses.

Polymer	**R11**
Intercept	43.644
Intercept p-value	0.017
Slope	-32.235
Slope-value	0.016
Odds Ratio (OR)	187.598
95 % OR Lower confidence interval limit	1.347
95 % OR Upper confidence interval limit	> 999.999

Inhibition Assays: We also observed that the polymer **R11** (100 nM) was effective in inhibiting the activity of the enzyme MMP-9 (Figure 16). These observations suggest that the

inhibitor on the polymers interact with the active site of MMP-9 and the charged amino acids are forming additional interactions with the amino acid residues on the surface of the enzyme. To test this hypothesis, we synthesized a polymer **RX** (M_w = 77,485) with 30 mole % inhibitor monomer (10 mole % lysine monomer, 10 mole % aspartic acid monomer, 10 mole % dansyl monomer and 40 mole % alcohol monomer) and tested its activities against MMP-9. However, increasing the amount of inhibitor monomer to 30 mol% in the polymers did not improve the selective binding to MMP-9 (Figure 17). So polymer with 20 mole % of the inhibitor (**R11**) was taken to be the optimal composition for MMP-9 interaction.

Next it was determined if the selective interactions of the polymer **R11** was maintained in a complex mixture of proteins. The fluorescence emission from the polymer-incorporated dansyl group (λ_{ex} = 325 nm) was found to increase and blue-shift (about 100 nm; Figure 18) in the presence of dilute (less than 5% by volume) human serum in phosphate buffer (pH = 7.4). When this dilute human serum contained 200 nM of MMP-9 (levels of this enzyme in bronchial lavage fluid from lung cancer patients), the emission intensity was substantially increased and blue-shifted (Figure 18, blue trace). The same trends were observed when the human serum contained either 200 nM MMP-7 (Figure 18, olive trace) or 200 nM MMP-10 (Figure 18, magenta trace). This indicated that the polymer-incorporated dansyl fluorophore was experiencing a more hydrophobic microenvironment in the presence of dilute human serum and the MMPs. Clearly, the emission intensity in the presence of MMP-9 was substantially more pronounced in the presence of MMP-9 compared to MMP-7 and -10. Increasing the amount of human serum to more than 5% (by volume) led to the loss of the selective enhancements of the polymer emission intensity in the presence of MMP-9.

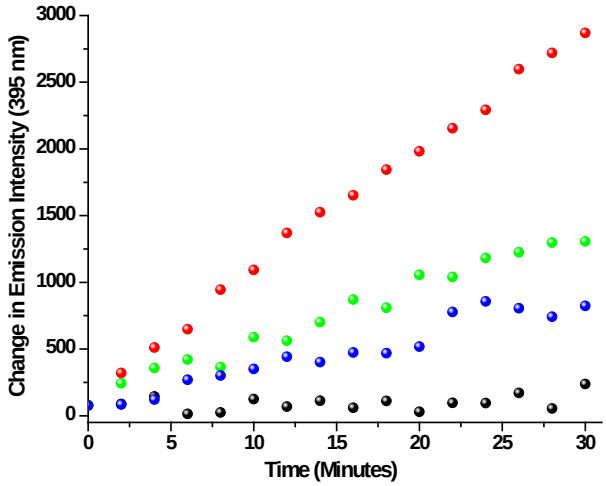

Figure 16. Emission intensity changes (395 nm) for MMP-9 inhibition assay in the absence (red spheres) and in the presence of 50 nM (green spheres) and 100 nM (blue spheres) polymer **R11** are shown. The black spheres are the blank and indicate the emission changes in the absence of MMP-9. These experiments were conducted in 25 mM HEPES buffer (pH = 8.0) with excitation at 325 nm.

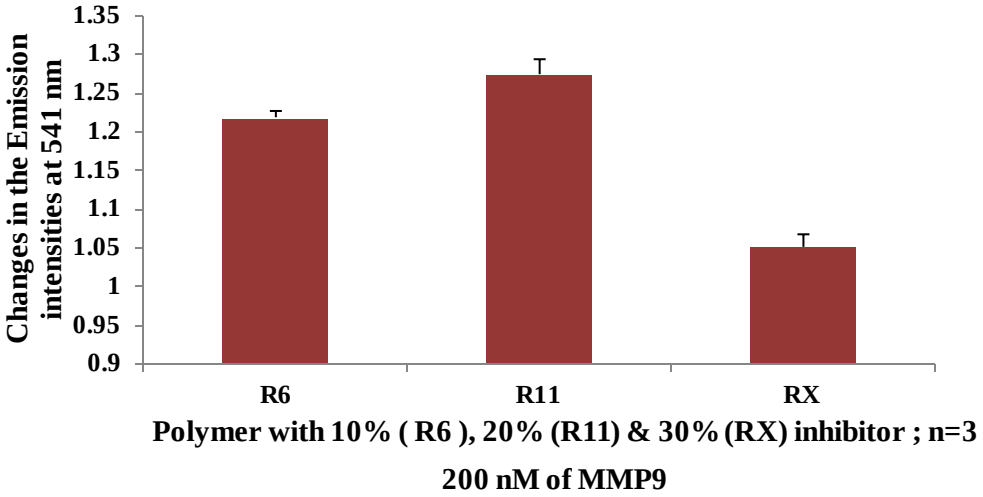

Figure 17. Emission Intensity changes at 541 nm for polymers **R6** (with 10 mole % inhibitor monomer), **R11** (with 20 mole % inhibitor monomer) and **RX** (with 30 mole % inhibitor monomer) for MMP-9.

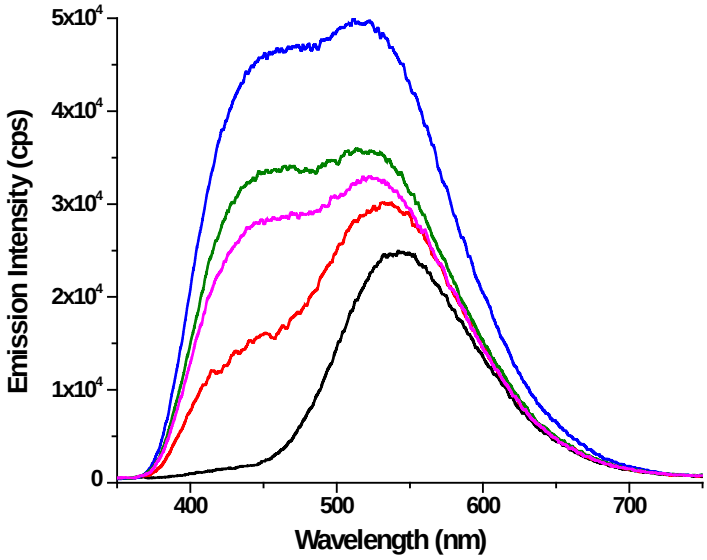

Figure 18. The fluorescence emission spectra of polymer **R11** (50 nM) in phosphate buffer (30 mM, pH = 7.4, λ_{ex} = 325 nm; black trace) was found to increase and blue-shift in the presence of dilute (2% by volume) human serum (red trace). The emission intensity changes were more pronounced when the dilute serum contained 200 nM MMP-9 (blue trace) compared to 200 nM MMP-7 (olive trace) or 200 nM MMP-10 (magenta trace).

Conclusion

In conclusion, we have synthesized flexible, water-soluble polymers containing charges and a weak inhibitor for the MMPs. The fluorescence emission data of the interactions of the polymers with the isozymes were analyzed by statistical tools and one of the polymers, **R11** was found to significantly interact with MMP-9 compared to MMP-7 and MMP-10. Polymer **R11** also demonstrated selective interactions with the isozyme MMP-9 compared to MMP-7 and -10, even in a complex mixture of proteins (e.g., dilute human serum). A second batch of **R11**was synthesized and fluorescence experiments with MMP-7, -9 and -10 were performed separately. The ratios generated from the second batch of the polymer **R11**with the isozymes were almost similar compared to the first batch of the polymer. We anticipate that by incorporating more

potent and selective MMP inhibitors in the polymer and by optimizing the polymer structures, the selectivity of the interactions with MMP-9 could be further enhanced.

CHAPTER II. DIFFERENTIATION OF CANCER CELL LINES USING WATER-SOLUBLE FLUORESCENT POLYMERS

Abstract

Cancer cells overexpress various extracellular enzymes e.g. MMP-7, MMP-9, urokinase plasminogen activator (uPA) and also membrane–bound enzymes such as a disintegrin and a metalloproteinase (ADAMs) in different amounts. Prostate cancer is among the most frequent cancers among men and breast cancer is among women. Early stage prostate cancer cause no symptoms, however, analysis of blood, urine and use of tumor biomarkers such as prostate – specific antigen (PSA) are the conventional methods of clinical diagnosis of early prostate cancer. But in many cases the PSA analysis leads to over diagnosis of the cancer stage. In case of breast cancer, symptoms such as occurrence of a new lump of mass and pain allows for early diagnosis with imaging tests such as x-rays (mammograms), magnetic fields, sound waves and use of radioactive substances. Although tissue biopsy is performed for laboratory examination of breast cancer cells, distinguishing breast cancer cells from non cancerous cells and subtyping of various cancers cell types require new non-invasive techniques.

Fluorescent polymers have been reported to distinguish between different proteins, isozymes and were shown to differentiate between cancerous cell lines from non cancerous cell lines. But for clinical diagnosis polymers have not been used yet. In this chapter we have discussed the applicability of the polymer **R11** synthesized and characterized in chapter 1 to differentiate between prostate cancer cell lines from non cancerous cell lines and also for subtyping breast cancer cells. Polymer **R11** was used for distinguishing 22Rv1 from PC3 (both prostate cancer cell lines) and through linear discriminant analysis (LDA) it was to proved that

the polymer could not only discriminate between various prostate cell lines but also PANC1 (pancreatic cancer) and noncancerous cell line (HEK-293). Similarly the LDA analysis also suggested that **R11** was able to distinguish between two breast cancer cell lines (MDA-MB-231 and MCF-7), non-breast cancer cell line (HeLa) and a non-cancerous cell line (HEK-293).

Introduction

Prostate cancer is the one of the most malignant cancers among men in the United States (*131*). For early diagnosis and treatment, prostate specific antigen (PSA) screening is the widely used technique followed by digital rectal examination (DRE) and trans-rectal ultrasound (TRUS) imaging. Also needle biopsy and radioimmunoassay of PSA are also prevalent (*132*). Usually the PSA level rises up in the cancerous condition and is considered as a biological tumor marker for that reason (*133*). The U.S. Food and Drug Administration (FDA) have approved the PSA test with DRE for prostate cancer detection in men older than 50 years. However, the PSA level does not give a full proof of the presence of cancer and often the physicians consider it as a first-hand approach for proceeding for further symptoms. So researchers are also striving for other methods of detection along with PSA and DRE (*134*). These include recognizing the micro-RNA pattern, gene fusion, non-mutation gene alterations (*135*), (*136*). Park et al showed *TMPRSS2-ERG* gene fusion was the basis of detection which was found to be positive in prostate cancer. Anti-ERG monoclonal antibody was implemented for immunoblot analysis together with immunohistochemistry and *in situ* fluorescence hybridization (*137*).

Breast cancer is among the most prevalent cancers among women (16 %) and is diagnosed in women of all ages (mostly above 50 years). The survival rate is almost 80 % in the developed nations and the success mainly depends on its early detection and treatment. There are various methods available for breast cancer detection like screening the cancer at an early

stage, examination and mammography (*138*). Screening could be dependent on self examination or clinical examination but the mammography is regarded as the best way to detect and improve the cancer. Mammography is primarily X-ray imaging and 80 to 90 % of the results are found to be accurate. Although screen-film mammography and other imaging techniques provide nearly accurate and acceptable outcomes, there are limitations in these techniques. The imaging techniques usually require trained technicians and developed instruments and various chemicals. Moreover, the process also requires radiation exposure and often the compression leads to patient discomfort. Other instrument aided modalities for detection involve the use of computer-aided detection (CAD), full-field digital mammography (FFDM), sonomammography using ultrasound (US), magnetic resonance imaging (MRI) and various nuclear medicines using thallium and technetium radioisotopes. Positron emission mammography (PET), diffuse optical imaging using near infrared light, thermography and Raman spectroscopy in tissue samples are some of the other methods for breast cancer detection known till date (*139*). Use of diffuse reflectance spectroscopy (DRS) and intrinsic fluorescence spectroscopy (IFS) were explored by Volynskaya et al for identification and detection of breast cancer lesions. These techniques are optical spectroscopic-based in nature and are used to differentiate between malignant and non-malignant tissues (*140*).

In case of breast cancer various hormone receptor markers are usually targeted for prognosis and therapy. For most of the breast cancer cases, estrogen receptor (ER) and progesterone (PR) expression have been related to this kind of pathology and have been validated from the clinical point of view. These receptors are usually detected by immunohistochemistry (ICH) and require anti-ER and anti-PR antibodies. An important oncogene transmembrane glycoprotein is human epidermal receptor protein-2 (c-erbB-2 or

HER2) which belongs to the epidermal growth factor receptor class. HER2 overexpression is considered to be a crucial biomarker for breast cancer and treatment with trastuzumab (monoclonal antibody) has been proven to be very effective in reducing the mortality rate in early-stage patients. In addition to ICH, fluorescence *in situ* hybridization (FISH) is an alternative way for detection, however, various disagreements exist between the results from ICH and FISH (*141*). Implementing unique detection method and choice of a prognostic biomarker can yield better treatment scope for this disease condition.

Conventional methods of cancer cells detection rely on the detection of the specific markers on the cells surface and creating appropriate ligands for those receptors. Usually antibody-based biomarkers are explored for targeting diverse cancer cell surface receptor targets. However, these techniques although useful require extensive knowledge of the cell surface morphology and ligand designing. An alternative strategy could be based on creating biosensors which would be more general and the binding with the various cells would be based on merely electrostatic interaction rather than traditional receptor-ligand 'lock and key' binding. Various researchers have actually developed biosensing synthetic polymers that could bind to the cancer cells surface on the basis of charged interactions (*142*).

For *in vitro* detection of cancer cell lines various systems such as nanoparticles and polymers have been developed which have been conjugated with a fluorophore imparting optical labels and better sensitivity. Maldiney et al showed the use of modified persistent luminescence nanoparticles (PLNPs) to detect prostate cancer cells (PC3) *in vitro* (*143*). Miranda et al used conjugated polymers (functionalized poly (p-phenyleneethynylene) for sensing both metalloproteinases as well as nonmetalloproteinases. It was found that the fluorescence emissions from the poly (p-phenyleneethynylene) (PPE) polymers were quenched upon

differential protein binding (*144*). In another report the same group reported how nanoparticles could be used as "chemical noses" or sensors for detection of not only proteins but also bacteria and cells. Gold nanoparticles conjugated fluorescent polymers worked as fluorescent switch on/off sensors thus creating finger print responses for individual different proteins (*145*). Folate acid grafted PPE polymers were also applied by Kim et al for *in vitro* targeting of KB cancer cells providing better photochemical stability and minimum cytotoxicity (*146*).

Rotello et al. have demonstrated the use of conjugated polymers for detection of various types of cell lines. These polymers acted as biosensor responding to the environmental change thus undergoing conformational modifications. The fluorophores in these polymers signaled these changes and thus give an indication of binding interactions with the various analytes. Detection of cancer cells from normal cells were achieved by PPE-based fluorescent polymers which were comprised of various charged residues in them and varied in degree of polymerization among them. The novelty in these polymers were that they were not based on any specific ligand or receptor targeted and solely depends on electrostatic interactions between the ionic polymers and general cell surface lipids, proteins and various polysaccharides. With the help of linear discriminant analysis (LDA), it was proved that these polymers can serve as useful tools for differentiating various cancerous cell lines having the same genetic basis (*142*).

In this chapter my optimal polymer, **R11** from the previous study has been used to subtype cancer cells as well as to differentiate cancer cells from non-cancerous cells based on the secretion of MMP-9 levels from these cell lines. These studies were performed separately for prostate cancer cell lines and breast cancer cell lines to understand how this polymer behave and to what extent it could serve the dual purpose of subtyping and differentiation among various cell lines.

Materials and Methods

Synthesis and characterization of Polymer R11: Monomers (as reported in chapter 1) were used to prepare polymer **R11** using AIBN as the free-radical initiator. In chapter 1 it was already reported that polymer **R11** was optimal for distinguishing recombinant human MMP-9 from MMP-7 and MMP-10. Polymer **R11** was prepared using the monomers with methacrylamide as the polymerizable group containing 50 mole % of the alcohol monomer, 10 mole % of the lysine monomer, 10 mole % of the aspartic acid monomer, 10 mole % of the dansyl (fluorophore) monomer and 20 mole % of the inhibitor monomer (details Chapter 1). The synthesized polymer was characterized by gel permeation chromatography (GPC) (Table 10). Polymer solutions were made in 30 mM phosphate buffer, pH 7.4 and final concentration used in all the fluorescence studies was 31 nM.

Table 10. Molecular weights of polymer **R11** determined by GPC.

Polymer	M_w	M_n	Polydispersity index (P.I.)
R11	117191	64577	1.81

Cellular Studies: All cell lines were obtained from American Tissue Culture Consortium (ATCC) and were cultured as instructed and maintained at 37ºC in an atmosphere of 5 % CO_2 in humidified air. For the breast cancer subtyping studies, HEK-293, MCF-7 and HeLa were all grown in MEM media with 10 % fetal bovine serum (FBS) and 1 % antibiotics. MDA-MB-231 was grown in DMEM media with 10 % FBS and 1 % antibiotics. PANC-1 was grown in DMEM media and 22Rv1 and PC3 were grown in RPMI media for the prostate cancer studies. The cells were all sub-cultured (each 3-5 days) until confluency and were splitted thrice in their respective phenol red containing media. The cells were then splitted twice (each 3-5 days) in

their respective dye-free media. HBSS and Trypsin-Versene were used for every split. Upon reaching confluency, the cells were then aseptically transferred from the culture flask into centrifuge tube. The cells were then centrifuged down at 1500 rpm for 8 minutes to pellet and remove any remaining cells and the supernatant was stored at -20ºC for fluorescence studies.

ELISA (Enzyme-linked Immunosorbent Assay): For the evaluation of the concentration of the MMP-9 in the conditioned media, we performed ELISA using our conditioned media from the cell lines. Human MMP-9 ELISA Kit from RayBiotech, Inc. (Cat # ELH-MMP9-001), was used following the instructions within the kit. Calibration curves were made using the recorded absorbance of the solutions at 450 nm and the concentrations of MMP-9 in the different conditioned cell culture media (50 µL) were determined from the calibration curve. Calibration curves were made separately for breast and prostate cancer cell lines and the concentrations of MMP-9 in each cell lines were calculated accordingly (Appendix Figure A.2.1 and Figure A.2.2).

Fluorescence Spectroscopy Studies: The fluorescence experiments were performed using Fluoromax-4 Spectrofluorometer by Horiba Jobin Yvon. 2 mg of polymer **R11** was weighed and properly diluted in 30 mM phosphate buffer solution, pH 7.4 to achieve 31 nM concentration in the cuvette. 50 µL of conditioned cell culture media was added to 200 µL solution of the polymer and mixed in the cuvette. The solution was excited at 325 nm and the emission spectra were recorded between 350 nm to 700 nm. The first peak was noticed at 420 nm and a second peak at 541 nm. The same procedure was followed for recording the emission spectra of the polymer in the presence of unconditioned media i.e. dye-free media before cell culture.

Fluorescence Ratio Determination: In order to mathematically eliminate the fluorescence signal contributions from the media, we choose to calculate the ratios of the conditioned cell culture media over the corresponding unconditioned media at different wavelengths. Since cells were grown in various different cell culture media like DMEM, MEM, RPMI, any potential variation that might be caused due to the unconditioned media was eliminated by performing the ratio step. The ratios were calculated at three different emission wavelengths 420 nm, 523nm and 541 nm for 8 cycles each (Appendix Table A.2.5 for prostate cancer cell lines and Appendix Table A.2.6 for breast cancer cell lines).

$$\text{Ratio of fluorescence intensity at particular emission wavelength} = \frac{\text{Fluorescence intensity for conditioned cell culture dye-free media}}{\text{Fluorescence intensity for specific unconditioned dye-free media}}$$

Statistical Data Analysis: The ratios were collected and subjected to linear discriminant analysis (LDA) to accurately quantify the fluorescent trends. LDA was performed separately for the prostate cancer cell lines and breast cancer cell lines ratios.

Results and Discussions

The polymer **R11** was expected to interact with MMP-9 using a variety of noncovalent interactions. The polymer contains an attached MMP inhibitor (from the inhibitor monomer 5). The hydroxamic acid moiety interacted with the Zn^{2+} ion in the active site pocket. In chapter 1 it has been already demonstrated that 100 nM of the polymer effectively inhibit 250 nM recombinant MMP-9. This interaction could serve as the initial anchoring site for MMP-9 to the polymer **R11** and facilitate the formation of the additional surface binding interactions to the enzyme. The polyamide backbones of the polymers can form hydrogen bonds with enzyme surface. Lysine (positive charge) and aspartic acid (negative charge groups on the polymers can

interact with complementary charges on the enzyme's surface. Hydrogen bonding interactions with the enzyme are also possible from the polymerized alcohol monomer.

The fluorescence experiments revealed variations in emission spectra of the polymer **R11** when exposed to the conditioned cell culture media from different cells. The emission spectra of the polymer in the presence of media before cell culture were used as the control for these experiments. The control emission spectra of the polymer were subtracted from the emission spectra in the presence of the conditioned media to generate the corresponding difference spectra. (Figure 19 for prostate cancer cell lines and Figure 20 for breast cancer cell lines).

The emission spectra of **R11** were found to be blue-shifted in the presence of the conditioned cell culture media, indicating the dansyl fluorophores in the polymer were experiencing more hydrophobic microenvironment. The emission intensity of the polymer increased in the presence of the conditioned media from the cells 22Rv1 and HEK-293 and decreased in the presence of the conditioned media from PANC-1 and PC3 (Figure 19).

The difference spectra (Figure 20) indicated that each polymer responded differently to the conditioned cell culture media tested. In the presence of most of the conditioned media (excepting MDA-MB-231cells), the emission from the dansyl groups increased in intensity and the emission maxima were blue-shifted. This indicated that the dansyl groups in the polymer were experiencing more hydrophobic micro-environments in the presence of conditioned cell culture media. This behaviour of the different spectral pattern observed due to the presence of the conditioned media from the multi-drug resistant MDA-MB-231 is ambiguous and requires further studies.

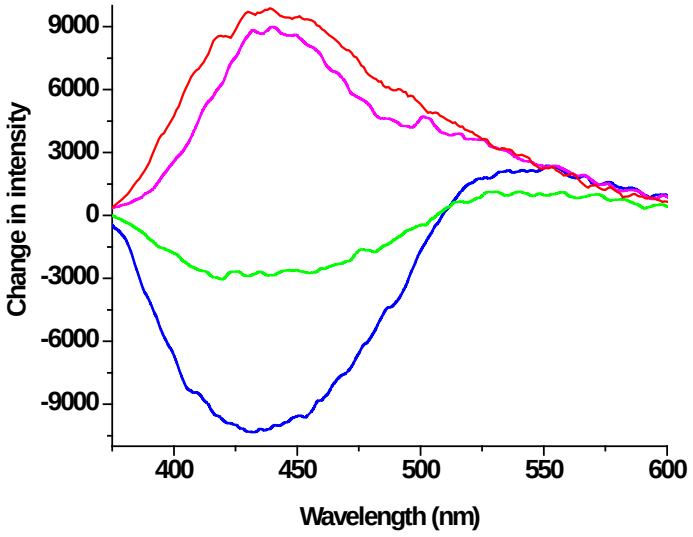

Figure 19. The difference emission spectra for the polymer **R11** in the presence of conditioned cell culture media from the cancer cells PANC-1 (blue trace), PC3 (green trace), 22Rv1 (pink trace) and HEK-293 (red trace). The emission spectra in the presence of unconditioned media were subtracted from the emission spectra in the presence of conditioned media to generate these plots.

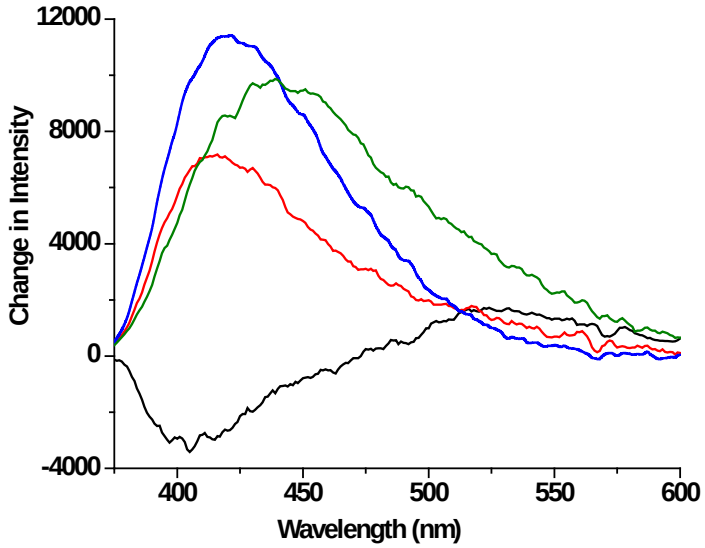

Figure 20. The difference emission spectra for polymer **R11** in the presence of conditioned cell culture media from MCF-7 (red), MDA-MB-231 (black), HeLa (blue), and HEK-293 (green). The plots were generated by subtracting unconditioned media from conditioned media.

ELISA: In order to find whether these intensity changes correlate with the levels of MMP-9 secreted by the cells, the total concentration of MMP-9 (active and inactive both) was determined in the conditioned cell culture media employing a commercial available ELISA kit. For the prostate cancer cell line study, it was observed that the PANC-1 cells secreted the highest amount of MMP-9 in the conditioned media (2 ng/mL) and the amounts of MMP-9 secreted by the other cells (PC3, 22Rv1 and HEK-293) were similar (740-780 pg/mL) (Appendix Table A.2.4). The concentrations of MMP-9 in the conditioned cell culture media for breast cancer cell studies indicate 170.5 pg/mL of MMP-9 for MDA-MB-231, 162 pg/mL for HEK-293, 268.75 pg/mL for HeLa and 969.5 pg/mL for MCF-7 (Appendix Table A.2.2). Clearly, the changes in the emission intensity of the polymer did not correlate with the concentration of the secreted MMP-9. Other proteins in the conditioned media are interacting with the polymer, causing the observed intensity changes, we reasoned that these differential modulations can be used to distinguish the cancer cells.

Statistical Data Analysis: Linear Discriminant Analysis has been used extensively in the literature and within this analysis, we assess the LDA results using several standard metrics. Standard F tests and Wilks' Lambda values were used to access mean differences across each of our cell lines and identify the ability of the predictor variables (the emission intensities for the polymer **R11**) to discriminate across the four cell lines. The significance of the canonical correlations discriminant functions were assessed using chi-square tests. An overall "potency index" for the predictor variable (emission intensity) was used to identify the predictor variables which play the largest role in the entire system of canonical discriminant functions. Higher values for each index signaled the overall importance of each predictor variable to the model as a whole. Overall model fit was assessed by examining canonical function plots to identify whether

each of the group centroids (one for each of the four cell lines) is sufficiently distinct. A large amount of overlap between the data points of two or more groups indicated poor discrimination across the cell lines, and by extension poor model fit. The model's internal validity was assessed by comparing the percentage of cell line observations that were correctly predicted by the model. All predicted values were computed using both traditional and (leave one out) cross-validation techniques. Models with a high degree of internal validity should correctly predict a high percentage of observations, and display consistency in predicted values across both techniques. All statistical analyses were conducted using the PASW (formerly SPSS) Statistical Package, Version 18.

The polymer **R11** exhibited multiple peak emission intensity ratios at 420 nm, 523 nm and 541 nm. The appearance of multiple peaks was an issue which potentially confounds the empirical analysis. Any results are potentially confounded without first identifying a true peak value, since the given polymer found to be inferior. This may be because the polymer does not adequately discriminate between the different cell lines or because the emission intensities recorded for the polymer-cell line pair in question were not evaluated at their maximum values. Linear discriminant analysis was applied in a stepwise manner for each kind (prostate and breast cancer separately) to account for this possibility.

LDA for breast cancer cell lines: LDA was applied to evaluate which of the three ratios provided the maximum discrimination (*i.e.* best predictor) between the cell lines. First, LDA was applied to the polymer, where each potential peak value based on its ability to discriminate between (or predict) the four cell lines (MCF-7, MDA-MB-231, HeLa and HEK-293) were evaluated. Each of these analyses was conducted using 32 observations (4 cell lines x 8 replications) and 4 variables (the cell line indicator and the three emission intensity wavelength

variables). This LDA analyses step identified the optimal intensity of 420 nm for the **R11** polymer. Because there is prior information identifying each of these wavelengths (420 nm, 523 nm and 541 nm) as potential candidates for inclusion in the final analysis (as well as a sufficient number of observations), the conservative approach of including all three wavelengths in a given LDA procedure was taken, as opposed to using a second stepwise procedure where wavelengths are eliminated using a Wilks' Lambda or F-statistic prior for identifying the discriminant functions. The analysis was replicated using a second set of stepwise LDA procedures, and these replications produced very similar results. Once the optimal emission intensities for each polymer are identified, a third application of LDA was used to compare the optimal wavelengths that were identified in the previous two applications of LDA.

As noted earlier, the emission intensity giving polymer **R11** the "best" predictive power occurred at 420 nm. Table 11 shows F-statistics and Wilks' Lambda values for the polymer, disaggregated by cell line type. All F-statistics have associated p-values less than 0.05 indicating significant differences exist across group means for each cell lines. Additionally, the HeLa cell line exhibits the highest mean emission intensity value, while the MDA-MB-231 cell line exhibits the lowest mean value. For the MDA-MD-231 cell line, the 541 nm emission intensity appears to be the highest value. For all other cell lines, the highest mean emission intensities appear at 420 nm. Wilks' Lambda values are lowest for 420 nm, followed by 523 nm and 541 nm.

Figure 21 contains a canonical function plot of the first two canonical functions (explaining 99.9% of the variation in the cell lines) (details Appendix Table A.2.7-A.2.10). It is noted that each of the cell line is clearly distinguished as a group in the plot. Moreover,

traditional and cross-validated discriminant functions each correctly predicted 100 % of the cell lines, respectively, indicating a high likelihood of interval validity.

Table 11. Tests of equality of group means for polymer **R11** at the three wavelengths for breast cancer cell line studies.

Cell lines	Polymer **R11** 420 nm[a,b]	Polymer **R11** 523 nm[a,b]	Polymer **R11** 541 nm[a,b]
MDA-MB-231	0.930	1.059	1.066
MCF-7	1.675	1.085	1.065
HeLa-293	2.032	1.067	1.030
HEK-293	1.805	1.253	1.189
Wilk's Lambda	0.016	0.065	0.072
F-Statistic	570.909	134.082	120.093
P-value	< 0.001	<0.001	<0.001

[a] first panel provides group-specific means [b] second panel provides statistics and p-values.

On total, the LDA had a clear and intuitive interpretation. The results in Table 11 suggested that the first canonical function was, by far, the most important discriminant function. Appendix Table A.2.9 and Appendix Table A.2.10 jointly suggested that the 420 nm variable contributeed the most towards the first canonical discriminant function, while the 523 nm and 541 nm variables contributed relatively more to the second and third canonical discriminant functions. This implied that the 420 nm emission intensity was the "best" determinant of the cell lines for the polymer.

LDA for prostate cancer cell lines: Table 12 provided means, F-statistics and Wilks' Lambda values for the polymer **R11** emission intensities at 420 nm, 523 nm and 541 nm, and for each cell line type (PANC-1, PC3, 22Rv1 and HEK-293). All F-statistics had significant p-values (less than 0.05), indicating that significant (joint) differences existed across group means for each cell lines. For the HEK-293 and 22Rv1 cell lines, 420 nm emission intensity appeared

to be the highest value. It was found that 541 nm intensity to be highest for the PANC-1 and PC3 cell lines. Wilks' Lambda values were lowest for 420 nm, followed by 523nm and 541 nm.

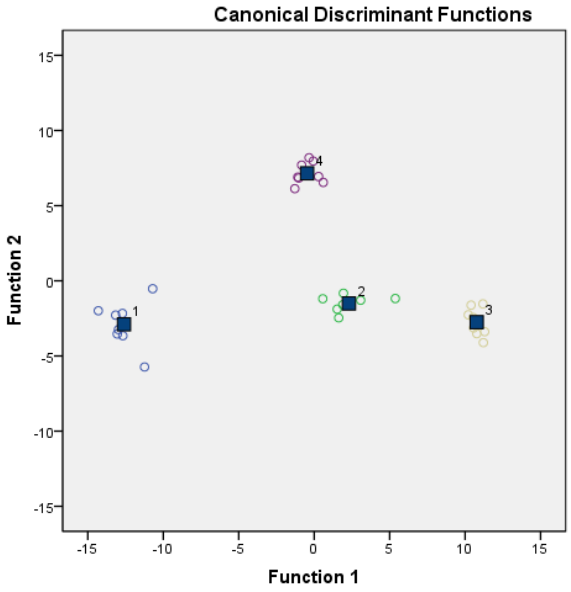

Figure 21. Polymer **R11**'s canonical correlation plot between two largest canonical correlations and each of the four cell lines: MDA-MB-231 (group 1), MCF-7 (group 2), HeLa (group 3) and HEK-293 (group 4).

Table 12. Tests of equality of group means for polymer **R11** at the three wavelengths for prostate cancer cell line studies.

Cell lines	Polymer **R11** 420 nm[a,b]	Polymer **R11** 523 nm[a,b]	Polymer **R11** 541 nm[a,b]
PANC-1	0.769	1.060	1.092
PC3	0.850	1.051	1.066
22Rv1	1.462	1.219	1.163
HEK-293	1.805	1.253	1.189
Wilk's Lambda	0.020	0.069	0.206
F-Statistic	466.379	126.376	36.067
P-value	< 0.001	<0.001	<0.001

[a] first panel provides group-specific means [b] second panel provides statistics and p-values.

Figure 22 contained the canonical function plot of the first two canonical functions (explaining 99.8% of the variation in the cell lines) (details Appendix Table A.2.11-A.2.13). All four cell lines were clearly distinguished as unique groups in the plot (although the PANC-1 and PC3 lines were relatively close together). Traditional and cross-validated discriminant functions each correctly predicted 93.8 % and 87.5 % of the cell lines, respectively, indicating a reasonable degree of interval validity.

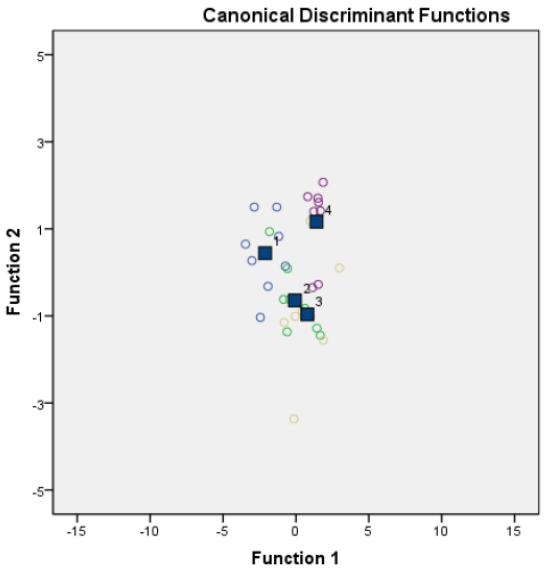

Figure 22. Polymer **R11**'s canonical correlation plot between two largest canonical correlations and each of the four cell lines: PANC-1 (group 1), PC3 (group 2), 22Rv1 (group 3) and HEK-293 (group 4).

Conclusion

In conclusion, the optimized polymer **R11** containing an inhibitor for the Zn^{2+} containing metalloenzyme MMP-9 showed differential modulations in emission spectra in the presence of conditioned cell culture media from various cancer cells. The ELISA assays indicated lack of correlations with the amount of secreted MMP-9 in the conditioned media, which suggested that other proteins in the conditioned media are nonspecifically interacting with the polymer. Due to

the hydrophilic nature of the polymer, surface binding interactions with MMP-9 could be the main binding event, although other contributing factors including a reduction in flexibility and increased steric hindrance should not be overlooked. The polymer accomplished the overall goal of simple, inexpensive and robust methodology for subtyping various prostate as well as breast cancer cell lines.

CHAPTER III. DISTINGUISHING CARBONIC ANHYDRASE ISOZYMES EMPLOYING WATER-SOLUBLE FLUORESCENT POLYMERS

Abstract

Carbonic anhydrases (CAs) are zinc containing metalloenzymes and are responsible for the reversible hydration of carbon dioxide to bicarbonate and proton. As such they are quite important in physiological conditions and their over expression leads to various pathologic conditions which cannot be overlooked. This enzyme family constitute of 16 isozymes of which some share their role in diseases such as glaucoma, diabetes, epilepsy and even cancer. Although pharmaceutical industries have come up with inhibitors for treating glaucoma and epilepsy, for the treatment of cancer more information is needed for each isozymes. These 16 isozymes work in various biochemical pathways and their functions are interrelated. Keeping this knowledge in mind and from the encouraging results obtained from my previous work on matrix metalloproteinases, we became interested in selective recognition of one isozyme of the CA enzyme family. Since the isozymes catalyze the same chemical reaction, their active sites are similar. However, the solvent-exposed surfaces of the isozymes are not under evolutionary pressure and thus not conserved. It is because that the surface patterns of the amino acids are different, we reasoned that flexible polymers can be suitably constructed to achieve selective binding to an isozyme. Specifically, if a modest inhibitor for the enzyme family is incorporated, it will serve as the initial anchoring site for the proteins on the polymer and facilitate the formation of additional simultaneous and complementary interactions between the polymer and the isozymes. Herein, report of a set of fluorescent, inhibitor incorporated, flexible, water-

soluble polymers and their selective interaction with carbonic anhydrases (CAs) isozymes CA II, CA VII, CA XII has been elaborately discussed. It was observed that the selective binding of one of the polymers to CA II was retained even in a complex mixture of biomolecules, e.g., cell culture medium containing 10% by volume of fetal bovine serum.

Introduction

Carbonic Anhydrases (CAs, EC 4.2.1.1) are a family of Zn^{2+} metalloenzymes responsible for catalyzing the reversible hydration of carbon dioxide to bicarbonate and proton. α, β, γ and δ forms of CA are found of which the latter two are abundant in bacteria, archaea and plants. Among higher vertebrates 16 different isoforms of α-CA are isolated. Out of these, CA I, II, III and VII are cytosolic, CA V is found in mitochondria, CA VI gets secreted in the saliva and CA IV, IX, XII and XIV are all membrane-bound. The rest CA VIII, CA X and CA XI are acatalytic forms and are called as CA related proteins or CARP (*147*).

The α-CAs have metal zinc in the active site co-ordinated with three histidine residues (His 94, His 96 and His 119) and a water or hydroxide ion which acts as a nucleophile (*50*). CA II is involved in glaucoma, hypertension, diabetes, epilepsy, and various cancers (*48*). Currently, clinically approved inhibitors for CA II are used for the treatment of glaucoma and epilepsy (*148*). While the specific role of CA VII is not clearly established, CA XII is found to be overexpressed in breast and renal cancers (*55*), (*149*).

Although much research has been carried out to study the behaviour of CA IX in tumour and various organ cancers and its role as a prognostic marker in these pathologies has been established, CA XII and CA II are equally responsible for numerous diseases including von Hippel-Lindau tumours, polycystic kidneys, pancreatitis and hypoxic tumours (*150*), (*147*).

Numerous inhibitors have been designed for the active site pocket of the enzymes of

which 4-substituted-ureido-benzenesulphonamides directed for the CA II active site pocket by Pacchiano et al deserves worth mentioning. These inhibitors could inhibit the isozyme in nanomolar concentrations by binding to the selective hydrophobic pocket of the enzyme (*151*). Nitro derivatives of sulphonamides were found to be highly effective as potent CA IX and XII inhibitors. These bioreductive inhibitors were able to inhibit not only the above isozymes (K_{is} = 5.4-653 nM) but also CA II (K_{is} = 8.8-4975 nM) effectively thus targeting the hypoxic tumours specifically (*152*). Various anticancer drugs targeting the CA isozymes have been discovered of which Indisulam, a sulphonamide derivative is under clinical trials (Phase II). Although innumerable drugs are in the market for inhibiting the CAs, but unfortunately these classical inhibitors cannot selectively inhibit a particular isozyme and often ends up in inhibiting other isozymes which are of physiological relevance (*153*).

Not only in treatment, in the field of cancer diagnosis also, are the same difficulties faced when targeting a particular isozyme. Since CA XI and XII are overexpressed in hypoxic tumours, they serve as the biomarkers as mentioned earlier. Fluorescent sulphonamides are used as probes for CA I and CA II where a series of naphthalene sulphonamide derivatives were tested for their change in fluorescence properties in absence and presence of the human recombinant isozymes (CA I and II) (*154*). Another ideal candidate for imaging purpose is fluorescein isothiocyanate (FITC) and its sulphonamide derivatives have been reported as excellent fluorescent probes for hypoxic tumour marker CA IX (*155*).

In the endeavour to selectively detect CA isozymes we undertook the polymeric approach consisting of the naphthalene sulphonamide as the fluorescent reporter as well as the active site inhibitor for enhanced signalling. Distinctive selectivity was achieved by the differential charged moieties on the polymer scaffold thus interacting differently with the isozymes based on

their charged surface differences. Designing of synthetic receptors to bind selectively to protein surfaces have been mentioned in the literature. These molecules have tremendous potential as sensors, selective imaging agents (*72*). Besides small molecules, the molecular imprinting technique has been developed to prepare polymers for selective protein recognition. However, this approach requires the use of excess cross-linkers and the resultant polymers usually have rigid structures (*156*). As an alternative, Schrader's group has recently demonstrated the use of flexible polymers for protein surface recognition (*124*). These polymers contain hydrophilic, charged and hydrophobic residues and due to the inherent structural flexibility, can interact with multiple sites on the surface of proteins (*121*). Structurally different proteins can be recognized employing these polymers (*119*).

Our lab has previously reported the applicability of the "multi-prong" approach for isozyme selective inhibition of MMPs (*130*). Even in case of CAs, "two-prong" approach was followed where a benzenesulphonamide was attached to iminodiacetate-Cu (II) via a spacer to bind to CA isozymes. The idea behind the study was that since the active sites of the isozymes are similar, the inhibitor would bind to the pocket unanimously, however, due to the difference in the surface exposed histidine groups, the Cu (II) would bind selectively to different CAs, thus producing varied inhibition constants. It was actually found that the "two-prong" approach was able to generate different binding constants for CA-I and CA-II and changing the spacer chain length resulted in creating potent selective inhibitors (*118*), (*65*). Based on these encouraging results, we report in this chapter use of fluorescent polymers for isozyme selective interactions with CA isozymes based on polyvalence and protein surface recognition in isozyme detection.

Materials and Methods

Commercial reagents were purchased from Alfa Aesar, TCI America and Aldrich. Solvents for synthesis were used as purchased without purification. Most of the syntheses were carried out under nitrogen. Rotary evaporator was used for solvent evaporation, desiccators for drying, automated flash chromatography (Combiflash RF system by Teledyne Isco) for purification, 300, 400 and 500 MHz (Varian) spectrometers for ^{1}H and ^{13}C NMR spectra. NMR solvents used were $CDCl_3$, D_2O, CD_3OD with TMS as the internal standard. TLC plates used were Adsorbosil plus IP, 20 X 20 cm plate, 0.25 mm (Altech Associates, Inc.). Chromatography plates were visualized under UV or iodine chamber. Melting points of the compounds were determined with a micro melting point apparatus. Polymers were characterized using Gel permeation chromatography (Waters 2690) and dimethylformamide as the solvent. Fluorescence spectroscopic studies including lifetime decay experiments were carried out using a Fluoromax-4 fluorescence instrument by Horiba Jobin-Yvon and its TCSPC hub with the DataStation software respectively. Isothermal Titration Microcalorimetry experiments were performed in NanoITC Standard Volume (TA instruments, USA). For inhibition studies, Spectramax Spectrophotometer was used. MMP-2/MMP-7 commercial fluorogenic substrate (MCA-Pro-Leu-Gly-Leu-Dpa-Ala-Arg-NH_2. TFA) and Human Serum were purchased from Calbiochem, (Cat. 03-32-5032) and BioWhittaker, Lonza respectively.

The monomers required for the polymers were synthesized in our laboratory (Scheme 3). Monomers **2**, **3** and **4** were synthesized for experiments in chapter 1 and used in this chapter also for synthesizing the polymers (for synthetic details vide chapter 1). A set of 4 polymers were prepared with different composition of the monomers (Table 14) using free radical polymerization with AIBN as the initiator. The molecular weights and polydispersity indices

(P.I.) of the polymers were determined by gel permeation chromatography (Table 15). The polymers were found to have molecular weights ranging from 111,000 to 121,000 with P.I. of 2.1 – 2.5. The polymers were soluble in aqueous phosphate buffer (30 mM, pH = 7.4) upto a concentration of 10 mg/mL.

As discussed in chapter 1, dansylamide (DA) was used as the reporter molecule for the recognition of the enzyme matrix metalloproteinase-9 (MMP-9). In these polymers, the inhibitor and the reporter groups were not conjugated. Consequently, the changes in fluorescence spectra of the fluorophore in the presence of MMPs were not optimal. Hence, in this chapter a fluorogenic CA inhibitor was conjugated to the polymerizable methacrylamide moiety directly (compound **1**, Scheme 3) for enhanced signals. The K_D of the 5-(dimethylamino) naphthalene-1-sulphonamide (DA) for CAII and CA XII are reported to be 360 and 80 nM respectively in literature (*157*), (*158*). Thus, we expected that naphthalenesulphonamide (NS) will act both as the initial anchoring site as well as the fluorescence reporter group. A diethyleneglycol spacer was introduced between NS and the methacrylamide groups to avoid any steric hindrance. To impart water solubility, methacrylamide derivative of the alcohol (Scheme 3, compound **2**) and to incorporate charges, the lysine and aspartic acid monomers (Scheme 3, compounds **3** and **4**) were used. The amount (mole %) of fluorogenic inhibitor monomer **1** was kept constant in these polymers for consistent fluorescence signals (Table 13).

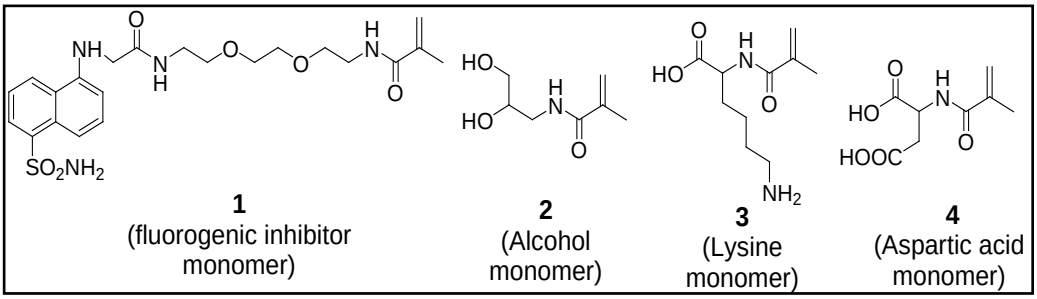

Scheme 3. Structures of the monomers used in the polymers (**F1-F4**).

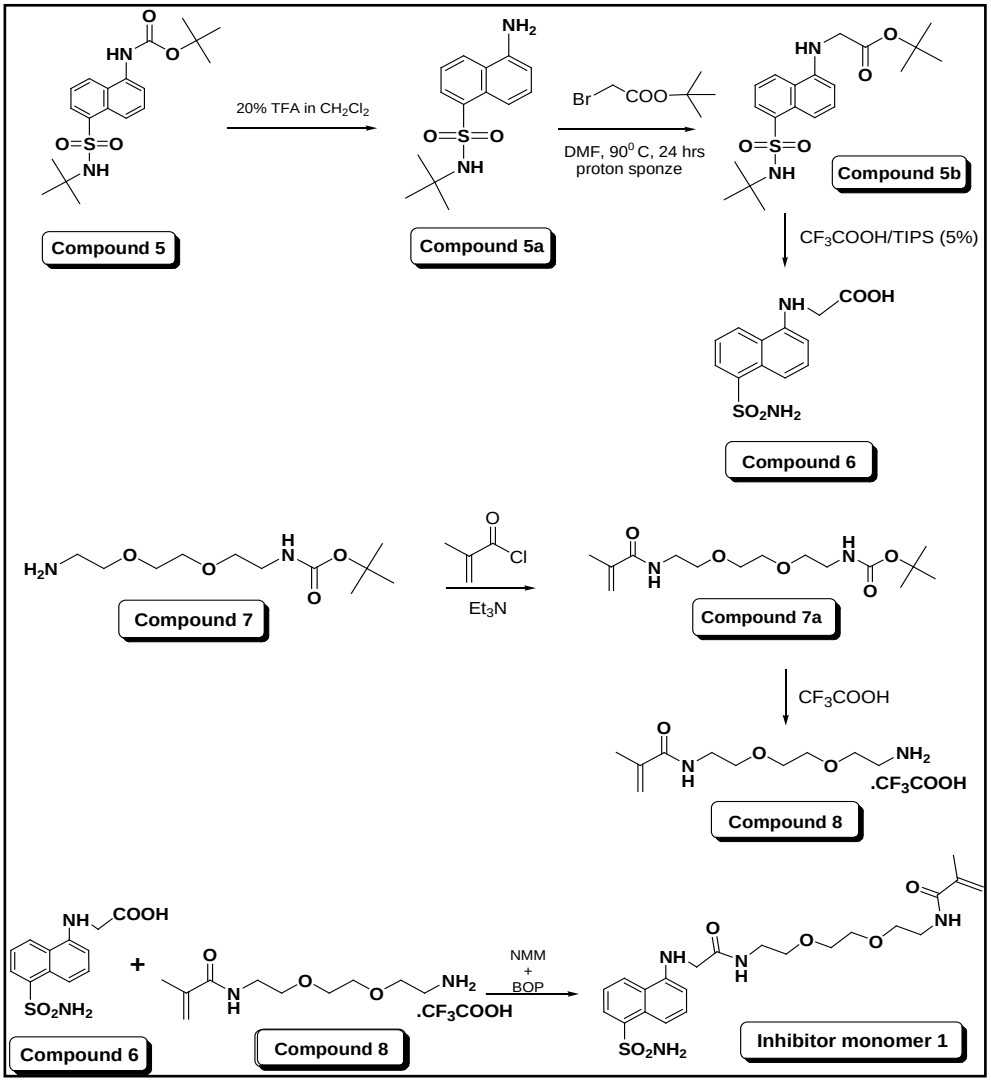

Scheme 4. Synthetic scheme of the inhibitor monomer **1**.

Compound 5a: Compound **5** {(5-tert-Butylsulfamoyl-naphthalen-1-yl)-carbamic acid tert-butyl ester}(*154*) (2.6 g, 6.87 mmol) was treated with 25 mL of 20% trifluoroacetic acid in dichloromethane for 2 hours. After removal of the solvent under reduced pressure, the residue was treated with 5% $NaHCO_3$ solution for 30 minutes. Filtration of the solid followed by air drying afforded the product as a yellow powder. Yield: 1.8 g (94%).

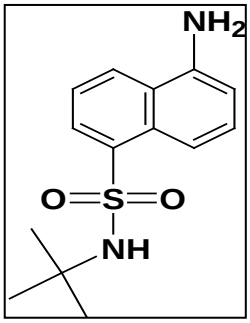

Compound 5a

Compound 5a: ^{1}H NMR (400 MHz, CD_3OD) δ: 1.09 (s, 9H), 6.89-6.91 (d, 1H, J = 7.6 Hz), 7.38-7.48 (m, 2H), 7.99-8.01 (d, 1H, J = 8.4 Hz), 8.19-8.21 (dd, 1H, J = 1.2, 7.2 Hz), 8.27-8.30 (d, 1H, J = 7.6Hz).

Compound 5b: Compound **5a** (1.5 g, 5.39 mmol) was treated with proton sponge (1.156 g, 5.39 mmol) and t-butyl bromoacetate (0.999 g, 5.12 mmol) in DMF (40 mL) at 90^0 C for overnight. The solvent was evaporated under reduced pressure and ethyl acetate was added to it, causing precipitation. The precipitate was filtered and the organic layer was washed with brine, 10% citric acid and 4% sodium bicarbonate solution. The product was purified by flash chromatography (**R_f = 0.6**; 3:1 hexane/ethyl acetate) yielding 1.6 g (76%) of a cream colored solid.

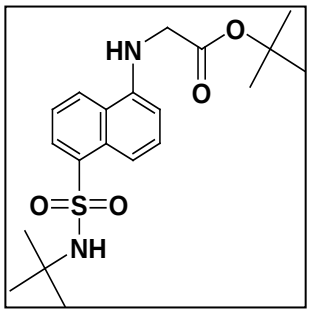

Compound 5b

Compound 5b: ^{1}H NMR (400 MHz, $CDCl_3$) δ: 1.14 (s, 9H), 1.55 (s, 9H), 3.96 (s, 2H), 4.63 (s, 1H), 6.51-6.55 (d, 1H, J = 7.8 Hz), 7.49-7.51 (m, 2H), 7.94-7.96 (d, 1H, J = 9 Hz), 8.17-8.19 (d, 1H, J = 7.2 Hz), 8.32-8.33 (d, 1H, J =7.8 Hz).

Compound 6: The tert-butyl protected compound **5b** (1.1 g, 2.80 mmol) was treated with 5% triisopropylsilane in trifluoroacetic acid (10 mL) overnight at room temperature. After evaporation of the solvent, hexane was added to the residue followed by 5% $NaHCO_3$ solution. Organic layer was separated and the aqueous layer was again extracted with dichloromethane. Finally, acidification of the aqueous phase to pH = 4 afforded precipitation of the product. The precipitate was filtered, air dried and was used as such for the next step. Yield: 0.73 g, (93%).

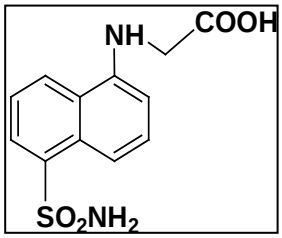

Compound 6

Compound 6: ^{1}H NMR (400 MHz, CD_3OD) δ: 4.09 (s, 2H), 6.59-6.60 (d, 1H, J = 7.8 Hz), 7.46-7.49 (m, 2H), 7.99-8.01 (d, 1H, J = 9 Hz), 8.21-8.23 (d, 1H, J = 7.2 Hz), 8.31-8.33 (d, 1H, J = 8.7 Hz).

Compound 7a: tert-Butyl 8-amino-3, 6-dioxaoctylcarbamate (1.0 g, 4.02 mmol) (*159*) and triethylamine (1.11 mL, 8.04 mmol) were dissolved in 25 mL of dry dichloromethane. Methacryloyl chloride (0.42 g, 4.02 mmol) was dissolved in 25 mL dichloromethane and added drop wise to the above reaction mixture while stirring at 0° C. The reaction was stirred under nitrogen at room temperature overnight. Subsequently, the reaction mixture was washed with 15% brine, 10% citric acid (2X) followed by 4% sodium carbonate solution (2X). The organic

layer was dried over sodium sulfate, filtered and the solvent was removed under reduced pressure. The oily liquid was purified by flash chromatography (silica gel, 10:1 dicholoromethane/methanol, $\mathbf{R_f = 0.6}$) to yield 0.9 g (71%) of the pure product as a viscous oil.

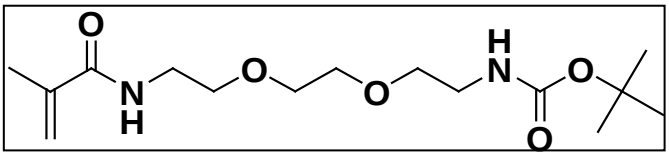

Compound 7a

Compound 7a: ^{1}H NMR (300 MHz, $CDCl_3$) δ ppm 1.44 (s, 9H), 1.97 (s, 3H), 2.17 (s, 1H), 3.31-3.62 (m, 12H), 5.33 (br. s. 1 H), 5.71 (s, 1H), 8.04 (br. s. 1H).

Compound 8: The tertiary butyl group of the compound **7a** obtained in the previous reaction (0.9 g, 2.84 mmol) was removed by adding 3 mL of trifluoroacetic acid followed by four hour stirring under nitrogen. The solvent was evaporated under vacuum and the dried product was stored in the freezer and was used without further purification. Yield: 0.6 g (81%).

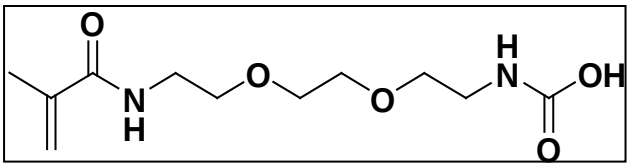

Compound 8

Compound 8: ^{1}H NMR (300 MHz, CD_3OD) δ ppm 1.70 (s, 3H), 2.87 (m, 3H), 3.07-3.43 (m, 9H), 5.14 (s, 1H), 5.46 (br. s. 1 H).

Compound 1: To a stirred solution of compound **6** (0.35 g, 1.25 mmol) in DMF (3 mL), compound **8** (0.332 g, 1.31 mmol) was added followed by NMM (412 µL, 3.75 mmol). After 5 minutes of stirring at room temperature, BOP (0.581 g, 1.31 mmol) was added. The reaction mixture was allowed to stir at room temperature for 24 hours and then poured into brine. The

precipitate was filtered, dissolved into dichloromethane/methanol (9:1) and was directly taken for purification. Flash chromatography with silica gel (**R_f = 0.1** in 5% MeOH in dichloromethane) afforded a brownish semisolid as the pure compound **1**. Yield : 0.25 g, (42%).

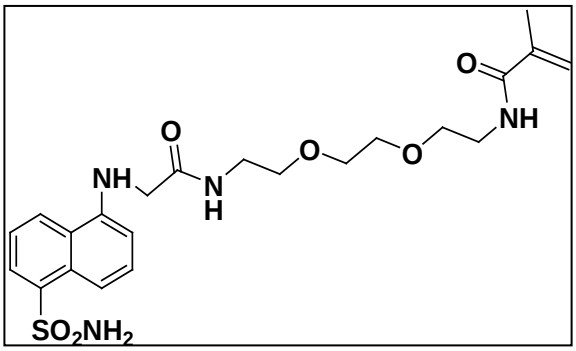

Compound 1

Compound1: ^{1}H NMR (500 MHz,$CDCl_3$/CD_3OD) δ: 1.88 (s, 3H), 2.14 (s, 2H), 3.20-3.35 (m, 12H), 3.92 (s, 2H), 5.29 (s, 1H), 5.66 (s, 1H), 6.52 (d, 1H, J = 7.68 Hz), 6.88 (br. s, 1H), 7.33 (m, 1H), 7.43-7.46 (m, 2H), 7.98 (d, 1H, J = 8.54 Hz), 8.18 (d, 2H, J = 7.68 Hz). ^{13}C NMR (400 MHz, $CDCl_3$/CD_3OD) δ: 18.25, 38.89, 43.69, 47.69, 53.49, 63.97, 69.39, 69.65, 70.00, 105.51, 114.28, 120.06, 122.91, 124.18, 125.94, 127.37, 128.82, 137.87, 139.4, 143.36, 164.85, 170.84. HRMS: exact mass calculated for $C_{22}H_{30}N_4O_6S$ $[M+H]^+$ was 478.19, Found 479.2 (Figure 23).

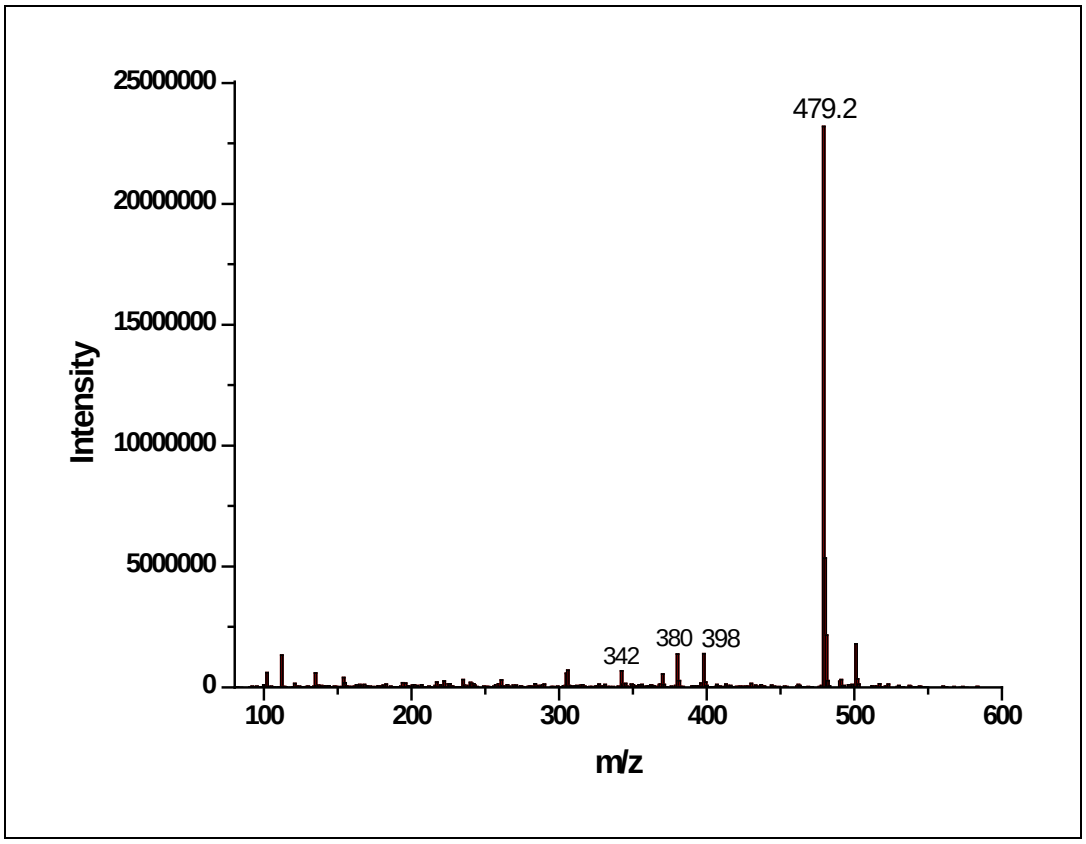

Figure 23. Calculated mass for inhibitor monomer **1** $[M+H]^+$ = 479.2.

General Polymerization Procedure: For each polymer, all the required methacrylamide-based monomers were weighed in certain mole % (Table 13) and dissolved in DMF. A catalytic amount of AIBN in DMF (15-30 mgs) was added to the reaction mixtures (Table 14). The reaction mixtures were then degassed for 15 minutes and stirred for 24 hours at 60-62°C. The reaction mixtures were next diluted with 3 mL of methanol and the whole mixtures were added to excess ethylacetate (10 times with respect to reaction mass volume) dropwise at room temperature. The polymers started precipitating out immediately. The solutions were kept in the freezer for 2-3 hours, centrifuged, washed with ethylacetate twice, dried under vacuum and stored in the freezer.

Table 13. Amounts (mole %) of the different monomers used to prepare the polymers (**F1–F4**).

Polymer	Inhibitor (1)	Alcohol (2)	Lysine (3)	Aspartic acid (4)
F1	10	90	-	-
F2	10	80	10	-
F3	10	80	-	10
F4	10	70	10	10

Table 14. Initial monomer compositions for the polymers (**F1-F4**).

Polymers	Alcohol (mg)	Lysine (mg)	Aspartic acid (mg)	Inhibitor (mg)	AIBN (mg)	Yield (mg)
F1	30	-	-	10	18	36 (62%)
F2	63	10	-	24	30	58 (46%)
F3	59	-	10	22	22	62 (55%)
F4	38	7.3	7	16	15	48 (58%)

Table 15. Molecular weights and polydispersity indices of the polymers (**F1-F4**).

Polymers	M_w	M_n	Polydispersity Indices
F1	112,149	44,110	2.54
F2	112,293	52,522	2.14
F3	121,933	58,079	2.09
F4	111,490	51,720	2.16

Fluorescence Spectroscopic Studies: The monomer inhibitor **1** was dissolved in DMSO (0.01% final concentration) and further diluted in 30 mM phosphate buffer (pH = 7.4) to a final concentration of 10 μM (402 μL) solution in the cuvette. To this, 8 μL of CA II (bovine erythrocyte, stock solution of 25 μM) was added to reach 500 nM of final concentration. Similar experiments were conducted for the CA VII (recombinant human) and CA XII (recombinant human). For the polymers, samples (2 mg) were weighed and dissolved in 1 mL of the 30 mM phosphate buffer (pH = 7.4). Proper dilutions were performed to achieve the desired concentration in the cuvette. CA II (8 μL of the 25 μM) was added to the cuvette and the

solution was excited at 325 nm. The emission spectra were recorded between 350 nm and 750 nm. The same experiments were repeated for the CA VII and CA XII.

Lifetime studies were performed using Horiba Data Station (v2.6) Single Photon Counting Controller: FluoroHub with 340 nm Nano LED and 10 nm bandpass. The polymer solutions (402 μL, 50 nM) in 30 mM phosphate buffer (pH = 7.4) were used and the emission wavelengths studied were 460 nm (490 nm for **F3**) and 522 nm. For each of the polymers (50 nM) with the added CA II (500 nM, total volume of 410 μL), same experiments were repeated with the two emission wavelengths. The biexponential decay results were analyzed using Decay Analysis Software (DAS6, v6.6).

For the fluorescence titrations experiments, 400 μL of the initial polymer **F4** (33 nM) was taken and then 2 μL of CA II (25 μM) was added at each step till 12 μL. After each addition, the solution mixture in the cuvette was excited at 325 nm and the emission spectra from 350 nm to 750 nm were recorded (Figure 24). The fluorescence intensities of the initial solution (before addition of enzyme) and after addition of enzyme at 458 nm (emission wavelength) were noted. The initial intensity was subtracted from each of the observation and the ratio $[(I_{final}-I_{initial}) / I_{initial}]$ was plotted against [CA II] / [**F4**] where [CA II] and [**F4**] represents the concentrations of CA II and polymer **F4** at each titration point. For CA VII and CA XII, similar experiments were performed (Appendix Figure A.3.4 and Figure A.3.5) and the calculations were done at 492 nm emission wavelength for CA VII and at 457 nm for CA XII. All the other parameters were kept constant and the experiments were conducted in 30 mM phosphate buffer (pH = 7.4).

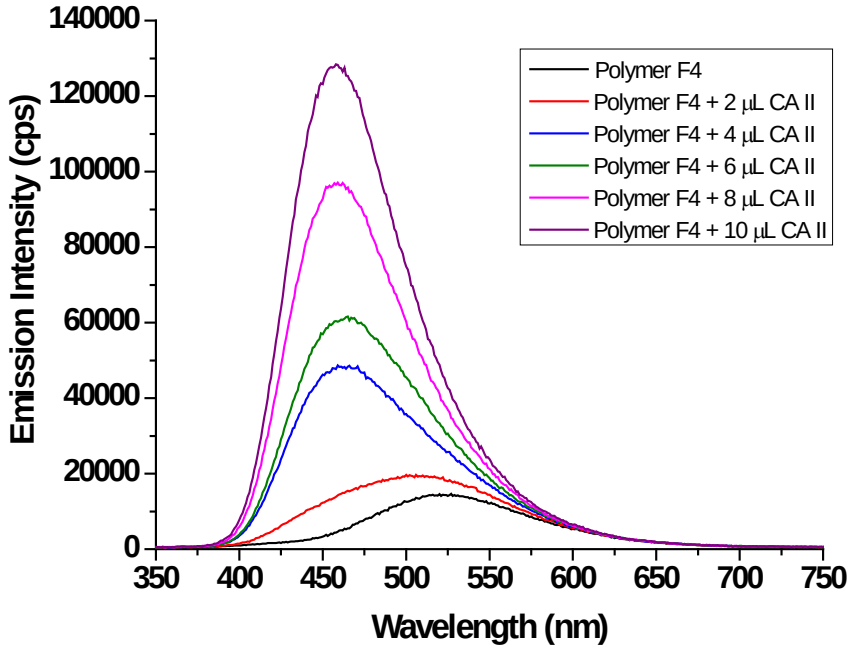

Figure 24. Fluorescence titration plot for polymer **F4** against increasing amount of added CA II. The solutions were excited at 325 nm and were conducted in 30 mM phosphate buffer (pH = 7.4).

Isothermal Titration Microcalorimetry Studies: The isothermal titrations of the monomer and the polymer **F4** against CA II were conducted using a NanoITC Standard Volume (TA instruments, USA). For all the ligands, titrations were performed in 25 mM phosphate buffer (pH = 7.4) at 25 °C with cell volume 950 μL, injection volume 10 μL (total 25 injections), and injection interval of 400 seconds. Water was taken in the reference cell. The data obtained were analyzed on Nanoanalyze data analyzer software (version: 2.1.13, TA Instruments). DMSO (1.5%) was added to low salt phosphate buffered saline (pH = 7.4) in order to dissolve the monomer completely. Appropriate blank experiments were conducted to subtract the effect of DMSO in the heat changes.

Inhibition Assays: To check the inhibition of the polymers against the inhibitor monomer **1**, esterase inhibition assay using *p*-nitrophenyl acetate (PNPA) as the substrate was

performed. CA II (1 μM) and PNPA (1 mM, prepared with 1 % DMSO) was used. The monomer was dissolved in 25 mM HEPES buffer (pH 7.4) to make various concentrations (50 nM – 10 μM) in the wells of a microplate. The absorbance was monitored at 348 nm for 30 minutes. For comparison, the assay was performed using 10 μM solution of acetazolamide (with 2.2 % of DMSO) which is a potent CA inhibitor. For polymers, 1 μM final concentration was used in the wells. Other parameters were kept constant as the monomer.

Inhibition assays for MMP-7 and -9 with polymer **F4** were performed using a commercially-available fluorogenic substrate (Calbiochem, Cat. 03-32-5032). In the assays, 500 nM of the MMPs (both for MMP-7 and MMP-9), 25 mM HEPES buffer (pH 8.0), containing 10 mM $CaCl_2$, 100 mM NaCl, and 10 μM $ZnCl_2$ were used. Polymer concentrations used were 500 nM and 1 μM. Final concentration of the substrate in the 96-well plate was 28 μM. The samples were excited at 325 nm and the emission was monitored at 395 nm for 30 minutes.

Results and Discussions

Upon addition of CA isozymes (500 nM solutions of CA II, CA VII and CA XII) separately to a solution of the monomer **1** (10 μM) in phosphate buffer, it was observed that the emission spectra of NS moiety of **1** (λ_{ex} = 325 nm) were significantly blue shifted (from 522 nm to 460 nm) and intensity was increased in the presence of CA II and CA XII (Figure 25). This observation indicated that the fluorophore was experiencing a more hydrophobic microenvironment inside the active site of CA II and CA XII. No such intensity enhancement was observed in the presence of CA VII (Figure 25).

Isothermal titration microcalorimetry (ITC) studies were conducted with 150 μM monomer **1** against 20 μM CA II in phosphate buffered saline (pH = 7.4). The isothermal titration profiles indicated that monomer **1** was binding to CA II in 1:1 stoichiometry with an

association constant of 2.55 x 10^5 M^{-1} when fitted in a single binding model (Figure 26). The reported association constant between Dansylamide (DA) and CA II is 2.78 x 10^6 M^{-1} (*157*). Hence, conjugation of the spacer and the polymerizable moiety to the naphthalenesulphonamide (NS) resulted in ten-fold decrease in binding affinity to CA II.

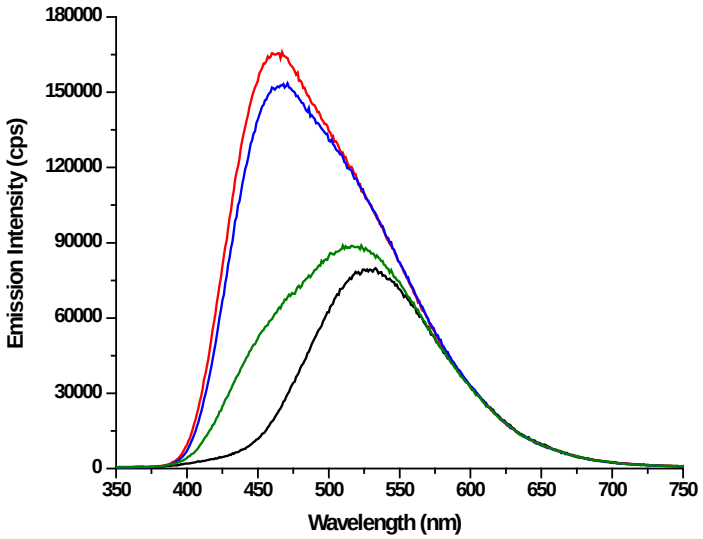

Figure 25. The emission spectra of 10 μM solution of the inhibitor monomer **1** (λ_{ex} = 325 nm) in the absence (black trace) and in the presence of 500 nM of CA II (red trace), CA VII (green trace) and CA XII (blue trace). These experiments were conducted in 30 mM phosphate buffer, pH=7.4.

To optimize the interactions with the CAs, 50 nM of the polymers (**F1 to F4**) in phosphate buffer were titrated with increasing concentrations of CA II (50–500 nM). Samples were excited at 325 nm and the emission spectra were recorded from 350 nm to 700 nm. The emission maximum from the polymer-incorporated NS group was found to increase and blue-shifted (from 522 nm to 460 nm) in presence of added CA II (Figure 27). The emission intensity and spectral shift were found to be largest in the presence of 500 nM of added CA II. Since

more than this concentration of CA II is physiologically irrelevant, we used 500 nM of the isozymes in our studies.

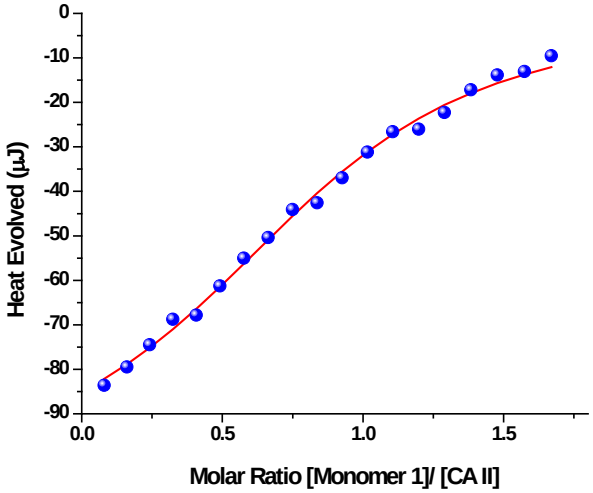

Figure 26. The isothermal titration profiles for 150 µM monomer **1** against 20 µM CA II in phosphate buffered saline (pH = 7.4). The red line indicates the fitted curve for one-site independent binding model.

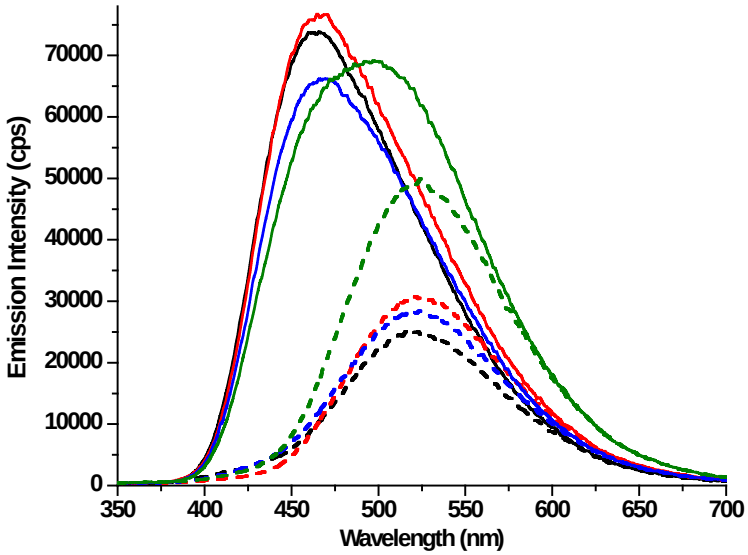

Figure 27. The emission spectra of the polymers **F1–F4** (50 nM each; λ_{ex} = 325 nm) in the absence and presence (dashed and solid line respectively, **F1**: blue; **F2**: red; **F3**: olive; **F4**: black) of CA II (500 nM).

Polymer **F3** in the absence of CA II showed higher emission intensity compared to the polymers **F1**, **F2** and **F4**. However, in the presence of added CA II, the blue-shifting of the emission maximum of **F3** was less compared to those of the other polymers. The blue shifting and enhancement of emission intensities for **F2** were similar to those for **F4**.

Calculation of the surface electrostatic potential map indicated that CA II had a patch of negative charge close to the active site (Figure 28). It is likely that the negative charges from the polymer-incorporated aspartate groups of **F3** are interfering with efficient binding to the active site of CA II. The ratio of the emission intensities (after and before the addition of CA II) was highest for **F4**.

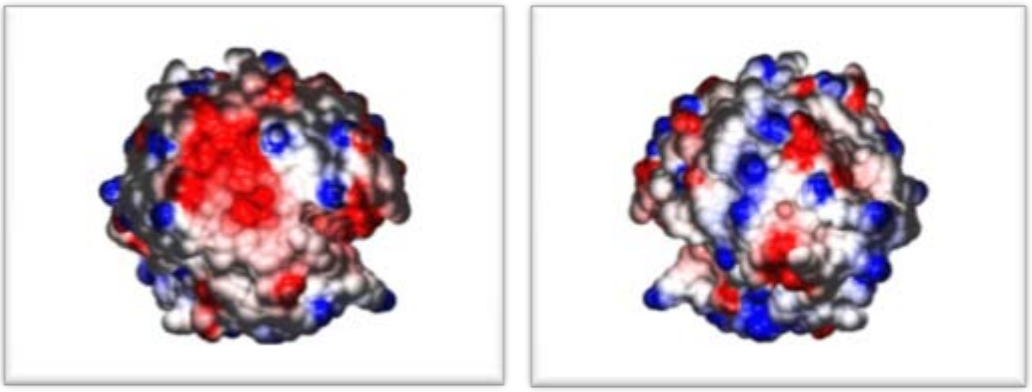

Figure 28. The X-ray crystallographic structures of CA II (3OYQ) obtained from the RCSB Protein Data Bank. The molecular surface electrostatic potentials were calculated by the Poisson-Boltzmann equation as implemented in the program GRASP2. The calculations were run with Coulombic boundary conditions and the values for internal and external dielectric and salt concentration were set at 4, 80 and 0.1M respectively. The electrostatic surface potential of CA II front, facing the active site (left) and back (right). The color range of the electrostatic potential maps reflects a range from red (−5 *k*T/mol) via white (neutral) to blue (5 *k*T/mol). The molecular surface of CA II appears to have predominantly negative electrostatic potential around the active site (front).

When similar concentration (500 nM) of the isozymes CA VII and CA XII were added to a solution of the polymer **F4** (50 nM), no significant changes in emission spectra were observed (Figure 29). Clearly, the emission from the polymer-incorporated NS group changed

substantially only in the presence of CA II (Figure 29, red trace). We repeated similar experiments with a solution of polymer **F2** also. Blue shifting and intensity enhancement of the NS emission were observed for both CA II and CA XII (Figure 30). Surface electrostatic potential calculations indicated that CA II and XII have a cluster of negative charges close to the active site (Figure 28 and Figure 31 respectively).

CA VII on the other hand does not have a similar region of dominating electrostatic potential (either negative or positive) on any side of the molecular surface (Appendix Figure A.3.3). Possibly the positive charges on polymer **F2** are interacting favorably with the negative charges close to the active site of CA XII. However, we do not yet have an explanation for the selective interaction of **F4** with CA II. Similar experiments were performed for polymers **F1** and **F3** also with the isozymes (vide Appendix Figure A.3.1 and Figure A.3.2)

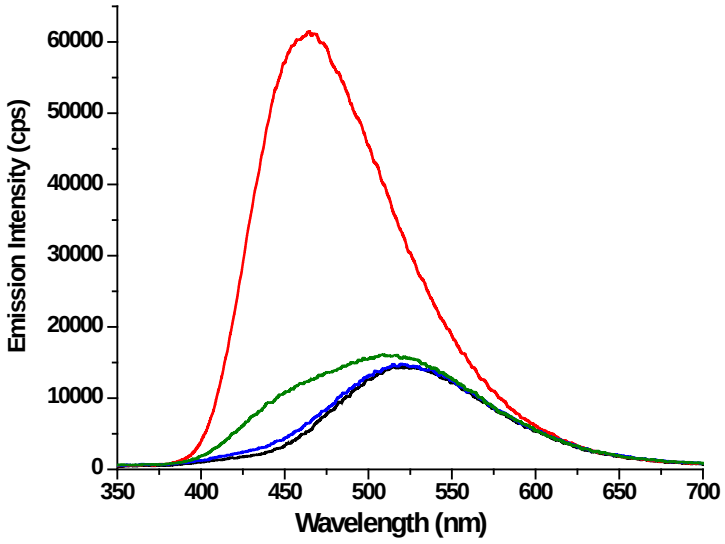

Figure 29. Fluorescence emission spectra of polymer **F4** (50 nM; λex = 325 nm, black trace) in presence of 500 nM of CA II (red trace), CA XII (green trace) and CA VII (blue trace) each.

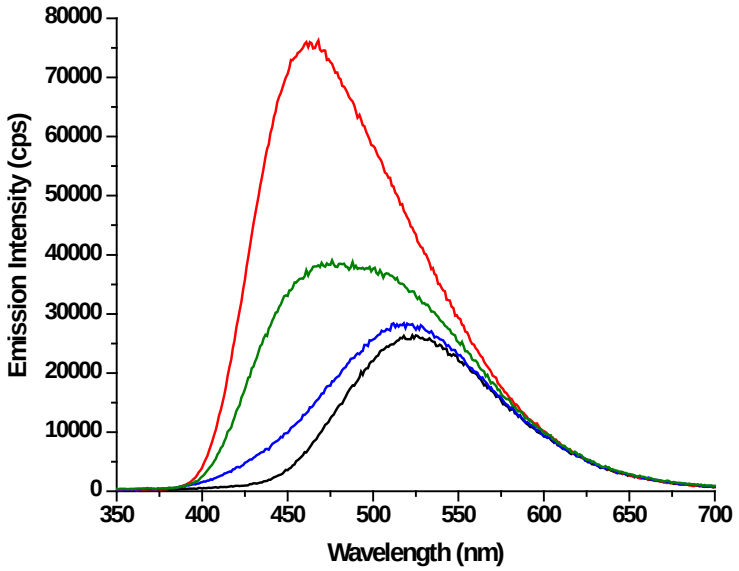

Figure 30. Fluorescence emission spectra of polymer **F2** (50 nM; λex = 325 nm, black trace) in presence of 500 nM of CA II (red trace), CA XII (green trace) and CA VII (blue trace) each.

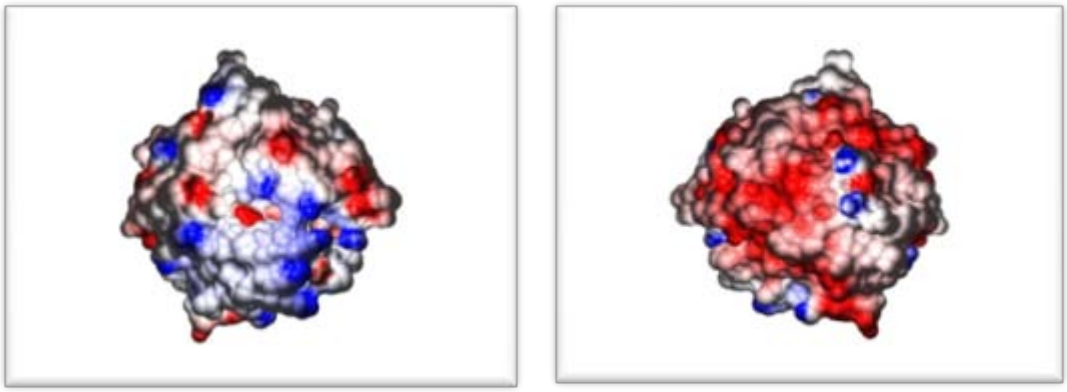

Figure 31. The X-ray crystallographic structures of CA XII (1JCZ) obtained from the RCSB Protein Data Bank. The molecular surface electrostatic potentials were calculated by the Poisson-Boltzmann equation as implemented in the program GRASP2. The calculations were run with Coulombic boundary conditions and the values for internal and external dielectric and salt concentration were set at 4, 80 and 0.1M respectively. The color range of the electrostatic potential maps reflects a range from red (-5 *k*T/mol) via white (neutral) to blue (5 *k*T/mol). The electrostatic surface potential of CA XII front, facing the active site (left) and back (right). CA XII appears to have extensive negative electrostatic potential on the back.

The blue shifted and increased emission of **F4** in the presence of CA II indicates that NS fluorophores were experiencing more hydrophobic microenvironment in the presence of the

enzyme. We reasoned that this change in the microenvironment should be reflected in the excited-state lifetime of the polymer-incorporated fluorophores. Hence, we excited the polymer **F4** (340 nm) in the absence and in the presence of 500 nM CA II and measured the excited-state lifetimes at 460 nm (Figure 32) and at 522 nm (Figure 33). In the absence of CA II, the polymer-incorporated NS groups exhibited biexponential decay at 460 nm with lifetimes of 9.7 + 0.12 and 1.9 + 0.02 ns; in the presence of added CA II, the lifetimes increased to 20.2 + 0.05 ns and 2.9 + 0.05 ns. The excited state lifetimes at 522 nm were also found to increase in the presence of added CA II. The excited-state lifetimes of the other polymers in the presence of CA II are in Table 16.

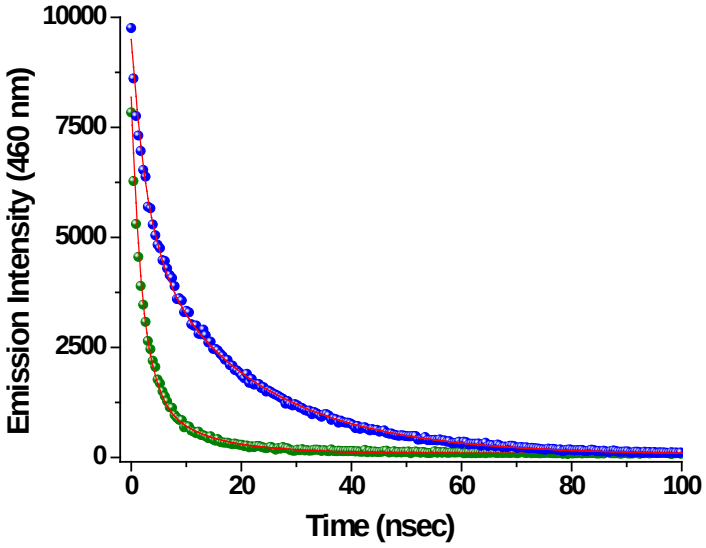

Figure 32. The emission intensity decay profiles at 460 nm (λ_{ex} = 340 nm) for polymer **F4** (50 nM in phosphate buffer) in the absence (green circles) and in the presence of CA II (500 nM, blue circles). The red lines indicate the fitted curve using a biexponential decay equation.

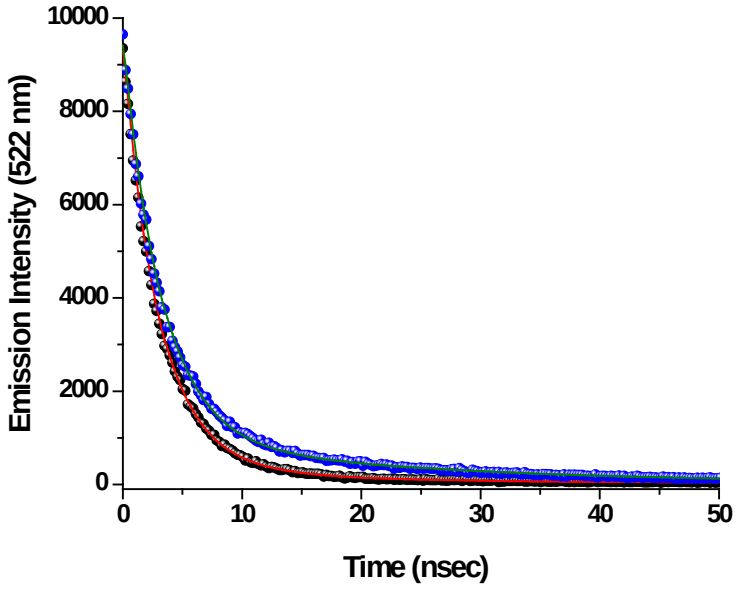

Figure 33. The emission intensity decay profiles at 522 nm (λ_{ex} = 340 nm) for polymer **F4** (50 nM in 30 mM phosphate buffer, pH = 7.4) in the absence (black circles) and in the presence of added CA II (500 nM, blue circles) are shown. The red and green lines indicate the fitted curves using biexponential decay equation.

Table 16. Excited state decay profiles of the polymers (**F1-F4)** for CA II.

λ_{Ex} = 325 nm λ_{Em} = 460 nm (490 nm for F3)	τ_1 (nsecs)	τ_2 (nsecs)	λ_{Ex}= 325 nm λ_{Em}= 522 nm	τ_1 (nsecs)	τ_2 (nsecs)
F1	2.2 ± 0.03	13.1 ± 0.13	**F1**	2.9 ± 0.03	10.1 ± 0.16
F1 + CA II	2.9 ± 0.06	20.5 ± 0.05	**F1** + CA II	3.2 ± 0.02	19.6 ± 0.12
F2	0.03± 0.01	4.0 ± 0.03	**F2**	2.8 ± 0.04	8.2 ± 0.15
F2 + CA II	2.7 ± 0.05	20.7 ± 0.06	**F2** + CA II	3.2 ± 0.02	20.1 ± 0.15
F3	2.5 ± 0.03	8.1 ± 0.10	**F3**	2.8 ± 0.03	7.8 ± 0.10
F3 + CA II	3.2 ± 0.03	19.1 ± 0.09	**F3** + CA II	3.3 ± 0.03	17.5 ± 0.14
F4	9.7 ± 0.12	1.9 ± 0.02	**F4**	2.7 ± 0.03	9.4 ± 0.17
F4 + CA II	2.9 ± 0.05	20.2 ± 0.05	**F4** + CA II	3.0 ± 0.02	19.3 ± 0.14

The binding constant for the polymer **F4** with CA II was determined by ITC. A solution of **F4** in phosphate buffer was titrated with increasing concentrations of CA II. The ITC binding isotherm for **F4** and CA II was best fitted with two types of binding sites with different stoichiometry (n) and association constants (Figure 34). The binding constants for these two sites are higher (10–100 times) compared to that of the monomer **1** (Table 17).

Table 17. Binding parameters of the monomer **1** and the polymer **F4** for CA II as determined by isothermal titration microcalorimetry.

Compound	K_a (M^{-1})	ΔH (kJ/mol)	(n)	ΔG (kJ/mol)	ΔS (kJ/mol.K)
1	(3.3 ± 2.1) x10^5	– 63.7 ± 13.3	1.07 ± 0.12	–31.4 ± 6.2	–0.11 ± 0.02
F4	(3.9 ± 1.6) x10^6	–195 ± 8	1.9 ± 0.04	–37.6 ± 1.5	–0.53 ± 0.02
	(5 ± 1.8) x 10^7	–55 ± 5	0.10 ± 0.01	–43.9 ± 3.8	–0.037 ± 0.004

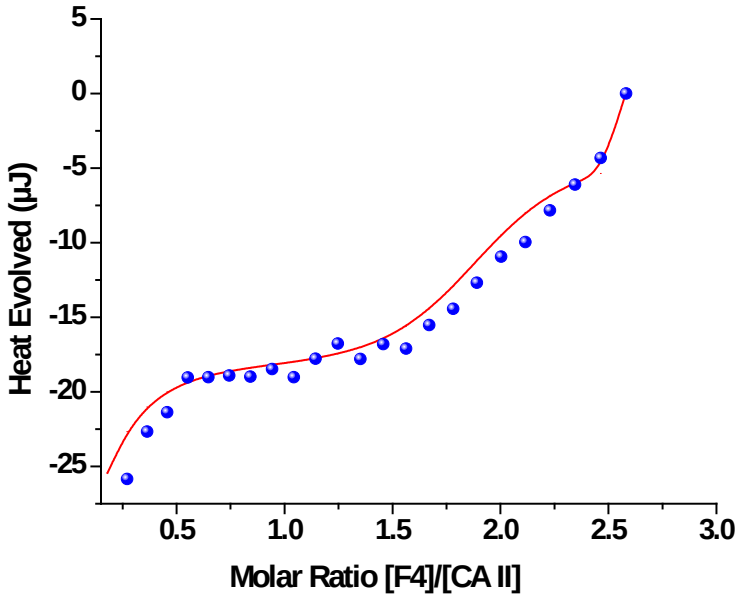

Figure 34. The isothermal titration profiles (blue circles) for 75 µM **F4** against 10 µM CA II in phosphate buffered saline (pH = 7.4). The red line indicates the fitted curve for multiple binding model.

It is likely that the polymer structure is heterogeneous and the charge distribution surrounding the inhibitor is making one site tighter binding compared to the other. The lack of sufficient amounts of recombinant CA VII and CA XII prevented us from determining the association constants of these isozymes for the monomer **1** and **F4** employing ITC. Fluorescence titrations plots were fitted in Hill equation model and were found to be sigmoidal in nature (Figure 35-37). The binding constant was found to be greater for **F4** and CA II followed by CA VII and XII. The details of the values generated from the models are given in Appendix (Table A.3.1-A.3.3). Inhibition assays confirmed that **F4** was binding to the active site of CA II and was a more potent inhibitors compared to the monomer **1** (Figure 38). We performed the inhibition assays with polymer **F2** and **F3** (both 1μM) to check their binding efficiencies against CA II and found that polymer **F4** was better than polymer **F2** (Figure 39) and **F3** (Figure 40) in binding CA II.

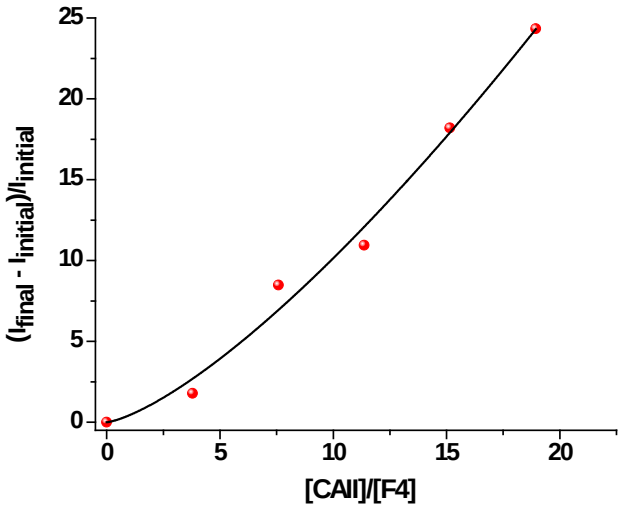

Figure 35. Fluorescence titration plots of CA II vs. polymer **F4** at 458 nm emission wavelength. Polymer concentration ranges from 33 nM to 32 nM whereas enzyme concentrations range from 0 to 728 nM. The solutions were excited at 325 nm after each enzyme addition. The experiments were conducted in 30 mM phosphate buffer, pH = 7.4.

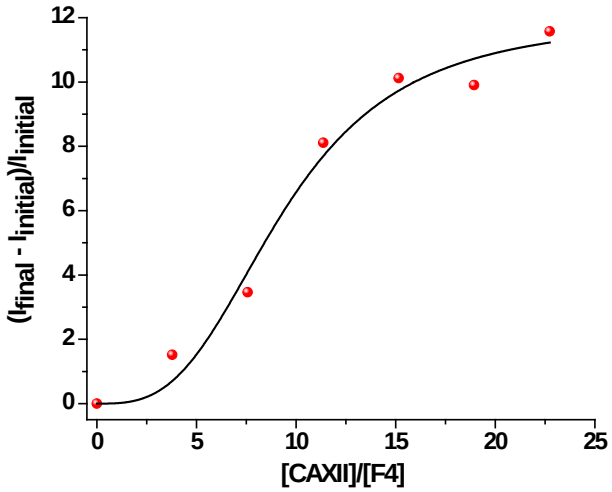

Figure 36. Fluorescence titration plots of CA XII vs. polymer **F4** at 457 nm emission wavelength. Polymer concentration ranges from 33 nM to 32 nM whereas enzyme concentrations range from 0 to 728 nM. The solutions were excited at 325 nm after each enzyme addition. The experiments were conducted in 30 mM phosphate buffer, pH = 7.4.

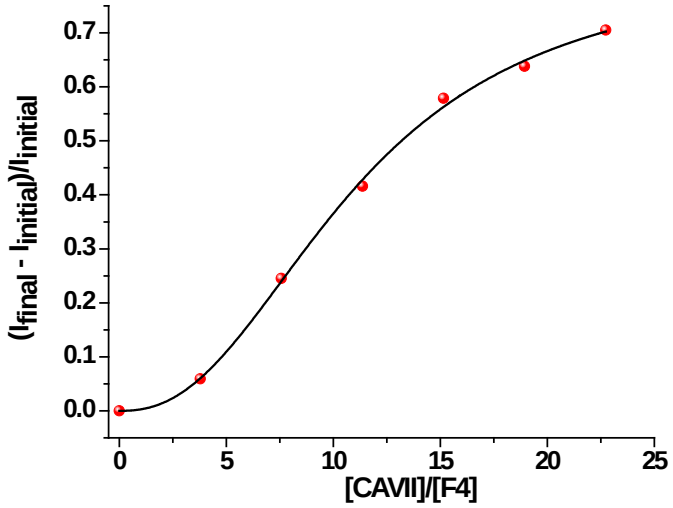

Figure 37. Fluorescence titration plots of CA VII vs. polymer **F4** at 492 nm emission wavelength. Polymer concentration ranges from 33 nM to 32 nM whereas enzyme concentrations range from 0 to 728 nM. The solutions were excited at 325 nm after each enzyme addition. The experiments were conducted in 30 mM phosphate buffer, pH = 7.4.

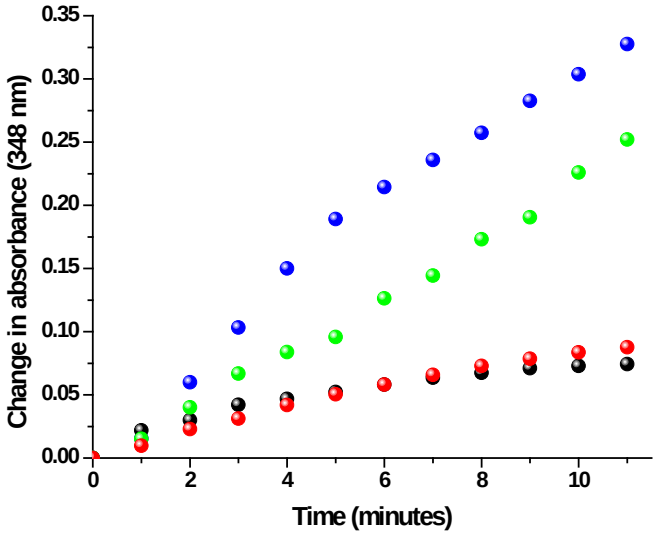

Figure 38. PNPA esterase assay of CA II in the absence (blue circles) and presence of 10 μM of inhibitor monomer **1** (green circles) and 1 μM polymer **F4** (red circles) are shown. For comparison, the results obtained with 10 μM concentration of acetazolamide are also included in the plot (black circles). The assays were conducted in 25 mM HEPES buffer (pH = 7.4).

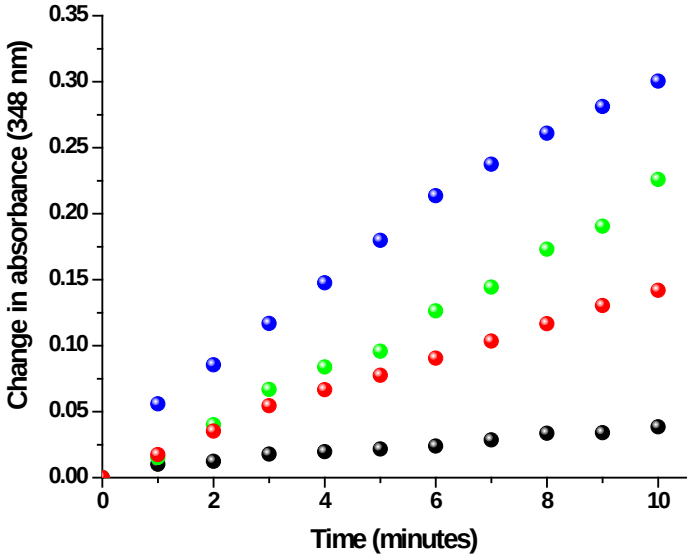

Figure 39. PNPA esterase assay of CA II in the absence (blue circles) and presence of 10 μM of inhibitor monomer **1** (green circles) and 1 μM polymer **F2** (red circles) are shown. For comparison, the results obtained with 10 μM concentration of acetazolamide are also included in the plot (black circles). The assays were conducted in 25 mM HEPES buffer (pH = 7.4).

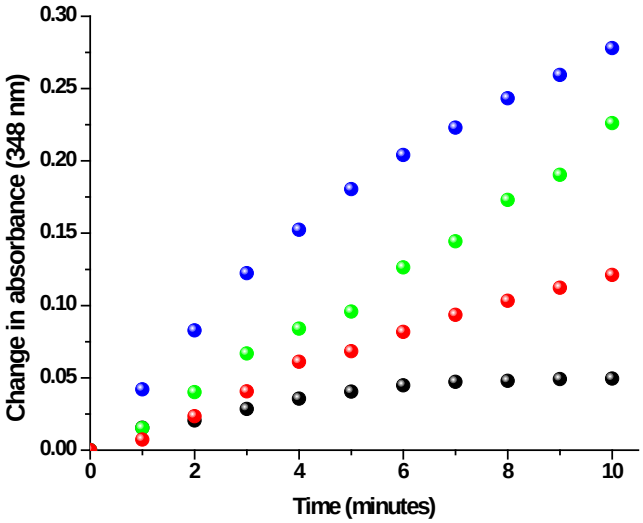

Figure 40. PNPA esterase assay of CA II in the absence (blue circles) and presence of 10 μM of inhibitor monomer **1** (green circles) and 1 μM polymer **F3** (red circles) are shown. For comparison, the results obtained with 10 μM concentration of acetazolamide are also included in the plot (black circles). The assays were conducted in 25 mM HEPES buffer (pH = 7.4).

To determine the extent of electrostatic interactions in the overall binding process, we measured the emission spectra of a mixture of polymer **F4** (50 nM in phosphate buffer) and CA II (500 nM) in presence of increasing concentrations of NaCl (0–275 mM). The emission intensity (at 460 nm) was found to remain constant up to 60 mM NaCl concentration (Figure 41) and then decreased (by 22%) with higher concentrations of added sodium chloride (60–175 mM). The emission intensity (460 nm) remained constant with further addition of salt (175–275 mM).

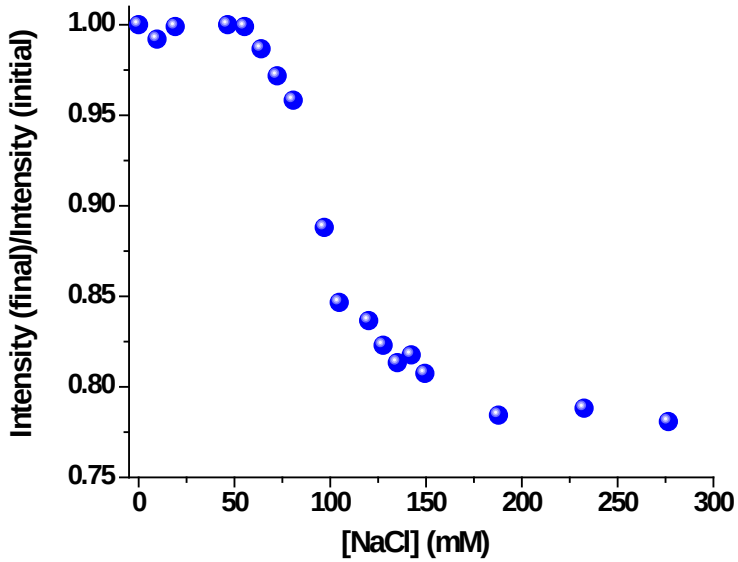

Figure 41. The ratios of emission intensities at 460 nm (λ_{ex} = 325 nm) of **F4** (50 nM) and CA II (500 nM) in the presence of added NaCl (0–275 mM).

These results (Figure 41) indicate that the overall binding of polymer **F4** to CA II is mediated by both electrostatic and inhibitor-active site interactions. Since **F4** incorporates both aspartic acid and lysine based monomers, the flexible polymer interacts with the surface charges of CA II, enhancing the overall affinity to CA II. It is important to note that the polymer incorporated inhibitor and the charges contributed to the selective interactions of polymer **F4** with CA II. The electrostatic interactions of **F4** with the surface charged residues of CA will be different for the three isozymes tested and is likely contributing to the selectivity of interactions of **F4** with CA II.

In order to probe the selectivity of the interactions, we decided to determine interactions of polymer **F4** with several isozymes of matrix metalloproteinases (MMPs), another Zn^{+2} containing family of enzymes (*98*). Aberrant expressions of many MMP isozymes (especially MMP-2, -7 and -9) contribute to the invasion and metastasis of a large number of cancers (*160*),

(*15*), (*46*). MMP-7 has several positively and negatively charged amino acid side chains on the surface and this feature has been used for selective interactions of this isozyme with appropriately-formulated liposomes (*18*). However, NS is reported to be a weak inhibitor for the MMPs (*161*). When **F4** (50 nM) was exposed to recombinant human MMP-9 or MMP-7 or MMP-10 (final concentration: 500 nM) no change in the emission spectra of the polymer incorporated NS groups were observed (Figure 42).

Functional assays of MMP-7 and MMP-9 with polymer **F4** showed very weak inhibition (Figure 43 and Figure 44). These observations indicate that the inhibitor group in the polymer is playing an important role in the overall binding of the enzymes to the proteins.

Subsequently, we determined if the selective interactions of **F4** with CA II were retained in a complex mixture of biomolecules. As a representative complex mixture, 10% (by volume) of fetal bovine serum (FBS) was added to the McCoy's cell culture media without the dye phenol red. This media (100 µL) was added to a 400 µL solution of **F4** (50 nM) and the emission spectra (λ_{ex} = 325 nm; Figure 45, red trace) were recorded. Blue shift was observed from 522 nm to 415 nm and an increase in intensity.

This indicates that the reporter groups of **F4** are experiencing a more hydrophobic microenvironment. However, when CA II was added to this mixture (final concentration of 500 nM), a more pronounced emission peak was observed at 455 nm (Figure 45, blue trace) indicating that **F4** is able to selectively interact with CA II even in the presence of a complex mixture of biomolecules.

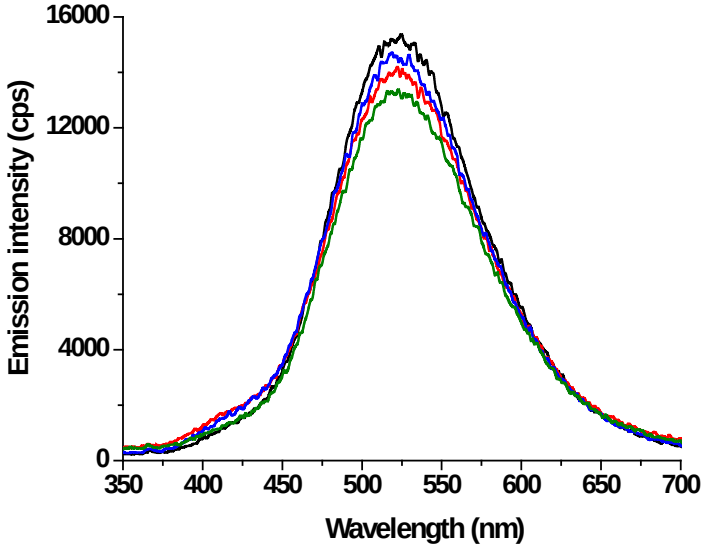

Figure 42. The emission spectra of a 50 nM solution of polymer **F4** (λ_{ex} = 325 nm) in the absence (black trace) and in the presence of 500 nM each of added MMP-7 (blue trace), MMP-9 (red trace) and MMP-10 (green trace).

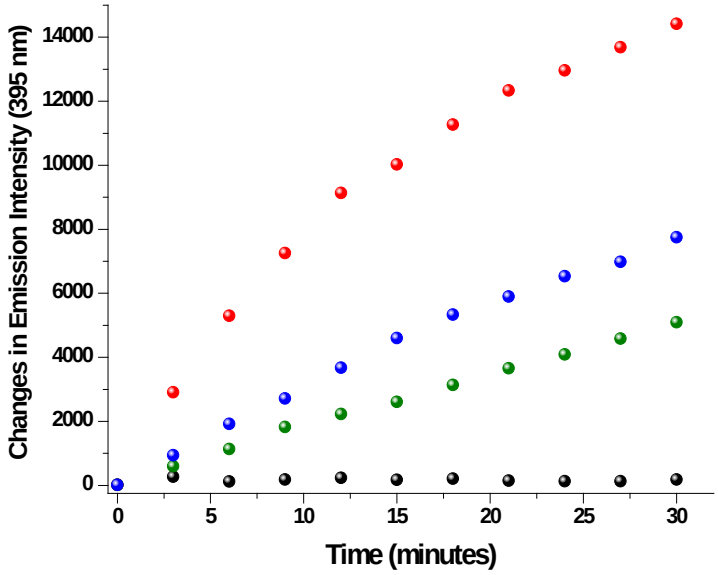

Figure 43. Emission intensity changes (395 nm) for MMP-7 inhibition assay in the absence (red spheres) and in the presence of 500 nM (blue spheres) and 1 μM (olive spheres) polymer **F4** are shown. The black spheres are the blank and indicate the emission changes in the absence of MMP-7. These experiments were conducted in 25 mM HEPES buffer (pH = 8.0) with excitation at 325 nm.

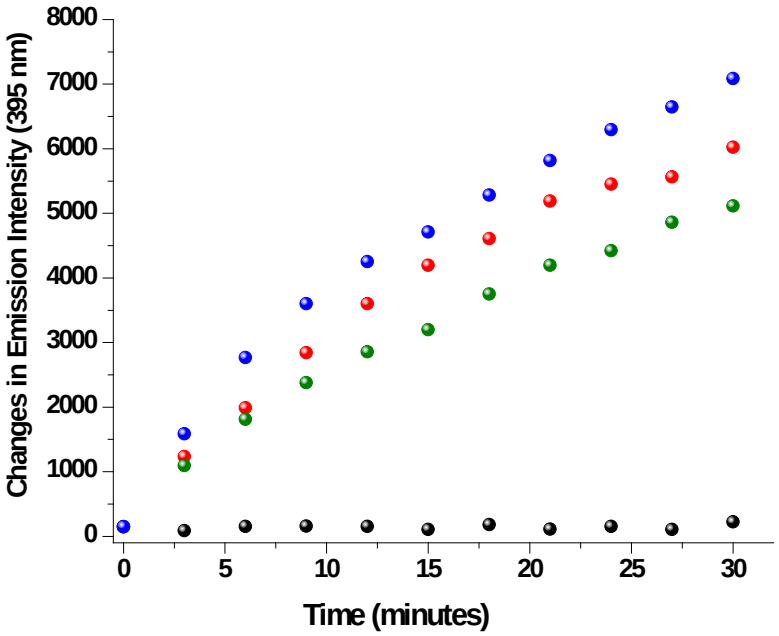

Figure 44. Emission intensity changes (395 nm) for MMP-9 inhibition assay in the absence (blue spheres) and in the presence of 500 nM (red spheres) and 1 μM (green spheres) polymer **F4** are shown. The black spheres are the blank and indicate the emission changes in the absence of MMP-9. These experiments were conducted in 25 mM HEPES buffer (pH = 8.0) with excitation at 325 nm.

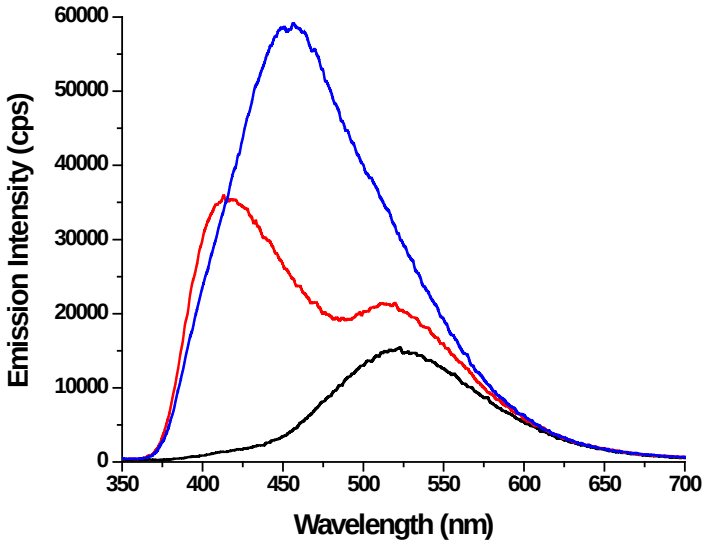

Figure 45. The emission spectra of a 50 nM solution of polymer **F4** (λ_{ex} = 325 nm) in the absence (black trace), in the presence of 10% (by volume) of FBS-containing McCoy's cell culture media (red trace) and with added CA II (final concentration: 500 nM, blue trace).

Conclusion

In conclusion, we have successfully synthesized a set of water-soluble, random copolymers incorporating a fluorogenic inhibitor for the enzyme carbonic anhydrase (CA). The polymer **F4** showed selective interactions with CA II compared to CA VII, CA XII, MMP-7, -9 and -10. The selective interactions of **F4** with CA II was maintained in a complex mixture of biomolecules (McCoy's cell culture media containing 10 % of fetal bovine serum). The fluorescence and isothermal titration microcalorimetry results indicate that the naphthalene sulfonamide inhibitor is bound to the active site of CA II and that the charges on the polymer were electrostatically interacting with the charged amino acid residues on the surface of the enzyme.

CHAPTER IV. DETECTION OF MATRIX METALLOPROTEINASE-7 (MMP-7) EMPLOYING DYE-ENCAPSULATED LIPOSOMES

Abstract

Matrix metalloproteinase-7 (MMP-7) is one of the smallest proteases among the members of the Matrix metalloproteinase class and is found to be overexpressed in many diseases including cancer (*162*). Usual detection strategies of MMPs involve antibody-based ELISA or zymography. Liposomes have been widely used as drug delivery carriers for targeting both cell-surface receptors as well as extracellular components found in tumors and around its environment. Liposomes have been used also in the field of detection of biomarkers where the liposomal surfaces are modified with antibodies, enzymes, peptides and fluorescent tags. In chapter 1 we have used our synthesized polymers for detecting total enzymes (both active and inactive). Herein we report the liposomal formulations designed for detecting active MMP-7 with the help of fluorescence signals from an encapsulated dye. Various commercial lipids as well as synthesized lipids were used for the development of carboxyfluorescein dye encapsulated liposomal formulations. Various MMP-7 cleavable specific peptides were synthesized and were incorporated within the lipid bilayer of the liposomes. We have conjugated the short peptides with our synthesized lipids present in the bilayer of the liposomes using 'click' reaction and then treated these liposomes with active MMP-7. We hypothesized that cleavage of the peptide by MMP-7 would cause a disturbance in the lipid bilayer of the liposomes, releasing the dye in the buffer solution. The released dye was monitored by the changes in the fluorescence intensities (excitation/emission wavelengths = 480 nm/518 nm). We observed that instead of increasing, the fluorescence intensity of the released dye in presence of MMP-7 decreased. These

contradictory results proved that the presence of bipolar charges in the enzyme stabilized the liposomal bilayer. These results will be addressed in further studies.

Introduction

Liposomes are spherical bilayer vesicles and are extensively used as drug delivery and tumor targeting agents (*86*). Because of their sizes (< 500 nm), they have become ideal candidates for site targeted drug delivery vehicle in diagnosing and in the treatment of cancer (*163*). Liposomes can reach the target due to EPR effect (as discussed previously) because of their nanosizes. Moreover, they have been modified as "Stealth" liposomes that can stay in the plasma for long and can bypass the RES (*164*). Currently more than 10 formulations are available in the market that has been approved by the US Food and Drug Administration. Liposomes have been applied not only for drug delivery but also for gene delivery (*165*), (*166*). In case of activating lymphocytes (T-cells), liposomes act as immunological adjuvant and vaccines thus influencing the immune response (*167*). In case of antibody and peptide-drug conjugates, liposomes have proved to be helpful agents in targeting tumor as well as in other pathogenic conditions (*168*).

Liposomal release can be achieved by various triggering agents such as, light, pH, metal ions, enzymes, ultrasound and temperature (*169*), (*86*), (*47*), (*170*). Zhao and coworkers utilized pH and redox potentials as stimuli for controlled release of dye from cleavable polymerized liposomes (*171*). "Click' reaction was used by the Zhao group for polymerization of the alkyne derivative of POPE with the azide of a cross linker containing the cleavable disulfide linkage. Reducing thiol dithiothreitol (DTT) and weakly acidic conditions were used as the cleaving agents for the liposomal content release. "Click" reaction created more stable liposomes in regards to polymerization and the polymer-oriented biodegradability aspect was avoided (*171*).

"Click" reaction has many attributes which has made it an efficient tool for chemists. The reaction is easy to carry out at room temperature with easily available reagents (Cu^{+} ion catalysts), easily removable solvent (preferably water) and the end-products are usually clean without requiring further chromatographic purifications (usually used are distillation/crystallization). The concept of this famous "Click" chemistry was first mentioned by Barry Sharpless at the Scripps Research Institute in 2001. Out of the many "click" chemistries, azide-alkyne Huisgen cycloaddition has been widely mentioned as the "click" reaction (*172*). From its initial introduction "click" reaction have been extensively applied not only by organic chemists but also by pharmaceutical chemists for synthesis of liposomes, dendrimers and for surface modifications primarily for conjugation of ligands (*173*), (*174*). In this chapter we have used "click" reaction to attach an alkyne-based MMP-7 cleavable peptide (5-hexynoic acid) with the azide group present in the synthesized lipids that are part of the liposomal bilayer.

Mallik et al have demonstrated the use of liposomes composed of protease-cleavable peptides for detection of matrix metalloproteinase-9 (MMP-9) based on its natural substrate triple-helical collagen substrate (*46*). Not only were these liposomes used for detecting recombinant human MMP-9, these liposomes could detect MMP-9 secreted in the conditioned media from MCF-7 cancer cell lines which over express MMP-9 (*98*). These liposomes could detect active enzymes which were manifested by the increased fluorescence of the encapsulated carboxyfluorescein dye which was released as the enzyme cleaved the peptide scissile bond and thus disturbing the liposomal bilayer.

Matrix metalloproteinases are extracellular matrix degrading enzymes which are found to be overexpressed in various diseases and their tight regulation is required for maintaining

proper physiological functions (*175*). Usually under normal conditions these endopeptidases function in a well-regulated biochemical network and are controlled by multiple signaling pathways. Since these enzymes contain zinc in their active sites, their substrates bind to the zinc ion for directing their catalysis. All the 26 isozymes in this Metzincin family work in a channelized fashion among themselves and with their natural inhibitors (TIMPS, tissue inhibitor of matrix metalloproteinases) for modeling and remodeling the extracellular matrix components (*176*). Any abnormal functioning or unlike signaling step leads to pathological symptoms and outcomes like cancer, arthritis, periodontal diseases, tumor invasion and metastasis (*177*).

MMP-7 or Matrilysin is the smallest and simplest isozyme in the Matrix metalloproteinase family consisting of a pre-peptide, a propeptide and a catalytic domain in its latent stage. This isozyme is devoid of any hinge-region or hemopexin like domain (*4*). Although the isozyme is simple in nature, it is found to be overexpressed frequently in tumor cells. In fact, the first human MMP-7 was isolated from the cDNA of mixed tumor profile and was expressed in the eukaryotic system for its characterization (*178*). The 28 kDa zymogen when gets activated (19 kDa active enzyme) acts on various surface proteins such as Fas-ligands, syndecan-1 and pro-TNF-α including E-cadherin (*15*), (*17*). It has been reported that both pro and active matrilysins are activated by various sulfated glycoaminoglycans or GAGS such as heparin, dermatan sulfate and chondroitin-4,6-sulfate (*179*). MMP-7 is mostly expressed in glandular epithelium and of various organs such as liver, pancreas, prostate, parotid and prebonchial glands (*16*). However they are not expressed in the stromal cells (*17*).

Since most of the MMP inhibitors have failed in the clinical trials due to various adverse side effects and overlapping of the functions of each other isozymes, various peptide based substrates have been designed for isozyme selective interactions (*32*). Particularly in MMP

detection, a peptide-based library have been created depending on the subsites and pockets design of each isozyme. Usually a fluorescent reporter is attached to the peptide substrate which gives the signal upon enzyme cleavage mostly by FRET or normal fluorescence (*180*).

Peptides are designed based on their cleavage site motif by a particular isozyme (*181*). In protease peptide this motif is usually the scissile bond between the N and C-terminals of P1 and P1´ residues of the P3-P2-P1-P1´-P2´-P3´ respectively. Turk et al showed that presence of hydrophobic amino acid leucine in the P1´ and and serine in the P1 sites had the highest k_{cat}/K_M value for MMP-7 when compared with other MMPs. This was followed by glycine in the P1 motif (VPLG-LTMG; $V_{max}/K_M = 75 \pm 8\ s^{-1}$) (*182*).

Ganguly et al demonstrated that MMP-7 interacts differently with charged lipid membranes mimicking the biological plasma membrane. The enzyme was found to be inhibited when positively charged liposomes were used and in presence of negative and neutral ones, MMP-7 stayed fully active. This was inferred when compared with the electrostatic potential maps of the enzyme where 'bipolar' distribution of charge was noticed with negative potential round the active site region and positive charge on the opposite end of the enzyme's surface. Thus the result was in full agreement with the structure that positively charged moieties could have an inhibitory effects on the isozyme (Figure 46) (*18*).

Our goal in this chapter was to prepare dye encapsulated liposomes composed of MMP-7 cleavable peptide to detect active MMP-7 by monitoring the fluorescence intensity changes of the released dye.

We used "click" reaction for conjugating our peptide with the available azides on the surface of the liposomes and then the activity of the enzyme was monitored indirectly from the enhanced fluorescence intensities with time.

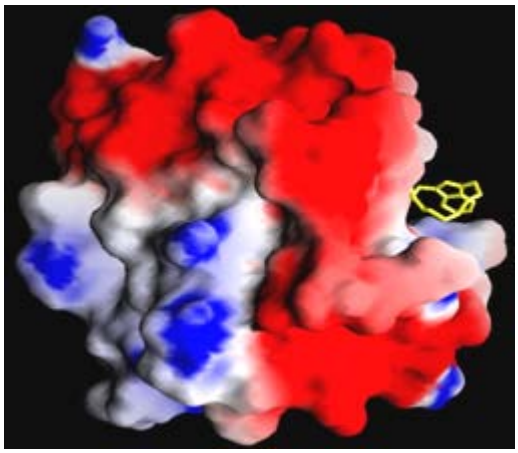

Figure 46. Electrostatic potentials map of hydroxamate (yellow) inhibitor-bound MMP-7. The red-colored region depicts the negatively charged region; the blue-colored region depicts the positively charged region respectively. (Used with permission from Ref.18).

Materials and Methods

All the reagents were purchased commercially from TCI America, Alfa Aesar, Peptide International, Chem-Impex International, Advanced Chem Tech, Chem Pep and Mallinkrodt Chemicals. Fmoc-Gly-Clear Amide resin was used for the solid support for peptide synthesis. All the solvents used were HPLC grade and were used as such. The peptides were synthesized using microwave –assisted peptide synthesizer and purified by semi-preparative HPLC. The molecular weights of the purified peptides were determined by MALDI-ToF mass spectrometry. For analyses and cleaving experiments analytical columns were used. The liposomes sizes were analyzed by dynamic light scattering. The osmolality of the buffer was checked in the Osmometer (Fiske).

Synthesis of the Lipids: All the reagents were purchased from Alfa Aesar, TCI America and Aldrich. Solvents were used as purchased without further purification. Syntheses were carried out under a nitrogen atmosphere. Automated flash chromatography (Combiflash RF

system by Teledyne Isco) was used for purification of the compounds. For ^{1}H and ^{13}C NMR spectra, 300 and 400 MHz (Varian) spectrometers were used. NMR solvents used were $CDCl_3$ and D_2O with TMS as the internal standard. NMR spectral data processing was performed using ACD Labs software processor. TLC plates used were Adsorbosil plus IP, 20 X 20 cm plate, 0.25 mm (Altech Associates, Inc.). Chromatography plates were visualized under UV or iodine chamber.

Compound 1a: 2-Bromoethylamine hydrobromide (4.1 g, 20 mmol, 1 equiv.) was added to Boc-anhydride (8.72 g, 40 mmol, 2 equiv.) in methanol (200 mL) in presence of triethylamine (at 0 ºC) under nitrogen. The reaction was carried out overnight at room temperature under the nitrogen atmosphere. The organic solvent was evaporated and the residue was taken in hexane and washed with water (2 X 20 mL). The product was purified by automated flash chromatography over silica gel with ethylacetate/hexane (**R_f = 0.4**; EtOAc : Hex = 1 : 9) as the mobile phase. The solvent was removed under pressure and a yellowish white sticky solid was found as the product (compound **1a**). Yield : 3.4 g (76.2 %).

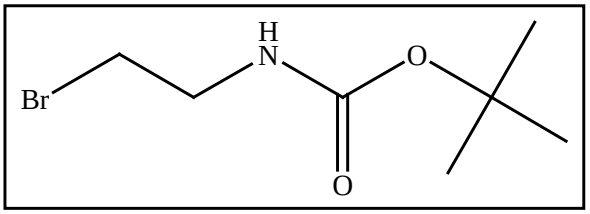

Compound 1a

Compound 1a: ^{1}H NMR (400 MHz, $CDCl_3$) δ ppm 1.44 (s, 10 H), 3.44 (br. s., 2 H), 3.52 (br. s., 2 H), 5.00 (br. s., 1 H).

Compound 1b. To compound **1a** (2.505 g, 11.23 mmol, 1 equiv.), sodium azide (1.46 g, 22.47 mmol, 2 equiv.) was added in DMF (40 mL) and the reaction was carried out at 90 ºC

overnight. The solvent was removed by distillation and the product was washed with dichloromethane and water (2 X 20 mL) and extracted in dichloromethane. TLC was checked with dichloromethane/methanol mobile phase ($\mathbf{R_f}$ **= 0.2**; CH_2Cl_2 : MeOH = 10 : 1) and pure product was found compared with the starting materials. The solvent was removed by evaporation to yield a sticky liquid (compound **1b**). Yield : 1.8 g (86 %).

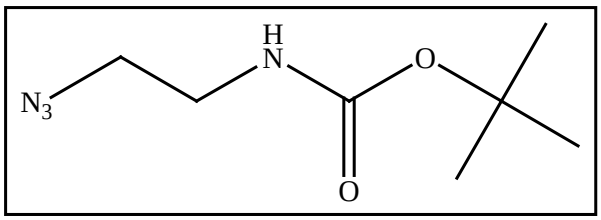

Compound 1b

Compound 1b: ^{1}H NMR (400 MHz, $CDCl_3$) δ ppm 1.45 (s, 9 H), 3.30 (br. s., 2 H), 3.41 (br. s., 2 H), 4.86 (br. s., 1 H).

Compound 1c. HCl (4N) in dioxane (8 mL) was added to the compound **1b** for deprotection and stirred under nitrogen atmosphere at room temperature for 3 hours to yield compound **1c**. The solvent was evaporated under vacuum and the dried brownish product was stored in the freezer. Yield : 1.15 g (92 %).

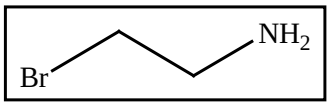

Compound 1c

Compound 1c: ^{1}H NMR (400 MHz, D_2O) δ ppm 3.18 (br. s., 2 H), 3.71 (br. s., 2 H).

Lipid 1. Stearic acid (0.5 g, 1.74 mmol, 1 equiv.) was added to compound **1c** (0.15 g, 1.74 mmol, 1 equiv.) in presence of BOP (0.77 g, 1.74 mmol, 1 equiv.) and triethylamine (0.53 g, 0.523 mmol, 3 equiv.) in 25 mL chloroform. The reaction was carried out at room

temperature with stirring under nitrogen atmosphere. The solution was extracted with chloroform/water system (3 X 20 mL). The solvent was evaporated and the product was purified in the flash chromatography with ethylacetate/hexane (**R_f = 0.2**; EtOAc : Hex = 1 : 3) as the mobile phase. White crystalline flakes were found as the product after drying. Yield : 0.4 g (65 %).

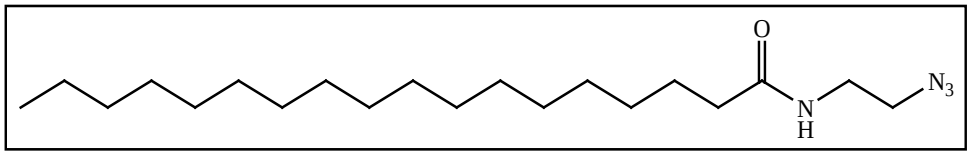

Lipid 1

Lipid 1: ^{1}H NMR (400 MHz, $CDCl_3$) δ ppm 0.89 (s, 3 H), 1.26 (s, 25 H), 1.58 (br. s., 4 H), 2.05 (s, 1 H), 2.20 (s, 2 H), 3.45 (s, 3 H), 3.71 (s, 1 H). ^{13}C NMR (101 MHz, $CDCl_3$) δ ppm 13.79 (s, 1 C), 22.59 (s, 1 C), 25.30 (s, 1 C), 29.01 (s, 1 C), 29.38 (s, 10 C), 31.60 (s, 1 C), 36.42 (s, 1 C), 38.54 (s, 1 C), 44.69 (s, 1 C), 50.73 (s, 1 C), 175.00 (s, 1 C). HRMS: exact mass calculated for $C_{20}H_{40}N_4O$ $[M-H]^-$ was 352.3, Found 351.2.

Lipid 2. Oleic acid (0.49 g, 1.74 mmol, 1 equiv.) was added to compound **1c** (0.15 g, 1.74 mmol, 1 equiv.) in presence of BOP (0.77 g, 1.74 mmol, 1 equiv.) and triethylamine (0.53 g, 0.523 mmol, 3 equiv.) in 30 mL chloroform. The reaction was carried out at room temperature with stirring under nitrogen atmosphere. The solution was extracted with chloroform/water system (3 X 20 mL). The solvent was evaporated and the product was purified in the flash chromatography with ethylacetate/hexane (**R_f = 0.2**; EtOAc : Hex = 1 : 3) as the mobile phase. White sticky solid was obtained as the product after drying. Yield : 0.4 g (59 %).

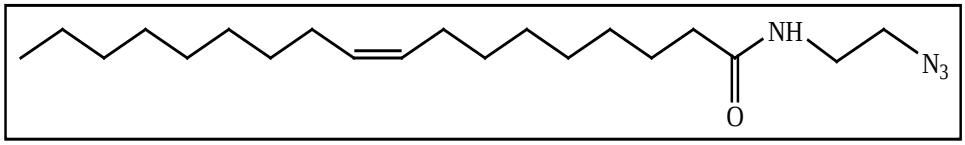

Lipid 2

Lipid 2: ^{1}H NMR (400 MHz, $CDCl_3$) δ ppm 0.88 (s, 3 H), 1.30 (br. s., 21 H), 1.63 (br. s., 2 H), 2.01 (br. s., 4 H), 2.19 (s, 2 H), 3.44 (s, 4 H), 5.34 (br. s., 2 H), 5.82 (br. s., 1 H). ^{13}C NMR (101 MHz, $CDCl_3$) δ ppm 14.11 (s, 1 C), 22.69 (s, 1 C), 25.60 (s, 1 C), 27.17 (s, 1 C), 27.22 (s, 1 C), 29.12 (s, 1 C), 29.24 (s, 1 C), 29.32 (s, 1 C), 29.53 (s, 1 C), 29.70 (s, 1 C), 29.77 (s, 1 C), 31.90 (s, 1 C), 36.70 (s, 1 C), 38.87 (s, 1 C), 46.01 (s, 1 C), 51.04 (s, 1 C), 58.13 (s, 1 C), 129.73 (s, 1 C), 130.02 (s, 1 C), 182.95 (s, 1 C). HRMS: exact mass calculated for $C_{20}H_{38}N_4O$ $[M-H]^-$ was 350.3, Found 349.3.

Peptide Synthesis: All the peptides were synthesized in the microwave-assisted peptide synthesizer using the standard Fmoc protected amino acids in the 0.1 mmol scale and Fmoc-Gly-CLEAR-amide resin as the solid support. CEM Discover microwave chamber was used for the reaction in a 30 mL reaction vessel within it and attached with the synthesizer. Mixture of HOBT/HBTU was used as the coupling reagents and each of the coupling steps was performed once (except Arg) at 50 ºC under 25 W microwave power (300 seconds). For the Arg coupling initial reaction was performed at 25 ºC for 1500 seconds with no microwave. After that 25 W microwave power was used at 25 ºC for 300 seconds. For the activator base, mixture of DIEA and NMP were used and piperazine was used as the deprotector. All the reagents were used five-fold in excess and were dissolved in equivalent amounts of DMF. The initial deprotection was carried out with 35 W microwave power for 30 seconds at 75 ºC. Final deprotection and cleavage of the peptides from the resin were not carried out in the machine. A mixture of

trifluoroacetic acid-tri-isopropylsilane-water (TFA-TIPS-H_2O = 95 % - 2.5 % - 2.5 %) was used as the cleaving solution (20 mL) and the cleaving was carried out in the bench top for 3 hours. The crude peptides were precipitated as solids with ice-cold diethyl ether and centrifuged. The supernatant was discarded and the precipitates were dried and the crude peptides were purified by reversed-phase semi-preparatory HPLC.

Semi-preparatory HPLC: For the hexynoic acid peptides, a Princeton Chromatography C18 column was used with a linear gradient of 0 to 80 % acetonitrile in water for 50 minutes at a flow rate of 4.5 mL/min. Both water and acetonitrile contained 0.1% TFA and the solvents were degassed for 10 minutes before each run. For the stearic acid peptide a Princeton Chromatography diphenyl column was used with a linear gradient of 10 to 80 % acetonitrile and water for 40 minutes at a flow rate of 4.5 mL/min. All the purifications were monitored at the detector wavelength of 235 nm. The purified samples were collected in vials and dried overnight in the lyophilizer.

Mass spectroscopy (MALDI-ToF): The dried samples from semi-preparatory HPLC were sent for molecular weight analysis by MALDI-ToF at the Proteomics Core Center Facility at the University of North Dakota.

Analytical HPLC: All the peptide cleaving experiments by MMPs were carried out with the analytical columns (C18 for hexynoic acid peptides and diphenyl for stearic acid peptides) with the same gradient as the semi-preparatory column but with 1.5 mL/min flow rate for 30 minutes. The detector wavelength was kept at 235 nm and the mobile phase contained 0.1% TFA in each.

Buffer Solutions: For all the MMP experiments, 25 mM HEPES buffer was used (pH = 8.0) with 10 mM $CaCl_2$, 10 µM $ZnCl_2$ and 100 mM NaCl. For the liposomal formulations,

carboxyfluorescein was dissolved in 25 mM HEPES Buffer (pH =8.0) with 10 mM $CaCl_2$, 10 µM $ZnCl_2$. To the buffer solution, 100 mM NaCl was added initially and during column equilibration, liposomes elution from the column and all the release experiments, the osmolality was adjusted by adding NaCl.

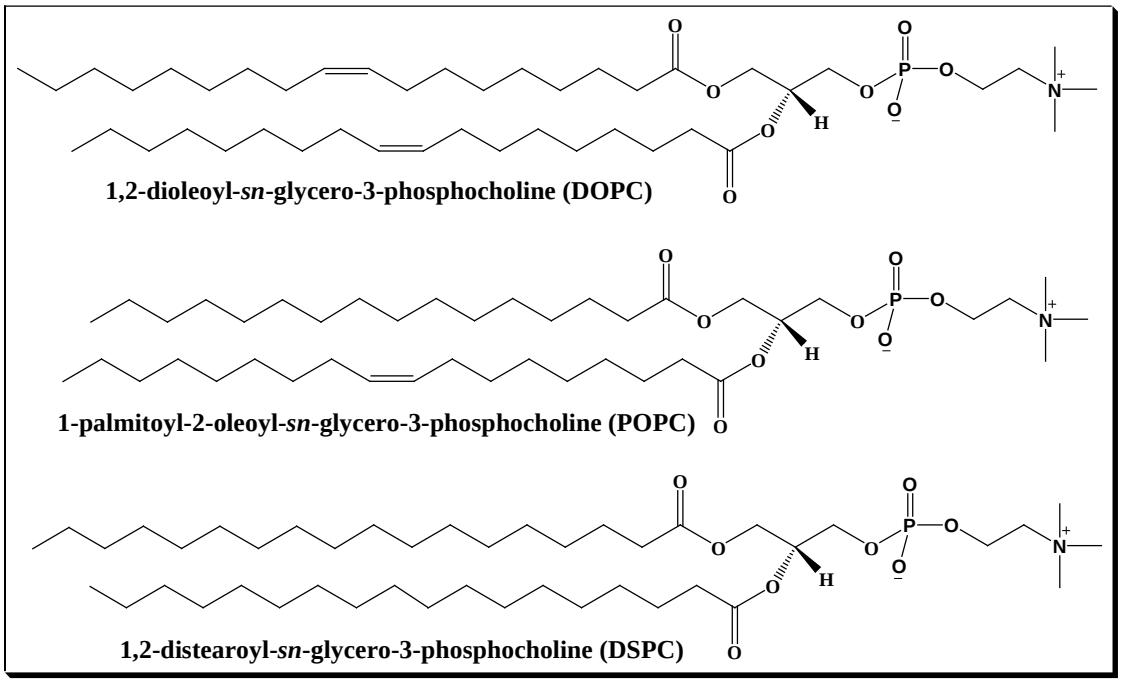

Figure 47. Structures of commercial phospholipids used for liposome formulations.

Liposome Preparation: Weighed amounts of synthesized lipids were dissolved in chloroform/methanol solution (5:1) to a concentration of 2 mg/mL. Commercial phospholipids such as, POPC, DOPC and DSPC (Figure 47) were made in stock with 2 mg/mL concentration and then in a 25 mL round bottomed flask appropriate amount of both the lipids were mixed and then evaporated while stirring in the rotary evaporator to form a thin film. In some liposomes, along with the commercial lipids, lipopeptides were used instead of the synthesized lipids (vide later). Once a thin film is made, it was kept in the desiccator under high vacuum overnight to remove all traces of the organic solvents. Next day the thin film was hydrated with 1.5 mL

carboxyfluorescein dye (100 mM) in buffer for 60 minutes at 50 ºC under stirring condition. The hydration was then carried out at the room temperature by storing for another 60 minutes followed by bath sonication at 50 ℃ for 30 minutes to form unilamellar vesicles from multilamellar vesicles. After sonication, 10 freeze-thaw cycles were performed in liquid nitrogen for better encapsulation. The solution then was extruded first through 800 nm and then 200 nm polycarbonate filters (Avanti Polar lipids, AL) at 70 ºC for 20 times each. The solution was then passed through the Sephadex G-50 column which was equilibrated with the properly adjusted osmolal HEPES buffer (same as the extruded solution) to remove the unencapsulated dye. The reason for keeping the osmolality of the extruded carboxyfluorescein liposomal solution and the buffer same was to prevent the release of the liposomal content from osmotic shock.

Size determination using Dynamic Light Scattering: For determination of the sizes of the liposomes, the eluted liposomes were diluted 20 times in the same osmolality adjusted buffer and then checked in the Zetasizer instrument for Z-average diameter and polydispersity index. For each sample, 3 runs were taken (11 measurements for each run, with 10 seconds delay) at 25 ºC.

Preparation of Cu complex for "click" reaction: For the $CuCl_2$ stock solution preparation, PMDETA (*N*,*N*,*N'*,*N'*,*N''*-pentamethyldiethylenetriamine) was mixed to the aqueous solution of $CuCl_2$ and stirred for 2 hours at room temperature to make a final Cu-complex solution of concentration 0.053 M. This stock solution was used in all the conjugation reactions with proper dilutions. This step was performed to avoid precipitation which usually occurs upon mixing just the $CuCl_2$ solution in the buffer solutions containing the liposomes.

Conjugation of the peptides with the liposomes: For the liposomes which were composed of synthesized lipids and phospholipids, the MMP-7 cleavable hexynoic acid peptides were conjugated using 'click reaction'. The eluted liposomes (1 mL) were mixed with the equivalent amount of peptide (1:1 according to azide and alkyne concentrations in the synthesized lipids and hexynoic acid peptide respectively) in presence of $CuCl_2$ solution (1.5 equivalents) (prepared previously) and sodium ascorbate (4 equivalents) solutions. The 'click' reaction was carried overnight with slight stirring at room temperature. Next day the solution was passed through Sephadex G-50 column to separate the Cu and leaked carboxyfluorescein from the conjugated liposomes. For the liposomes which were made of the lipopeptides and phospholipids, this conjugation step is not performed as the MMP-7 cleavable peptide was incorporated within the lipid bilayer of the liposomes.

Release experiments: The liposomes both before and after conjugation were subjected to release experiments. For the MMP-7 mediated release experiments, 25 µM stock solution of the recombinant enzyme was added to liposomal solution in the HEPES buffer (pH=8.0, 10 mM $CaCl_2$, 10 µM $ZnCl_2$ and 100 mM NaCl and osmolality adjusted) to achieve 1 µM and 2 µM concentrations of the enzymes separately in the wells to a total volume of 200 µL. These releases were compared with wells containing no MMP-7 which served as the controls. The release experiments were monitored at 518 nm with 480 nm as the excitation wavelength for 30 minutes with 20 seconds interval in the spectrofluorometer (Spectramax, Molecular Devices). All the experiments were conducted in triplicate using 96 well plates for fluorescent studies. The averages of the three measurements were taken finally. After that 10 µL of Triton-X was added to each well to rupture the liposomes for release the dye completely. For all the human recombinant MMP-7 release experiments, the activity of the enzyme was checked every time

with the commercially available substrate prior to the release experiments. The percentage leakage was calculated using the following formula:

$$\% \text{ leakage} = \{(I_t - I_0) / (I_{triton} - I_0)\} \times 100 \qquad \textbf{(Equation 4)}$$

Results and Discussions

In order to detect active MMP-7 with the help of liposomes, we started with designing MMP-7 cleavable peptides. Our original goal was to incorporate MMP-7 cleavable peptide within the lipid bilayer of liposomes along with commercial lipids and then monitor the release of liposomal content, in our case a fluorogenic dye, carboxyfluorescein. By this way we could indirectly detect the activity of MMP-7 which is found to be overexpressed in various cancers as mentioned at the beginning of the chapter. Zheng et al (*183*) used the short peptide sequence G*PLG*LARK where the cleavage site for MMP-7 was between G and L. We investigated this peptide sequence and tried to modify it for incorporating in the liposomes. The peptide needed to be attached to some lipid tail for forming lipid bilayer. We tried attaching a saturated fatty acid, stearic acid to the N-terminus of the modified sequence and synthesized peptide **Rd-A** (Table 18) in our microwave-assisted peptide synthesizer. The HPLC purification trace and the MALDI-ToF spectra of the purified peptide **Rd-A** are shown in Figure 48 and Figure 49 respectively.

Table 18. Names and amino acid sequences of the synthesized peptides.

Name of Peptides	Peptide Structure
Rd-A	Stearic acid-GPL*G-L*ARKG
Rd-B	Stearic acid-mini-PEG-GPL*G-L*ARKG
Rd-C	Hexynoic acid-GPL*G-L*ARKG
Rd-D	Hexynoic acid-GPL*G-L*AEEG

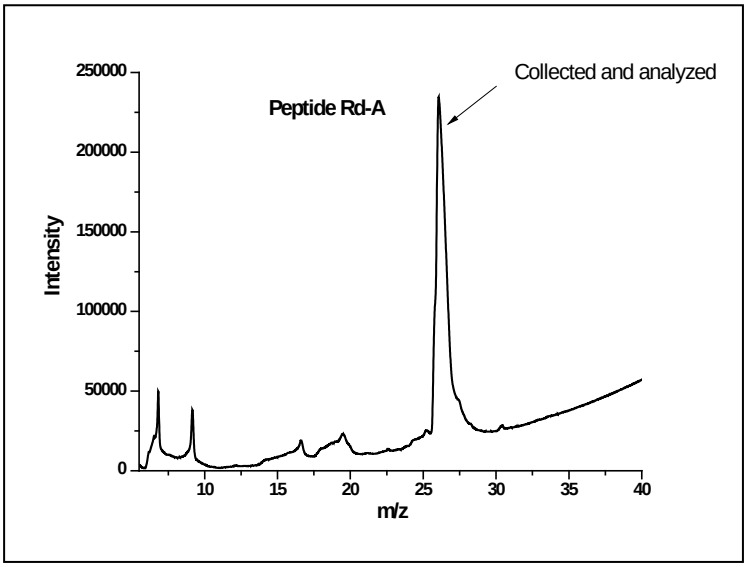

Figure 48. HPLC purification trace of the peptide **Rd-A.**

The purified product was then tested to check if MMP-7 was cleaving the peptide and for this analytical diphenyl column was used. The peptide **Rd-A** (100 μM) was incubated with 100 nM of active MMP-7 and then 100 μL was aliquoted at 30, 60 and 120 minutes time point and the reaction was stopped at each point by adding 4 μL TFA. Next, 100 μL of these aliquots were injected in the HPLC to check the peptide peak intensity change before and after MMP-7 incubation.

Even after 120 minutes, no change in the original peptide peak was noticed suggesting that MMP-7 was not cleaving the peptide. Increasing the amount of active MMP-7 to 1 μM caused no cleaving as observed from the HPLC chromatogram (Figure 50).

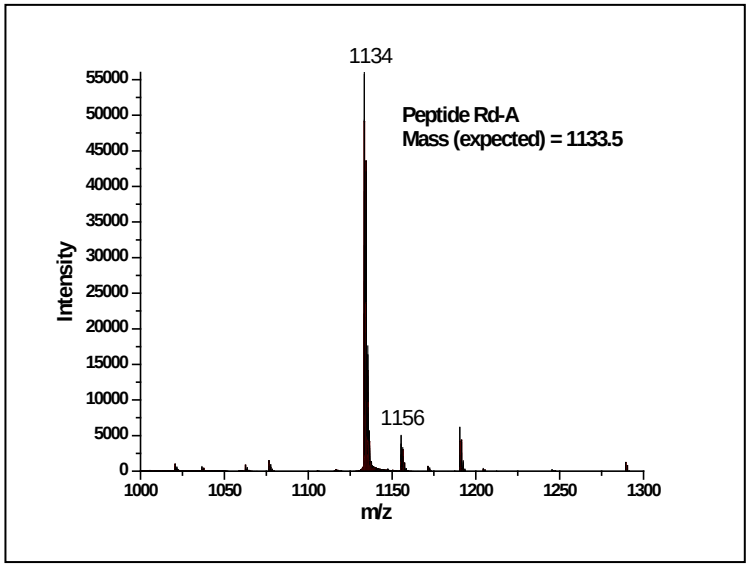

Figure 49. Mass spectra of the purified peptide **Rd-A**.

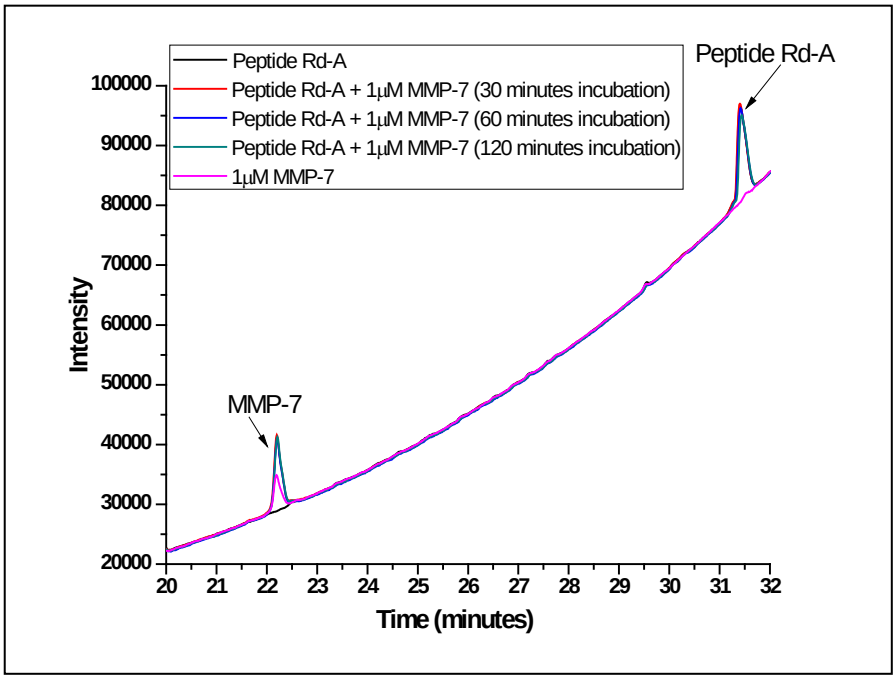

Figure 50. Cleaving experiment showing peptide **Rd-A** (100 μM) incubated with active recombinant hMMP-7 (1 μM) after incubating at 30, 60 and 120 minutes.

Although the peptide sequence was reported in the literature to be cleaved by MMP-7, we have not yet found any possible reason for this anomaly. One possible explanation could be that

the modified peptide contained stearic acid resulting in a micellar structure. As a result the polar head groups of the peptide (**Rd-A**) are not properly accessible to the enzyme as it would be for just the peptide alone. As an alternative approach, we tried to insert a mini-PEG between the stearic acid end and the peptide sequence in order to achieve better solubility. Peptide **Rd-B** (vide Table 18) was synthesized and purified in the semi-preparatory diphenyl column (Figure 51).

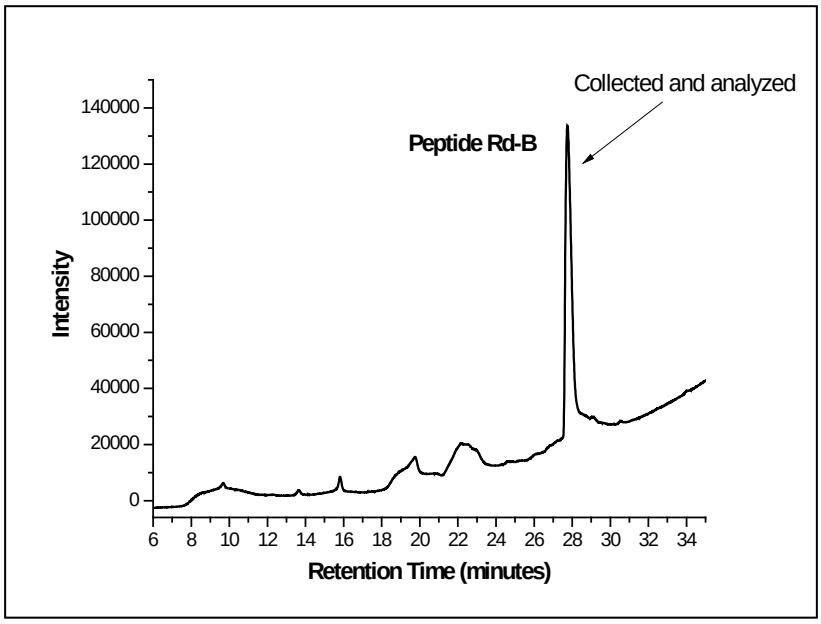

Figure 51. HPLC purification trace of the peptide **Rd-B**.

Although we obtained good separations in the column and the mass of the purified product was confirmed by MALDI-ToF (Figure 52), we faced difficulties in encapsulating the dye within the liposomes (**Rd-L7**, vide Table 19) formulated with the peptide **Rd-B** (discussed later).

We next attempted to synthesize another peptide by replacing the stearic acid with 5-hexynoic acid and keeping the rest of the sequence intact, to check whether the peptide was cleaved by MMP-7.

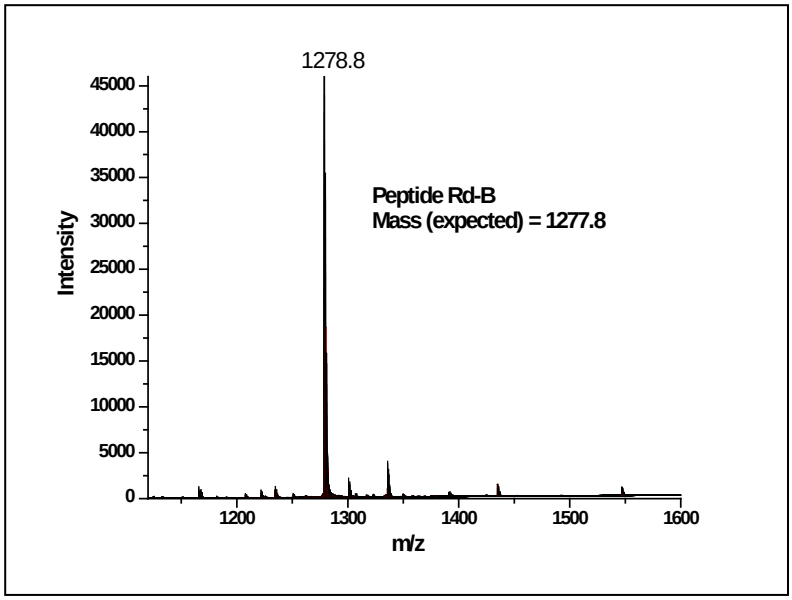

Figure 52. Mass spectra of the purified peptide **Rd-B**.

The peptide **Rd-C** (vide Table 18) was synthesized following the same conditions as earlier and the purification was carried out with C18 semi-preparatory column (Figure 53). The molecular weight of the purified peptide was confirmed by MALDI-ToF mass spectrometry (Figure 54). The pure peptide was next tested for cleaving by active MMP-7. With 100 nM of the active enzyme, 100 μM of the peptide was found to be cleaved as observed from the change in the HPLC chromatogram (Figure 55).

The cleaving experiment revealed that the original peptide peak decreased in intensity with time and new peaks corresponding to the peptide fragments (Figure 55; Peak A and Peak B) appeared at different retention times and those peaks increased in intensity with time proving that the peptide was cleaved by MMP-7. To confirm that the Peak A and Peak B (Figure 56 and Figure 57) were actually the fragments of the peptide **Rd-C**, MALDI-ToF mass spectral analyses were carried out on the 120 minutes MMP-7 incubated peptide (freeze-dried mixture). MALDI-ToF showed the masses of the peptide fragments were present along with the intact peptide

(Figure 58). From the peaks obtained from MALDI, we found that the peptide was cleaved at two points, between G and L, but also between L and G when compared with the calculated masses of the peptide fragments.

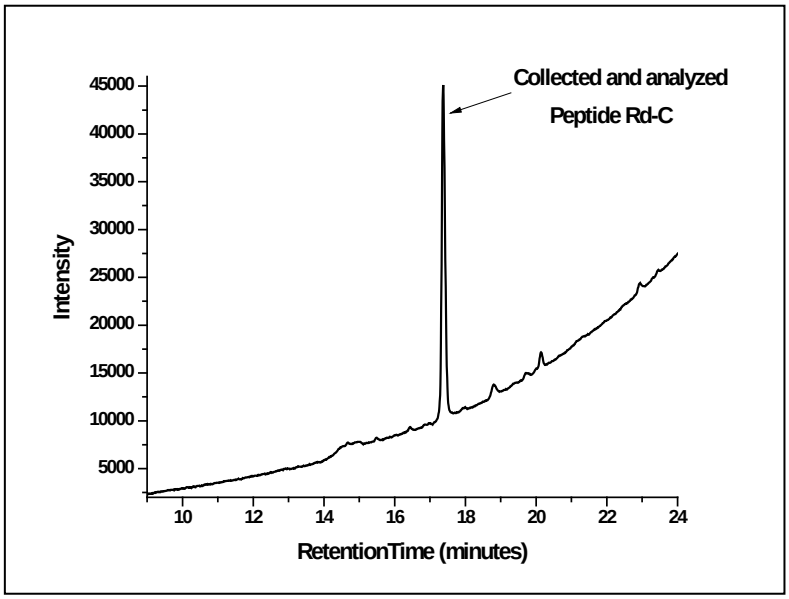

Figure 53. HPLC purification trace of the peptide **Rd-C**.

Once established that the peptide **Rd-C** was cleaved by active MMP-7, the selectivity of the peptide sequence was checked for hMMP-7 against active hMMP-9 and -10. The activities of hMMP-9 and -10 were checked with commercial fluorogenic substrate prior to the cleaving experiments. The cleaving experiments were repeated for MMP-9 and MMP-10 separately with the peptide **Rd-C** following the same incubation conditions and HPLC procedures. The experimental parameters were kept identical (peptide and enzyme concentrations) for MMP-9 and MMP-10 as was for MMP-7. For MMP-9, it was found that the peptide **Rd-C** was cleaved by the enzyme although the rate of cleaving was slow compared to MMP-7 as shown from the HPLC chromatogram (Figure 59 and Figure 60). For MMP-10, even after 2 hours, no noticeable

change was found in the original peptide peak proving that the peptide **Rd-C** was not cleaved by the MMP-10 under the same conditions (Figure 61).

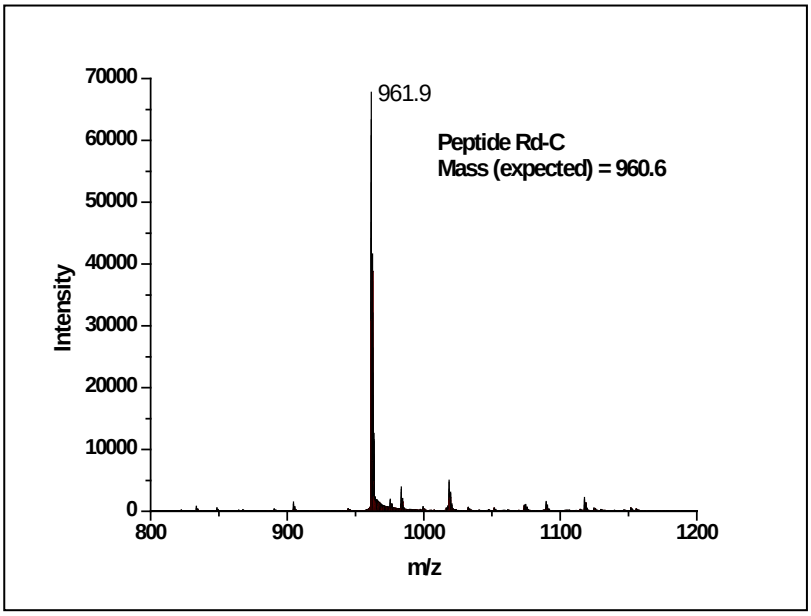

Figure 54. Mass spectra of the purified peptide **Rd-C**.

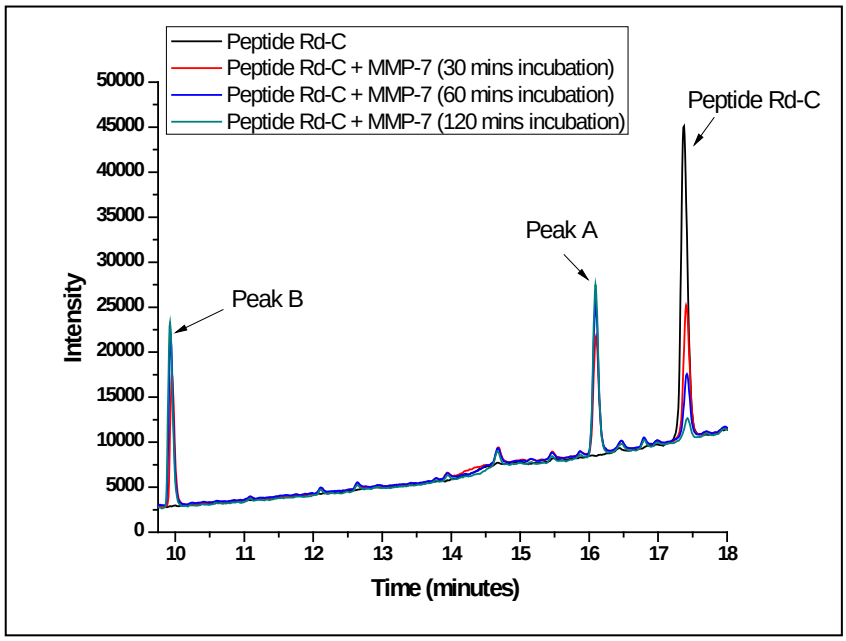

Figure 55. Cleaving experiment showing peptide **Rd-C** (100 μM) was cleaved by active recombinant hMMP-7 (100 nM) after incubating at 30, 60 and 120 minutes. The cleaved peptide fragments (Peak A and Peak B) with different retention times increased with time.

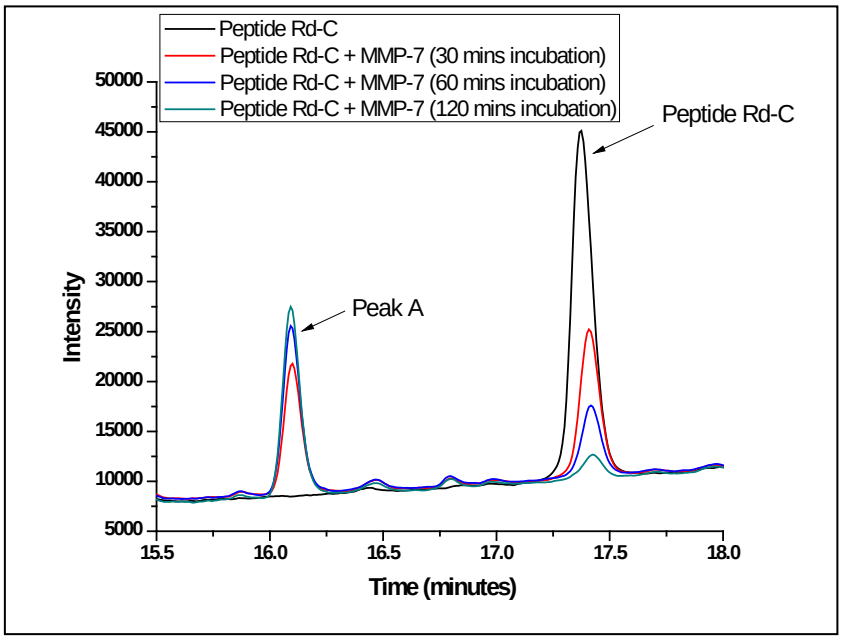

Figure 56. Cleaving experiment showing peptide **Rd-C** (100 μM) was cleaved by active recombinant hMMP-7 (100 nM) after incubating at 30, 60 and 120 minutes. The cleaved peptide fragments Peak A (magnified) with different retention time increased with time.

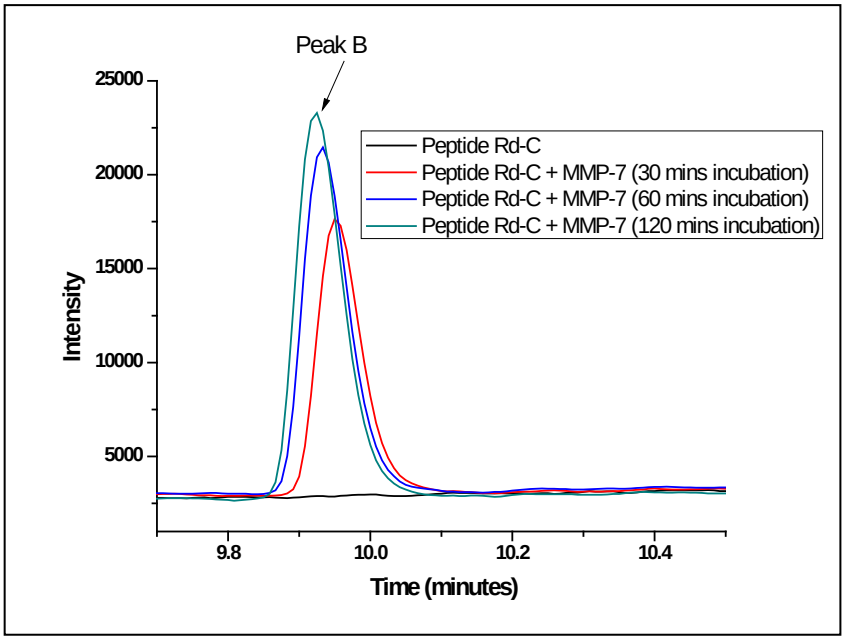

Figure 57. Cleaving experiment showing peptide **Rd-C** (100 μM) was cleaved by active recombinant hMMP-7 (100 nM) after incubating at 30, 60 and 120 minutes. The cleaved peptide fragments Peak B (magnified) with different retention time increased with time.

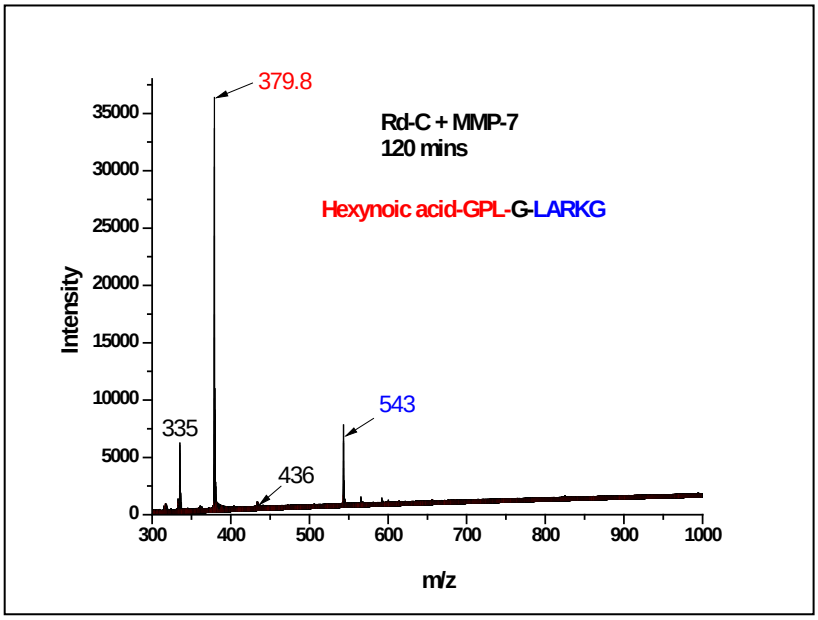

Figure 58. Mass spectra of the peptide **Rd-C** and its cleaved fragments after 2 hours incubation with active recombinant hMMP-7.

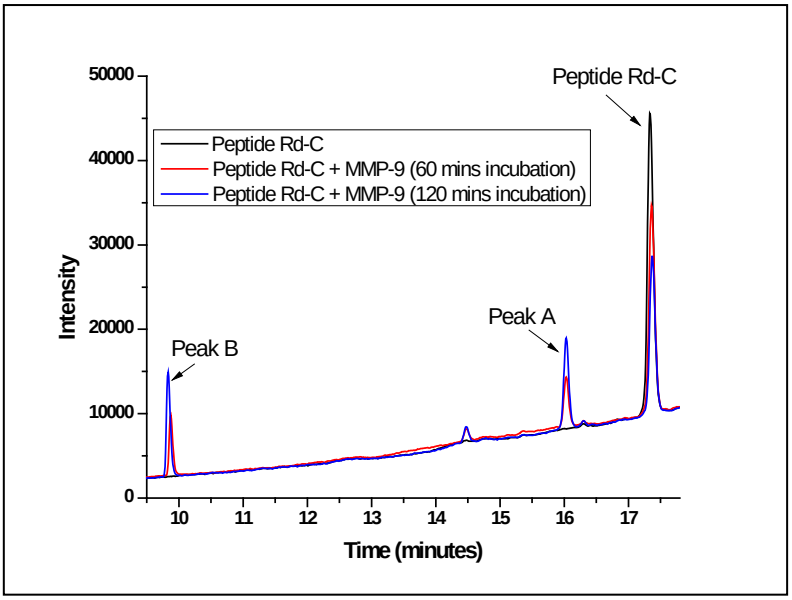

Figure 59. Cleaving experiment showing peptide **Rd-C** (100 μM) was cleaved by active recombinant hMMP-9 (100 nM) after incubating at 60 and 120 minutes. The cleaved peptide fragments (Peak A and Peak B) with different retention times increased with time.

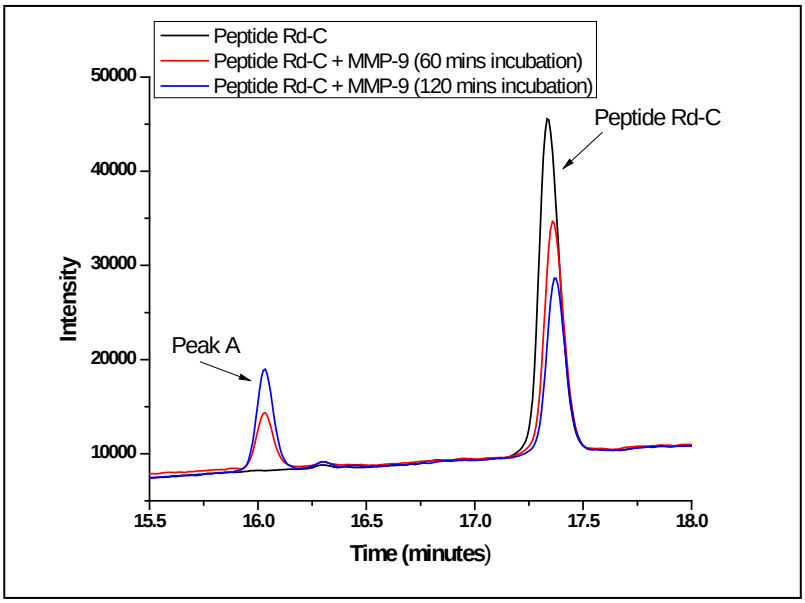

Figure 60. Cleaving experiment showing peptide **Rd-C** (100 μM) was cleaved by active recombinant hMMP-9 (100 nM) after incubating at 60 and 120 minutes. The cleaved peptide fragments Peak A (magnified) with different retention times increased with time.

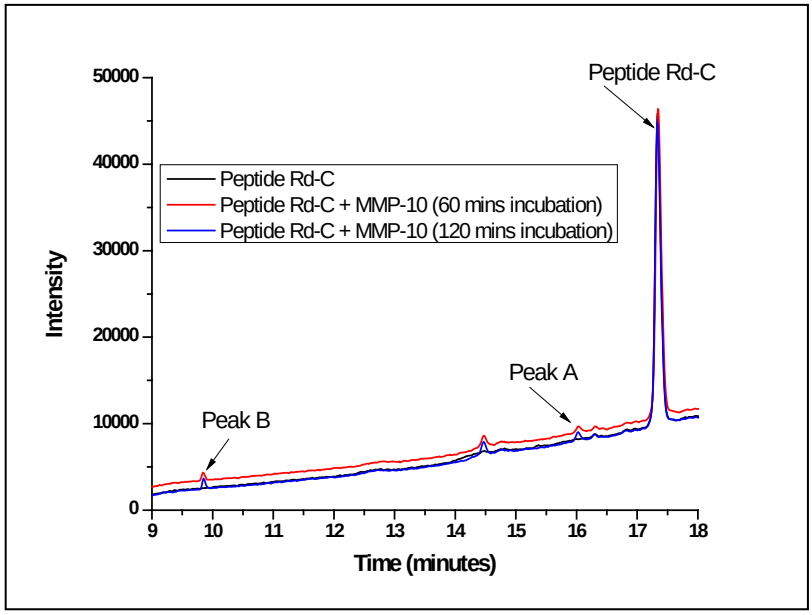

Figure 61. Cleaving experiment showing peptide **Rd-C** (100 μM) was cleaved by active recombinant hMMP-10 (100 nM) after incubating at 60 and 120 minutes. The cleaved peptide fragments (Peak A and Peak B) with different retention times did not increase significantly with time.

Since we found peptide **Rd-C** was cleaved by MMP-7, we next attempted to make liposomes with it. **Rd-L1** (Table 19) liposomes were composed of 70 mole % POPC and 30 mole % of the peptide **Rd-C** following the procedure discussed above and depicted in Scheme 5.

Table 19. Compositions of liposomes prepared.

Liposome Formulations	Commercial Lipids (mole %)	Synthesized Lipids (mole %)	Conjugated Peptide
Rd-L1	POPC (70)	-	Rd-C (30 mole %)
Rd-L2	POPC (70)	Lipid **1**(30)	Rd-C
Rd-L3	POPC (70)	Lipid **2**(30)	Rd-C
Rd-L4	DSPC (70)	Lipid **1**(30)	Rd-C
Rd-L5	DOPC (70)	Lipid **2**(30)	Rd-C
Rd-L6	POPC(70)	Lipid **1**(30)	Rd-D
Rd-L7	POPC(70)	-	Rd-B (30 mole %)

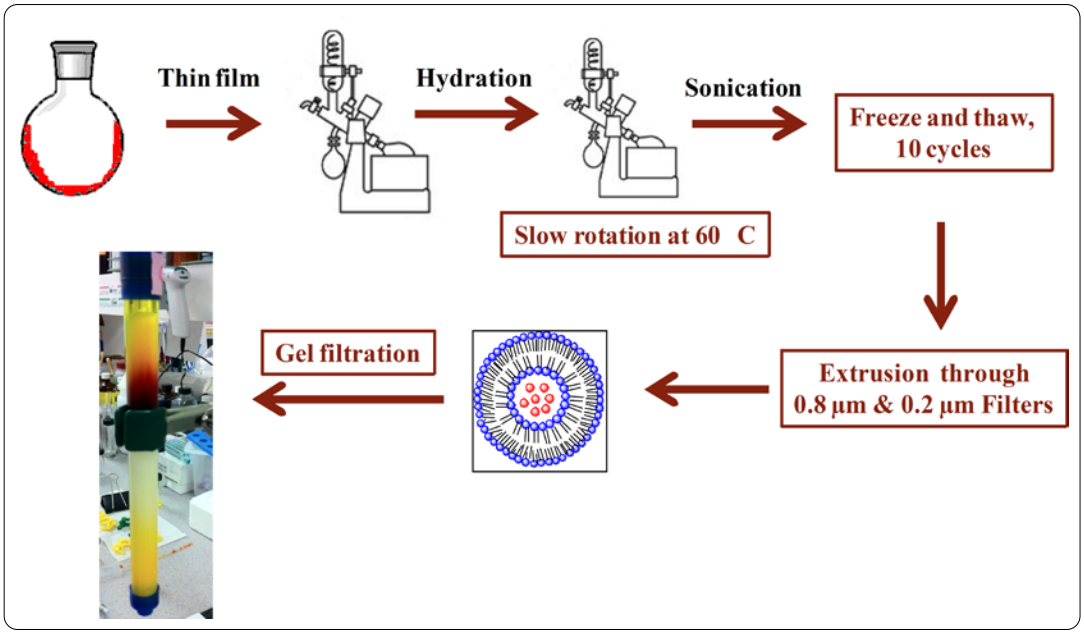

Scheme 5. Schematic diagram of liposome preparation steps.

Carboxyfluorescein encapsulated liposomes were prepared. It was hypothesized that active MMP-7 would cleave the peptide and that would disturb the stability of the liposomal bilayer resulting in the release of the dye. This disturbance would be monitored by the

fluorescence intensity changes of the released dye with time. The sizes of the liposomes were measured in the DLS and were found to be 139.1 ± 12.7 nm (Table 20).

In order to check the release of the dye, opaque 96 microwell plates were used. The concentrations of the liposomes were kept 0.1 mg/mL and for the active MMP-7 two concentrations, 1 μM and 2 μM were used in the wells. The releases were compared with just the liposomes without any enzyme to check the leakage. Each of the experiments was done in triplicates. At the end of 30 minutes, 10 μL of triton was added and the fluorescence intensity after 5 minutes was recorded. This intensity was considered to be from 100 % release of the dye as the liposomes ruptured in presence of triton. The percentage release was calculated using the equation mentioned earlier (Equation 4). But it was observed that the release from the control wells were more than from the wells containing MMP-7, suggesting that the dye leaked from the liposomes by itself faster than in the presence of MMP-7 (Figure 62). Another possibility could be that since the peptide has a short lipid, hexynoic acid, incorporation of the peptide in the liposomes could have affected the stability of the bilayer and that actually caused the greater release.

In order to address this problem, we sought to attach the hexynoic acid-peptide **Rd-C** with the synthesized stearic acid azide through "Click" reaction. The azide present in the stearic acid compound (Lipid **1**, described earlier) would react with the alkyne group of the peptide **Rd-C** and would form a five-membered ring structure. The reaction is a 1, 3-dipolar cycloaddition reaction and the product is a 1, 2, 3-triazole. By this way two purposes were served, one was the incorporation of a relatively long chain fatty acid within the liposomal bilayer and the second was the attachment of the known MMP-7 cleavable peptide with the liposomes (Scheme 6). We had also synthesized another lipid azide, oleic acid azide (Lipid **2**, described earlier) for

incorporation within the liposomal bilayer. Next, 30 mole % of the synthesized lipids and 70 mole % of the commercial lipids were used and liposomal formulations were made and then these were reacted with the peptide **Rd-C** through "click" reaction. In this way the following conjugated liposomal formulations, **Rd- L2**, **Rd- L3**, **Rd- L4** and **Rd- L5** (Table 19) were obtained. Other than POPC, DSPC and DOPC lipids were also used in these formulations. The sizes of the liposomes before and after the "click" reaction were checked in the DLS and are given below (Table 20).

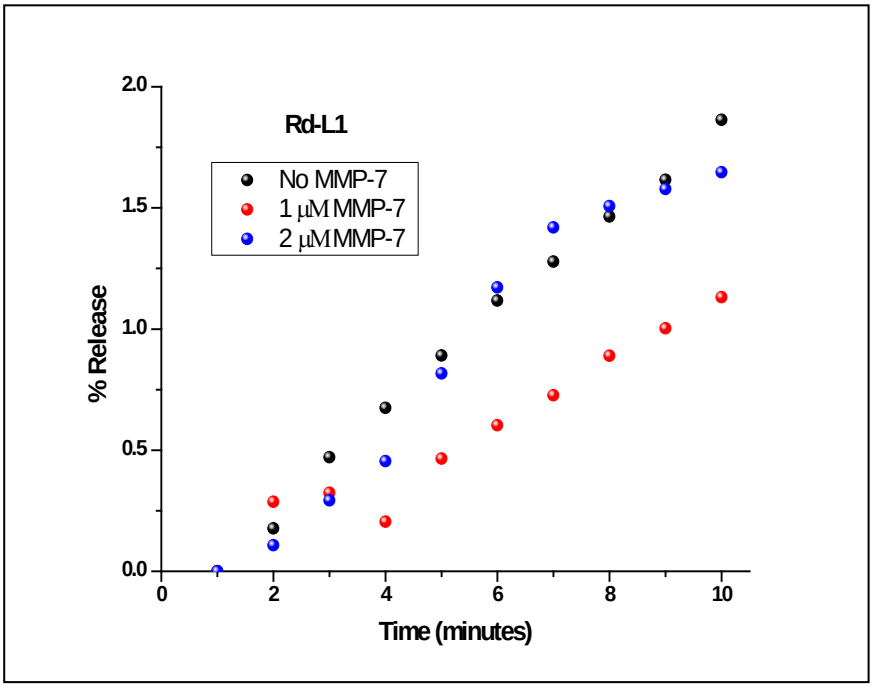

Figure 62. Release profile of the encapsulated dye carboxyfluorescein from the liposomes **Rd-L1** in absence (black circles) and presence of 1 µM (red circles) and 2 µM (blue circles) of active hMMP-7. The experiments were conducted with 25 mM HEPES buffer (pH =8.0) containing 10 mM $CaCl_2$, 10 µM $ZnCl_2$ and 100 mM NaCl and osmolality adjusted.

Table 20. Sizes of liposomes by Dynamic Light Scattering (DLS) before and after cross linking (n=3).

Liposomal Formulations	Size before "click" reaction (nm)	Size after "click" reaction (nm)	Polydispersity indices (P. I.) of liposomes after "click" reaction
Rd-L1	139.1 ± 12.7	-	0.2 ± 0.0
Rd-L2	144.2 ± 11.3	157.9 ± 1.6	0.2 ± 0.1
Rd-L3	146.2 ± 1.9	146.3 ± 11.1	0.4 ± 0.1
Rd-L4	62.4 ± 3.7	130.6 ± 12.9	0.6 ± 0.2
Rd-L5	166.4 ± 22.7	282.4 ± 6.9	0.2 ± 0.0
Rd-L6	75.4 ± 0.4	98.3 ± 0.8	0.2 ± 0.0
Rd-L7	153.5 ± 1.3	-	0.1 ± 0.0

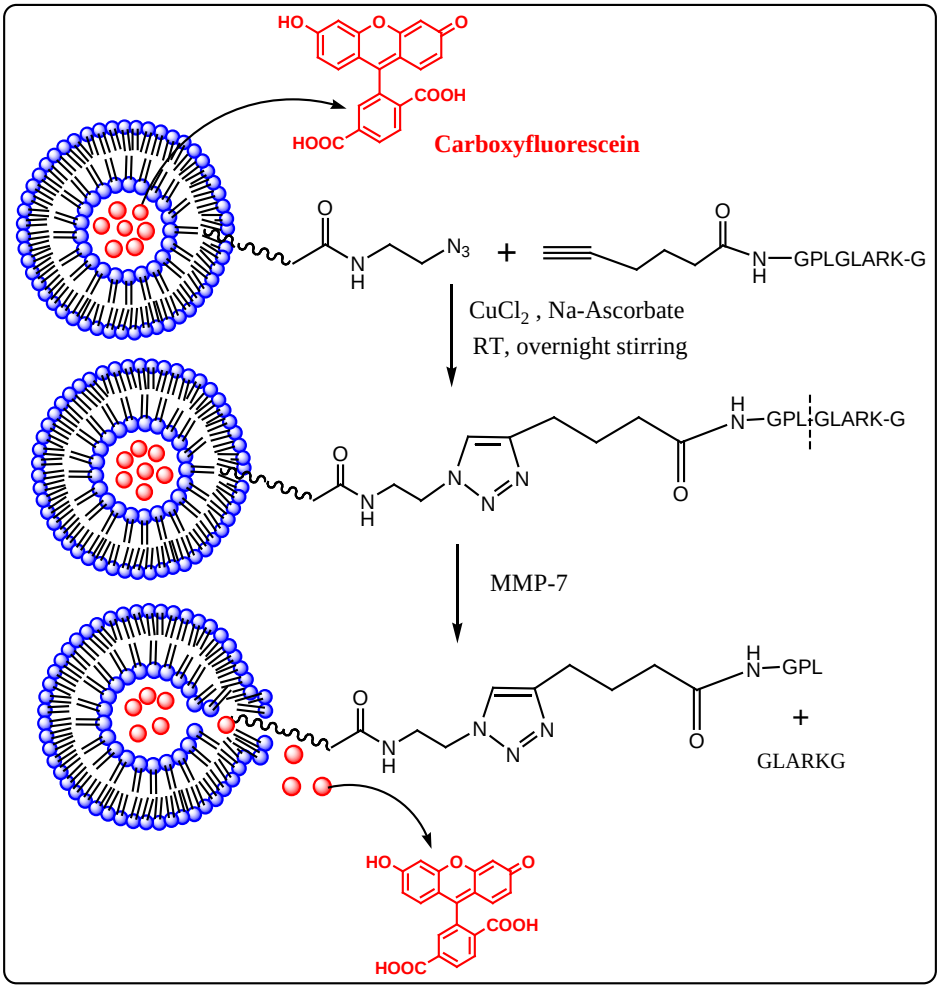

Scheme 6. Schematic representation of conjugating the peptides **Rd-C/Rd-D** with the carboxyfluorescein encapsulated liposomes by the "Click" reaction.

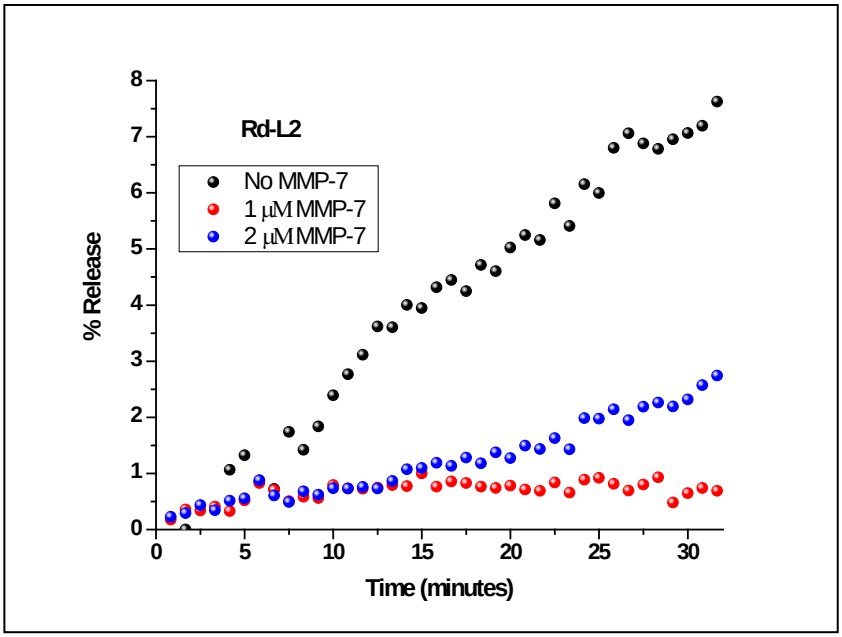

Figure 63. Release profile of the encapsulated dye carboxyfluorescein from the liposomes **Rd-L2** in absence (black circles) and presence of 1 µM (red circles) and 2 µM (blue circles) of active hMMP-7. The experiments were conducted with 25 mM HEPES buffer (pH =8.0) containing 10 mM $CaCl_2$, 10 µM $ZnCl_2$ and 100 mM NaCl and osmolality adjusted.

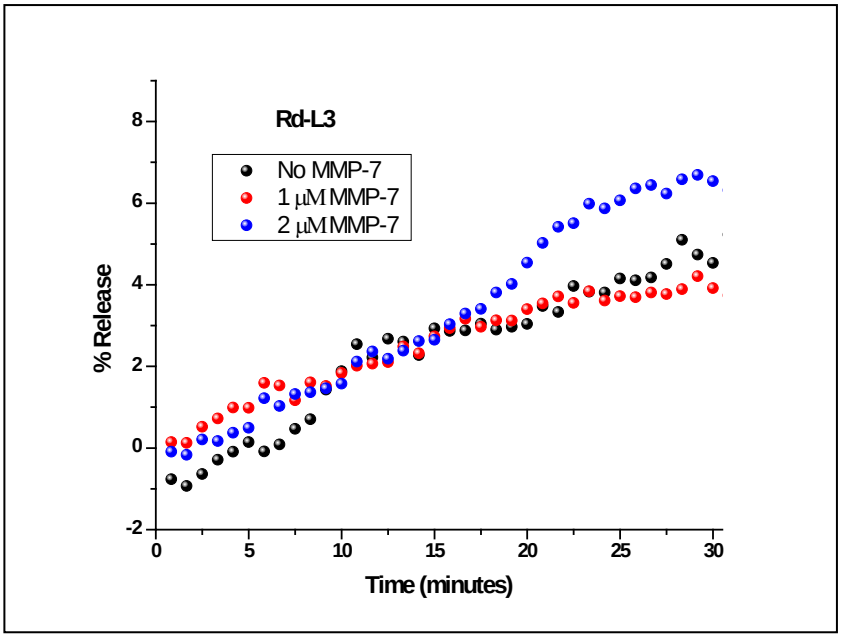

Figure 64. Release profile of the encapsulated dye carboxyfluorescein from the liposomes **Rd-L3** in absence (black circles) and presence of 1 µM (red circles) and 2 µM (blue circles) of active hMMP-7. The experiments were conducted with 25 mM HEPES buffer (pH = 8.0) containing 10 mM $CaCl_2$, 10 µM $ZnCl_2$ and 100 mM NaCl and osmolality adjusted.

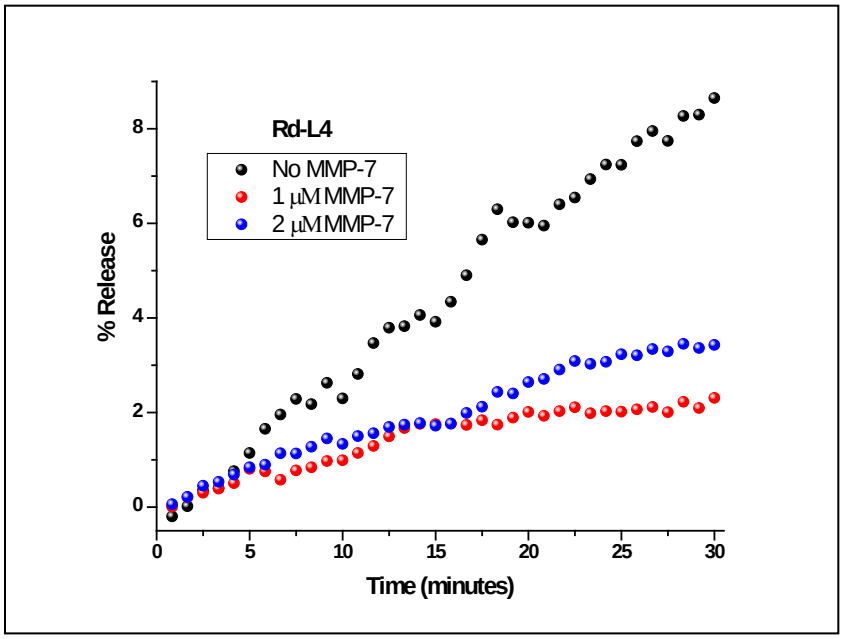

Figure 65. Release profile of the encapsulated dye carboxyfluorescein from the liposomes **Rd-L4** in absence (black circles) and presence of 1 μM (red circles) and 2 μM (blue circles) of active hMMP-7. The experiments were conducted with 25 mM HEPES buffer (pH = 8.0) containing 10 mM $CaCl_2$, 10 μM $ZnCl_2$ and 100 mM NaCl and osmolality adjusted.

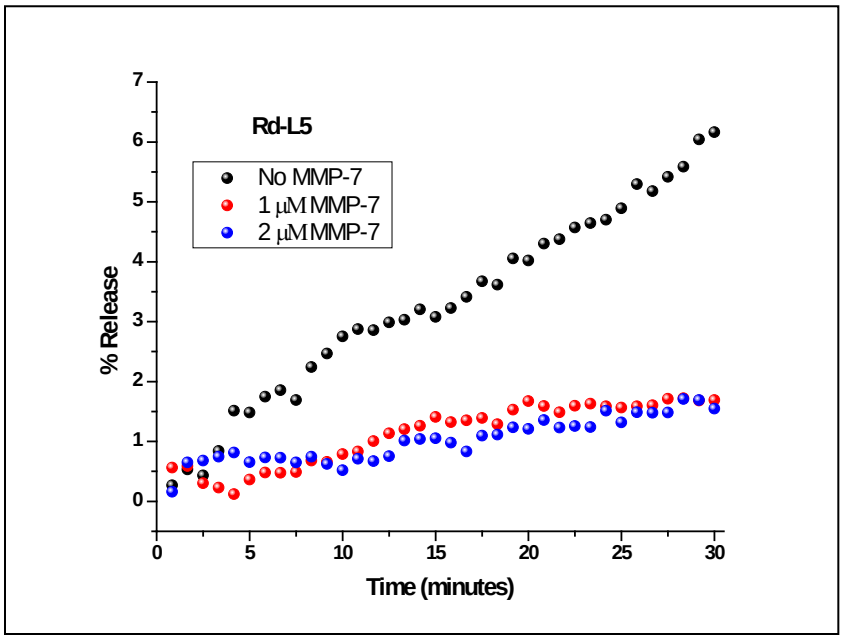

Figure 66. Release profile of the encapsulated dye carboxyfluorescein from the liposomes **Rd-L5** in absence (black circles) and presence of 1 μM (red circles) and 2 μM (blue circles) of active hMMP-7. The experiments were conducted with 25 mM HEPES buffer (pH = 8.0) containing 10 mM $CaCl_2$, 10 μM $ZnCl_2$ and 100 mM NaCl and osmolality adjusted.

In all the above formulations, we noticed that in absence of MMP-7 the percentage of release was highest than in the presence of the enzyme. However, the release was higher in presence of 2 µM MMP-7 than that in presence of 1 µM of MMP-7. This unusual behavior can be attributed to the fact that the peptide **Rd-C** is positively charged and therefore could have an inhibitory effect on the enzyme. So we proceeded to synthesize a negatively charged peptide **Rd-D**. The sequence of the peptide was hexynoic acid-GPL-GLAEEG where two Glu acids were incorporated to impart negative charge to the peptide. The peptide was synthesized previously described and was purified in the semi-preparatory. HPLC (Figure 67) and the mass of the purified fraction were confirmed in the MALDI-ToF (Figure 68). The cleaving of the peptide by hMMP-7 in the C18 analytical column was also checked (Figure 69). As the peptide was cleaved by the active enzyme, the original peptide peak decreased in intensity (Figure 70) and the cleaved peptide fragment peaks increased with time (Peak A, Figure 71 and Peak B, Figure 72).

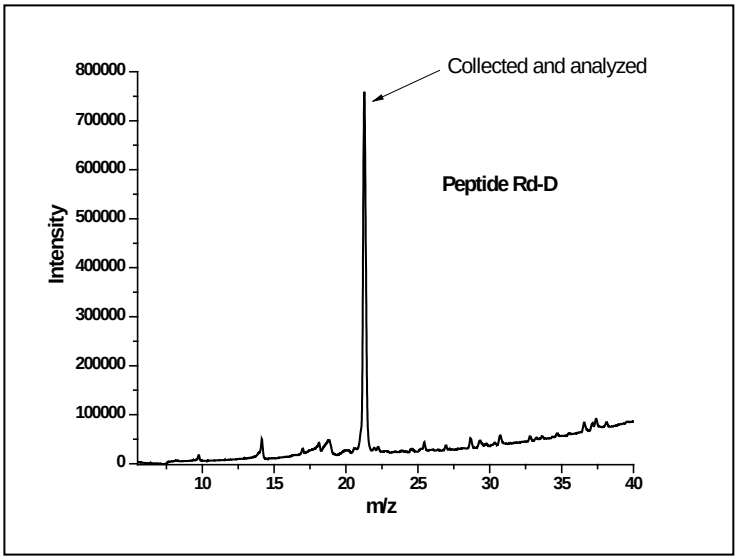

Figure 67. HPLC purification trace of the peptide **Rd-D**.

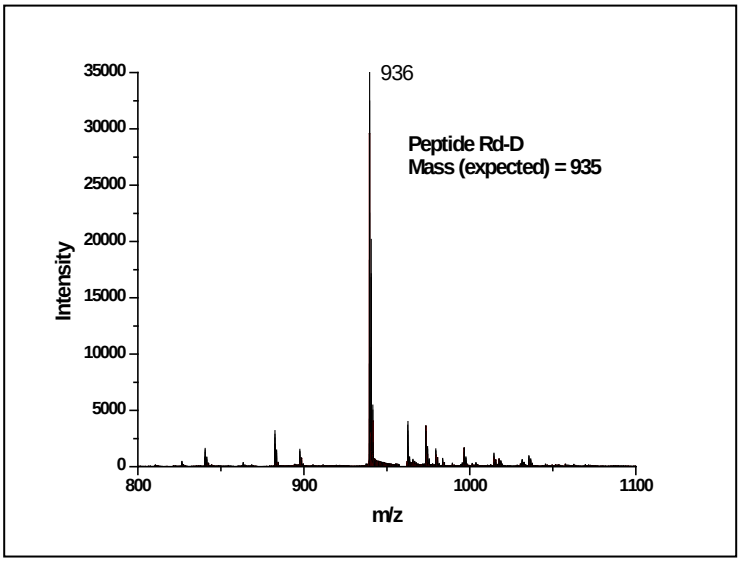

Figure 68. Mass spectra of the purified peptide **Rd-D**.

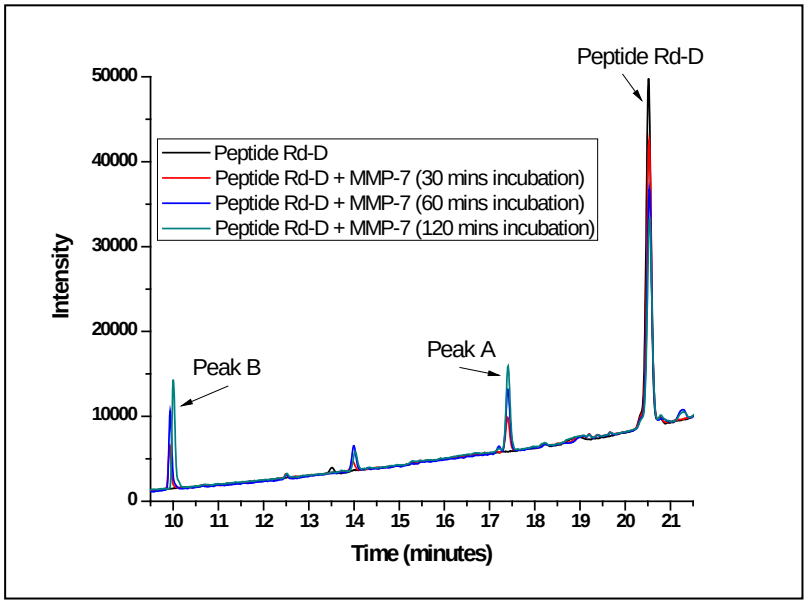

Figure 69. Cleaving experiment showing peptide **Rd-D** (100 µM) was cleaved by active recombinant hMMP-7 (100 nM) after incubating at 30, 60 and 120 minutes. The cleaved peptide fragments (Peak A and Peak B) with different retention times increased significantly with time.

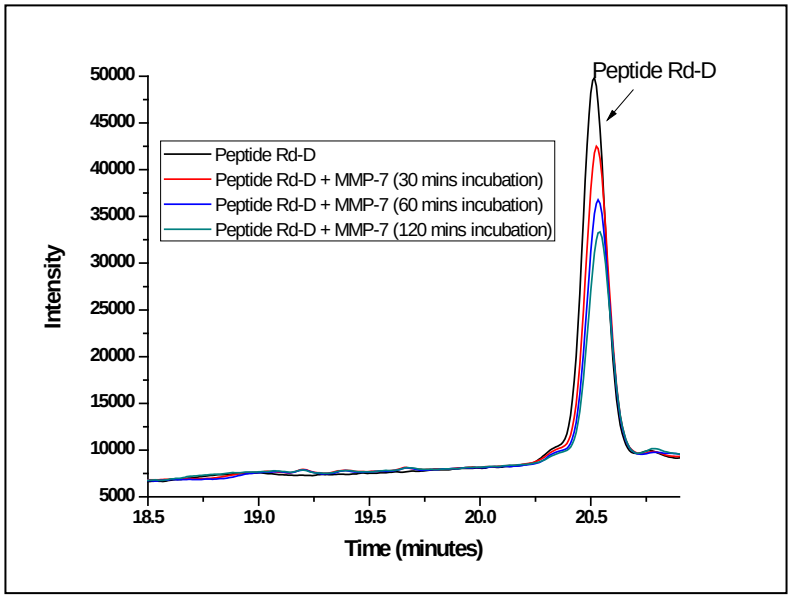

Figure 70. Cleaving experiment showing peptide **Rd-D** (100 μM) was cleaved by active recombinant hMMP-7 (100 nM) after incubating at 30, 60 and 120 minutes. The intensity of the peptide peak decreased with time.

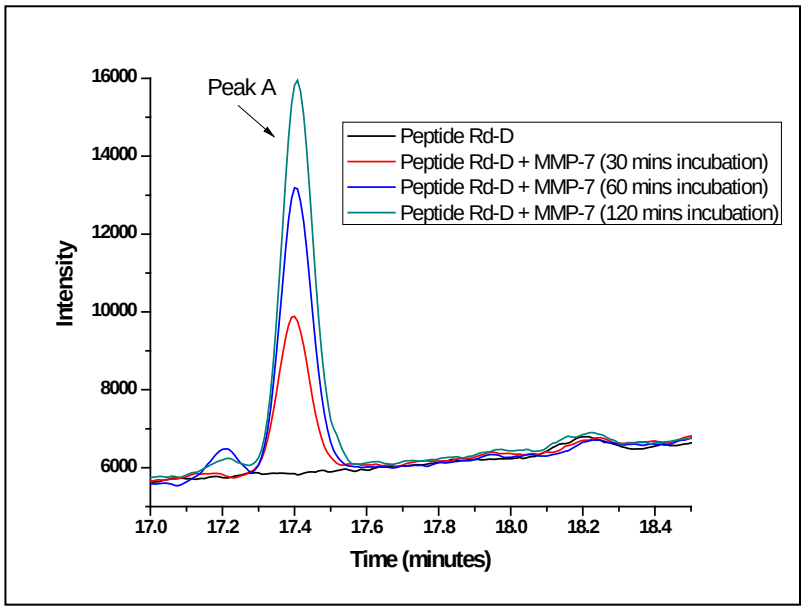

Figure 71. Cleaving experiment showing peptide **Rd-D** (100 μM) was cleaved by active recombinant hMMP-7 (100 nM) after incubating at 30, 60 and 120 minutes. The cleaved peptide fragment Peak A (magnified) with different retention time increased significantly with time.

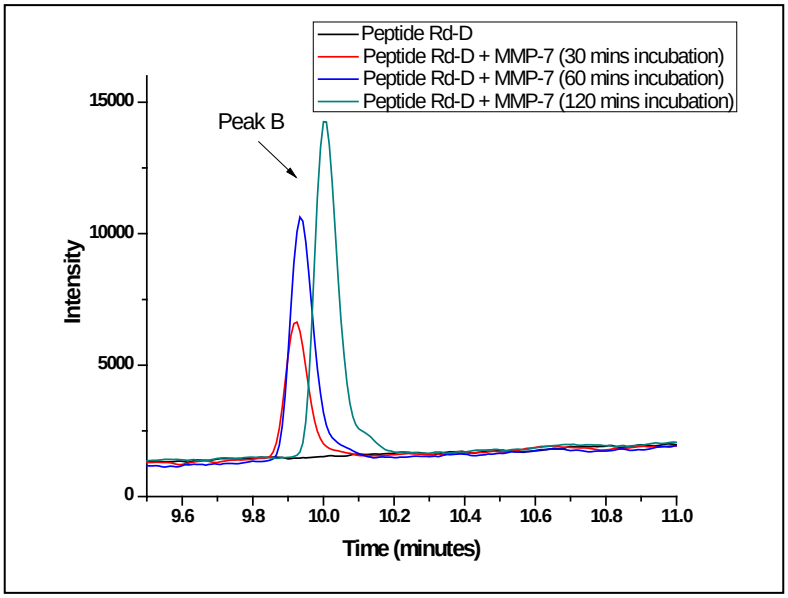

Figure 72. Cleaving experiment showing peptide **Rd-D** (100 μM) was cleaved by active recombinant hMMP-7 (100 nM) after incubating at 30, 60 and 120 minutes. The cleaved peptide fragments Peak B (magnified) with different retention time increased significantly with time.

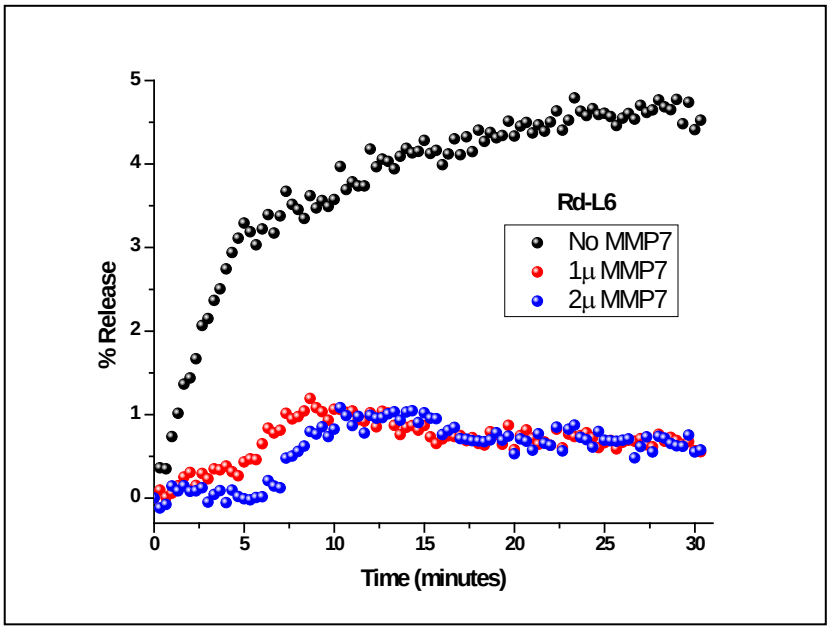

Figure 73. Release profile of the encapsulated dye carboxyfluorescein from the liposomes **Rd-L6** in absence (black circles) and presence of 1 μM (red circles) and 2 μM (blue circles) of active hMMP-7. The experiments were conducted with 25 mM HEPES buffer (pH = 8.0) containing 10 mM $CaCl_2$, 10 μM $ZnCl_2$ and 100 mM NaCl and osmolality adjusted.

Even though the negatively charged peptide was found to be cleaved by MMP-7, cleaving experiment for the encapsulated liposomes (**Rd-L6**) made with this peptide against MMP-7 did not improve the release profile of the dye carboxyfluorescein. In fact, the release for 1μM MMP-7overlapped with the 2 μM concentrations of MMP-7. The blank wells containing no enzyme showed the higher release of the dye.

Liposomes incorporating the peptide **Rd-A** and **Rd-B** were difficult to make as the thin films were very sticky and wouldn't detach from the round-bottomed flask. After vigorous sonication for 10 minutes, the thin films for these liposomes were hydrated with the buffer containing the dissolved carboxyfluorescein. During gel filtration from the Sephadex G-50 column, no separate yellow colored liposomal bands eluted. There can be multiple reasons for these observations. Since stearic acid was present in these peptides, it could cause the formation of micelle and were difficult to remove when the thin films were hydrated. Adding mini-PEG to this did not improve this step. Although the solubility of the **Rd-B** peptide was better than **Rd-A** peptide because of the addition of the mini-PEG, the liposomes were found difficult to encapsulate the dye. Absence of liposomal band in the column proved the inherent problem of proper formation of lipid bilayer in the liposomes. As a result although the solution was extruded out from 200 nm filter papers 20 times, carboxyfluorescein was not encapsulated in these liposomes as observed from the absence of the characteristic colored band in the column. We also observed that the peptide **Rd-A** was not cleaved by even higher concentration of MMP-7 (1 μM). Although the sequence when attached with the 5-hexynoic acid counterpart was cleavable by MMP-7 (Figure 55), attachment of the stearic acid to the sequence made the peptide uncleavable by MMP-7. If the **Rd-A** peptide had already formed micelle then the structure could cause hindrance to the enzyme accessibility for active site binding. This was manifested in the

cleaving experiments where no change in the original peptide peak was noticed with time (Figure 50).

Peptide **Rd-C** was found to be cleaved by active MMP-7 as observed from the cleaving experiments. Although the peptide itself was cleaved by the enzyme but formation of liposomes with this peptide (**Rd-L1**) was not easy as the length of the peptide was short and not appropriate for proper formation of lipid bilayer. The release profile of the dye encapsulated liposomes in presence of 2 μM MMP-7 overlapped with the control wells containing liposomes containing no enzymes proving that the peptide was not suitable for lipid bilayer formation in liposomes and the dye leaked as such. As a next step we ventured for a suitable method so that both the purposes of using the **Rd-C** peptide and formation of liposomes with it can be solved. As mentioned earlier, "click" reaction has been used extensively by pharmaceutical chemists for conjugation of ligands. Peptide **Rd-C** has alkyne group already incorporated in the N-terminus of the sequence. Lipid **1** and **2** were appropriate for lipid bilayer formation due to the presence of stearic acid and oleic acid moieties respectively. These lipids were synthesized to have an azide functional group on the carboxylic end of the lipids. "Click" reaction between **Rd-C** peptide and azide of the lipids (Lipid **1** and Lipid **2**) was carried out. However, poor solubility of the both the lipids in water as well as in other solvents (acetonitrile, DMSO, DMF) prevented us from attaching the peptide with the lipids. So we made liposomes with these lipids (30 mole %) along with the commercial lipids (70 mole %). We faced no problems in preparing or eluting out these liposomes from the column which we faced earlier with our Stearic acid peptides (**Rd-A** and **Rd-B**). Various compositions of liposomes were made by varying both the synthesized lipids (Lipid **1** and **2**) and commercial lipids (POPC, DOPC, and DSPC) and their sizes were checked by DLS. Formulations **Rd-L2**, **Rd-L3** and **Rd-L5** had sizes between 144 nm to 166

nm, however, liposomes **Rd-L4** sizes were found to be around 60 nm. All the formulations were next conjugated with the peptide **Rd-C** by "click" reaction and the sizes after the reactions were checked by DLS. All the liposomal formulations increased in size after the conjugation proving that the attachment of the peptide was successful with the protruding azides of the liposomal bilayer. Release experiments were performed with and without MMP-7 with all the formulations to check the releases (Figure 63-Figure 66) but in all cases, the percentage release was less in presence of the enzyme than in the absence of it. One possible explanation could be that since we know from the structure of MMP-7, it has a negative charge (Figure 46) around its active site, which could cause an inhibitory effect for the positively charged peptide (**Rd-C**). As an alternative strategy, we developed another peptide **Rd-D** by keeping the cleavage site identical and replacing the positive charged amino acids with glutamic acids imparting negative charge to the peptide. The peptide **Rd-D** was found to be cleaved by active MMP-7 (Figure 69). So we conjugated this peptide with the liposomes composed of POPC and Lipid **1**. The sizes of the liposomes before and after conjugation were around 75.39 ± 0.39 nm and 98.27 ± 0.8 nm respectively. The release experiments with these **Rd-L6** liposomes and MMP-7 revealed the liposomal bilayer was stabilized better in presence of the enzyme. The probable reason that might cause the greater release in absence of the enzyme was due to disturbances in the bilayer. These disturbances might be due to the long chain along with a bulky five-membered ring protruding out from the liposomes. As MMP-7 cleaves the peptide, the chain becomes shorter and thus the bilayer disturbance was avoided causing lesser release of the dye.

Conclusion

Both positively and negatively charged peptides were studied for preparing various liposomal formulations. The release experiments revealed that the presence of MMP-7 was

stabilizing the liposomal bilayer resulting in decreased percentage release of the encapsulated dye carboxyfluorescein from the liposomal aqueous core. For further studies these liposomal designs could be extended in future where mixing both the charged peptide could result in increased release of the dye from the liposomes in presence of the active enzymes. This could lead to the understanding of the mechanisms of interpretation between the active site of the enzyme and the charged peptides.

GENERAL CONCLUSION AND FUTURE STUDIES

Detection of biomarkers can be the preliminary step in any disease prognosis and treatment. Various enzymes are found to be overregulated in pathological conditions and their detection could serve as tools for better diagnosis and disease management. We studied two detection methodologies, water soluble fluorescent-polymers and liposomes for *in vitro* detection of two broad metalloenzyme classes, Matrix metalloproteinases (MMPs) and Carbonic anhydrases (CAs). In the first three chapters, polymeric detection systems were tested for isozyme selective detection of total (active + inactive) MMPs and CAs. Chapter IV deals with the investigation of dye-encapsulated liposomes for the detection of active MMP-7 isozyme.

We synthesized various monomers and attached methacrylamide moiety as the polymerizable group to these monomers. The monomers were characterized by ^{1}H and ^{13}C NMR spectroscopy. Alcohol monomers were used for imparting water solubility to the polymers. Lysine, Aspartic acid and alanine monomers added positive, negative and neutral charges respectively to the polymers while a hydroxamate monomer was incorporated for active site binding to the MMPs. For fluorescence signal dansylamide was used as the fluorophore. We tested the hypothesis that since the isozymes has the active site conserved in a particular enzyme class, difference in their surface residues can be targeted with our polyvalent polymers based on the concept of "Protein Surface Recognition" for isozyme selective interactions. Free radical copolymerization was used for synthesizing the polymers and their molecular weights were characterized by gel permeation chromatography. A library of polymers were constructed and their fluorescence were tested against three human recombinant MMP isozymes, MMP-7, -9 and -10. Statistical analysis (Logit Regression Analyses) of the data revealed one of the

polymers (**R11**) was able to detect MMP-9 significantly compared to MMP-7 and -10. This polymer could inhibit MMP-9 even in the presence of other proteins in human serum when spiked with this particular isozyme.

Chapter II consisted of studying our optimized polymeric system (**R11**) for differentiating cancer cell lines from non-cancerous cell lines based on the secreted amounts of MMP-9. Various breast cancer cell lines and prostate cancer cell lines were cultured and the conditioned media from these cell lines were tested against polymer **R11** for change in fluorescence signals. Not only differentiating cancer from non cancer cell lines, we also sought to apply the response for subtyping various breast and prostate cancer cell lines. The ratios from the control and test cell lines were analyzed by Linear Discriminant Analyses (LDA) and the canonical plots proved that the polymer **R11** was able to distinguish and subtype various cell lines. In future the polymeric strategy could be modified with better hydrophilic inhibitor for MMPs and incorporating other amino acids for better isozyme selective detection.

Detailed study of the synthesis and application of polymers for isozyme-selective detection of Carbonic Anhydrases were studied in Chapter III. In order to achieve enhanced fluorescence signals we conjugated the active site binding inhibitor with the fluorophore and synthesized the methacrylamide derivative of napthalenesulphonamide and incorporated in the polymers along with the other monomers such as alcohol, lysine and aspartic acid. Four polymers were constructed and tested against CA II, VII and XII for fluorescence, inhibition, isothermal titration microcalorimetry and lifetime studies. One of the polymers (**F4**) was actually able to discriminate between CA II from CA VII and CA XII even in mixture of biomacromolecules. These polymers can be evaluated further by incorporation of better

inhibitors and fluorophore like pyrene or pyranine for enhanced selectivity amongst other isozymes in the class.

In Chapter IV we investigated liposomal release of a self quenching dye for detection of active MMP-7. Carboxyfluorescein encapsulated liposomes were formulated and MMP-7 cleavable peptide was conjugated with fractions of the lipid bilayer of these liposomes through "click" reaction. It has been found that the release from these conjugated liposomes drastically decreased in presence of active MMP-7 suggesting that the cleaving of the peptide somehow had some stabilizing effect on the liposomal release. Both positively and negatively charged peptides were used for constructing the conjugated liposomes. In future mixing both these dual charged peptides for conjugating in the liposomal bilayer can be a potential way to increase the release of the dye from the liposomes in presence of the active enzymes.

Our polymeric and liposomal detection strategies might serve as an alternative way for potential detection kit other than ELISA in respect of stability, cost and yield.

REFERENCES

1. Page-McCaw, A., Ewald, A. J., and Werb, Z. (2007) Matrix metalloproteinases and the regulation of tissue remodelling, *Nat Rev Mol Cell Biol 8*, 221-233.
2. Chakraborti, S., Mandal, M., Das, S., Mandal, A., and Chakraborti, T. (2003) Regulation of matrix metalloproteinases: an overview, *Mol Cell Biochem 253*, 269-285.
3. Coussens, L. M., Fingleton, B., and Matrisian, L. M. (2002) Matrix metalloproteinase inhibitors and cancer: trials and tribulations, *Science 295*, 2387-2392.
4. Egeblad, M., and Werb, Z. (2002) New functions for the matrix metalloproteinases in cancer progression, *Nat Rev Cancer 2*, 161-174.
5. Bode, W., Fernandez-Catalan, C., Tschesche, H., Grams, F., Nagase, H., and Maskos, K. (1999) Structural properties of matrix metalloproteinases, *Cell Mol Life Sci 55*, 639-652.
6. Borkakoti, N. (2004) Matrix metalloprotease inhibitors: design from structure, *Biochem Soc Trans 32*, 17-20.
7. Rundhaug, J. E. (2003) Matrix metalloproteinases, angiogenesis, and cancer: commentary re: A. C. Lockhart et al., Reduction of wound angiogenesis in patients treated with BMS-275291, a broad spectrum matrix metalloproteinase inhibitor. Clin. Cancer Res., 9: 00-00, 2003, *Clin Cancer Res 9*, 551-554.
8. Verma, R. P., and Hansch, C. (2007) Matrix metalloproteinases (MMPs): chemical-biological functions and (Q)SARs, *Bioorg Med Chem 15*, 2223-2268.
9. Deryugina, E. I., and Quigley, J. P. (2006) Matrix metalloproteinases and tumor metastasis, *Cancer Metastasis Rev 25*, 9-34.

10. Hu, J., Van den Steen, P. E., Sang, Q. X., and Opdenakker, G. (2007) Matrix metalloproteinase inhibitors as therapy for inflammatory and vascular diseases, *Nat Rev Drug Discov 6*, 480-498.

11. Sternlicht, M. D., and Werb, Z. (2001) How matrix metalloproteinases regulate cell behavior, *Annu Rev Cell Dev Biol 17*, 463-516.

12. Massova, I., Kotra, L. P., Fridman, R., and Mobashery, S. (1998) Matrix metalloproteinases: structures, evolution, and diversification, *FASEB J 12*, 1075-1095.

13. Whittaker, M., Floyd, C. D., Brown, P., and Gearing, A. J. (1999) Design and therapeutic application of matrix metalloproteinase inhibitors, *Chem Rev 99*, 2735-2776.

14. Cha, H., Kopetzki, E., Huber, R., Lanzendorfer, M., and Brandstetter, H. (2002) Structural basis of the adaptive molecular recognition by MMP9, *J Mol Biol 320*, 1065-1079.

15. Ii, M., Yamamoto, H., Adachi, Y., Maruyama, Y., and Shinomura, Y. (2006) Role of matrix metalloproteinase-7 (matrilysin) in human cancer invasion, apoptosis, growth, and angiogenesis, *Exp Biol Med (Maywood) 231*, 20-27.

16. Harrell, P. C., McCawley, L. J., Fingleton, B., McIntyre, J. O., and Matrisian, L. M. (2005) Proliferative effects of apical, but not basal, matrix metalloproteinase-7 activity in polarized MDCK cells, *Exp Cell Res 303*, 308-320.

17. Higashi, S., Oeda, M., Yamamoto, K., and Miyazaki, K. (2008) Identification of amino acid residues of matrix metalloproteinase-7 essential for binding to cholesterol sulfate, *J Biol Chem 283*, 35735-35744.

18. Ganguly, B., Banerjee, J., Elegbede, A. I., Klocke, D. J., Mallik, S., and Srivastava, D. K. (2007) Intrinsic selectivity in binding of matrix metalloproteinase-7 to differently charged lipid membranes, *FEBS Lett 581*, 5723-5726.

19. Bord, S., Horner, A., Hembry, R. M., and Compston, J. E. (1998) Stromelysin-1 (MMP-3) and stromelysin-2 (MMP-10) expression in developing human bone: potential roles in skeletal development, *Bone 23*, 7-12.

20. Sirum, K. L., and Brinckerhoff, C. E. (1989) Cloning of the genes for human stromelysin and stromelysin 2: differential expression in rheumatoid synovial fibroblasts, *Biochemistry 28*, 8691-8698.

21. Cheng, X. C., Fang, H., and Xu, W. F. (2008) Advances in assays of matrix metalloproteinases (MMPs) and their inhibitors, *J Enzyme Inhib Med Chem 23*, 154-167.

22. Jacobsen, F. E., Lewis, J. A., and Cohen, S. M. (2007) The design of inhibitors for medicinally relevant metalloproteins, *ChemMedChem 2*, 152-171.

23. Vartak, D. G., and Gemeinhart, R. A. (2007) Matrix metalloproteases: underutilized targets for drug delivery, *J Drug Target 15*, 1-20.

24. Overall, C. M., and Kleifeld, O. (2006) Towards third generation matrix metalloproteinase inhibitors for cancer therapy, *Br J Cancer 94*, 941-946.

25. Overall, C. M., and Kleifeld, O. (2006) Tumour microenvironment - opinion: validating matrix metalloproteinases as drug targets and anti-targets for cancer therapy, *Nat Rev Cancer 6*, 227-239.

26. McQuibban, G. A., Gong, J. H., Tam, E. M., McCulloch, C. A., Clark-Lewis, I., and Overall, C. M. (2000) Inflammation dampened by gelatinase A cleavage of monocyte chemoattractant protein-3, *Science 289*, 1202-1206.

27. Overall, C. M., and Lopez-Otin, C. (2002) Strategies for MMP inhibition in cancer: innovations for the post-trial era, *Nat Rev Cancer 2*, 657-672.

28. Liu, S., Netzel-Arnett, S., Birkedal-Hansen, H., and Leppla, S. H. (2000) Tumor cell-selective cytotoxicity of matrix metalloproteinase-activated anthrax toxin, *Cancer Res 60*, 6061-6067.

29. Yin, H., and Hamilton, A. D. (2005) Strategies for targeting protein-protein interactions with synthetic agents, *Angew Chem Int Ed Engl 44*, 4130-4163.

30. Fingleton, B. (2007) Matrix metalloproteinases as valid clinical targets, *Curr Pharm Des 13*, 333-346.

31. Dursun, D., Kim, M. C., Solomon, A., and Pflugfelder, S. C. (2001) Treatment of recalcitrant recurrent corneal erosions with inhibitors of matrix metalloproteinase-9, doxycycline and corticosteroids, *Am J Ophthalmol 132*, 8-13.

32. Fisher, J. F., and Mobashery, S. (2006) Recent advances in MMP inhibitor design, *Cancer Metastasis Rev 25*, 115-136.

33. Dive, V., Andarawewa, K. L., Boulay, A., Matziari, M., Beau, F., Guerin, E., Rousseau, B., Yiotakis, A., and Rio, M. C. (2005) Dosing and scheduling influence the antitumor efficacy of a phosphinic peptide inhibitor of matrix metalloproteinases, *Int J Cancer 113*, 775-781.

34. Sang, Q. X., Jin, Y., Newcomer, R. G., Monroe, S. C., Fang, X., Hurst, D. R., Lee, S., Cao, Q., and Schwartz, M. A. (2006) Matrix metalloproteinase inhibitors as prospective agents for the prevention and treatment of cardiovascular and neoplastic diseases, *Curr Top Med Chem 6*, 289-316.

35. Kawagishi, H., Hamajima, K., and Inoue, Y. (2002) Novel hydroquinone as a matrix metallo-proteinase inhibitor from the mushroom, Piptoporus betulinus, *Biosci Biotechnol Biochem 66*, 2748-2750.

36. Fingleton, B. (2003) Matrix metalloproteinase inhibitors for cancer therapy:the current situation and future prospects, *Expert Opin Ther Targets 7*, 385-397.

37. Pavlaki, M., and Zucker, S. (2003) Matrix metalloproteinase inhibitors (MMPIs): the beginning of phase I or the termination of phase III clinical trials, *Cancer Metastasis Rev 22*, 177-203.

38. Paemen, L., Martens, E., Norga, K., Masure, S., Roets, E., Hoogmartens, J., and Opdenakker, G. (1996) The gelatinase inhibitory activity of tetracyclines and chemically modified tetracycline analogues as measured by a novel microtiter assay for inhibitors, *Biochem Pharmacol 52*, 105-111.

39. Ratnikov, B., Deryugina, E., Leng, J., Marchenko, G., Dembrow, D., and Strongin, A. (2000) Determination of matrix metalloproteinase activity using biotinylated gelatin, *Anal Biochem 286*, 149-155.

40. Baragi, V. M., Shaw, B. J., Renkiewicz, R. R., Kuipers, P. J., Welgus, H. G., Mathrubutham, M., Cohen, J. R., and Rao, S. K. (2000) A versatile assay for gelatinases using succinylated gelatin, *Matrix Biol 19*, 267-273.

41. Catterall, J. B., and Cawston, T. E. (2003) Assays of matrix metalloproteinases (MMPs) and MMP inhibitors: bioassays and immunoassays applicable to cell culture medium, serum, and synovial fluid, *Methods Mol Biol 225*, 353-364.

42. Zucker, S., Mancuso, P., DiMassimo, B., Lysik, R. M., Conner, C., and Wu, C. L. (1994) Comparison of techniques for measurement of gelatinases/type IV collagenases: enzyme-linked immunoassays versus substrate degradation assays, *Clin Exp Metastasis 12*, 13-23.

43. Terato, K., Nagai, Y., Kawanishi, K., and Yamamoto, S. (1976) A rapid assay method of collagenase activity using 14C-labeled soluble collagen as substrate, *Biochim Biophys Acta 445*, 753-762.

44. Sunada, H., and Nagai, Y. (1980) A rapid micro-assay method for gelatinolytic activity using tritium-labeled heat-denatured polymeric collagen as a substrate and its application to the detection of enzymes involved in collagen metabolism, *J Biochem 87*, 1765-1771.

45. Kurien, B. T., and Scofield, R. H. (2006) Western blotting, *Methods 38*, 283-293.

46. Elegbede, A. I., Banerjee, J., Hanson, A. J., Tobwala, S., Ganguli, B., Wang, R., Lu, X., Srivastava, D. K., and Mallik, S. (2008) Mechanistic studies of the triggered release of liposomal contents by matrix metalloproteinase-9, *J Am Chem Soc 130*, 10633-10642.

47. Banerjee, J., Hanson, A. J., Nyren-Erickson, E. K., Ganguli, B., Wagh, A., Muhonen, W. W., Law, B., Shabb, J. B., Srivastava, D. K., and Mallik, S. (2010) Liposome-mediated amplified detection of cell-secreted matrix metalloproteinase-9, *Chem Commun (Camb) 46*, 3209-3211.

48. Supuran, C. T., and Scozzafava, A. (2007) Carbonic anhydrases as targets for medicinal chemistry, *Bioorg Med Chem 15*, 4336-4350.

49. Sly, W. S., and Hu, P. Y. (1995) Human carbonic anhydrases and carbonic anhydrase deficiencies, *Annu Rev Biochem 64*, 375-401.

50. Supuran, C. T., Scozzafava, A., and Casini, A. (2003) Carbonic anhydrase inhibitors, *Med Res Rev 23*, 146-189.

51. Breton, S. (2001) The cellular physiology of carbonic anhydrases, *JOP 2*, 159-164.

52. Nogradi, A. (1998) The role of carbonic anhydrases in tumors, *Am J Pathol 153*, 1-4.

53. Leppilampi, M., Koistinen, P., Savolainen, E. R., Hannuksela, J., Parkkila, A. K., Niemela, O., Pastorekova, S., Pastorek, J., Waheed, A., Sly, W. S., Parkkila, S., and Rajaniemi, H. (2002) The expression of carbonic anhydrase II in hematological malignancies, *Clin Cancer Res 8*, 2240-2245.

54. Chiche, J., Ilc, K., Laferriere, J., Trottier, E., Dayan, F., Mazure, N. M., Brahimi-Horn, M. C., and Pouyssegur, J. (2009) Hypoxia-inducible carbonic anhydrase IX and XII promote tumor cell growth by counteracting acidosis through the regulation of the intracellular pH, *Cancer Res 69*, 358-368.

55. Ivanov, S., Liao, S. Y., Ivanova, A., Danilkovitch-Miagkova, A., Tarasova, N., Weirich, G., Merrill, M. J., Proescholdt, M. A., Oldfield, E. H., Lee, J., Zavada, J., Waheed, A., Sly, W., Lerman, M. I., and Stanbridge, E. J. (2001) Expression of hypoxia-inducible cell-surface transmembrane carbonic anhydrases in human cancer, *Am J Pathol 158*, 905-919.

56. Kallio, H., Pastorekova, S., Pastorek, J., Waheed, A., Sly, W. S., Mannisto, S., Heikinheimo, M., and Parkkila, S. (2006) Expression of carbonic anhydrases IX and XII during mouse embryonic development, *BMC Dev Biol 6*, 22.

57. Hsieh, M. J., Chen, K. S., Chiou, H. L., and Hsieh, Y. S. (2010) Carbonic anhydrase XII promotes invasion and migration ability of MDA-MB-231 breast cancer cells through the p38 MAPK signaling pathway, *Eur J Cell Biol 89*, 598-606.

58. Abbate, F., Casini, A., Scozzafava, A., and Supuran, C. T. (2003) Carbonic anhydrase inhibitors: X-ray crystallographic structure of the adduct of human isozyme II with the

perfluorobenzoyl analogue of methazolamide. Implications for the drug design of fluorinated inhibitors, *J Enzyme Inhib Med Chem 18*, 303-308.

59. Alterio, V., Vitale, R. M., Monti, S. M., Pedone, C., Scozzafava, A., Cecchi, A., De Simone, G., and Supuran, C. T. (2006) Carbonic anhydrase inhibitors: X-ray and molecular modeling study for the interaction of a fluorescent antitumor sulfonamide with isozyme II and IX, *J Am Chem Soc 128*, 8329-8335.

60. Maren, T. H. (1967) Carbonic anhydrase: chemistry, physiology, and inhibition, *Physiol Rev 47*, 595-781.

61. Sugrue, M. F. (2000) Pharmacological and ocular hypotensive properties of topical carbonic anhydrase inhibitors, *Prog Retin Eye Res 19*, 87-112.

62. Patil, S., Reshetnikov, S., Haldar, M. K., Seal, S., and Mallik, S. (2007) Surface-derivatized nanoceria with human carbonic anhydrase II inhibitors and fluorophores: A potential drug delivery device, *J Phys Chem C 111*, 8437-8442.

63. Maren, T. H., and Conroy, C. W. (1993) A new class of carbonic anhydrase inhibitor, *J Biol Chem 268*, 26233-26239.

64. Popescu, A., Simion, A., Scozzafava, A., Briganti, F., and Supuran, C. T. (1999) Carbonic anhydrase inhibitors. Schiff bases of some aromatic sulfonamides and their metal complexes: towards more selective inhibitors of carbonic anhydrase isozyme IV, *J Enzyme Inhib 14*, 407-423.

65. Banerjee, A. L., Swanson, M., Roy, B. C., Jia, X., Haldar, M. K., Mallik, S., and Srivastava, D. K. (2004) Protein surface-assisted enhancement in the binding affinity of an inhibitor for recombinant human carbonic anhydrase-II, *J Am Chem Soc 126*, 10875-10883.

66. Jude, K. M., Banerjee, A. L., Haldar, M. K., Manokaran, S., Roy, B., Mallik, S., Srivastava, D. K., and Christianson, D. W. (2006) Ultrahigh resolution crystal structures of human carbonic anhydrases I and II complexed with "two-prong" inhibitors reveal the molecular basis of high affinity, *J Am Chem Soc 128*, 3011-3018.

67. Voet, D., and Voet, J. G. (2004) *Biochemistry*, 3rd ed., J. Wiley & Sons, New York.

68. Jain, R., Ernst, J. T., Kutzki, O., Park, H. S., and Hamilton, A. D. (2004) Protein recognition using synthetic surface-targeted agents, *Mol Divers 8*, 89-100.

69. Peczuh, M. W., and Hamilton, A. D. (2000) Peptide and protein recognition by designed molecules, *Chem Rev 100*, 2479-2494.

70. Park, H. S., Lin, Q., and Hamilton, A. D. (1999) Protein surface recognition by synthetic receptors: A route to novel submicromolar inhibitors for alpha-chymotrypsin, *Journal of the American Chemical Society 121*, 8-13.

71. Stites, W. E. (1997) Proteinminus signProtein Interactions: Interface Structure, Binding Thermodynamics, and Mutational Analysis, *Chem Rev 97*, 1233-1250.

72. Schrader, T., and Koch, S. (2007) Artificial protein sensors, *Mol Biosyst 3*, 241-248.

73. Korn, A. P., and Burnett, R. M. (1991) Distribution and complementarity of hydropathy in multisubunit proteins, *Proteins 9*, 37-55.

74. Jones, S., and Thornton, J. M. (1995) Protein-protein interactions: a review of protein dimer structures, *Prog Biophys Mol Biol 63*, 31-65.

75. Puerta, D. T., Lewis, J. A., and Cohen, S. M. (2004) New beginnings for matrix metalloproteinase inhibitors: identification of high-affinity zinc-binding groups, *J Am Chem Soc 126*, 8388-8389.

76. Dutta, R., Scott, M. D., Haldar, M. K., Ganguly, B., Srivastava, D. K., Friesner, D. L., and Mallik, S. (2011) Fluorescent water soluble polymers for isozyme-selective interactions with matrix metalloproteinase-9, *Bioorg Med Chem Lett 21*, 2007-2010.

77. Jain, R. K., and Hamilton, A. D. (2000) Protein surface recognition by synthetic receptors based on a tetraphenylporphyrin scaffold, *Org Lett 2*, 1721-1723.

78. Gradl, S. N., Felix, J. P., Isacoff, E. Y., Garcia, M. L., and Trauner, D. (2003) Protein surface recognition by rational design: nanomolar ligands for potassium channels, *J Am Chem Soc 125*, 12668-12669.

79. Whitcombe, M. J., Chianella, I., Larcombe, L., Piletsky, S. A., Noble, J., Porter, R., and Horgan, A. (2011) The rational development of molecularly imprinted polymer-based sensors for protein detection, *Chem Soc Rev 40*, 1547-1571.

80. Samad, A., Sultana, Y., and Aqil, M. (2007) Liposomal drug delivery systems: an update review, *Curr Drug Deliv 4*, 297-305.

81. Bangham, A. D., and Horne, R. W. (1964) Negative Staining of Phospholipids and Their Structural Modification by Surface-Active Agents as Observed in the Electron Microscope, *J Mol Biol 8*, 660-668.

82. Mufamadi, M. S., Pillay, V., Choonara, Y. E., Du Toit, L. C., Modi, G., Naidoo, D., and Ndesendo, V. M. (2011) A review on composite liposomal technologies for specialized drug delivery, *J Drug Deliv 2011*, 939851.

83. Maruyama, K. (2011) Intracellular targeting delivery of liposomal drugs to solid tumors based on EPR effects, *Adv Drug Deliv Rev 63*, 161-169.

84. Li, Y., Wang, J., Wientjes, M. G., and Au, J. L. (2011) Delivery of nanomedicines to extracellular and intracellular compartments of a solid tumor, *Adv Drug Deliv Rev*.

85. Sadzuka, Y., Nakade, A., Hirama, R., Miyagishima, A., Nozawa, Y., Hirota, S., and Sonobe, T. (2002) Effects of mixed polyethyleneglycol modification on fixed aqueous layer thickness and antitumor activity of doxorubicin containing liposome, *Int J Pharm 238*, 171-180.

86. Jesorka, A., and Orwar, O. (2008) Liposomes: technologies and analytical applications, *Annu Rev Anal Chem (Palo Alto Calif) 1*, 801-832.

87. Coldren, B., van Zanten, R., Mackel, M. J., Zasadzinski, J. A., and Jung, H. T. (2003) From vesicle size distributions to bilayer elasticity via cryo-transmission and freeze-fracture electron microscopy, *Langmuir 19*, 5632-5639.

88. Simard, P., and Leroux, J. C. (2009) pH-sensitive immunoliposomes specific to the CD33 cell surface antigen of leukemic cells, *Int J Pharm 381*, 86-96.

89. Negishi, Y., Omata, D., Iijima, H., Takabayashi, Y., Suzuki, K., Endo, Y., Suzuki, R., Maruyama, K., Nomizu, M., and Aramaki, Y. (2010) Enhanced laminin-derived peptide AG73-mediated liposomal gene transfer by bubble liposomes and ultrasound, *Mol Pharm 7*, 217-226.

90. Sakaguchi, N., Kojima, C., Harada, A., and Kono, K. (2008) Preparation of pH-sensitive poly(glycidol) derivatives with varying hydrophobicities: their ability to sensitize stable liposomes to pH, *Bioconjug Chem 19*, 1040-1048.

91. Kawamoto, M., Horibe, T., Kohno, M., and Kawakami, K. (2011) A novel transferrin receptor-targeted hybrid peptide disintegrates cancer cell membrane to induce rapid killing of cancer cells, *BMC Cancer 11*, 359.

92. Kakudo, T., Chaki, S., Futaki, S., Nakase, I., Akaji, K., Kawakami, T., Maruyama, K., Kamiya, H., and Harashima, H. (2004) Transferrin-modified liposomes equipped with a

pH-sensitive fusogenic peptide: an artificial viral-like delivery system, *Biochemistry 43*, 5618-5628.

93. Sasaki, K., Kogure, K., Chaki, S., Nakamura, Y., Moriguchi, R., Hamada, H., Danev, R., Nagayama, K., Futaki, S., and Harashima, H. (2008) An artificial virus-like nano carrier system: enhanced endosomal escape of nanoparticles via synergistic action of pH-sensitive fusogenic peptide derivatives, *Anal Bioanal Chem 391*, 2717-2727.

94. Ferrara, K. W. (2008) Driving delivery vehicles with ultrasound, *Adv Drug Deliv Rev 60*, 1097-1102.

95. Chandra, B., Mallik, S., and Srivastava, D. K. (2005) Design of photocleavable lipids and their application in liposomal "uncorking", *Chem Commun (Camb)*, 3021-3023.

96. Ong, W., Yang, Y., Cruciano, A. C., and McCarley, R. L. (2008) Redox-triggered contents release from liposomes, *J Am Chem Soc 130*, 14739-14744.

97. Lopez-Otin, C., and Hunter, T. (2010) The regulatory crosstalk between kinases and proteases in cancer, *Nat Rev Cancer 10*, 278-292.

98. Banerjee, J., Hanson, A. J., Gadam, B., Elegbede, A. I., Tobwala, S., Ganguly, B., Wagh, A. V., Muhonen, W. W., Law, B., Shabb, J. B., Srivastava, D. K., and Mallik, S. (2009) Release of liposomal contents by cell-secreted matrix metalloproteinase-9, *Bioconjug Chem 20*, 1332-1339.

99. Songjun Li, J. S., He Li, Ipsita A. Banerjee, (Ed.) (2011) *Biosensor Nanomaterials*, Wiley-VCH.

100. Santos, M., Roy, B. C., Goicoechea, H., Campiglia, A. D., and Mallik, S. (2004) An investigation on the analytical potential of polymerized liposomes bound to lanthanide ions for protein analysis, *J Am Chem Soc 126*, 10738-10745.

101. Elegbede, A. I., Haldar, M. K., Manokaran, S., Mallik, S., and Srivastava, D. K. (2007) Recognition of isozymes via lanthanide ion incorporated polymerized liposomes, *Chem Commun*, 4495-4497.

102. Kullberg, M., Mann, K., and Owens, J. L. (2009) A two-component drug delivery system using Her-2-targeting thermosensitive liposomes, *J Drug Target 17*, 98-107.

103. Pan, X. Q., and Lee, R. J. (2005) In vivo antitumor activity of folate receptor-targeted liposomal daunorubicin in a murine leukemia model, *Anticancer Res 25*, 343-346.

104. Kawano, K., Onose, E., Hattori, Y., and Maitani, Y. (2009) Higher liposomal membrane fluidity enhances the in vitro antitumor activity of folate-targeted liposomal mitoxantrone, *Mol Pharm 6*, 98-104.

105. Suzuki, R., Takizawa, T., Kuwata, Y., Mutoh, M., Ishiguro, N., Utoguchi, N., Shinohara, A., Eriguchi, M., Yanagie, H., and Maruyama, K. (2008) Effective anti-tumor activity of oxaliplatin encapsulated in transferrin-PEG-liposome, *Int J Pharm 346*, 143-150.

106. Zheng, Y., Chen, H., Liu, X. P., Jiang, J. H., Luo, Y., Shen, G. L., and Yu, R. Q. (2008) An ultrasensitive chemiluminescence immunosensor for PSA based on the enzyme encapsulated liposome, *Talanta 77*, 809-814.

107. Kamidate, T., Maruya, M., Tani, H., and Ishida, A. (2009) Application of 4-iodophenol-enhanced luminol chemiluminescence to direct detection of horseradish peroxidase encapsulated in liposomes, *Anal Sci 25*, 1163-1166.

108. Viswanathan, S., Rani, C., Vijay Anand, A., and Ho, J. A. (2009) Disposable electrochemical immunosensor for carcinoembryonic antigen using ferrocene liposomes and MWCNT screen-printed electrode, *Biosens Bioelectron 24*, 1984-1989.

109. Vamvakaki, V., Fournier, D., and Chaniotakis, N. A. (2005) Fluorescence detection of enzymatic activity within a liposome based nano-biosensor, *Biosens Bioelectron 21*, 384-388.

110. Edwards, K. A., and Baeumner, A. J. (2007) DNA-oligonucleotide encapsulating liposomes as a secondary signal amplification means, *Anal Chem 79*, 1806-1815.

111. Egashira, N., Morita, S., Hifumi, E., Mitoma, Y., and Uda, T. (2008) Attomole detection of hemagglutinin molecule of influenza virus by combining an electrochemiluminescence sensor with an immunoliposome that encapsulates a Ru complex, *Anal Chem 80*, 4020-4025.

112. Zaytseva, N. V., Montagna, R. A., Lee, E. M., and Baeumner, A. J. (2004) Multi-analyte single-membrane biosensor for the serotype-specific detection of Dengue virus, *Anal Bioanal Chem 380*, 46-53.

113. Tai, J. H., Ewert, M. S., Belliot, G., Glass, R. I., and Monroe, S. S. (2003) Development of a rapid method using nucleic acid sequence-based amplification for the detection of astrovirus, *J Virol Methods 110*, 119-127.

114. Haack, T., Peczuh, M. W., Salvatella, X., Sanchez-Quesada, J., de Mendoza, J., Hamilton, A. D., and Giralt, E. (1999) Surface recognition and helix stabilization of a tetraaspartate peptide by shape and electrostatic complementarity of an artificial receptor, *Journal of the American Chemical Society 121*, 11813-11820.

115. Tominey, A. F., Liese, J., Wei, S., Kowski, K., Schrader, T., and Kraft, A. (2010) RAFT polymers for protein recognition, *Beilstein J Org Chem 6*.

116. Meireles, L. M., Domling, A. S., and Camacho, C. J. (2010) ANCHOR: a web server and database for analysis of protein-protein interaction binding pockets for drug discovery, *Nucleic Acids Res 38*, W407-411.

117. Leung, D. K., Yang, Z., and Breslow, R. (2000) Selective disruption of protein aggregation by cyclodextrin dimers, *Proc Natl Acad Sci U S A 97*, 5050-5053.

118. Banerjee, A. L., Eiler, D., Roy, B. C., Jia, X., Haldar, M. K., Mallik, S., and Srivastava, D. K. (2005) Spacer-based selectivity in the binding of "two-prong" ligands to recombinant human carbonic anhydrase I, *Biochemistry 44*, 3211-3224.

119. Dongming He, W. S., Thomas Schrader, Mathias Ulbricht. (2009) Protein adsorbers from surface-grafted copolymers with selective binding sites, *Journal of Materials Chemistry 19*, 253-260.

120. Koch, S. J., Renner, C., Xie, X., and Schrader, T. (2006) Tuning linear copolymers into protein-specific hosts, *Angew Chem Int Ed Engl 45*, 6352-6355.

121. Renner, C., Piehler, J., and Schrader, T. (2006) Arginine- and lysine-specific polymers for protein recognition and immobilization, *J Am Chem Soc 128*, 620-628.

122. Sun, W., Bandmann, H., and Schrader, T. (2007) A fluorescent polymeric heparin sensor, *Chemistry 13*, 7701-7707.

123. You, C. C., Miranda, O. R., Gider, B., Ghosh, P. S., Kim, I. B., Erdogan, B., Krovi, S. A., Bunz, U. H., and Rotello, V. M. (2007) Detection and identification of proteins using nanoparticle-fluorescent polymer 'chemical nose' sensors, *Nat Nanotechnol 2*, 318-323.

124. Wenck, K., Koch, S., Renner, C., Sun, W., and Schrader, T. (2007) A noncovalent switch for lysozyme, *J Am Chem Soc 129*, 16015-16019.

125. Fisher, J. F., and Mobashery, S. (2010) Mechanism-based profiling of MMPs, *Methods Mol Biol 622*, 471-487.

126. Klein, G., Vellenga, E., Fraaije, M. W., Kamps, W. A., and de Bont, E. S. (2004) The possible role of matrix metalloproteinase (MMP)-2 and MMP-9 in cancer, e.g. acute leukemia, *Crit Rev Oncol Hematol 50*, 87-100.

127. Chang, Y. H., Lin, I. L., Tsay, G. J., Yang, S. C., Yang, T. P., Ho, K. T., Hsu, T. C., and Shiau, M. Y. (2008) Elevated circulatory MMP-2 and MMP-9 levels and activities in patients with rheumatoid arthritis and systemic lupus erythematosus, *Clin Biochem 41*, 955-959.

128. Paczek, L., Michalska, W., and Bartlomiejczyk, I. (2008) Trypsin, elastase, plasmin and MMP-9 activity in the serum during the human ageing process, *Age Ageing 37*, 318-323.

129. Hurst, N. G., Stocken, D. D., Wilson, S., Keh, C., Wakelam, M. J., and Ismail, T. (2007) Elevated serum matrix metalloproteinase 9 (MMP-9) concentration predicts the presence of colorectal neoplasia in symptomatic patients, *Br J Cancer 97*, 971-977.

130. Banerjee, A. L., Tobwala, S., Haldar, M. K., Swanson, M., Roy, B. C., Mallik, S., and Srivastava, D. K. (2005) Inhibition of matrix metalloproteinase-9 by "multi-prong" surface binding groups, *Chem Commun (Camb)*, 2549-2551.

131. Moeketsi Mokete, D. C. S., Christopher D. Betts, Kieran J. O'Flynn, Noel W. Clarke. (2005) The increased rate of prostate specific antigen testing has not affected prostate cancer presentation in an inner city polulation in the UK, *BJU International 97*, 266-269.

132. Pu, Y., Wang, W. B., Das, B. B., Achilefu, S., and Alfano, R. R. (2008) Time-resolved fluorescence polarization dynamics and optical imaging of Cytate: a prostate cancer receptor-targeted contrast agent, *Appl Opt 47*, 2281-2289.

133. Cooperberg, M. R., Lubeck, D. P., Meng, M. V., Mehta, S. S., and Carroll, P. R. (2004) The changing face of low-risk prostate cancer: trends in clinical presentation and primary management, *J Clin Oncol 22*, 2141-2149.

134. Catalona, W. J., Richie, J. P., Ahmann, F. R., Hudson, M. A., Scardino, P. T., Flanigan, R. C., deKernion, J. B., Ratliff, T. L., Kavoussi, L. R., Dalkin, B. L., and et al. (1994) Comparison of digital rectal examination and serum prostate specific antigen in the early detection of prostate cancer: results of a multicenter clinical trial of 6,630 men, *J Urol 151*, 1283-1290.

135. Porkka, K. P., Pfeiffer, M. J., Waltering, K. K., Vessella, R. L., Tammela, T. L., and Visakorpi, T. (2007) MicroRNA expression profiling in prostate cancer, *Cancer Res 67*, 6130-6135.

136. Nupponen, N. N., Hyytinen, E. R., Kallioniemi, A. H., and Visakorpi, T. (1998) Genetic alterations in prostate cancer cell lines detected by comparative genomic hybridization, *Cancer Genet Cytogenet 101*, 53-57.

137. Park, K., Tomlins, S. A., Mudaliar, K. M., Chiu, Y. L., Esgueva, R., Mehra, R., Suleman, K., Varambally, S., Brenner, J. C., MacDonald, T., Srivastava, A., Tewari, A. K., Sathyanarayana, U., Nagy, D., Pestano, G., Kunju, L. P., Demichelis, F., Chinnaiyan, A. M., and Rubin, M. A. (2010) Antibody-based detection of ERG rearrangement-positive prostate cancer, *Neoplasia 12*, 590-598.

138. Reljin, B., Paskas, M., Reljin, I., and Konstanty, K. (2011) Breast cancer evaluation by fluorescent dot detection using combined mathematical morphology and multifractal techniques, *Diagn Pathol 6 Suppl 1*, S21.

139. Nover, A. B., Jagtap, S., Anjum, W., Yegingil, H., Shih, W. Y., Shih, W. H., and Brooks, A. D. (2009) Modern breast cancer detection: a technological review, *Int J Biomed Imaging 2009*, 902326.

140. Volynskaya, Z., Haka, A. S., Bechtel, K. L., Fitzmaurice, M., Shenk, R., Wang, N., Nazemi, J., Dasari, R. R., and Feld, M. S. (2008) Diagnosing breast cancer using diffuse reflectance spectroscopy and intrinsic fluorescence spectroscopy, *J Biomed Opt 13*, 024012.

141. Gown, A. M. (2008) Current issues in ER and HER2 testing by IHC in breast cancer, *Mod Pathol 21 Suppl 2*, S8-S15.

142. Bajaj, A., Miranda, O. R., Phillips, R., Kim, I. B., Jerry, D. J., Bunz, U. H., and Rotello, V. M. (2010) Array-based sensing of normal, cancerous, and metastatic cells using conjugated fluorescent polymers, *J Am Chem Soc 132*, 1018-1022.

143. Maldiney, T., Byk, G., Wattier, N., Seguin, J., Khandadash, R., Bessodes, M., Richard, C., and Scherman, D. (2012) Synthesis and functionalization of persistent luminescence nanoparticles with small molecules and evaluation of their targeting ability, *Int J Pharm 423*, 102-107.

144. Miranda, O. R., You, C. C., Phillips, R., Kim, I. B., Ghosh, P. S., Bunz, U. H., and Rotello, V. M. (2007) Array-based sensing of proteins using conjugated polymers, *J Am Chem Soc 129*, 9856-9857.

145. Miranda, O. R., Creran, B., and Rotello, V. M. (2010) Array-based sensing with nanoparticles: 'chemical noses' for sensing biomolecules and cell surfaces, *Curr Opin Chem Biol 14*, 728-736.

146. Kim, I. B., Shin, H., Garcia, A. J., and Bunz, U. H. (2007) Use of a folate-PPE conjugate to image cancer cells in vitro, *Bioconjug Chem 18*, 815-820.

147. Scozzafava, A., and Supuran, C. T. (2000) Carbonic anhydrase and matrix metalloproteinase inhibitors: sulfonylated amino acid hydroxamates with MMP inhibitory properties act as efficient inhibitors of CA isozymes I, II, and IV, and N-hydroxysulfonamides inhibit both these zinc enzymes, *J Med Chem 43*, 3677-3687.

148. De Simone, G., Di Fiore, A., Menchise, V., Pedone, C., Antel, J., Casini, A., Scozzafava, A., Wurl, M., and Supuran, C. T. (2005) Carbonic anhydrase inhibitors. Zonisamide is an effective inhibitor of the cytosolic isozyme II and mitochondrial isozyme V: solution and X-ray crystallographic studies, *Bioorg Med Chem Lett 15*, 2315-2320.

149. Tureci, O., Sahin, U., Vollmar, E., Siemer, S., Gottert, E., Seitz, G., Parkkila, A. K., Shah, G. N., Grubb, J. H., Pfreundschuh, M., and Sly, W. S. (1998) Human carbonic anhydrase XII: cDNA cloning, expression, and chromosomal localization of a carbonic anhydrase gene that is overexpressed in some renal cell cancers, *Proc Natl Acad Sci U S A 95*, 7608-7613.

150. Ilie, M., Mazure, N. M., Hofman, V., Ammadi, R. E., Ortholan, C., Bonnetaud, C., Havet, K., Venissac, N., Mograbi, B., Mouroux, J., Pouyssegur, J., and Hofman, P. (2010) High levels of carbonic anhydrase IX in tumour tissue and plasma are biomarkers of poor prognostic in patients with non-small cell lung cancer, *Br J Cancer 102*, 1627-1635.

151. Pacchiano, F., Aggarwal, M., Avvaru, B. S., Robbins, A. H., Scozzafava, A., McKenna, R., and Supuran, C. T. (2010) Selective hydrophobic pocket binding observed within the carbonic anhydrase II active site accommodate different 4-substituted-ureido-

benzenesulfonamides and correlate to inhibitor potency, *Chem Commun (Camb) 46*, 8371-8373.

152. D'Ambrosio, K., Vitale, R. M., Dogne, J. M., Masereel, B., Innocenti, A., Scozzafava, A., De Simone, G., and Supuran, C. T. (2008) Carbonic anhydrase inhibitors: bioreductive nitro-containing sulfonamides with selectivity for targeting the tumor associated isoforms IX and XII, *J Med Chem 51*, 3230-3237.

153. Thiry, A., Supuran, C. T., Masereel, B., and Dogne, J. M. (2008) Recent developments of carbonic anhydrase inhibitors as potential anticancer drugs, *J Med Chem 51*, 3051-3056.

154. Banerjee, J., Haldar, M. K., Manokaran, S., Mallik, S., and Srivastava, D. K. (2007) New fluorescent probes for carbonic anhydrases, *Chem Commun (Camb)*, 2723-2725.

155. Cecchi, A., Hulikova, A., Pastorek, J., Pastorekova, S., Scozzafava, A., Winum, J. Y., Montero, J. L., and Supuran, C. T. (2005) Carbonic anhydrase inhibitors. Design of fluorescent sulfonamides as probes of tumor-associated carbonic anhydrase IX that inhibit isozyme IX-mediated acidification of hypoxic tumors, *J Med Chem 48*, 4834-4841.

156. Jie Hu, X. M., Shunsheng Cao, Xinhua Yuan. (2010) Recognition of Proteins and Peptides: Rational development of Molecular Imprinting Technology, *Polymer Science 52*, 328-339.

157. Day, Y. S., Baird, C. L., Rich, R. L., and Myszka, D. G. (2002) Direct comparison of binding equilibrium, thermodynamic, and rate constants determined by surface- and solution-based biophysical methods, *Protein Sci 11*, 1017-1025.

158. Manokaran, S., Zhang, X., Chen, W., and Srivastava, D. K. (2010) Differential modulation of the active site environment of human carbonic anhydrase XII by cationic quantum dots and polylysine, *Biochim Biophys Acta 1804*, 1376-1384.

159. Mart, R. J., Liem, K. P., Wang, X., and Webb, S. J. (2006) The effect of receptor clustering on vesicle-vesicle adhesion, *J Am Chem Soc 128*, 14462-14463.

160. Jani, M., Tordai, H., Trexler, M., Banyai, L., and Patthy, L. (2005) Hydroxamate-based peptide inhibitors of matrix metalloprotease 2, *Biochimie 87*, 385-392.

161. Cheng, X. C., Wang, Q., Fang, H., and Xu, W. F. (2008) Role of sulfonamide group in matrix metalloproteinase inhibitors, *Curr Med Chem 15*, 368-373.

162. Miyata, Y., Iwata, T., Ohba, K., Kanda, S., Nishikido, M., and Kanetake, H. (2006) Expression of matrix metalloproteinase-7 on cancer cells and tissue endothelial cells in renal cell carcinoma: prognostic implications and clinical significance for invasion and metastasis, *Clin Cancer Res 12*, 6998-7003.

163. Torchilin, V. P. (2005) Recent advances with liposomes as pharmaceutical carriers, *Nat Rev Drug Discov 4*, 145-160.

164. Immordino, M. L., Dosio, F., and Cattel, L. (2006) Stealth liposomes: review of the basic science, rationale, and clinical applications, existing and potential, *Int J Nanomedicine 1*, 297-315.

165. Hashida, M., Nishikawa, M., Yamashita, F., and Takakura, Y. (2001) Cell-specific delivery of genes with glycosylated carriers, *Adv Drug Deliv Rev 52*, 187-196.

166. Huang, S. L. (2008) Liposomes in ultrasonic drug and gene delivery, *Adv Drug Deliv Rev 60*, 1167-1176.

167. Kunisawa, J., Nakagawa, S., and Mayumi, T. (2001) Pharmacotherapy by intracellular delivery of drugs using fusogenic liposomes: application to vaccine development, *Adv Drug Deliv Rev 52*, 177-186.

168. Maurer, N., Fenske, D. B., and Cullis, P. R. (2001) Developments in liposomal drug delivery systems, *Expert Opin Biol Ther 1*, 923-947.

169. Gerasimov, O. V., Boomer, J. A., Qualls, M. M., and Thompson, D. H. (1999) Cytosolic drug delivery using pH- and light-sensitive liposomes, *Adv Drug Deliv Rev 38*, 317-338.

170. Huang, S. L., and MacDonald, R. C. (2004) Acoustically active liposomes for drug encapsulation and ultrasound-triggered release, *Biochim Biophys Acta 1665*, 134-141.

171. Zhang, S., and Zhao, Y. (2011) Controlled release from cleavable polymerized liposomes upon redox and pH stimulation, *Bioconjug Chem 22*, 523-528.

172. Kolb, H. C., Finn, M. G., and Sharpless, K. B. (2001) Click Chemistry: Diverse Chemical Function from a Few Good Reactions, *Angew Chem Int Ed Engl 40*, 2004-2021.

173. O'Neil, E. J., DiVittorio, K. M., and Smith, B. D. (2007) Phosphatidylcholine-derived bolaamphiphiles via click chemistry, *Org Lett 9*, 199-202.

174. Iha, R. K., Wooley, K. L., Nystrom, A. M., Burke, D. J., Kade, M. J., and Hawker, C. J. (2009) Applications of orthogonal "click" chemistries in the synthesis of functional soft materials, *Chem Rev 109*, 5620-5686.

175. Chen, E. I., Li, W., Godzik, A., Howard, E. W., and Smith, J. W. (2003) A residue in the S2 subsite controls substrate selectivity of matrix metalloproteinase-2 and matrix metalloproteinase-9, *J Biol Chem 278*, 17158-17163.

176. Chung, L., Dinakarpandian, D., Yoshida, N., Lauer-Fields, J. L., Fields, G. B., Visse, R., and Nagase, H. (2004) Collagenase unwinds triple-helical collagen prior to peptide bond hydrolysis, *EMBO J 23*, 3020-3030.

177. Nagase, H., Fields, C. G., and Fields, G. B. (1994) Design and characterization of a fluorogenic substrate selectively hydrolyzed by stromelysin 1 (matrix metalloproteinase-3), *J Biol Chem 269*, 20952-20957.

178. Itoh, M., Osaki, M., Chiba, T., Masuda, K., Akizawa, T., Yoshioka, M., and Seiki, M. (1997) Flow injection analysis for measurement of activity of matrix metalloproteinase-7 (MMP-7), *J Pharm Biomed Anal 15*, 1417-1426.

179. Ra, H. J., Harju-Baker, S., Zhang, F., Linhardt, R. J., Wilson, C. L., and Parks, W. C. (2009) Control of promatrilysin (MMP7) activation and substrate-specific activity by sulfated glycosaminoglycans, *J Biol Chem 284*, 27924-27932.

180. Thomas, D. A., Francis, P., Smith, C., Ratcliffe, S., Ede, N. J., Kay, C., Wayne, G., Martin, S. L., Moore, K., Amour, A., and Hooper, N. M. (2006) A broad-spectrum fluorescence-based peptide library for the rapid identification of protease substrates, *Proteomics 6*, 2112-2120.

181. Pham, W., Choi, Y., Weissleder, R., and Tung, C. H. (2004) Developing a peptide-based near-infrared molecular probe for protease sensing, *Bioconjug Chem 15*, 1403-1407.

182. Turk, B. E., Huang, L. L., Piro, E. T., and Cantley, L. C. (2001) Determination of protease cleavage site motifs using mixture-based oriented peptide libraries, *Nat Biotechnol 19*, 661-667.

183. Zheng, G., Chen, J., Stefflova, K., Jarvi, M., Li, H., and Wilson, B. C. (2007) Photodynamic molecular beacon as an activatable photosensitizer based on protease-

controlled singlet oxygen quenching and activation, *Proc Natl Acad Sci U S A 104*, 8989-8994.

APPENDIX

Supplementary Material for Chapter I

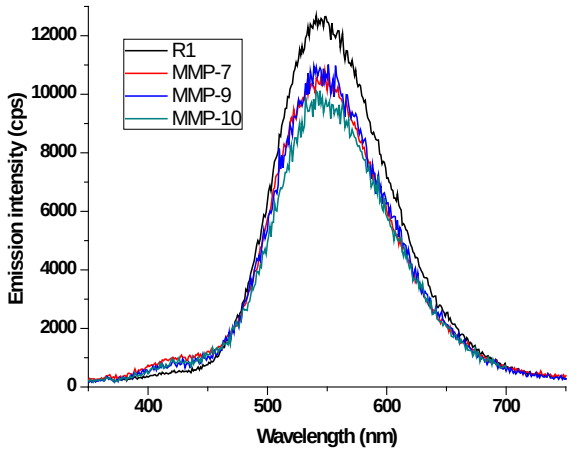

Figure A.1.1. Fluorescence emission spectra of the polymer **R1** (27 nM in 30 mM phosphate buffer, pH = 7.4, λ_{ex} = 325 nm, black trace) in presence of 200 nM of recombinant human MMP-7 (red trace), MMP-9 (blue trace) and MMP-10 (green trace).

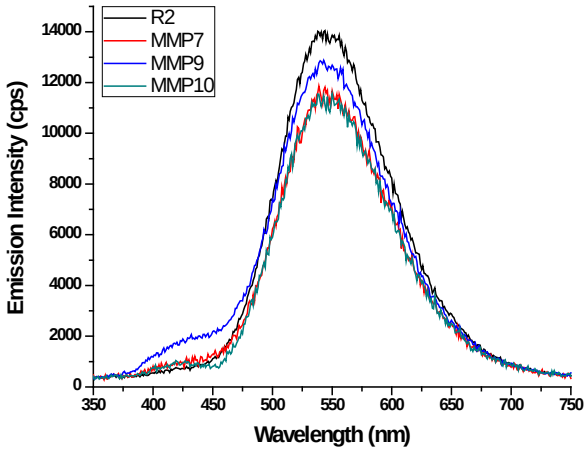

Figure A.1.2. Fluorescence emission spectra of the polymer **R2** (34 nM in 30 mM phosphate buffer, pH = 7.4, λ_{ex} = 325 nm, black trace) in presence of 200 nM of recombinant human MMP-7 (red trace), MMP-9 (blue trace) and MMP-10 (green trace).

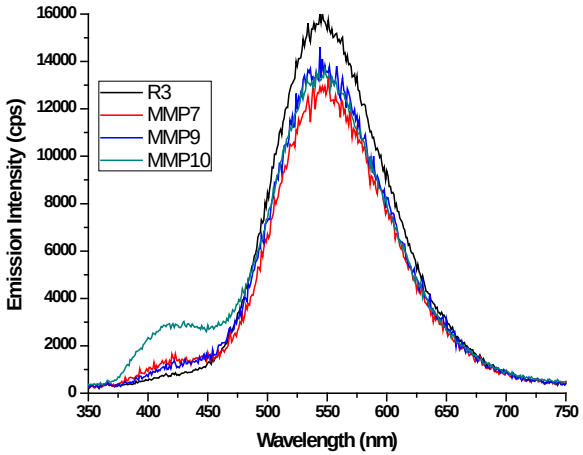

Figure A.1.3. Fluorescence emission spectra of the polymer **R3** (31 nM in 30 mM phosphate buffer, pH = 7.4, λ_{ex} = 325 nm, black trace) in presence of 200 nM of recombinant human MMP-7 (red trace), MMP-9 (blue trace) and MMP-10 (green trace).

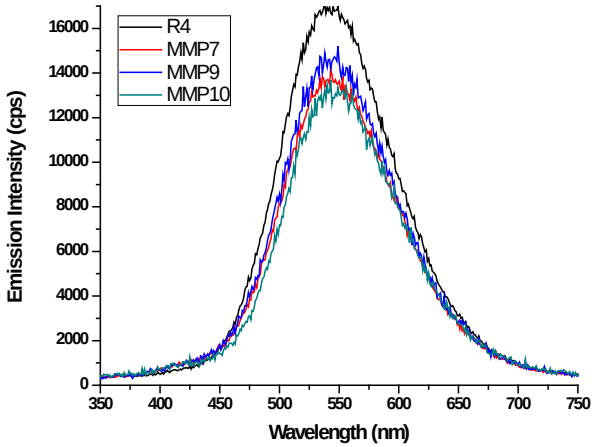

Figure A.1.4. Fluorescence emission spectra of the polymer **R4** (28 nM in 30 mM phosphate buffer, pH = 7.4, λ_{ex} = 325 nm, black trace) in presence of 200 nM of recombinant human MMP-7 (red trace), MMP-9 (blue trace) and MMP-10 (green trace).

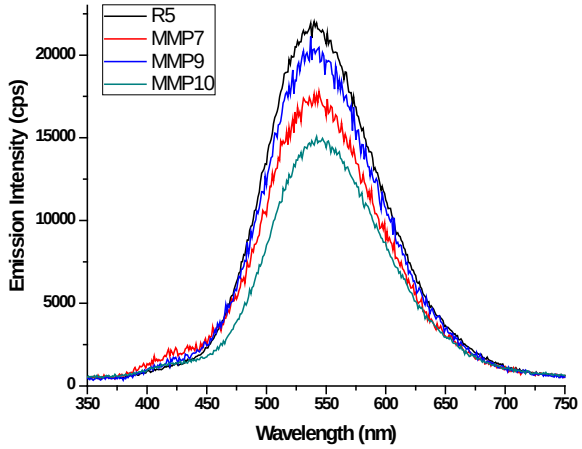

Figure A.1.5. Fluorescence emission spectra of the polymer **R5** (32 nM in 30 mM phosphate buffer, pH = 7.4, λ_{ex} = 325 nm, black trace) in presence of 200 nM of recombinant human MMP-7 (red trace), MMP-9 (blue trace) and MMP-10 (green trace).

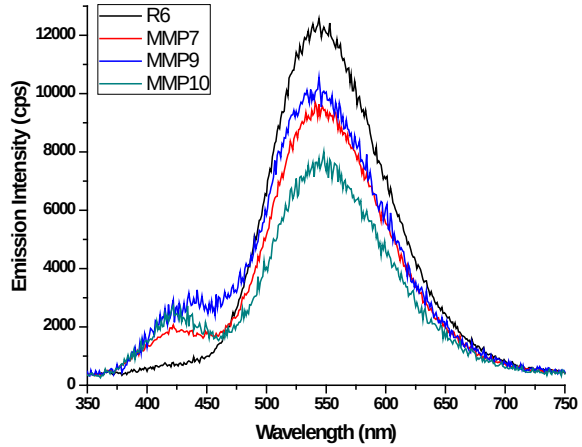

Figure A.1.6. Fluorescence emission spectra of the polymer **R6** (34 nM in 30 mM phosphate buffer, pH = 7.4, λ_{ex} = 325 nm, black trace) in presence of 200 nM of recombinant human MMP-7 (red trace), MMP-9 (blue trace) and MMP-10 (green trace).

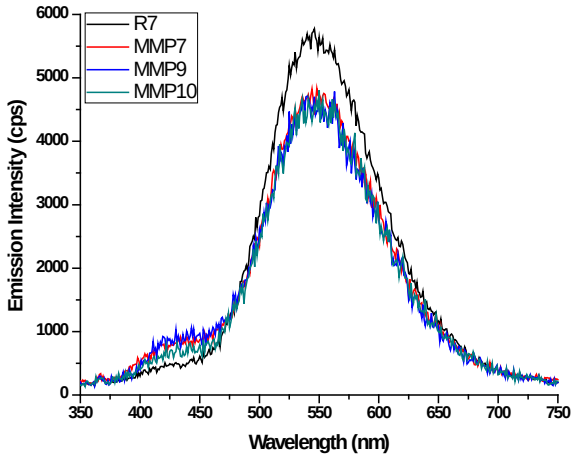

Figure A.1.7. Fluorescence emission spectra of the polymer **R7** (26 nM in 30 mM phosphate buffer, pH = 7.4, λ_{ex} = 325 nm, black trace) in presence of 200 nM of recombinant human MMP-7 (red trace), MMP-9 (blue trace) and MMP-10 (green trace).

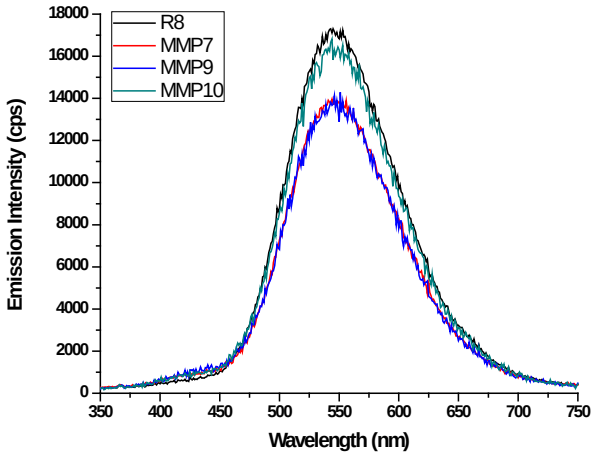

Figure A.1.8. Fluorescence emission spectra of the polymer **R8** (36 nM in 30 mM phosphate buffer, pH = 7.4, λ_{ex} = 325 nm, black trace) in presence of 200 nM of recombinant human MMP-7 (red trace), MMP-9 (blue trace) and MMP-10 (green trace).

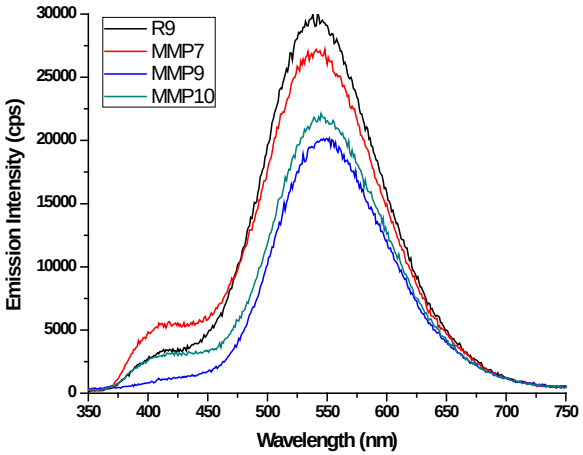

Figure A.1.9. Fluorescence emission spectra of the polymer **R9** (27 nM in 30 mM phosphate buffer, pH = 7.4, λ_{ex} = 325 nm, black trace) in presence of 200 nM of recombinant human MMP-7 (red trace), MMP-9 (blue trace) and MMP-10 (green trace).

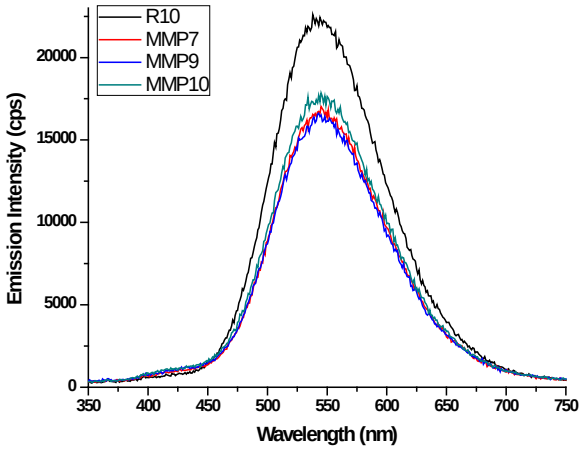

Figure A.1.10. Fluorescence emission spectra of the polymer **R10** (30 nM in 30 mM phosphate buffer, pH = 7.4, λ_{ex} = 325 nm, black trace) in presence of 200 nM of recombinant human MMP-7 (red trace), MMP-9 (blue trace) and MMP-10 (green trace).

Table A.1.1. Fluorescence ratios at 541 nm for polymers **R1-R11** against MMP-7 for 6 repetitions.

Polymers	Cycle 1	Cycle 2	Cycle 3	Cycle 4	Cycle 5	Cycle 6
R1	1.202	1.208	1.226	1.229	1.213	1.236
R2	1.227	1.202	1.214	1.188	1.118	1.148
R3	1.253	1.217	1.170	1.250	1.186	1.158
R4	1.227	1.215	1.180	1.200	1.163	1.189
R5	1.270	1.239	1.202	1.203	1.195	1.150
R6	1.250	1.291	1.214	1.166	1.187	1.163
R7	1.184	1.149	1.146	1.137	1.163	1.096
R8	1.231	1.300	1.259	1.235	1.230	1.175
R9	1.069	1.209	1.265	1.246	1.276	1.296
R10	1.361	1.278	1.169	1.185	1.181	1.210
R11	1.523	1.566	1.495	1.465	1.444	1.439

Table A.1.2. Fluorescence ratios at 541 nm for polymers **R1-R11** against MMP-10 for 6 repetitions.

Polymers	Cycle 1	Cycle 2	Cycle 3	Cycle 4	Cycle 5	Cycle 6
R1	1.255	1.225	1.151	1.133	1.060	1.006
R2	1.265	1.223	1.156	1.150	1.075	1.078
R3	1.150	1.137	1.114	1.077	1.048	1.062
R4	1.282	1.266	1.175	1.148	1.142	1.171
R5	1.464	1.218	1.172	1.097	1.085	1.012
R6	1.268	1.210	1.184	1.084	1.096	1.086
R7	1.201	1.233	1.189	1.147	1.097	1.099
R8	1.046	1.055	1.066	1.093	1.129	1.082
R9	1.093	1.067	1.026	1.031	1.047	1.057
R10	1.152	1.170	1.133	1.136	1.128	1.115
R11	1.572	1.498	1.461	1.446	1.413	1.414

Table A.1.3. Logit analysis of MMP-9 versus MMP-7/MMP-10 for **R1-R11**. Dependent variable: (Binary variable identifying MMP-9).

Variable	Coeff.	Std.Err.	Chi-Square Stat.	P-value	
Binary Variables Identifying the Polymer					
R1 (Control Polymer)	-16.173	12.466	1.683	0.195	
R2 (Control Polymer)	42.982	21.560	3.975	0.046	*
R3	16.851	11.767	2.051	0.152	
R4	23.016	18.612	1.529	0.216	
R5	12.656	9.762	1.681	0.195	
R6	5.278	9.583	0.303	0.582	
R7	-28.919	16.574	3.044	0.081	
R8	-5.942	7.658	0.602	0.438	
R9	0.916	6.598	0.019	0.890	
R10	-23.984	10.757	4.972	0.026	*
R11	43.644	18.308	5.683	0.017	*

Table A.1.4. Slope dummy interaction terms between Fluorescence and polymers.

R1*Fluorescence	12.853	10.207	1.586	0.208	
R2*Fluorescence	-39.385	19.777	3.966	0.046	*
R3*Fluorescence	-15.546	10.550	2.171	0.141	
R4*Fluorescence	-20.033	15.825	1.603	0.206	
R5*Fluorescence	-11.552	8.560	1.821	0.177	
R6*Fluorescence	-5.028	8.175	0.378	0.539	
R7*Fluorescence	23.998	14.010	2.934	0.087	
R8*Fluorescence	4.534	6.486	0.489	0.485	
R9*Fluorescence	-1.350	5.806	0.054	0.816	
R10*Fluorescence	18.816	8.581	4.808	0.028	*
R11*Fluorescence	-32.235	13.425	5.765	0.016	*

Table A.1.5. Chi-Square Test and degrees of freedom for polymers **R1-R11**.

-2*Log-Likelihood Function		228.0710		
-2*Restricted Log-Likelihood Function		299.6960		
Chi-Square Test Statistic Value		71.6245	< 0.0001	*
Degrees of Freedom		22		
Number of Observations		198		
* Indicates statistical significance at the 5 percent level or better				
# Indicates a significant odds ratio that predicts the ommitted category (0)				

Table A.1.6. Odd Ratio Estimates of the polymers.

	Odds Ratio Estimates			
Evaluated at Grand Sample Mean of Fluorescence				
	95% Profile	95% Profile	Evaluated	
	CI	CI	at	
Odds	Lower	Upper	Fluorescence	
Ratio	Limit	Limit	Mean Value	
0.424	0.131	1.375	1.192	
0.019	<0.001	1.270	1.192	
0.188	0.028	1.268	1.192	
0.425	0.136	1.329	1.192	
0.330	0.084	1.297	1.192	
0.490	0.174	1.380	1.192	
0.723	0.236	2.222	1.192	
0.583	0.215	1.580	1.192	
0.500	0.154	1.621	1.192	
0.209	0.043	1.020	1.192	
187.598	1.347	>999.999	1.192	*

Supplementary Material for Chapter II

Table A.2.1. Calculation of subtracted initial absorbance against concentrations of MMP-9 for the ELISA calibration curve (for breast cancer cell line studies).

Conc. of MMP-9 (pg/mL)	Abs.	Initial Abs. subtracted
0	0.1188	0
8.23	0.1716	0.0528
24.69	0.1857	0.0669
74.07	0.2029	0.0841
222.2	0.2426	0.1238
666.7	0.3407	0.2219
2000	0.6151	0.4963
6000	1.2891	1.1703

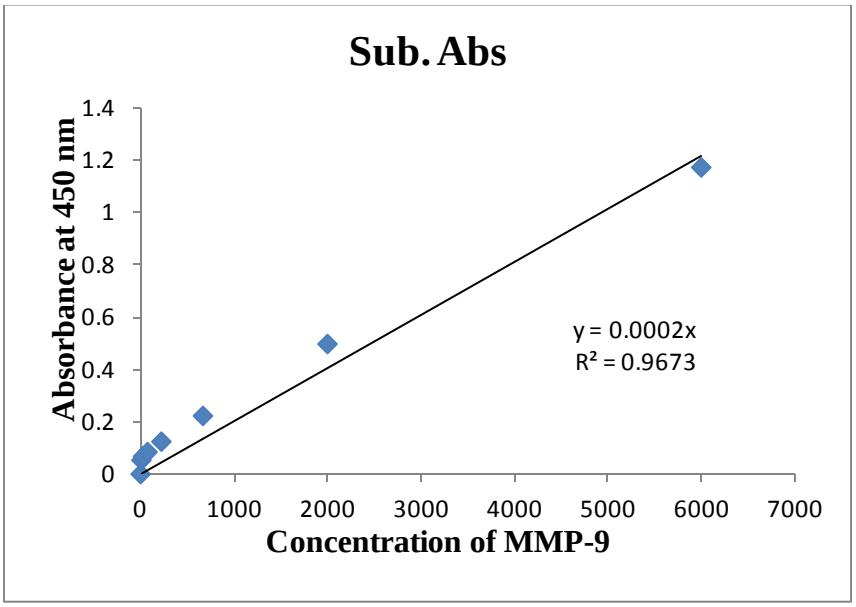

Figure A.2.1. Calibration curve from the ELISA kit for breast cancer cell lines.

Table A.2.2. Concentrations of MMP-9 in the conditioned cell culture media (determined by ELISA from Appendix Figure A.2.1).

Conditioned media from cell lines	Concentration of MMP-9 (pg/mL)
MCF 7	969.5
HEK	162
HELA	268.75
MDA-MB-231	170.5

Table A.2.3. Calculation of subtracted initial absorbance against concentrations of MMP-9 for the ELISA calibration curve (for prostate cancer cell line studies).

Conc. of MMP-9 (pg/mL)	Initial absorbance subtracted
6000	1.7415
2000	0.657
666.7	0.1985
222.2	0.0585
0	0

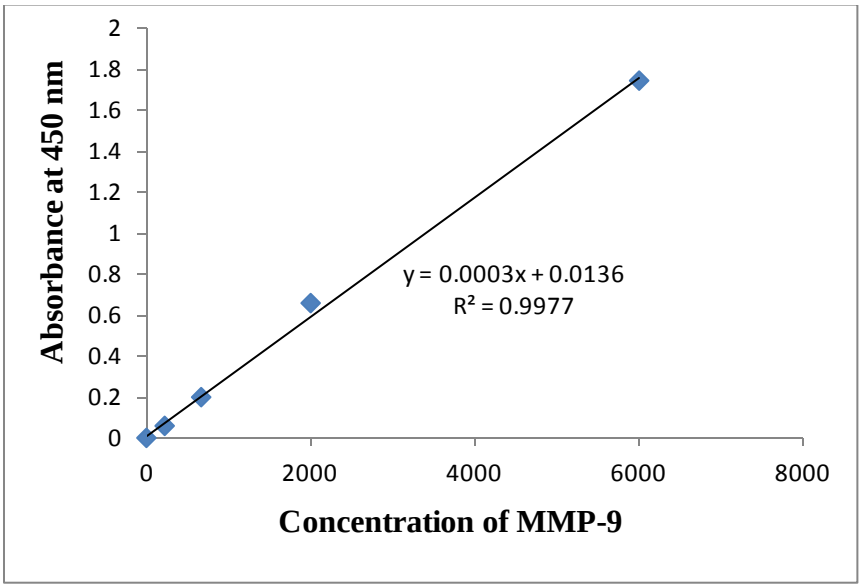

Figure A.2.2. Calibration curve from the ELISA kit for prostate cancer cell lines.

Table A.2.4. Concentrations of MMP-9 in the conditioned cell culture media (determined by ELISA from Appendix Figure A.2.2).

Conditioned media from cell lines	Concentration of MMP-9 (pg/mL)
PANC1	2053
PC3	739.67
22Rv1	773
HEK	771.33

Statistical Data Analysis : LDA for breast cancer cell lines : LDA extracted two canonical variables, each with its own discriminant function. At the 5% level, chi-square tests indicate that both canonical functions significantly explain the four cell lines. The first canonical function is the more important of the two, as it explains 98.3% of the variation across cell lines, while the remaining function explains only 1.7% of this variation. Analysis of these canonical functions suggests that the polymer contributes relatively more to the first canonical function.

Table A.2.5. Table of ratios (R) generated from fluorescent experiments for prostate cancer cell lines.

Polymer	Cell Line	Run 1	Run 2	Run 3	Run 4	Run 5	Run 6	Run 7	Run 8
R11	PANC-$1_{420\ nm}$	0.754512	0.787304	0.803593	0.788134	0.752842	0.764749	0.739391	0.75971
	PC-$3_{420\ nm}$	0.793168	0.839454	0.840286	0.84325	0.837371	0.851493	0.89816	0.897751
	22Rv$1_{420\ nm}$	1.197853	1.460126	1.459727	1.515055	1.447846	1.498209	1.563769	1.550487
	HEK-$293_{420\ nm}$	1.734831	1.766465	1.841755	1.788262	1.767768	1.851178	1.846879	1.842947
	PANC-$1_{523\ nm}$	1.096931	1.088802	1.054943	1.046537	1.078234	1.066194	1.048481	1.001006
	PC-$3_{523\ nm}$	1.061301	1.047744	1.046535	1.02048	1.032212	1.112304	1.069226	1.017869
	22Rv$1_{523\ nm}$	1.23598	1.26203	1.21424	1.192433	1.210153	1.190576	1.236044	1.211034
	HEK-$293_{523\ nm}$	1.234752	1.251697	1.234789	1.288396	1.248991	1.264972	1.266787	1.236204
	PANC-$1_{541\ nm}$	1.129329	1.105367	1.116404	1.072364	1.116948	1.067953	1.059361	1.067068
	PC-$3_{541\ nm}$	1.080923	1.105098	1.031855	1.039193	1.049868	1.122354	1.081042	1.01804
	22Rv$1_{541\ nm}$	1.205429	1.183399	1.141565	1.13724	1.169841	1.150047	1.134717	1.181879
	HEK-$293_{541\ nm}$	1.174917	1.181515	1.185666	1.174749	1.186022	1.203861	1.209758	1.197237

Table A.2.6. Table of ratios (R) generated from fluorescent experiments for breast cancer cell lines.

Polymer	Cell Line	Run 1	Run 2	Run 3	Run 4	Run 5	Run 6	Run 7	Run 8
R11	MDA-MB-$231_{420\ nm}$	1.080916	0.940839	0.932647	0.911347	0.881809	0.902869	0.887206	0.905851
	MCF-$7_{420\ nm}$	1.606264	1.62015	1.841565	1.708477	1.654629	1.679794	1.676482	1.611221
	HeLa$_{420\ nm}$	2.03411	2.01602	2.0644	2.078443	2.010565	2.026123	2.010012	2.017582
	HEK-$293_{420\ nm}$	1.734831	1.766465	1.841755	1.788262	1.767768	1.851178	1.846879	1.842947
	MDA-MB-$231_{523\ nm}$	1.119972	1.082309	1.055043	1.038331	1.069302	1.045312	1.050322	1.008249
	MCF-$7_{523\ nm}$	1.07821	1.087998	1.07334	1.103308	1.081348	1.095925	1.083516	1.078523
	HeLa$_{523\ nm}$	1.067634	1.083515	1.065766	1.105408	1.060263	1.07273	1.051424	1.032221
	HEK-$293_{523\ nm}$	1.234752	1.251697	1.234789	1.288396	1.248991	1.264972	1.266787	1.236204
	MDA-MB-$231_{541\ nm}$	1.081602	1.066703	1.089008	1.073585	1.086683	1.053653	1.053267	1.019529
	MCF-$7_{541\ nm}$	1.041337	1.051019	1.081892	1.053521	1.066059	1.076953	1.062204	1.083289
	HeLa$_{541\ nm}$	1.039678	1.031022	1.067872	1.032628	1.02431	1.003782	1.020121	1.018158
	HEK-$293_{541\ nm}$	1.174917	1.181515	1.185666	1.174749	1.186022	1.203861	1.209758	1.197237

Table A.2.7 contains the structure matrix and the cumulative potency indices, which can be used to assess the overall contribution of the polymer (evaluated at the "best" emission intensity) to the ability of LDA to discriminate between (or predict) the four cell lines. The potency indices (0.922) suggest that the polymer provides the largest overall contribution to the model's ability to distinguish between the cell lines.

Table A.2.7. The potency index of various functions for the polymer **R11.**

Parameters	Polymer R-11
Function 1	0.968
Function 2	-0.250
Potency Index	0.922

Table A.2.8 identifies the number of significant canonical correlations and canonical functions. At the 5% level, two of three canonical functions significantly explain the four cell lines. Of these, the first canonical function is most important, as it explains 80.2% of the variation across cell lines. The remaining functions explain 19.8% and 0.0002%, respectively. As in the previous analysis, these results lead us to focus primarily on the first discriminant function.

Table A.2.8. Canonical function summary[a] for breast cancer cell lines studies.

Function	Eigen value	Pct. of variance explained	Canonical Correlation	Wilk's Lambda[a]	Chi Square Statistics	p-value
1	80.085	80.2	0.994	0.001	204.861	<0.001
2	19.806	19.8	0.976	0.047	83.985	<0.001
3	0.019	0.0002	0.136	0.981	0.516	0.473

[a] Lower values for Wilks' Lambda indicate greater discrimination. Wilks' Lambda and chi-square tests apply sequentially. [b] tests functions 1 – 3 cumulatively. [c] tests functions 2 – 3 cumulatively [d] tests function 3.

To assess the overall contribution of each emission intensity to the discriminatory power of the LDA, Table A.2.9 contains the structure matrix and the cumulative potency indices. The potency indices suggest that 420 nm emission intensity provides the largest overall contribution to the model's ability to distinguish between the cell lines.

Table A.2.9. Structure matrix and potency index for breast cancer cell lines studies.

Predictor	Canonical Function 1	Canonical Function 2	Canonical Function 3	Potency Index
420 nm	0.832	0.537	0.139	0.612
523 nm	0.010	0.851	-0.525	0.144
541 nm	-0.088	0.789	0.608	0.130

Table A.2.10 contains the standardized discriminant function coefficients, which measure the relative contributions of each emission intensity to a specific discriminant function. For function 1, the 420 nm wavelength exhibits the highest coefficient in absolute value. Additionally, the 523 nm and 541 nm emission intensities carry values which (in absolute magnitude) are much smaller in absolute magnitude than for 420 nm.

Table A.2.10. Standardized canonical discriminant function coefficients (breast cancer).

Predictor	Canonical Function 1	Canonical Function 2	Canonical Function 3
420 nm	1.152	0.050	0.103
523 nm	-0.268	0.641	0.525
541 nm	-0.495	0.542	0.628

Concomitantly, the 523 nm exhibits the highest value for the second function, while 541 nm has the largest coefficient for the third (insignificant) canonical function. In both the second and third canonical functions, the coefficient values for the 420 nm variable suggest that the 420 intensities have very little contribution to the second and third canonical discriminant functions. On the other hand, the 523 nm and 541 nm coefficient values for the second and third functions

are large in absolute value, implying that these predictors contribute substantially to these functions.

Statistical Data Analysis : LDA for prostate cancer cell lines : Table A.2.11 identifies the number significant eigen values, canonical correlations and canonical functions. At the 5% level, all three canonical functions are significant. The first canonical explains 99.3% of the variation across cell lines. The remaining functions explain 0.05% and 0.2% respectively. Based on these results, we focus primarily on the first discriminant function.

Table A.2.11. Canonical function summary[a] for prostate cancer cell lines studies.

Function	Eigen value	Pct. of variance explained	Canonical Correlation	Wilk's Lambda[a]	Chi Square Statistics	p-value
1	71.429	99.3	0.993	0.009	129.534	<0.001
2	0.331	0.5	0.498	0.652	11.762	<0.001
3	0.153	0.2	0.364	0.868	3.907	0.048

[a] Lower values for Wilks' Lambda indicate greater discrimination. Wilks' Lambda and chi-square tests apply sequentially. [b] tests functions 1 – 3 cumulatively. [c] tests functions 2 – 3 cumulatively [d] tests function 3.

Table A.2.12 contains the standardized discriminant function coefficients, which measure the relative contributions of each emission intensity to a specific discriminant function. For function 1, the 420 nm wavelength exhibits the highest coefficient in absolute value. 523 nm exhibits the highest value for the second function, while 541 nm has the largest coefficient for the third canonical function.

Table A.2.12. Standardized canonical discriminant function coefficients (prostate cancer).

Predictor	Canonical Function 1	Canonical Function 2	Canonical Function 3
420 nm	0.928	-0.446	0.049
523 nm	0.428	0.942	-0.781
541 nm	0.176	-0.147	1.306

Table A.2.13 contains the structure matrix and the cumulative potency indices, which can be used to assess the overall contribution of each emission intensity to the discriminatory power of the LDA. The potency indices suggest that 420 nm emission intensity provides the largest overall contribution to the model's ability to distinguish between cell lines. These result should not be surprising considering that the 420 nm variable is the primary determinant of the first canonical correlation. This variate (and its corresponding discriminant function) xplains over 99 % of the variation in the cell lines.

Table A.2.13. Structure matrix and potency index for prostate cancer cell lines studies.

Predictor	Canonical Function 1	Canonical Function 2	Canonical Function 3	Potency Index
420 nm	0.832	0.537	0.139	0.612
523 nm	0.010	0.851	-0.525	0.144
541 nm	-0.088	0.789	0.608	0.130

Supplementary Material for Chapter III

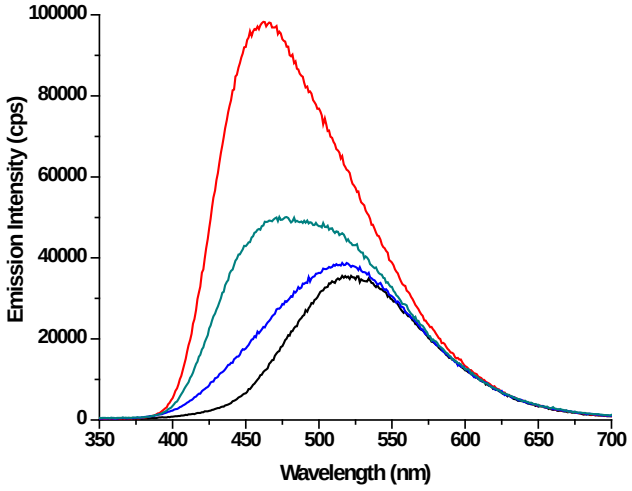

Figure A.3.1. Fluorescence emission spectra of polymer **F1** (50 nM; λex = 325 nm, black trace) in presence of 500 nM of CA II (red trace), CA XII (green trace) and CA VII (blue trace) each.

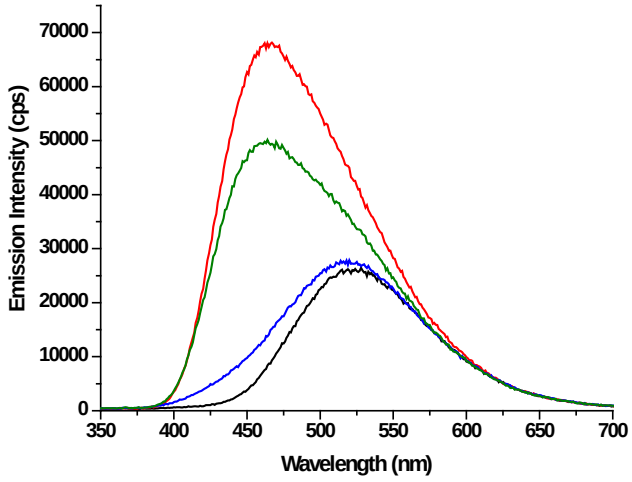

Figure A.3.2. Fluorescence emission spectra of polymer **F3** (50 nM; λex = 325 nm, black trace) in presence of 500 nM of CA II (red trace), CA XII (green trace) and CA VII (blue trace) each.

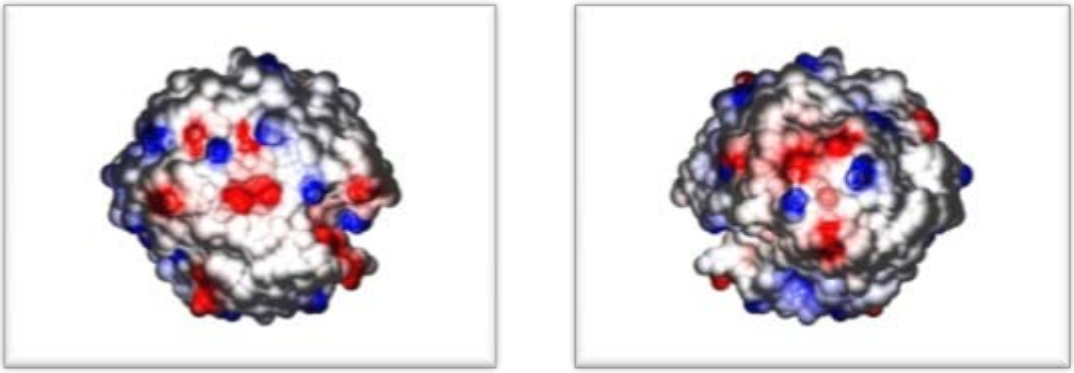

Figure A.3.3. The X-ray crystallographic structures of CA VII (3MDZ) obtained from the RCSB Protein Data Bank. The molecular surface electrostatic potentials were calculated by the Poisson-Boltzmann equation as implemented in the program GRASP2. The electrostatic surface potential of CA VII front, facing the active site (left) and back (right).

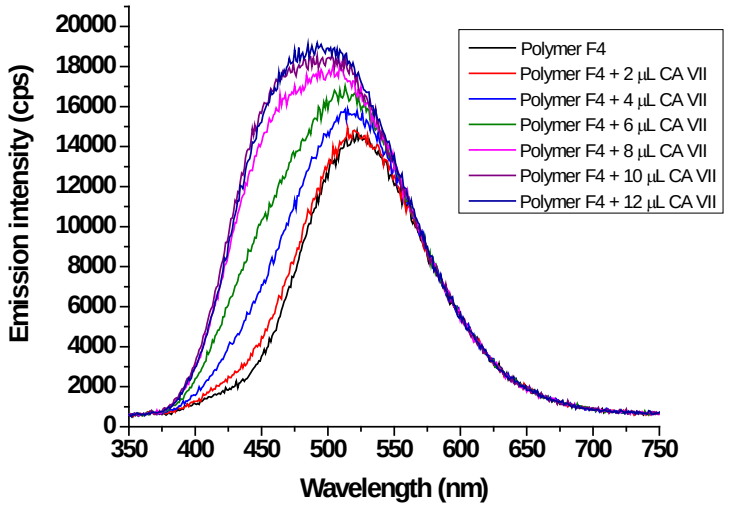

Figure A.3.4. Fluorescence titration plot for polymer **F4** against increasing amount of added CA VII. The solutions were excited at 325 nm and were conducted in 30 mM phosphate buffer (pH = 7.4).

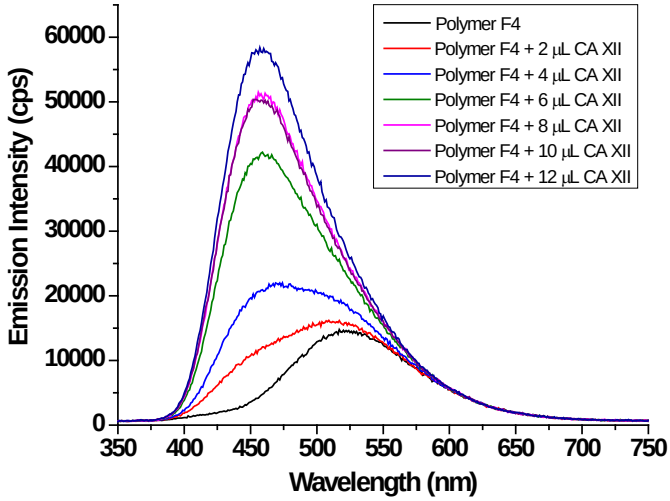

Figure A.3.5. Fluorescence titration plot for polymer **F4** against increasing amount of added CA XII. The solutions were excited at 325 nm and were conducted in 30 mM phosphate buffer (pH = 7.4).

.

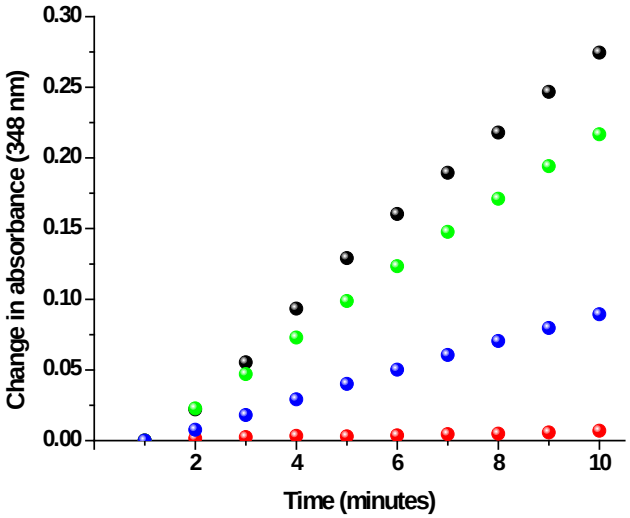

Figure A.3.6. Absorbance change (348 nm) during the esterase inhibition assay of CA II in the absence (black trace) and in the presence of 10 μM (blue trace) and 1 μM (green trace) inhibitor monomer **1** are shown. The red trace indicates the absorption changes in the presence of 10 μM acetazolamide solution. These experiments were conducted in 25 mM HEPES buffer (pH=7.4).

Table. A.3.1. Fluorescence titration plots fitted in Hill equation and values generated for polymer **F4** and CA II.

V_{max}		k		n		Statistics	
Value	Standard error	Value	Standard error	Value	Standard error	Reduced Chi-Square.	Adj. R-Square.
37705.9	3.85E7	4053.12	3.04E6	1.369	0.55	1.53	0.98

Table. A.3.2. Fluorescence titration plots fitted in Hill equation and values generated for polymer **F4** and CA VII.

V_{max}		k		n		Statistics	
Value	Standard error	Value	Standard error	Value	Standard error	Reduced Chi-Square.	Adj. R-Square.
0.83	0.038	11.06	0.56	2.4	0.18	1.38E-4	0.99

Table.A.3.3. Fluorescence titration plots fitted in Hill equation and values generated for polymer **F4** and CA XII.

V_{max}		k		n		Statistics	
Value	Standard error	Value	Standard error	Value	Standard error	Reduced Chi-Square.	Adj. R-Square.
11.97	1.21	9.38	0.98	3.05	0.84	0.55	0.97